Gran Sasso Science Institute

Scuola Internazionale Superiore di Studi Avanzati

Open problems in neutrino astrophysics

Thesis advisor:
Francesco Vissani

Dissertation by:
Carlo Mascaretti

PhD in Astroparticle Physics, XXXII cycle

April 2020

Abstract

Context The physics of neutrinos is one of the richest and most intriguing fields of research in modern physics. One reason is their ambiguous role in the Standard Model of particle physics, within and beyond the Standard Model of electroweak interaction: they are categorised as neutral leptons which obey the gauge structures of the Standard Model Lagrangian, with which it is possible to precisely compute the neutrino interaction rates, yet they have mass and are subject to flavour oscillations, which cannot be reconciled with the minimal formulation of the Standard Model. Flavour oscillations are explained with nonzero masses of neutrinos, the nature of which (Dirac or Majorana) is still under experimental investigation. Also the flavour oscillations of neutrinos are still studied, and are currently tested over 9 decades in energy, from MeV to PeV.

Another reason for the interest in neutrinos is that they are very elusive, which means that experimental results come with enormous effort and large timescales. For example, out of more than 60 billion solar neutrinos that every second go through any square centimeter of the Earth, Borexino, one of the most sensitive modern detectors, manages to reveal about 100 per day. Cosmic neutrino searches, which are currently led by IceCube, a km^3-scale telescope embedded in the depths of the Antarctic ice, deal with about 10 events per year, which is why an unequivocal source of neutrinos is yet to be found.

Another implication of their elusiveness is that neutrinos can travel for huge distances in the cosmos without being absorbed. In the context of astroparticle physics, neutrinos have a very peculiar role: they are assumed to be produced in the interaction of cosmic-rays with the gas or radiation fields that surround the accelerators of the cosmic rays themselves, and do not suffer deviation from magnetic fields, like charged particles, nor absorption, like photons. Neutrinos

are also produced in the thermonuclear reactions that make stars burn, in the explosions of Supernovae, which are phenomena that are still poorly understood, and in the collisions between cosmic rays and the nuclei in the atmosphere.

All the features mentioned above make neutrinos very peculiar particles, as they are simultaneously the probe for fundamental (particle) physics, for cosmic-ray acceleration and propagation, and, potentially, tomographic study of the objects which produce them.

Original contributions This thesis is focussed on the astroparticle nature of neutrinos. A first technical but novel result is the update of the survival/oscillation probabilities for cosmic neutrinos using the most recent oscillation parameters available at the time, and we exploited them to critically investigate the results on astrophysical neutrinos obtained by IceCube.

The spectrum of cosmic neutrinos has been a focal point of interest, as the results of the IceCube analyses, based on the HESE and through-going muons data samples, lead to problems in their interpretation. These results have been critically discussed, pointing out the potential reasons for such discrepancy [1]. In the same work, we also quantitatively predicted the number of ν_τ-induced events and Glashow events, i.e. resonant interactions of $\overline{\nu}_e + e^- \to W^-$ ($E_{\overline{\nu}_e} \gtrsim 6.3\,\mathrm{PeV}$), based on a cosmic neutrino spectrum which we modelled from the experimental data. Different hypotheses on the cosmic neutrino spectrum were used to compute the rate of ν_τ-induced events in the present and future neutrino telescopes, and to discuss the dramatic implications of the failure to observe them [2].

Atmospheric neutrinos have been studied in the context of their connection to the cosmic-ray spectrum [3] and as a background to astrophysical neutrino analyses [4]. Atmospheric neutrinos are in fact generated in the collisions of cosmic rays with the nuclei in the atmosphere, and are expected to follow an energy spectrum which maintains information on that of the incident particles. This led us to assessing the possibility of identifying the rigidity of the most prominent feature in the cosmic-ray spectrum, the knee, with atmospheric neutrinos [3]. The knee is associated with the end of the light component (protons and Helium nuclei) of the cosmic-ray spectrum, which is supposedly connected to the end of the spectrum of conventional atmospheric neutrinos. Different primary cosmic-ray flux models have been defined, corresponding to two alternative parametrizations

of the knee, and to the fits to two different knee rigidities, which result from the measurements by ARGO-YBJ and KASCADE-Grande. These primary cosmic-ray flux models have been used to compute the atmospheric neutrino fluxes, which have been compared to experimental data for the discrimination of the knee and the discussion of the experimental results.

The atmospheric neutrino models which resulted from this work were also used in [4]: in this work the contribution to the IceCube cascade dataset of the prompt component of the atmospheric spectrum has been computed - the prompt component is yet to be measured, despite the high degree of certainty about its existence. The cascade topology is the most relevant in this context, as it is mainly due to electron and tau neutrinos: in the muon neutrino spectrum, the prompt component is practically dominated by the conventional one up to about 1 PeV. A cosmic neutrino model has been obtained by combining the expectations from starburst Galaxies by Loeb & Waxman and the fit to the through-going muons dataset by IceCube, so as to have a precise, phenomenological muon neutrino flux. The cosmic neutrino fluxes of the other flavours have been obtained exploiting the connection among each other via their relation to the gamma-ray flux, with the underlying hypothesis of a hadronic mechanism of production. These fluxes have been convolved with the IceCube effective areas for cascade-like events, taking into account the presence of the veto for atmospheric neutrinos. We highlighted how to help the detection of prompt neutrinos and their possible impact on the interpretation of the IceCube signals.

Lastly, we studied solar neutrinos in the context of the luminosity constraint, which is a very powerful tool that allows to connect the power emitted by the Sun in photons to that emitted in neutrinos. We re-derived the standard luminosity constraint in a simpler and clearer formulation; this description is based on the assumption that the Sun accumulates only ^{4}He, while all the other reactions are in equilibrium, and that its total power is emitted in photons and neutrinos. Motivated by a very precise, recent measurement of the solar luminosity in photons, we showed how to extend the luminosity constraint with the inclusion of the effects of other accumulating nuclear species, and of the variation over time of the gravitational potential of the Sun due to its expansion. We discussed the relevance and power of this updated luminosity constraint in the context of CNO neutrino (predicted from the Standard Solar Model, but never observed) detection, which is directly related to an accurate determination of the metallicity

(heavier-than-Helium element fraction) of the Sun.

Structure The layout of the thesis is the following:

1. Chapter 1 presents a brief history of neutrinos and reviews its description in elementary particle physics; neutrino masses are introduced both in the Dirac and Majorana formulations. After that, neutrino oscillations in vacuum and in matter are dealt with, and the update of the cosmic neutrino oscillation/survival probabilities is presented. We conclude the chapter with an overview on the types of neutrinos, ranging from relic neutrinos, produced in the early Universe, to the neutrinos produced on Earth.

2. Chapter 2 deals with solar neutrinos, the theoretical foundation of which is the Standard Solar Model; this is a model that relies on nuclear physics, thermodynamics, and hydrodynamics to reproduce the current features of the Sun. We then offer an overview of the experiments which detected, detect and will detect solar neutrinos, including their results both in the context of solar neutrino flux determination and of neutrino oscillations. We close the chapter by presenting the original work concerning the update of the luminosity constraint, which is close to publication.

3. Chapter 3 revolves about atmospheric neutrinos. Firstly, we cover the predictions and theoretical expectations on their energy spectrum and flavour composition, based on particle and cosmic-ray physics. We discuss the conventional and prompt components of the neutrino spectrum, which are produced, respectively, by the decay of light (mainly pions and kaons) and heavy (mainly charmed mesons and baryons) particles. Secondly, due to the connection of atmospheric neutrinos to the cosmic-ray flux, we briefly touch on the cosmic-ray spectrum and the cascade formalism, which is needed to compute secondary neutrino production from cosmic ray-nuclei collisions in the atmosphere. Thirdly, we present the experimental results on atmospheric neutrinos, both in the context of flux and neutrino mixing measurements. Finally, we present the original work on the connection between the cosmic-ray knee and atmospheric neutrinos.

4. Chapter 4 is about cosmic neutrinos. We open the chapter with a discussion on the commonly accepted set of expectations and assumptions regarding

the mechanisms of production and the candidate sources of high-energy neutrinos, stressing the fact that a definitive theoretical picture is still missing. This set of assumptions includes: standard-three flavour neutrino mixing, an unbroken power law as the energy spectrum of cosmic neutrinos, and isotropy for their angular distribution. We briefly overview the most popular types of cosmic neutrino sources, i.e. starburst Galaxies, blazars and gamma-ray bursts, and cover the recent evidence for a neutrino source, the blazar TXS 0506+056. After this phenomenological introduction, we present the current experimental results on astrophysical neutrinos, which are mainly obtained by IceCube, the first operating km^3-scale experiment. The types of datasets and the corresponding results are reviewed in depth, as they are the foundation of the phenomenological discussions presented in this thesis. We also cover the results by the ANTARES telescope, and briefly cover its upgrade KM3NeT. An overview of the experiments using Askaryan radio emission - ARIANNA, ARA, and ANITA - is also present, with a short presentation of the very unexpected events detected by ANITA. These experiments, with Auger and POEMMA, provide the best sensitivities to the ultra-high-energy neutrino flux. We close the chapter with the presentation of three original works on the compatibility of the IceCube results with a universal neutrino spectrum, on the importance of cosmic tau neutrino detection, and on the role of prompt neutrinos for the interpretation of the IceCube signals.

Results In [1] we discussed the difficulty of the interpretation of the IceCube results as an isotropic cosmic neutrino flux with an unbroken power-law distribution. A two-component model of the astrophysical neutrino spectrum has been proposed, and standard three-flavour oscillations have been used to compute the cosmic flux of each neutrino flavour. Such astrophysical neutrino model proved to be compatible with the IceCube measurements, and has been used to compute the rate of events due to Glashow resonances and due to double cascades in IceCube. Moreover, a preference for pion decay as a neutrino production mechanism has been found.

In [2] we computed the rate of ν_τ-induced events in IceCube, KM3NeT and IceCube-gen2, quantifying the amount of time needed to observe a double-cascade event at 99% C.L. for each detector. To do this, we convoluted the cosmic ν_τ

spectrum, which we obtained on the bases of standard three-flavour neutrino oscillations and of the IceCube results, with the effective areas for double-cascade events. Analytical approximations for the relevant effective areas of all these detectors have been proposed and used to predict that the IceCube detector was close to see the first double cascade events - let us stress that the first preliminary data agree with such prediction. We considered the possibility that these events would not be observed, and discussed the consequent implications.

In [3] we tested the possibility to use atmospheric neutrinos to determine the position of the knee of the cosmic-ray spectrum. A primary cosmic-ray flux model has been introduced to fit the knee positions as measured by ARGO-YBJ and KASCADE-Grande. The resulting spectra were used as input to a numerical code for the computation of the corresponding atmospheric neutrino fluxes: these have been then compared with the available data to discriminate the better knee model. A slight preference for the knee as measured by the KASCADE-Grande collaboration has been found, but the experimental uncertainties on the atmospheric neutrino flux are too large to unequivocally discriminate the two models.

In [4] we investigated the role of the yet undetected prompt neutrino flux for the interpretation of the IceCube results. We adopted the procedure of [3] to model the atmospheric component, with the choice of the KASCADE-Grande knee. The assumptions of a hadronic mechanism of astrophysical neutrino production in starburst Galaxies and of standard three-flavour neutrino oscillations led us to formulate a phenomenologically precise astrophysical flux. This flux is obtained as a combination of the theoretical expectation for astrophysical neutrinos produced in starburst Galaxies [5] with the experimental results of the through-going muons neutrino analyses. All the components of the neutrino flux have been obtained for every flavour, which clearly showed why prompt neutrinos cannot be detected in ν_μ-rich datasets. The cascade dataset has been considered as a better option to detect prompt neutrinos: in order to assess this, the yearly rates of shower-like events due to the various components of the neutrino spectrum have been computed. It resulted that the event rate due to prompt neutrinos is about 3% of that due to conventional ones in the cascade dataset between 1 TeV and 10 PeV. However, the prompt signal may be extracted using a higher energy threshold and discarding horizontal cascades, so as to reduce the contribution due to conventional neutrino. It was also found that prompt

neutrinos can contribute to the discrepancy of the IceCube results from different datasets.

Lastly, we proposed a clearer and simpler formulation of the luminosity constraint. We generalised it, allowing for the accumulation of other elements than ^{4}He, in particular ^{3}He and ^{14}N, which are the "bottlenecks" respectively of the *pp*-chain and of the CNO cycle. With the new, very precise value of the solar luminosity in photons we assessed that the contribution to the luminosity constraint of these out-of-equilibrium nuclear species is sizable, and so is the impact of the variation of the solar gravitational potential due to the expansion of the Sun. We thus obtained a more general and more powerful luminosity constraint, and showed how strictly it links the fluxes of *pp* and CNO neutrinos. This is particularly relevant for detectors like Borexino, which already measure *pp* neutrinos and have the potential to detect CNO neutrinos, and for a determination of the metallicity of the Sun, as it is directly connected to the flux of CNO neutrinos.

Summary of my PhD activity My PhD work resulted in the following publications:

1. *On the compatibility of the IceCube results with a universal neutrino spectrum*, with A. Palladino and F. Vissani, EPJC, 77:684 (2017), DOI: 10.1140/epjc/s10052-017-5273-z;

2. *The importance of observing astrophysical tau neutrinos*, with A. Palladino and F. Vissani, JCAP, **2018** (2018), DOI: 10.1088/1475-7516/2018/08/004;

3. *Introduction to neutrino astronomy*, with A. Gallo Rosso, A. Palladino and F. Vissani, EPJ Plus, 133:267 (2018), DOI: 10.1140/epjp/i2018-12143-6;

4. *Atmospheric neutrinos and the knee of the cosmic ray spectrum*, with P. Blasi and C. Evoli, Astroparticle Physics, **114** (2020) 22-29, DOI: 10.1016/j.astropartphys.2019.06.002;

5. *On the relevance of prompt neutrinos for the interpretation of the IceCube signals*, with F. Vissani, JCAP, **2019** (2019), DOI: 10.1088/1475-7516/2019/08/004;

6. *Exploring the assumption of hadron-hadron collisions for high energy neutrino production*, with F. Vissani, PoS (ICRC2019) 959 358.

There is another article, which is yet to be submitted, on which I worked in collaborations with Francesco Vissani, Diego Vescovi, Oscar Straniero, and Luciano Piersanti. It is about the update of the luminosity constraint, and is contained in §2.3.

I presented my work to the scientific community on the following occasions:

1. *Perspectives in Astroparticle physics from High Energy Neutrinos*, 25-26 September 2017, Napoli. Poster: *Cosmic neutrino oscillations and τ neutrinos in IceCube*;

2. *The High Energy Universe: Gamma Ray, Neutrino, and Cosmic Ray Astronomy*, 12-23 March 2018, Munich. Talk: *Neutrino oscillations and astrophysical tau neutrinos*;

3. the 36^{th} International Cosmic Ray Conference, July 24 - August 1 2019, Madison, USA. Talk: *Exploring the assumption of hadron-hadron collisions for high-energy neutrino production*;

4. *Heavy-Quark Hadroproduction from Collider to Astroparticle Physics*, 6-12 September 2019, Mainz. Talk: *Detecting prompt neutrinos at neutrino telescopes: theoretical predictions and experimental data*;

and attended the following schools/conferences:

- *Cross sections for Cosmic Rays*, 29-31 March 2017, CERN;
- *International School of Space Science*, 12-16 June 2017, L'Aquila;
- *Cosmic Ray Transport and Energetic Radiations*, May 28 - June 1 2018, L'Aquila;
- DIAS Summer School in High-Energy Astrophysics, 19-29 June 2018, Dublin.

Contents

Neutrinos alone, among all the known particles,
have ethereal properties that are striking and romantic
enough both to have inspired a poem by John Updike
and to have sent teams of scientists deep underground
for 50 years to build huge science-fiction-like contraptions
to unravel their mysteries.
Laurence M. Krauss

Alle mie nonne,
Bianca e Paola.
Le parole
non basteranno mai
per esprimere
ciò che siete state,
fortunatamente
vivete ancora
dentro di noi.

1

Introduction

Neutrino physics is largely an art
of learning a great deal
by observing nothing.
Haim Harari

In this chapter we introduce neutrinos mainly from the particle physics perspective: in section 1.1 we briefly overviews the history of this particle, from its theorization to the latest experimental results, while section 1.2 is a review on neutrinos both in the Standard Model (SM) of Elementary Particles and out of it. Finally, in section 1.3 we will cover the mechanisms that can produce these particles.

The original work on the update of the oscillation/survival probabilities, presented in §1.2.3, has been used in [1, 2, 4].

1.1 A brief history of the neutrino

With this section we aim at briefly overviewing the steps that neutrino physics has taken, from theorization to the latest experimental results; for a more in-depth review, we suggest consulting [6] and references therein.

In 1930 Wolfgang Pauli proposed the existence of a 1/2-spin particle with

zero charge and almost zero mass as a desperate remedy to the apparent non-conservation of energy in β decays of radioactive nuclei [7]. It is interesting to note that such proposal was considered back then as "something very bad", since "proposing a particle that cannot be detected" "is something no theorist should ever do". It is also worth mentioning that another solution, proposed by Niels Bohr, to the same problem, i.e. the continuity of the β energy spectrum, was the violation of the principle of energy conservation.

In 1932 Chadwick discovered the existence of the neutron, which is a neutral particle with 1/2 spin, but way too massive to be Pauli's particle. Just two years later, in 1934, Enrico Fermi formulated a quantitative theory of nuclear decays [8], a prototype of today's theory of weak interactions (or, rather, its low-energy limit), and named Pauli's particle "neutrino", so as to distinguish it from Chadwick's neutron [9].

In 1956 Reines and Cowan, inspired by Bruno Pontecorvo, detected antineutrinos produced in the decay of radioactive substances in nuclear reactors [10]. Reines was awarded the Nobel prize just after 40 years, when Cowan had, sadly, already passed away.

Between 1957 and 1967 Bruno Pontecorvo formulated the theory of neutrino oscillations; the idea of neutrino mixing has been first introduced by Maki, Nakagawa and Sakata. After five years, at Brookhaven, it was shown that there are at least two species of neutrinos; Lederman, Schwartz and Steinberger observed that neutrinos from the decay of pions and muons interact with matter differently from those produced in β decays.

In 1968, Ray Davis, in collaboration with John Bahcall and others, detected neutrinos produced in the thermonuclear reactions in the Sun with the Homestake mine experiment [11] - only in amounts incompatibly smaller than predicted by Bahcall' Standard Solar Model (SSM): the so-called solar neutrino problem was born. Only thirty years later the Super-Kamiokande collaboration presented atmospheric neutrino measurements which suggested that nothing was wrong with Davis' experiment or Bahcall's predictions, as neutrino do change flavour on their way to Earth, and the Homestake experiment was sensitive to only one flavour. The final word on the solar neutrino problem arrived only in 2001, when the experiment at the Sudbury Neutrino Observatory (SNO), sensitive to all neutrino flavours, confirmed the original predictions by Bahcall [12, 13].

In the same year, the DONUT collaboration reported the detection of ν_τ, the

third type of neutrinos [14], which had been predicted almost thirty years before, after the discovery of the τ lepton at the Stanford Linear Accelerator (SLAC).

In 1987 Kamiokande II, IBM and Baksan (also the Mont Blanc liquid scintillator, but this is generally considered as a spurious measurement) detected bursts of events compatible with the neutrino emission from the explosion of a type-II Supernova; see [15] for a review and [16] for a discussion on these measurements. This remains the one and only case of detection of neutrinos from a Supernova.

In 2013 the IceCube collaboration announced the discovery of an extra-galactic flux of neutrinos [17], and, in 2018, they reported the coincident observation of a neutrino with the flaring of a known blazar, TXS 0506+056 [18]. This is the first hint at a source of cosmic rays.

1.2 Neutrinos in (and out of) the Standard Model

In this section we review the treatment of neutrinos both as an element of the Standard Model of elementary particles and as an outsider: neutrino oscillations are, in fact, one of the few solid and clear evidences of physics beyond the Standard Model (BSM).

In 1.2.1 we will review then the SM Lagrangian, focussing on its electro-weak part, which contains neutrinos; we will also cover how the mass of neutrinos can be added to the SM Lagrangian with the Dirac and Majorana approach.

Neutrino oscillations in vacuum and in matter will be introduced in 1.2.2.

Finally, in 1.2.3, we will present our contribution to the determination of the oscillation and survival probabilities of cosmic neutrinos.

1.2.1 Standard Model neutrinos

The Standard Model (SM) of elementary particles is the model that, at present, best describes the phenomena occurring at the smallest scales accessible to us via particle accelerators. The elementary processes among these particles are coded in a Lagrangian density, in which bosons and fermions appear as quantum fields subject to peculiar group properties. This formulation is the result of decades of efforts, both theoretical and experimental, in which the forces have been shown to follow local symmetries, which are called "gauge" symmetries. A complete

overview of the SM Lagrangian is, of course, way beyond the scope of this thesis, so that we will refer the interested reader to benchmark works such as [19, 20, 21].

Let us face directly the SM Lagrangian:

$$\mathcal{L} = -\frac{1}{4}F_{\mu\nu}F^{\mu\nu} + i\overline{\psi}\not{D}\psi + \psi_i y_{ij}\psi_j\phi + |D_\mu\phi|^2 - V(\phi) + \text{h.c.} \tag{1.1}$$

This is a very compact expression for the whole SM Lagrangian before the symmetry breaking gives mass to the particles: we are interested in a more transparent one (in which masses are present) for the electro-weak part. After symmetry breaking, the fermion section of the electro-weak Lagrangian reads:

$$\begin{aligned}\mathcal{L}_{\text{EW,F}} = &\sum_i \overline{\psi}_i \left[i\not{\partial} - m_i(1 - H/v)\right] \psi_i \\ &- \frac{g}{2\sqrt{2}} \sum_i \overline{\psi}_i \gamma^\mu (1-\gamma^5)(T^+ W_\mu^+ + T^- W_\mu^-)\psi_i \\ &- e\sum_i Q_i \overline{\psi}_i \gamma^\mu \psi_i A_\mu - \frac{g}{2\cos\theta_W}\sum \overline{\psi}_i \gamma^\mu (g_V^i - g_A^i \gamma^5)\psi_i Z_\mu\end{aligned} \tag{1.2}$$

The index i labels the SU(2) fermion fields, i.e.:

$$\psi_i = \begin{cases} \begin{pmatrix}\nu_i \\ \ell_i^-\end{pmatrix} & \text{for leptons} \\ \begin{pmatrix}u_i \\ d_i'\end{pmatrix} & \text{for quarks}\end{cases}$$

where $d_i' = V_{ij}d_j$, and V is the Cabibbo-Kobayashi-Maskawa mixing matrix. In Eq. (1.2) we can more clearly see:

- a kinetic term, and a mass term, in which the strength of the coupling to the Higgs boson H is proportional to the mass of the particles (first line);
- the interaction term with the charged $W^\pm$ bosons, in which we can notice the presence of the $(1-\gamma^5)$ projector, which causes only the left-handed fields to interact via charged weak currents (second line);

- the interaction term with the photon A_μ, which couples equally to left- and right-handed fields with eQ_i = charge of the field i as strength of the interaction (third line, first term);
- the interaction term with the Z^0, which couples unequally to left-handed and right-handed fields.

The basic neutrino interactions can be represented, at tree-level, by the following Feynman graphs:

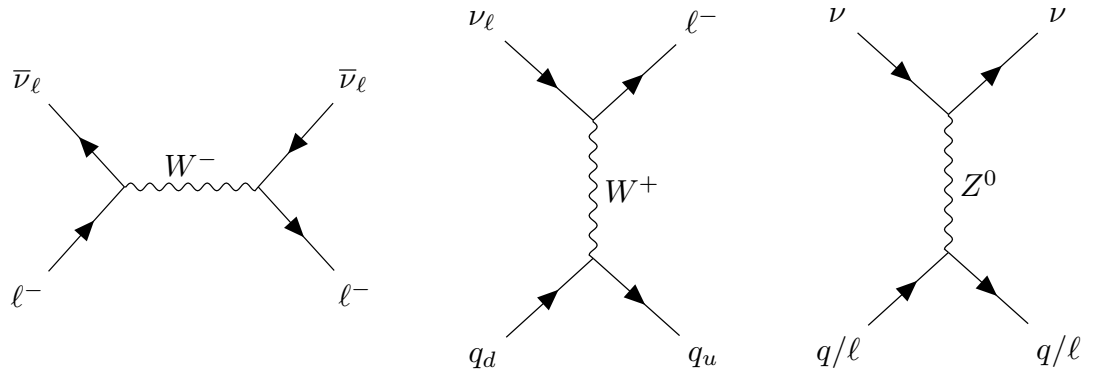

and by the graphs obtained by charge conjugation and "rotation" (from channel s to channel t and viceversa) of the graphs above.

To give a handle on the typical cross sections for neutrino experiments, let us consider neutrino - electron scattering with $\sqrt{s} \gg m_e$; for electron neutrinos, it can occur both in t-channel version of the leftmost and rightmost graphs, and has a total cross section of

$$\sigma(\nu_e + e^- \to \nu_e + e^-) \simeq \frac{G_F^2 s}{4\pi}\left[\left(1 + 2\sin^2\theta_W\right)^2 + \frac{4}{3}\sin^4\theta_W\right] \simeq 93\,\frac{s}{\mathrm{MeV}^2}\,10^{-46}\,\mathrm{cm}^2$$

The same scattering cross section for an electron antineutrino, a muon/tau neutrino and a muon/tau antineutrino would be about 42%[1], 16% and 14%, respectively, of $\sigma(\nu_e + e^- \to \nu_e + e^-)$. Electron antineutrinos, in fact, can interact

[1]Unless the center-of-mass energy approaches the W^- mass, $\sqrt{s} \approx m_W$, in which case the cross-section increases due to the resonance. This occurs for $E_{\overline{\nu}_e} \simeq 6.3\,\mathrm{PeV}$, and is referred to as *Glashow resonance*, which is clearly visible in Fig. 1.2.

with electrons with the leftmost and the rightmost graph, which is the only one available to muon and tau (anti)-neutrinos.

For ν_μ charged-current inclusive scattering cross sections (per nucleon), we have:

$$\sigma(\nu_\mu + N \to \mu^- + X) \simeq 0.7 \, \frac{E_\nu}{\mathrm{GeV}} \times 10^{-38} \, \mathrm{cm}^2$$

which is another interesting process for high-energy neutrino detection. These cross sections are very small compared to, say, that of an electromagnetic process like $\gamma + \gamma \to$ hadrons, which is around $10^{-28} \, \mathrm{cm}^2$ for $\sqrt{s} \in [1, 10^4] \, \mathrm{GeV}$.

The most peculiar trait of neutrinos is their mass, which is directly related to their oscillatory behaviour. Before the discovery of neutrino flavour oscillations, in fact, neutrinos were assumed to be massless; as we will see in the following, the fact that their flavour can change over time is related to a nonzero neutrino mass. This creates a distinction between the neutrino eigenstates of interaction, which are labelled by flavour, and of propagation (the free Hamiltonian), which are labelled by mass. A fermion mass term arises usually from the coupling of particles with nonzero hypercharge Y to the Higgs boson; since right-handed neutrinos do not have hypercharge, adding a mass term to the SM means extending the standard model. In order to clarify this point, let us look at the mass term for the leptons:

$$\mathcal{L}_{\mathrm{M,L}} = - \sum_{i,j=e,\mu,\tau} y^{\ell\prime}_{ij} \overline{\psi}'_{i,L} \phi \, \ell'_{j,R} + \mathrm{h.c.} \tag{1.3}$$

It is clear that such term can be written only if all the involved fields have nonzero hypercharge.

The mass of the neutrino is nowadays one of the most important mysteries in physics; the squared mass differences between the three[2] mass eigenstates are known, but only upper limits, at about 1 eV, on the absolute mass are available. Such a small value for the mass of the neutrinos is believed to be due to mechanisms like the *see-saw mechanism*, in which a new high-energy scale generates a suppression of the neutrino mass. An in depth coverage of the problem of the neutrino mass is beyond the scope of this thesis; the interested reader may find useful material in [22, 23] and references therein. Here we will present briefly the two common approaches to extend the SM Lagrangian with the addition of neutrino mass terms.

[2] There are at least three.

Dirac neutrinos In the Dirac approach to neutrino masses, the mass term in Eq. (1.3) is extended with the introduction of a right-handed neutrino:

$$\mathcal{L}_{\mathrm{M}_D,\mathrm{L}} = -\sum_{i,j=e,\mu,\tau} y^{\ell\prime}_{ij}\overline{\psi}'_{i,L}\phi\,\ell'_{j,R} - \sum_{i,j=e,\mu,\tau} y^{\nu\prime}_{ij}\overline{\psi}'_{i,L}\tilde{\phi}\,\nu'_{j,R} + \mathrm{h.c.} \tag{1.4}$$

The primed Yukawa matrices stand for the fact that neither y^{ℓ}_{ij} nor y^{ν}_{ij} are diagonal in the chosen, primed, bases; we can diagonalise them with the use of appropriate 3×3 unitary matrices:

$$\begin{cases} V_L^{\ell\dagger} y^{\ell\prime} V_R^{\ell} = y^{\ell} & y^{\ell}_{ij} = y^{\ell}_i \delta_{ij} \\ V_L^{\nu\dagger} y^{\nu\prime} V_R^{\nu} = y^{\nu} & y^{\nu}_{ij} = y^{\nu}_i \delta_{ij} \end{cases}$$

such that

$$n_{j,L} = V^{\nu\dagger}_{ij}\nu'_{i,L} \qquad n_{j,R} = V^{\nu\dagger}_{ij}\nu_{i,R}$$

The diagonalised form of Eq. (1.4) in the unitary gauge reads:

$$\mathcal{L}_{\mathrm{M}_L,\mathrm{F}} = -\left(\frac{v+H}{\sqrt{2}}\right)\left[\sum_{i=e,\mu,\tau} y^{\ell}_i\,\overline{\ell}_{i,L}\ell_{i,R} + \sum_{i=1}^{3} y^{\nu}_i\,\overline{n}_{i,L}n_{i,R}\right] + \mathrm{h.c.} \tag{1.5}$$

from which we can see that the neutrino masses are given by:

$$m_{\nu_i} = \frac{v y^{\nu}_i}{\sqrt{2}} \tag{1.6}$$

i.e. they are proportional to the Higgs vacuum expectation value (vev) v, just like the masses of charged leptons and quarks. As in the case of the Higgs mechanism for these particles, such formulation for the neutrino masses leaves open the question of their origin and value.

The interaction term between charged leptons and neutrinos will look like:

$$j^{\mu}_{W,L} = 2\overline{\boldsymbol{\nu}}'_L\gamma^{\mu}\boldsymbol{\ell}'_L = 2\overline{\boldsymbol{n}}_L V_L^{\nu\dagger}\gamma^{\mu}V_L^{\ell}\boldsymbol{\ell}_L$$

which, with the introduction of the neutrino mixing matrix (which will be the subject of discussion in the following):

$$U = V_L^{\ell\dagger}V_L^{\nu} \tag{1.7}$$

becomes:

$$j^{\mu}_{W,L} = 2\overline{\boldsymbol{n}}_L U^{\dagger}\gamma^{\mu}\boldsymbol{\ell}_L \tag{1.8}$$

Usually U is represented as the product of three rotation matrices with up to three CP-violating phases:

$$U = \begin{pmatrix} 1 & 0 & 0 \\ 0 & c_{23} & s_{23} \\ 0 & -s_{23} & c_{23} \end{pmatrix} \begin{pmatrix} c_{13} & 0 & s_{13}e^{-i\delta} \\ 0 & 1 & 0 \\ -s_{13}e^{i\delta} & c_{13} & 0 \end{pmatrix} \begin{pmatrix} c_{12} & s_{12} & 0 \\ -s_{12} & c_{12} & 0 \\ 0 & 0 & 1 \end{pmatrix} \tag{1.9}$$

where δ is the Dirac CP-violating phase and $s_{ij} = \sin\theta_{ij}$ and $c_{ij} = \cos\theta_{ij}$. If neutrinos are Majorana particles, there is an additional diagonal matrix with two Majorana CP-violating phases. It is customary to introduce the left-handed flavour neutrino fields $\boldsymbol{\nu}_L$ as:

$$\boldsymbol{\nu}_L = U\boldsymbol{n}_L = V^{\ell\dagger}_L \boldsymbol{\nu}'_L \tag{1.10}$$

so that Eq. (1.8) becomes:

$$j^{\mu}_{W,L} = 2\overline{\boldsymbol{\nu}}_L\gamma^{\mu}\boldsymbol{\ell}_L = 2\sum_{i=e,\mu,\tau} \overline{\nu}_{i,L}\gamma^{\mu}\ell_{i,L} \tag{1.11}$$

It is interesting to immediately see the non-conservation of single-flavour lepton number. In fact, given the definition of mixing matrix as in Eq. (1.10), the mass terms of the Lagrangian in Eq. (1.5) becomes:

$$\mathcal{L}_{\mathrm{M}_D,\mathrm{L}} = -\left(\frac{v+H}{\sqrt{2}}\right)\sum_{i=e,\mu,\tau}\left[y^{\ell}_i\overline{\ell}_{i,L}\ell_{i,R} + \overline{\nu}_{i,L}\sum_{k=1}^{3}U_{ik}y^{\nu}_k\nu_{k,R}\right] + \text{h.c.} \tag{1.12}$$

The kinetic term, instead, looks like:

$$\mathcal{L}_{\text{kin.}} = \sum_{k=1}^{3}\overline{\nu}_k\, i\partial\!\!\!/\,\nu_k = \sum_{i=e,\mu,\tau}\overline{\nu}_{i,L}\, i\partial\!\!\!/\,\nu_{i,R} + \sum_{k=1}^{3}\overline{\nu}_{k,R}\, i\partial\!\!\!/\,\nu_{k,R} \tag{1.13}$$

We can see now that:

- the weak charged-current in Eq. (1.11) is invariant under

  $$\ell_{j,L} \to e^{i\varphi_j}\ell_{j,L} \qquad \nu_{j_L} \to e^{i\varphi_j}\nu_{j,L}$$

  for $j = e, \mu, \tau$ and $\varphi_j \neq \varphi_k$ with $j \neq k$;

- the charged lepton terms in Eq. (1.12) are invariant under the above transformation of the left-handed ℓ fields if

$$\ell_{j,R} \to e^{i\varphi_j} \ell_{j,R}$$

- it is impossible to find any transformation of the $\nu_{k,R}$ fields that leaves invariant the neutrino mass term in Eq. (1.12) and Eq. (1.13), unless 1) all y^{ν}_{k} are equal or 2) $U = \mathrm{diag}(1,1,1)$ - i.e. there is no mixing.

Even though the single-flavour lepton number is not conserved, the total lepton number is; both the Yukawa and the kinetic parts of the Lagrangian are in fact invariant under the global U(1) transformation

$$\Psi_{x,L/R} \to e^{i\varphi} \Psi_{x,L/R}$$

where $\Psi = \ell, \nu$, $x = 1,2,3$ or $x = e, \mu, \tau$.

Majorana neutrinos Ettore Majorana, in 1937 [24], discovered that a four-component spinor is not necessary for the description of a massive particle. In fact, Dirac's equation:

$$(i\partial\!\!\!/ - m)\psi = 0 \tag{1.14}$$

for the chiral components reads:

$$\begin{cases} i\partial\!\!\!/ \psi_R = m\psi_L \\ i\partial\!\!\!/ \psi_L = m\psi_R \end{cases} \tag{1.15}$$

Taking the hermitian conjugate on the second line of Eq. (1.15) and multiplying on the right by γ^0, we have:

$$-i\partial_\mu \overline{\psi}_R \gamma^\mu = m\overline{\psi}_L \tag{1.16}$$

Now we can manipulate it so as to recover a form like that in Eq. (1.15): transposing Eq. (1.16) and multiplying it on the left with the charge conjugation matrix C we have:

$$i\partial\!\!\!/ C\overline{\psi}^T_R = mC\overline{\psi}^T_L \tag{1.17}$$

Setting now:

$$\psi_R = \xi C\overline{\psi}_L^T \tag{1.18}$$

where ξ is an arbitrary phase factor, i.e. $|\xi|^2 = 1$, which will be "rephased away", we obtain:

$$i\partial\!\!\!/\psi_L = m\xi C\overline{\psi}_L^T \tag{1.19}$$

The rephasing that leads us to Majorana's equation (1.20) is $\psi_L \to \xi^{1/2}\psi_L$:

$$i\partial\!\!\!/\psi_L = mC\overline{\psi}_L^T \tag{1.20}$$

The field ψ now has the property that:

$$\psi = \psi_L + \psi_R = \psi_L + C\overline{\psi}_L^T \implies \psi = C\overline{\psi}^T$$

Since neutrinos do not interact electromagnetically, their charge parity can be chosen arbitrarily, as it does not hold physical meaning. For simplicity, we can choose it equal to 1, so that, for neutrinos:

$$\psi_L^C := C\psi_L^T \implies \psi = \psi_L + \psi_L^C$$

This means that:

$$\psi = \psi^C \tag{1.21}$$

which can be written only for neutral fermions, for the same argument we just made for the charge parity of neutrinos.

Since in Majorana's formulation the spinors of neutral fermions have just two independent components, rather than four as in Dirac's formulation, one may consider it more natural, as it is simpler - which is why neutrinos are Majorana particles in most theories beyond the Standard Model. If neutrinos were massless, however, the two formulations would be completely equivalent: for massless particles, in fact, Dirac's equation (1.15) would decouple for the two chiral components, and the right-handed component would be irrelevant in both descriptions. It follows that the nature of the neutrino can be understood from some effect due to the neutrino mass - otherwise the massless theory works well; so far these tentatives consist in looking for the so-called "neutrinoless double beta decay", i.e. two simultaneous beta decays in which the neutrinos annihilate with one another.

A complete treatment of the quantisation of Majorana fields is beyond the scope of this thesis. We will now see the mass term in the Lagrangian for the simple case of one Majorana neutrino type ν:

$$\mathcal{L}_{M_{\mathrm{M}}} = -\frac{1}{2} m \overline{\nu}_L^C \nu_L + \mathrm{h.c.} \tag{1.22}$$

where $\nu_L^C = C\overline{\nu}_L^T$ is a right-handed function of ν_L which transforms as ν_L under Lorentz transformations. The full Majorana Lagrangian looks like:

$$\mathcal{L}_{\mathrm{M}} = \frac{1}{2}\left[\overline{\nu}_L \, i\partial\!\!\!/ \nu_L + \overline{\nu}_L^C \, i\partial\!\!\!/ \nu_L^C - m\left(\overline{\nu}_L^C \nu_L + \overline{\nu}_L \nu_L^C\right)\right] \tag{1.23}$$

where the 1/2, as in Eq. (1.22) avoids double counting due to relation between ν_L^C and $\overline{\nu}_L$.

Since in the Majorana case neutrinos and antineutrinos are the same object, the can be no conservation of leptonic number. However, it is possible to use an effective approach to assign a total lepton number which is conserved in all processes insensitive to the neutrino mass.

The Majorana mixing matrix has two more phases with respect to the one in Dirac's formulation: this is due to the fact that the Majorana mass Lagrangian is not invariant with respect to global U(1) gauge transformations

$$\nu_{k,L} \to e^{i\varphi_k} \nu_{k,L}$$

so that there is less freedom on the entries of the neutrino mixing matrix U. Therefore, the unitary 3×3 mixing matrix of Majorana neutrinos depends on three mixing angles and three physical CP-violating phases, rather than three mixing angles and one CP-violating phase, and is usually represented as the product of the Dirac mixing matrix times a diagonal unitary matrix with two independent Majorana phases:

$$U = U_D \begin{pmatrix} 1 & 0 & 0 \\ 0 & e^{i\lambda} & 0 \\ 0 & 0 & e^{i\theta} \end{pmatrix} \tag{1.24}$$

Now we will briefly cover flavour mixing in the Majorana formalism; with three generations of massive neutrinos, we will construct the Majorana mass term as

$$\mathcal{L}_{M_{\mathrm{M}}} = \frac{1}{2} \boldsymbol{\nu}_L'^T C^\dagger M_L \boldsymbol{\nu}_L' + \mathrm{h.c.} = \frac{1}{2} \sum_{i,j=e,\mu,\tau} \nu_{i,L}'^T C^\dagger M_{ij,L} \nu_{j,L}' + \mathrm{h.c.}$$

As in the case of Dirac neutrinos, the massive neutrino fields are the eigenstates of the mass matrix, which can be shown to be symmetric, so that there is a unitary V_L^ν such that:

$$(V_L^\nu)^T M_L V_L^\nu = M \qquad M_{ij} = m_i \delta_{ij}$$

The eigenstates of the mass matrix will once more be:

$$\boldsymbol{n}_L = V_L^{\nu\dagger} \boldsymbol{\nu}'_L$$

so that the mass term in the Majorana Lagrangian will look like:

$$\mathcal{L}_{M_\mathrm{M}} = -\frac{1}{2} \sum_{k=1}^{3} m_k \overline{\nu}_{k,L}^C \nu_{k,L} + \mathrm{h.c.}$$

and the three-generation Majorana Lagrangian will be:

$$\mathcal{L}_\mathrm{M} = \frac{1}{2} \overline{\boldsymbol{n}} \left(i \partial\!\!\!/ - M \right) \boldsymbol{n} \tag{1.25}$$

where $\boldsymbol{n} = \boldsymbol{n}_L + \boldsymbol{n}_L^C$. The interacting part of the Majorana Lagrangian is, as it must be, the same as the one in Dirac's treatment seen in Eq. (1.7) and the following ones.

1.2.2 Neutrino oscillations

Neutrino oscillations were suggested by Pontecorvo in the late 1950s when only one type of neutrino was supposed to exist. He introduced an additional, sterile, neutrino, which could oscillate into the active one in analogy to the $K^0 - \overline{K}^0$ oscillation. Since the discovery of the muon neutrino, it was clear that active neutrinos could oscillate into each other if they had different masses: a review by Bilenky and Pontecorvo, published in 1978, is [25]. So far, neutrino oscillations provide the clearest and best understood piece of evidence for physics Beyond the Standard Model (BSM).

In the following we will overview the standard derivation of neutrino oscillations in vacuum, and discuss what changes and how when neutrino oscillate through matter.

Oscillations in vacuum In the standard picture, neutrinos are produced with the corresponding antilepton or after the decay (or interaction) of the corresponding lepton. From Eq. (1.10) and the hypothesis that neutrinos are ultrarelativistic [26] follows that:

$$|\nu_\ell\rangle = \sum_k U^*_{\ell k} |\nu_k\rangle \tag{1.26}$$

in which the number of massive neutrinos is not limited; it must be larger or equal to the number of active neutrinos, i.e. ≥ 3. If additional neutrinos are present in the flavour basis, they must be sterile, and their existence can be proven only by the disappearance of active neutrinos.

Massive neutrinos are eigenstates of the Hamiltonian $\mathcal{H}$, so that:

$$|\nu_k(t)\rangle = e^{-iE_k t} |\nu_k\rangle \tag{1.27}$$

so that

$$|\nu_\ell(t)\rangle = \sum_k U^*_{\ell k} e^{-iE_k t} |\nu_k\rangle \tag{1.28}$$

The probability amplitude for the oscillation of the neutrino ℓ into the neutrino ℓ' is given by:

$$\mathcal{A}_{\ell\ell'}(t) := \langle \nu_{\ell'}(t) | \nu_\ell \rangle = \sum_k U_{\ell' k} U^*_{\ell k} e^{-iE_k t} \tag{1.29}$$

The transition probability is the square modulus of the equation above:

$$P_{\ell\ell'}(t) = |\mathcal{A}_{\ell\ell'}(t)|^2 = \sum_{k,j} U^*_{\ell' j} U_{\ell j} U_{\ell' k} U^*_{\ell k} e^{-i(E_k - E_j)t} \tag{1.30}$$

Neutrinos have been measured only in the ultrarelativistic regime, so that:

$$E_k \simeq E + \frac{m_k^2}{2E} \implies E_k - E_j = \frac{\Delta m^2_{kj}}{2E}$$

where Δm^2_{jk} is the squared mass difference:

$$\Delta m^2_{kj} = m^2_k - m^2_j \tag{1.31}$$

and $E = |\mathbf{p}|$ is the neutrino energy without the contribution from mass. The transition probability then becomes, using $t \approx L$ ($c = 1$):

$$P_{\ell\ell'}(L, E) = \sum_{k,j} U^*_{\ell' j} U_{\ell j} U_{\ell' k} U^*_{\ell k} \exp\left(-i \frac{\Delta m^2_{kj} L}{2E}\right) \tag{1.32}$$

L is the distance between the source of neutrinos and the detector, and, along with the neutrino energy E, is the experiment-related quantity on which the oscillation phases depend:

$$\Phi_{kj} = -\frac{\Delta m^2_{kj} L}{2E} \tag{1.33}$$

Of course the Δm^2_{kj} are physical constants, as well as the entries of U, which determine the amplitude of the oscillations.

It can be shown that the quartic products

$$U^*_{\ell' j} U_{\ell j} U_{\ell' k} U^*_{\ell k}$$

do not vary upon rephasing of the lepton and neutrino fields; this means that the Majorana nature of neutrinos cannot be determined with oscillation experiments, as these would be intrinsically blind to the Majorana phases. It can be shown that CP and T violations in neutrino oscillations depend only on the Dirac phase.

It is useful to write the oscillation probability of Eq. (1.32) as follows:

$$P_{\ell\ell'}(L, E) = \sum_k |U_{\ell k}|^2 |U_{\ell' k}|^2 + 2\,\mathrm{Re} \sum_{k>j} U^*_{\ell' j} U_{\ell j} U_{\ell' k} U^*_{\ell k} \exp\left(-2\pi i \frac{L}{L^{\mathrm{osc}}_{kj}}\right) \tag{1.34}$$

where a constant term has been extracted from the oscillating one and the oscillation length has been introduced as:

$$L^{\mathrm{osc}}_{kj} = \frac{4\pi E}{\Delta m^2_{kj}} \tag{1.35}$$

An interesting case for cosmic neutrinos is when neutrinos cover cosmic distances, or simply $L \gg L^{\mathrm{osc}}_{kj}$, so that we would have:

$$P_{\ell\ell'}(E, L) \to P_{\ell\ell'} = \sum_k |U_{\ell k}|^2 |U_{\ell' k}|^2 \tag{1.36}$$

Observing that $P_{\ell\ell'} = P_{\ell'\ell}$ reduces the degrees of freedom of the oscillation probability matrix $P_{\ell\ell'}$ from four:

$$\begin{cases} \sum_{\ell} P_{\ell\ell'} = 1 \\ \sum_{\ell'} P_{\ell\ell'} = 1 \end{cases} \implies P_{\ell\ell'} = \begin{pmatrix} x & y & 1-x-y \\ z & t & 1-z-t \\ 1-x-z & 1-y-t & x+y+z+t-1 \end{pmatrix}$$

with $0 \leq x, y, z, t \leq 1$ to three:

$$P_{\ell\ell'} = \begin{pmatrix} x & y & 1-x-y \\ y & t & 1-y-t \\ 1-x-y & 1-y-t & x+2y+t-1 \end{pmatrix}$$

This observation has been the starting point for [27], on which the update of the cosmic neutrino oscillation probabilities, described in 1.2.3, is based. This update has been used in [1, 4].

It can be shown that the maximum value for $P_{\ell\ell'}$, with $\ell \neq \ell'$, as well as the minimum value of $P_{\ell\ell}$ is $1/n$, where n is the number of massive neutrinos.

The matter effect Neutrinos propagating through matter are subject to a potential due to the scattering with the electrons and nucleons in the medium, which, in some cases, can cause the mixing angles in matter to become large, even if the mixing angles in vacuum is small. This was first discovered by Wolfenstein in 1978 [28], and later expanded by Mikheev and Smirnov, who discovered that there could be resonant flavour transitions in the case of media with varying density [29]; this is the so-called MSW mechanism. Also in this case we aim at collecting the fundamental results, which are particularly relevant for Solar neutrinos.

The propagation of the active neutrinos is affected by the presence of matter; since all neutrinos interact with ordinary matter via the Z^0 boson, we expect charged weak interactions to make a difference. These are effectively sensitive to the presence of electrons, and, in fact, it can be shown that the charged-current potential that neutrinos feel in matter is

$$V_{\mathrm{CC}} = \sqrt{2} G_{\mathrm{F}} N_e \tag{1.37}$$

where $G_{\rm F}$ is the Fermi constant and N_e is the local density of electrons. The total potential energy that left-handed neutrinos are subject to traversing matter is:

$$V_\ell = V_{\rm CC}\delta_{\ell e} + V_{\rm NC} = \sqrt{2}G_{\rm F}\left(N_e\delta_{\ell e} - \frac{1}{2}N_n\right) \tag{1.38}$$

where N_n is the local density of neutrons[3]. As one could expect, there is no difference between Dirac and Majorana neutrinos when calculating the matter effect on their way through media.

The evolution of neutrino flavours is quite simple:

$$i\frac{\mathrm{d}}{\mathrm{d}t}\left|\nu_\ell(t)\right\rangle = \mathcal{H}\left|\nu_\ell(t)\right\rangle \tag{1.39}$$

with

$$\mathcal{H}\left|\nu_\ell\right\rangle = \mathcal{H}_0\left|\nu_\ell\right\rangle + V_\ell\left|\nu_\ell\right\rangle$$

Eq. (1.39) can be written introducing $\psi_{\ell\ell'}(x) := \langle\nu_{\ell'}|\nu_\ell(x)\rangle$ $(x \approx t)$:

$$i\frac{\mathrm{d}}{\mathrm{d}x}\psi_{\ell\ell'}(x) = \sum_{\ell''}\left(\sum_k U_{\ell' k}\frac{\Delta m^2_{k1}}{2E}U^*_{\ell'' k} + \delta_{\ell' e}\delta_{\ell'' e}V_{\ell'}\right)\psi_{\ell\ell''}(x) \tag{1.40}$$

in which the contributions equal for all flavours, including those of neutral currents, have been neglected as they generate a common phase. Once more, neutrino oscillations depend on the squared mass differences.

To proceed, we consider the case of two-neutrino mixing, which is physically relevant as ν_μ and ν_τ suffer the same matter potential. Let us then consider $\nu_e - \nu_\mu$ mixing, with $|\nu_\ell(0)\rangle = |\nu_e\rangle$, as for Solar neutrinos. Eq. (1.40) can be diagonalized with a unitary matrix:

$$U_M = \begin{pmatrix} \cos\theta_{\rm M} & \sin\theta_{\rm M} \\ -\sin\theta_{\rm M} & \cos\theta_{\rm M} \end{pmatrix} \tag{1.41}$$

where

$$\tan 2\theta_{\rm M} = \frac{\tan 2\theta}{1 - \dfrac{2\sqrt{2}EG_{\rm F}N_e}{\Delta m^2\cos 2\theta}} \tag{1.42}$$

[3]The neutral-current contributions of protons and electrons cancel out due to opposite charge - we assume overall charge neutrality of the environment.

and θ is the two-neutrino mixing angle in vacuum. The diagonalized effective Hamiltonian in Eq. (1.40) reads:

$$\mathcal{H}_{\text{eff}} = \frac{1}{4E}\begin{pmatrix} -\Delta m^2_{\text{M}} & 0 \\ 0 & \Delta m^2_{\text{M}} \end{pmatrix} \tag{1.43}$$

From Eq. (1.42) it is clear that the mixing angle in matter can become maximal, i.e. $\theta_{\text{M}} = \pi/4$, when the resonance condition:

$$N_e|_{\text{R}} = \frac{\Delta m^2 \cos 2\theta}{2\sqrt{2}EG_{\text{F}}} \tag{1.44}$$

is fulfilled. This can lead to total transitions between the two flavours if the resonance region is wide enough, and this is the MSW effect. At the resonance, the effective squared mass difference in Eq. (1.43)

$$\Delta m^2_{\text{M}} = \sqrt{(\Delta m^2 \cos 2\theta - 2\sqrt{2}EG_{\text{F}}N_e)^2 + (\Delta m^2 \sin 2\theta)^2)} \tag{1.45}$$

has its minimum value

$$\Delta m^2\big|_{\text{R}} = \Delta m^2 \sin 2\theta \tag{1.46}$$

With definitions Eqs. (1.42) and (1.45), the evolution equation (1.40) can be written more transparently as:

$$i\frac{\text{d}}{\text{d}x}\begin{pmatrix} \psi_{ee} \\ \psi_{e\mu} \end{pmatrix} = \frac{1}{4E}\begin{pmatrix} -\Delta m^2_{\text{M}} \cos 2\theta_{\text{M}} & \Delta m^2_{\text{M}} \sin 2\theta_{\text{M}} \\ \Delta m^2_{\text{M}} \sin 2\theta_{\text{M}} & \Delta m^2_{\text{M}} \cos 2\theta_{\text{M}} \end{pmatrix}\begin{pmatrix} \psi_{ee} \\ \psi_{e\mu} \end{pmatrix} \tag{1.47}$$

With the diagonalization Eq. (1.41), Eq. (1.47) becomes:

$$i\frac{\text{d}}{\text{d}x}\begin{pmatrix} \phi_{e1} \\ \phi_{e2} \end{pmatrix} = \begin{pmatrix} -\Delta m^2_{\text{M}}/4E & -i\text{d}\theta_{\text{M}}/\text{d}x \\ i\text{d}\theta_{\text{M}}/\text{d}x & \Delta m^2_{\text{M}}/4E \end{pmatrix}\begin{pmatrix} \phi_{e1} \\ \phi_{e2} \end{pmatrix} \tag{1.48}$$

where the off-diagonal terms proportional to $\text{d}\theta_{\text{M}}/\text{d}x$ come from:

$$\Psi = U_{\text{M}}\Phi \implies \frac{\text{d}}{\text{d}x}\Psi = \frac{\text{d}U_{\text{M}}}{\text{d}x}\Phi + U_{\text{M}}\frac{\text{d}\Phi}{\text{d}x}$$

Since we have that:

$$\frac{\text{d}\theta_{\text{M}}}{\text{d}x} = \sqrt{2}EG_{\text{F}}\frac{\sin 2\theta_{\text{M}}}{\Delta m^2_{\text{M}}}\frac{\text{d}N_e}{\text{d}x} \tag{1.49}$$

the effective massive neutrinos are decoupled if the matter density is constant; conversely, there can be transitions between ν_1^{M} and ν_2^{M}. Such transitions are negligible if the off-diagonal terms in Eq. (1.48) are much smaller than the difference between the diagonal terms; to quantify the impact of the off-diagonal terms, the adiabaticity parameter is introduced as

$$\gamma = \frac{\Delta m^2_{\mathrm{M}}}{4E|\mathrm{d}\theta_{\mathrm{M}}/\mathrm{d}x|} \tag{1.50}$$

For $\gamma \gg 1$, the evolution is adiabatic, meaning that no transition between the two effective massive states is expected.

The applications of this formalism are found both in supernova and solar neutrinos, for which the common set of assumptions includes:

- high density of the medium, above the resonance, at production;
- propagation through a medium of monotonously decreasing density;
- detection practically in vacuum, far away (with respect to L_{osc}) from the source.

If the resonance is crossed in a non-adiabatic regime, $\nu_1^{\mathrm{M}} \leftrightarrow \nu_2^{\mathrm{M}}$ transitions can occur. It can be shown that, if P_c is the probability of such transition to take place at the resonance, the average survival probability for electron neutrinos is:

$$\langle P_{ee} \rangle = \frac{1}{2} + \left(\frac{1}{2} - P_c \right) \cos 2\theta_{\mathrm{M}} \cos 2\theta \tag{1.51}$$

where θ_{M} is the mixing angle at the production point. Eq. (1.51) is known as Parke formula, and has been widely used in the analyses of solar neutrino data.

It is interesting to take the limit of very large density of the production site of the neutrino of Eq. (1.51); in fact, if $N_e \to \infty$, the effective mixing angle in matter Eq. (1.42) is such that $\cos 2\theta_{\mathrm{M}} \to -1$. This means that the ν_e is produced in a pure ν_2^{M} state, which propagates unaffected towards the resonance. At the resonance, the density variation is very rapid in the case of extremely small adiabaticity $\gamma_{\mathrm{R}} \ll 1$, so that no flavour conversion has time to occur; the neutrino emerges then from the resonance as ν_e, and from there onwards, the

effective mixing and oscillations are equal to the vacuum ones. This is why, in the extreme nonadiabatic limit, we can write:

$$\langle P_{ee} \rangle = \frac{1}{2} - \frac{1}{2} \sin^2 2\theta$$

which is exactly what one would obtain assuming neutrino propagation in vacuum.

For Solar neutrinos, the production site is usually identified with the solar core, with matter density of about $150\,\mathrm{g\,cm^{-3}}$ and electron density of about $100 N_A\,\mathrm{cm^{-3}}$; the density is then larger than the resonance density if $\Delta m^2 \cos 2\theta \lesssim 10^{-4}\,\mathrm{eV}^2$. In such case, neutrinos can undergo MSW resonant transitions on their way out of the Sun. As of today, there is strong evidence towards large mixing angle (LMA) in vacuum, and Δm^2 is large (about $10^{-4}\,\mathrm{eV}^2$, see table 1.1); in such case, the resonance crossing is always adiabatic, as the effective mass difference Δm^2_{M} at the resonance is large with respect to $\mathrm{d}\theta_{\mathrm{M}}/\mathrm{d}x$, so that $\gamma > 1$. In particular, for $E \lesssim 2\,\mathrm{MeV}$ there is no resonance and

$$\langle P_{ee} \rangle = \frac{1}{2} - \frac{1}{2} \sin^2 2\theta$$

For $E \gtrsim 2\,\mathrm{MeV}$ the resonance is crossed adiabatically and the Parke formula Eq. (1.51) holds. For $E \gg 2\,\mathrm{MeV}$ the Sun density is much larger than the resonance density, so that θ_{M} at production is very close to $\pi/2$ and the survival probability is independent of energy:

$$\langle P_{ee} \rangle \simeq \sin^2 \theta$$

1.2.3 Update of the cosmic neutrino oscillation/survival probabilities

In this section we update the description of cosmic neutrino oscillations proposed in [27]. This consists in the use of three "natural" parameters to describe the probabilities of oscillations of cosmic neutrinos. After a brief review of [27], we discuss our updating procedure, which is based on the latest results on the oscillation parameters [30]. This update has been used in the original works [1, 2, 4].

The average survival/oscillation probabilities in vacuum are given by Eq. (1.36):

$$P_{\ell\ell'} = \sum_{k=1}^{n} |U_{\ell k}|^2 |U_{\ell' k}|^2$$

where $\ell, \ell' = e, \mu, \tau$ denotes the neutrino flavour, and U is the neutrino mixing matrix from Eq. (1.7). The approach of Palladino and Vissani in [27] to compute the average survival/oscillation probabilities of cosmic neutrinos in vacuum is based on two simple considerations:

- the matrix $P_{\ell\ell'}$ is symmetric under the exchange of the flavour indices $\ell \leftrightarrow \ell'$
- the elements of the mixing matrix must obey the condition $\sum_\ell P_{\ell\ell'} = 1$

For these reasons, the number of independent parameter is $n(n-1)/2$, where n is the number of neutrinos. For $n = 3$ we have just 3 independent parameters, which we label as P_0, P_1 and P_2: we can then rewrite the $P_{\ell\ell'}$ matrix as:

$$P = \frac{\mathbb{I}}{3} + \begin{pmatrix} 2P_0 & -P_0 + P_1 & -P_0 - P_1 \\ & P_0/2 - P_1 + P_2 & P_0/2 - P_2 \\ & & P_0/2 + P_1 + P_2 \end{pmatrix} \tag{1.52}$$

The expressions of these parameters in terms of the conventional oscillation parameters (3 mixing angles and one CP violating phase) are:

$$P_0 = \frac{1}{2}\left[(1-\epsilon)^2\left(1 - \frac{\sin^2 2\theta_{12}}{2}\right) + \epsilon^2 - \frac{1}{3}\right] \tag{1.53}$$

$$P_1 = \frac{1-\epsilon}{2}\left(\gamma \cos 2\theta_{12} + \beta\frac{1-3\epsilon}{2}\right) \tag{1.54}$$

$$P_2 = \frac{1}{2}\left[\gamma^2 + \frac{3}{4}\beta^2(1-\epsilon)^2\right] \tag{1.55}$$

where

$$\epsilon = \sin^2\theta_{13} \qquad \alpha = \sin\theta_{13}\cos\delta\sin 2\theta_{12}\sin 2\theta_{23}$$

$$\beta = \cos 2\theta_{23} \qquad \gamma = \alpha - \frac{\beta}{2}\cos 2\theta_{12}(1+\epsilon)$$

The values of the conventional oscillation parameters are given in [30]; in the following table we report their best fit values and the 68% confidence level interval. The normal hierarchy (NH) is the one for which

$$\Delta m^2 := m_3^2 - \frac{m_2^2 + m_1^2}{2} > 0 \tag{1.56}$$

whereas the inverted hierarchy (IH) is the one for which $\Delta m^2 < 0$. The other mass squared difference is:

$$\delta m^2 = m_2^2 - m_1^2 > 0 \tag{1.57}$$

parameter	NH	IH
$\sin^2\theta_{12}$	$0.297^{+0.017}_{-0.016}$	$0.297^{+0.017}_{-0.016}$
$\sin^2\theta_{23}$	$0.425^{+0.021}_{-0.015}$	$0.589^{+0.026}_{-0.022}$
$\sin^2\theta_{13}$	$0.022^{+0.001}_{-0.001}$	$0.022^{+0.001}_{-0.001}$
δ/π	$1.38^{+0.23}_{-0.20}$	$1.31^{+0.31}_{-0.19}$
Δm^2	$2.525^{+0.042}_{-0.030} \times 10^{-3}\,\mathrm{eV}^2$	$-2.505^{+0.034}_{-0.032} \times 10^{-3}\,\mathrm{eV}^2$
δm^2	$7.37^{+0.17}_{-0.16} \times 10^{-5}\,\mathrm{eV}^2$	$7.37^{+0.17}_{-0.16} \times 10^{-5}\,\mathrm{eV}^2$

Table 1.1: The best fit values and 68% intervals for the oscillation parameters as taken from [30].

The distributions of the oscillation parameters are sampled according to likelihood functions reported in figure 1 of [30]. This approach is necessary because the parameters $\sin^2\theta_{23}$ and δ/π are not Gaussian distributed. On the contrary, for $\sin^2\theta_{12}$ and $\sin^2\theta_{13}$ it is sufficient to use Gaussian distributions, with the central value as mean value and with the average of the errors quoted in the table above as the standard deviation. Performing Monte Carlo extractions according to such procedure, we obtain the distributions for P_0, P_1 and P_2 shown in figure 1.1; their best fit values and 68% CL intervals are reported in table 1.2.

ordering	P_0	P_1	P_2
NH	0.113 ± 0.006	$0.035^{+0.010}_{-0.012}$	$0.008^{+0.005}_{-0.004}$
IH		$0.029^{+0.010}_{-0.057}$	$0.008^{+0.005}_{-0.006}$

Table 1.2: The best fit values and 68% intervals for the natural parameters P_0, P_1 and P_2.

From table 1.2 it is clear that:

$$P_0 > P_1 > P_2 \tag{1.58}$$

P_0 is the largest parameter, and also the one with the smallest uncertainty. From Fig. 1.1 we see that the parameter P_2 satisfies the condition $P_2 > 0$, consistently with equation (1.55). The asymmetric errors quoted in the table are such that the integral of the normalized distribution $\mathcal{L}_P$ of a generic parameter P obeys the conditions:

$$\begin{cases} \displaystyle\int_{P_{\rm BF}-\Delta P_-}^{P_{\rm BF}+\Delta P_+} \mathcal{L}_P(t)\ dt = 0.68 \\ \mathcal{L}_P(P_{\rm BF} - \Delta P_-) = \mathcal{L}_P(P_{\rm BF} + \Delta P_+) \end{cases} \tag{1.59}$$

where $P_{\rm BF}$ is the best fit value and ΔP_+, ΔP_- are the asymmetric errors.

1.3 The types of neutrino

In this section we cover the mechanisms of neutrino production which are relevant for past, current and future neutrino detectors. Solar, atmospheric and cosmic neutrinos will be further discussed in the next chapters, as they have been object of my studies. In figure 1.2 we show the $\overline{\nu}_e + e^-$ cross section as a function of the anti-neutrino energy superimposed to the energy ranges for the commonly treated categories of neutrinos - with the exception of relic neutrinos, which have energies well below the plotted range.

1.3.1 Relic neutrinos

Just like the Cosmic Microwave Background (CMB), another direct leftover of the primordial Universe is predicted to exist: the Cosmic Neutrino Background, or CνB. In the hot plasma that filled the early Universe, neutrinos were at equilibrium with the other particles through the weak processes:

$$\nu + \overline{\nu} \leftrightarrow e^+ + e^-, \qquad \overline{\nu} + e^- \leftrightarrow \overline{\nu} + e^-$$

with interaction rate

$$\Gamma = n \langle \sigma c \rangle \approx n G_{\mathrm{F}}^2 T^2$$

where n is the density of target particles, σ is the cross section, T is the temperature of the thermal bath, and the neutrinos have been considered relativistic.

With decreasing temperature, the rate of neutrino interactions eventually became smaller than the expansion rate and they decoupled from the plasma. It can be shown that the decoupling temperature is [31]:

$$T_{e,\mathrm{dec}} \simeq 1.3\,\mathrm{MeV} \qquad T_{\mu,\tau,\mathrm{dec}} \simeq 1.5\,\mathrm{MeV} \tag{1.60}$$

The temperature is different for electron neutrinos as they interact more strongly with electrons and positrons than $\nu_{\mu,\tau}$. Due to the very small mass of the three known light neutrinos $m \simeq 1\,\mathrm{eV}$, they were relativistic at the freeze-out time, and thus are considered hot relics.

Another result from cosmology regards the present-day temperature of the CνB:

$$T_\nu^0 = \left(\frac{4}{11}\right)^{1/3} T_\gamma^0 = 1.945 \pm 0.001\,\mathrm{K} = (1.676 \pm 0.001) \times 10^{-4}\,\mathrm{eV} \tag{1.61}$$

Comparing this value with the constraint on the sum of the neutrino masses, which can be summarized into:

$$\sum_k m_k \lesssim 0.5 - 1\,\mathrm{eV}$$

we have that, since at least two neutrino masses are larger than about $5 \times 10^{-2}\,\mathrm{eV}$, the neutrinos belonging to these species are not relativistic in the CνB. With

massive nonrelativistic neutrinos, the cross section to detect them is of the order of:

$$\sigma \sim G_{\mathrm{F}}^2 (T_\nu^0)^2 \sim 10^{-64}\,\mathrm{cm}^2 = 10^{-40}\,\mathrm{b} \tag{1.62}$$

which makes them extremely difficult to detect, even though there is indirect evidence for the existence of the CνB [32].

1.3.2 Solar neutrinos

Electron neutrinos are produced in the thermonuclear reactions with which the Sun, as all stars, burns; many more details on this will follow later, in chapter 2,

The solar neutrino flux at Earth is about $6 \times 10^{10}\,\mathrm{cm}^{-2}\,\mathrm{s}^{-1}$, and is distributed up to about 10 MeV - even though it is almost entirely constituted by neutrinos generated in the proton-proton fusion (*pp* neutrinos). Despite such large flux, detecting solar neutrinos is difficult, and requires large detectors due to the smallness of the neutrino cross section - see figure 1.2 in the energy range $0.1 - 10\,\mathrm{MeV}$. Moreover, these detectors must be located underground to cut the background due to muons and other cosmic rays that would bury the neutrino signal under a much higher rate of events.

The detection of solar neutrinos, as discussed in section 1.1, dates back to the '70s, with the Homestake experiment. The confront of its results to the predictions of the Standard Solar Model by Bahcall gave rise to the solar neutrino problem, which turned into the search for the oscillated neutrinos. The story of solar neutrinos can be regarded as one of success:

- the seemingly undetectable particle that Pauli introduced was, indeed, detected;
- a theoretical model of the reactions that power the Sun could be precisely tested;
- neutrino oscillations have been discovered and are now subject of high-precision experiments - see the results in table 1.1.

As of now, there are two main open issues regarding solar neutrinos, and a secondary one:

1. test for the existence of the so-called CNO neutrinos, produced in the CNO cycle(s) which are thought to be active in the Sun;

2. use solar neutrinos to constrain the "metallicity" of the Sun, i.e. the fraction of elements heavier than Helium;

3. precisely measure neutrinos from the fusion of two protons.

In section 2.3 we will talk about the research work I contributed to in order to addess points 1 and 3.

1.3.3 Cosmic neutrinos

With cosmic neutrinos we refer to neutrinos produced outside of the Solar system. A further subdivision, justified by different production mechanisms, energetics and detection techniques, would be to separate neutrinos produced in the transition to the SuperNova (SN) phase of a star from those produced around more powerful accelerators, such as Starburst Galaxy Nuclei (SBGi), blazars, Gamma-Ray Bursts (GRBs), and Active Galactic Nuclei (AGNi) in general.

SuperNova Neutrinos SuperNovae (SNe) are the spectacular end of the life of some stars; they consist in the explosion of the star itself, in which some solar masses are ejected with a kinetic energy of the order of 10^{51} erg. The aftermath of a SN can be a compact object, such as a neutron star or a black hole.

In a very simple picture for core-collapse SNe, which are the most interesting type of SNe for us due to the very high neutrino fluxes they produce, such tremendous amount of energy comes from the gravitational collapse of the star itself, which, in the proximity of the star's death, cannot be balanced by the fusion processes. The contraction of the star causes the onset of the fusion of heavier elements, like carbon and oxygen [33], until the star has an onion-like structure with an iron core surrounded by layers of lighter elements. Iron is the most tightly bound nucleus, i.e. it does not work as themonuclear fuel: the core contracts due to gravity, which eventually overpowers the pressure due to degenerate relativistic electrons, and the high temperature causes the photodissociation of iron through

$$\gamma + {}^{56}\mathrm{Fe} \rightarrow 13\alpha + 4n$$

which absorbs energy and reduces the kinetic energy, and thus the pressure, of the electrons. Electrons are converted into neutrinos with the processes:

$$e^- + N(Z, A) \to N(Z-1, A) + \nu_e \qquad e^- + p \to n + \nu_e$$

which carry away most of the kinetic energy of the captured electrons. The combination of these processes decrease the electron pressure and favour the collapse, which accelerates.

The liberated gravitational energy is about 10^{53} erg, of which about 0.01% goes into electromagnetic radiation and about 1% is transformed into kinetic energy of the ejecta. The neutrinos produced in the electron capture processes can freely escape the star, and are characterized by a nonthermal spectrum with average energy of about 10 MeV. In the later stages of the collapse, the core density exceeds about $3 \times 10^{11}\,\mathrm{g\,cm^{-3}}$, trapping neutrinos as well.

Neutrinos of all flavours are produced in the hot core of the forming neutron star through pair annihilation:

$$e^+ + e^- \to \nu + \overline{\nu}$$

electron-nucleon and nucleon-nucleon bremsstrahlung:

$$e^\pm + N \to e^\pm + N + \nu + \overline{\nu} \qquad N + N \to N + N + \nu + \overline{\nu}$$

and photoannihilation:

$$\gamma + e^\pm \to e^\pm + \nu + \overline{\nu}$$

The sphere from which neutrinos can stream out freely is called *neutrinosphere*, which depends on flavour and energy; in particular, there are three energy-dependent neutrinospheres, one for ν_e, one for $\overline{\nu}_e$ and one for $\nu_{\mu,\tau}$ and $\overline{\nu}_{\mu,\tau}$, as ν_e and $\overline{\nu}_e$ interact (differently) with ordinary matter. This is why in the literature of SN neutrinos $\{\nu_{\mu,\tau}, \overline{\nu}_{\mu,\tau}\}$ are generically labelled by ν_x. Each neutrinosphere emits a pinched black body of neutrinos, with average time-integrated energies of

$$\langle E_{\nu_e} \rangle \approx 10\,\mathrm{MeV} \qquad \langle E_{\overline{\nu}_e} \rangle \approx 15\,\mathrm{MeV} \qquad \langle E_{\nu_x} \rangle \approx 20\,\mathrm{MeV}$$

A very important problem is the SN rate estimation; these rates depend on the galaxy type, and are important both for the study of the SN explosion dynamics

and for the estimation of the Relic Supernova Neutrino Background (RSNB). The rate of detectable core-collapse SNe in our Galaxy is estimated to be [34]:

$$R_{\text{cc-SN}} = 3.2^{+7.3}_{-2.6}\,\text{century}^{-1}$$

SN1987A has been the only case of direct detection of neutrinos from a Supernova. Four large underground neutrino detectors were in operation: Kamiokande-II [35], IMB [36], Baksan [37] and LSD [38]. These detectors observed an unusual number of events of about 10 MeV in a time span of about 10 seconds in the hours preceeding the optical observation of SN1987A. Kamiokande-II, IMB and Baksan observed the events at the same time (with some systematical uncertainties on the absolute time), whereas LSD detected events about five hours before them, in anticoincidence. For this reason, the LSD events are considered controversial [39] and are usually excluded by the analysis of SN1987A data.

Kamiokande-II and IMB were water-Cherenkov detectors, which are sensitive to neutrinos due to the light emitted by the charged leptons produced in neutrino interactions. This light is captured by photomultiplier tubes (PMTs) which can reconstruct the neutrino interaction point, the direction of the track and the energy of the produced lepton. Kamiokande, tailored to solar neutrino detection, measured neutrinos through the elastic scattering reaction:

$$\nu_\ell + e^- \to \nu_\ell + e^-$$

and with the inverse-beta decay (IBD):

$$\overline{\nu}_e + p \to e^+ + n \qquad E_{\overline{\nu}} \geq 1.8\,\text{MeV}$$

which has a much larger cross-section than the elastic scattering process.

Kamiokande measured 16 events during the burst, but some (6 or 7) of them are likely to be due to background.

IMB was aimed at atmospheric neutrino detection, and measured 35 ± 15 neutrino events with energy above 20 MeV in a time interval of 6 seconds, with a negligible background rate.

Baksan was an oil-based liquid scintillator, with a threshold E_ν of about 10 MeV and a rather large background due to cosmic ray muons and discharges in the photomultipliers. Also Baksan measured neutrinos with the reactions mentioned above, and detected 5 events within 10 seconds between 10 MeV and

25 MeV. The background rate was rather high, and there have been problems with the detector's clock; in [40] it has been shown, however, that the Baksan events are compatible with a SN signal.

What can be learned from SN neutrinos? [41]

- The total emitted energy can be determined with high accuracy by current and future scintillator-based neutrino detectors, and the same holds for the binding energy of the newly-formed neutron star.
- The equation of state of the proto-neutron star could be constrained, as well as some extended theories of gravity.
- Model-independent bounds on the mass of neutrinos can be set, by observing neutrinos in a time interval ΔT larger than the emission burst duration ΔT_0, one could measure directly the neutrino mass - if the distance of the SN and the energy of the neutrinos is measurable. This limit, for SN1987A, is rather weak: $m_{\nu_e} \lesssim 30\,\text{eV}$, to be compared with today's limits of 1 eV.
- The explosion mechanism can be thoroughly investigated through the neutrino light-curves, and the neutrino flavour conversion in the SN can be studied with the reconstruction of the energy spectra.
- Also the lifetime of electron neutrinos can be constrained; in the case of SN1987A, which is 50 kpc away, we have [42]

$$\tau_{\overline{\nu}_e} \gtrsim 1.6 \times 10^5 m_{\nu_e}/E_{\overline{\nu}_e}\ \text{yr}$$

The role of SNe is also crucial for the acceleration of Cosmic Rays (CRs) [43], which leads us to the next paragraph.

Neutrinos from the most powerful sources Since 2013 [17] we know that neutrinos with high (larger than 30 TeV) energy come from somewhere out of the Solar system. Measuring neutrinos of these energies requires huge volumes, as their interaction probability is very small and the energy to be contained is very large. Present day experiments are of the size of $1\,\text{km}^3$; we will cover the details about this in chapter 4.

One could have expected neutrinos from outer space considering their connection to cosmic rays, in that high-energy neutrinos are produced when high-energy cosmic rays collide with either gas (pp collisions) or background radiation ($p\gamma$ collisions). In those collisions, in fact, charged pions are produced:

$$\begin{cases} p_{\mathrm{CR}} + p_{\mathrm{gas}} \to X + \pi^+ + \pi^- + \pi^0 \\ p_{\mathrm{CR}} + \gamma_{\mathrm{bckgr}} \to X + \pi^+ + \pi^0 \end{cases}$$

which in turn decay into neutrinos:

$$\pi^+ \to \mu^+ + \nu_\mu \to e^+ + \nu_e + \overline{\nu}_\mu + \nu_\mu$$

$$\pi^- \to \mu^- + \overline{\nu}_\mu \to e^- + \overline{\nu}_e + \nu_\mu + \overline{\nu}_\mu$$

The pp mechanism of neutrino production is of course the same that generates the so-called atmospheric neutrinos, which we will cover more thoroughly later.

The phenomenology of high-energy neutrinos from outer space is still lacking solid theoretical bases and predictive power, mainly due to the fact that we do not know yet which are the sources that produce cosmic rays and how acceleration and propagation work - and this is true even in the case of the Milky Way, despite more than a century of measurements, which resulted into Fig. 1.3.

We suggest [45] and [46] as reviews respectively about the phenomenology of astroparticle physics in general and about the "zoo" of astrophysical objects commonly cited as sources.

In the simplest picture, the acceleration of cosmic rays takes place at the shocks generated by the explosion of a supernova; they can traverse the shocks multiple times thanks to diffusion through the turbulent magnetic field which surrounds the source and thus become more energetic. This is the so-called Diffusive Shockwave Acceleration (DSA); many improvements, reviewed in [43], have enriched the phenomenology of Galactic cosmic rays, but a completely satisfactory description of the experimental results is still missing.

While there is experimental evidence for leptonic acceleration[4] at the shock of Supernova Remnants (SNRs), i.e. the area which surrounds the remains of a Supernova explosion, there is no solid evidence for sources of cosmic rays. This is not really surprising, as the magnetic fields which permeate the intergalactic

[4] E.g. Tycho and the Crab Nebula.

and the interstellar medium curve the trajectories of cosmic rays, which as a result do not point anymore to their production site. For gamma rays, which are the most energetic photons, and neutrinos this is not the case; however, gamma rays can be produced with purely leptonic mechanisms, i.e. with the injection, acceleration and propagation of electron and positrons, and interact much more than neutrinos. These two facts imply that, unfortunately, 1) a gamma ray source does not necessarily coincide with a cosmic ray source, and 2) gamma rays have a horizon.

On the other hand, the detection of a source of neutrinos would coincide with the detection of a cosmic-ray source; so far, there is only one piece of evidence (of about 3.5σ of significance) for a neutrino source, which is TXS 0506+056 [18]. Many attempts have been done to model the detected neutrino as a product of TXS 0506+056, but the simplest and most satisfactory description of that source is that of a purely leptonic one [47].

TXS 0506+056 is classified as a blazar, i.e. an Active Galactic Nucleus (AGN) with a relativistic jet which points toward the Earth. An AGN is a compact region at the centre of a galaxy that has a much larger luminosity than a star; Active Galactic Nuclei emit persistently from the radio to the gamma-ray band, and are usually described as a black hole surrounded by an accretion disk, in which dissipative processes heat up the gas the disk. Some AGNs form jets of highly-collimated radiation, the origin of which is not yet completely understood.

We will not cover all possible cosmic neutrino sources, unless needed; for the moment we will mention two popular candidates, i.e. Gamma-Ray Bursts (GRBs), which are extremely energetic explosions - the brightest electromagnetic emitters - supposedly due to the accretion of matter around a black hole, and Starburst Galaxies (SBGs), which are Galaxies with a rate of star formation 10-100 times larger than that of the Milky Way.

1.3.4 Terrestrial neutrinos

With terrestrial neutrino we will mean neutrinos produced in reactors of nuclear power plants, in beam experiments, in the Earth and in the atmosphere.

Reactor neutrinos Reactor neutrinos are the neutrinos that result from the nuclear decays of the radioactive substances present in nuclear power plants.

The β decays of neutron-rich nuclei are in fact intense sources of $\overline{\nu}_e$; the main contributors are ^{235}U, ^{238}U, ^{239}Pu and ^{241}Pu.

Since the production of such neutrinos is isotropic, the flux at the detector scales as the inverse of the square of the distance to the reactor. This potential problem for oscillation experiments is somewhat mitigated by the fact that such neutrinos have an energy of the order of a few MeV, i.e. they have a rather short oscillation length. Only $\overline{\nu}_e$ disappearance can be studied with such setups, with the proviso that statistical fluctuations in the signal make it difficult to detect small mixing, which would result into small disappearance.

The main detection channel is based on the inverse beta decay, as for Supernova neutrinos; such process has a neutrino energy threshold of 1.806 MeV, which is surpassed by only about 25% of the antineutrinos produced in a reactor.

Beam neutrinos Beam neutrinos are produced at accelerators, and are usually classified according to the method of production of the neutrino beam: pion decay in flight, muon decay at rest and beam dump.

For pion decay in flight neutrino beams, a proton beam hits a target, producing pions and kaons; their decay produces neutrinos, as is the case for cosmic and atmospheric neutrinos. The beam is then composed mostly of ν_μ or $\overline{\nu}_\mu$, depending on the polarity of the apparatus that focalizes the pions and kaons. The typical energy of the neutrinos is of a few GeV, but it varies according to the energy of the proton beam. For short baseline experiments, the typical source-detector distance is of one kilometre, with coverage:

$$\frac{L}{E} \lesssim 1\,\mathrm{km\,GeV}^{-1} \implies \Delta m^2 \gtrsim 1\,\mathrm{eV}^2$$

To detect oscillated tau (anti-)neutrinos the energy must be of about one order of magnitude larger, as the τ lepton has a production threshold of about 3.5 GeV. One of the most notable experiments of this kind is OPERA, which first observed $\nu_\mu \to \nu_\tau$ oscillations [48].

Neutrinos can also come from the decay of muons which have been stopped; pions and kaons are produced as mentioned above, and π^- are usually absorbed by nuclei, leaving positive pions. Antimuons are then produced, which decay into (a positron,) an electron neutrino and a muon antineutrino; with these experiments, it is then possible to measure $\overline{\nu}_\mu \to \overline{\nu}_e$ oscillations, as $\overline{\nu}_e$ are not

directly produced. The energy of these neutrinos is of the order of several tens of MeV, and the relevant experiments have usually a coverage of:

$$\frac{L}{E} \lesssim 1\,\mathrm{m\,MeV^{-1}} \implies \Delta m^2 \gtrsim 1\,\mathrm{eV}^2$$

In beam dump experiments, a very high energy (hundreds of GeV) beam of protons is completely stopped in a thick target - the beam dump -, in which heavy hadrons are produced. Such hadrons decay promptly (more on this in section 4.5) and equally in muon and electron neutrinos with energies of the order of 10^2 GeV. A detector one kilometre away from the source could detect oscillations by measuring a ratio of the muon and electron neutrino fluxes different from 1. The typical coverage is:

$$\frac{L}{E} \lesssim 10^{-2}\,\mathrm{m\,MeV^{-1}} \implies \Delta m^2 \gtrsim 100\,\mathrm{eV}^2$$

In table 1.3 we shouw the coverage and sensitivity of the various kinds of oscillation experiments.

Geoneutrinos Geoneutrinos [49] are produced in the decay chains of the radioactive isotopes ^{238}U and ^{232}Th in the Earth's crust. With ^{40}K, the decay of such isotopes is one of the major sources of the heat generated in the Earth. KamLAND [50] has been the first experiment to detect the electron antineutrinos produced in the decay of the isotopes of uranium and thorium - those from potassium do not pass the energy threshold of 1.8 MeV; geoneutrinos showed up in the data as an excess over, among other backgrounds, reactor neutrinos, which, however, dominate above 2.3 MeV. This measurement is in agreement with the theoretical of the geophysical model, and may lead to a future way to investigate the composition of the Earth accurately.

More recently, the Borexino collaboration presented their results [51] on the measurement of geoneutrinos, which also documents improved techniques in the in-depth analysis of such kind of data and describes the substantial effort required to extract geoneutrino signals.

Atmospheric neutrinos These neutrinos are produced in the hadronic interactions of cosmic rays with the nuclei in the atmosphere, similarly to the *pp*

Type of experiment	L	E	Δm^2
Reactor SBL	10 m	1 MeV	$0.1\,\text{eV}^2$
Accelerator SBL (π decay)	1 km	1 GeV	$1\,\text{eV}^2$
Accelerator SBL (μ decay)	10 m	10 MeV	$1\,\text{eV}^2$
Accelerator SBL (beam dump)	1 km	100 GeV	$100\,\text{eV}^2$
Reactor LBL	1 km	1 MeV	$10^{-3}\,\text{eV}^2$
Accelerator LBL	10^3 km	1 GeV	$10^{-3}\,\text{eV}^2$
Atmospheric ν	20-10^4 km	0.5-100 GeV	$10^{-4}\,\text{eV}^2$
Reactor VLB	100 km	1 MeV	$10^{-5}\,\text{eV}^2$
Accelerator VLB	10^4 km	1 GeV	$10^{-4}\,\text{eV}^2$
Solar ν	10^8 km	0.2-15 MeV	$10^{-12}\,\text{eV}^2$

Table 1.3: The kinds of neutrino oscillation experiments with typical source-detector distance, energy and sensitivity to Δm^2, which is given by $\Delta m^2 L/2E \sim 1$ with E in GeV and L in km. SBL = short baseline, LBL = long baseline, VLB = very long baseline. The values reported here are indicative and can vary depending on the experiment; these can be sensitive to oscillations also for $\Delta m^2 L/2E \lesssim 1$; table taken from [6].

mechanism of cosmic neutrino production. We will cover atmospheric neutrinos in detail in §3, of which the following is a brief summary.

Their flux can be predicted on the bases of a model of the atmosphere, of the cosmic-ray flux up to a few PeV, and of the strong interactions between CRs (which are mostly protons and Helium nuclei) and the nuclei in the atmosphere. These interactions produce showers of particles, among which pions, kaons, and charmed mesons and baryons. Depending on their energy, pions and kaons can decay before losing energy in interactions, thus producing the so-called conventional component of neutrinos. Charmed mesons and baryons, on the other hand, have a very short lifetime of about 10^{-12} s at rest, so that they decay before interacting, thus producing a *prompt* component of neutrinos. As we will see, these two components differ in energy spectrum, flavour content at production and zenith dependence.

Due to the fact that the probability for pions and kaons to lose energy via interactions increases with energy, the spectrum of conventional neutrinos is expected to go like $E^{-3.7}$, i.e. to be suppressed by a $1/E$ factor with respect to the CR spectrum. Since pions and kaons have a large lifetime, of about 10^{-8} s, the more time they have to interact, that is, the thicker the atmosphere they can traverse, the more likely it is for them to decay in air producing neutrinos. This is why the conventional neutrino flux is expected to be minimum for the vertical direction and maximum for the horizontal one. The flavour content at production of conventional neutrinos goes from a $(\nu_e : \nu_\mu : \nu_\tau) \simeq (1 : 2 : 0)$ ratio at lower energies to about $(0 : 1 : 0)$ at higher energies, as the muon produced in the pion/kaon decay has a Lorentz-boosted mean free path which is too large for it to decay in the atmosphere.

Prompt neutrinos reflect the $E^{-2.7}$ spectrum of cosmic rays in the relevant energy range, as their parent particles immediately decay. Because of this short lifetime, it does not matter which direction the parent particle comes from, so that their zenith distribution is expected to be isotropic. It is also predicted that their parent particles produce electron and muon neutrinos in equal amounts, while the tau flavour is strongly suppressed as it mainly comes from the decay of the tau lepton.

The first, sought-after evidence for neutrino oscillations has been obtained with atmospheric neutrinos by the Super-Kamiokande collaboration [52], which measured the up-down asymmetry of muon neutrinos with a water-Cherenkov

detector. The presence of such asymmetry, as well as the L/E dependence of the distribution of μ-like events, was most probably due to neutrino oscillations, as the path covered by up-going neutrinos is much larger than that of down-going neutrinos.

The current generation of very large (0.1-1 km^3 for ANTARES and IceCube respectively) neutrino telescopes has performed measurements of the atmospheric neutrino spectrum which are in agreement with theory for energies between 100 GeV and 1 PeV, and are going to probe neutrino oscillations at such high energies. Since the sensitivity of Super-Kamiokande to neutrinos extends up to about 10 GeV, new instruments, like ORCA [53], are under construction to cover also the 10-100 GeV range of the spectrum of atmospheric neutrinos.

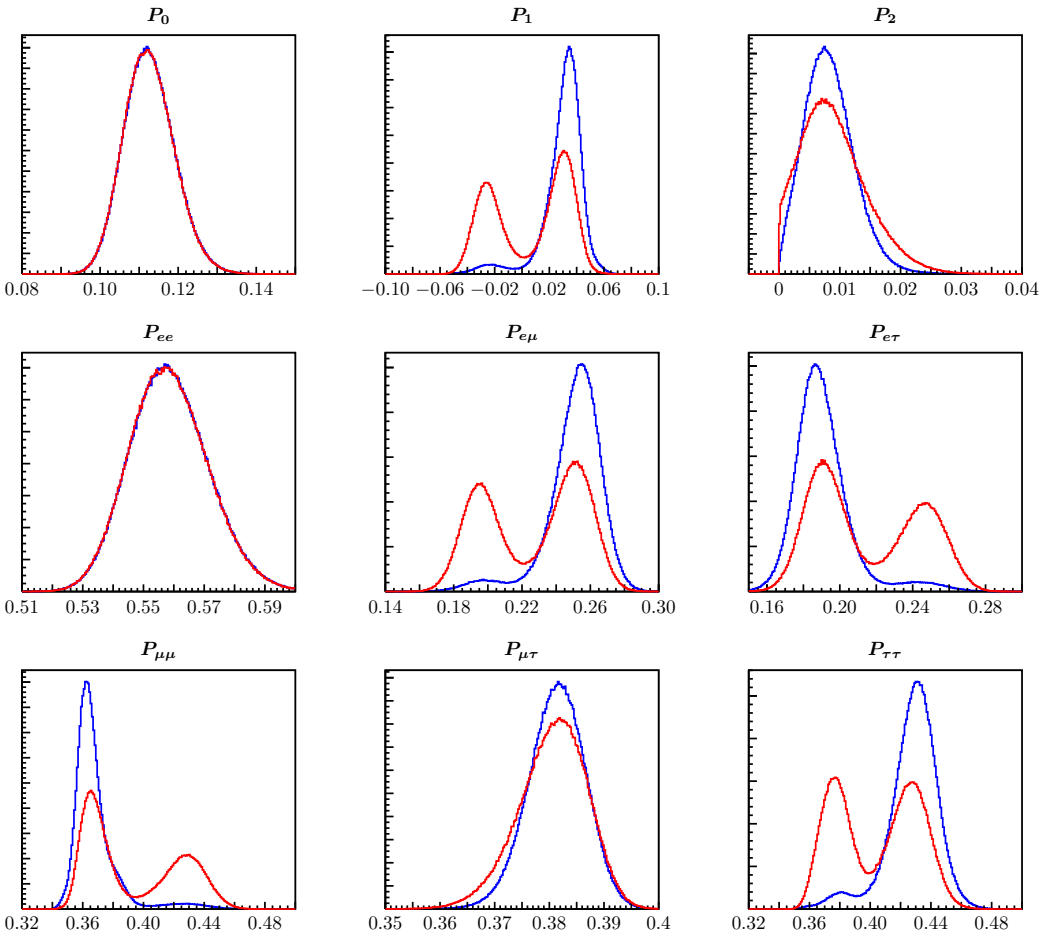

Figure 1.1: The distributions of the natural parameters P_0, P_1, P_2 Eq. (1.53)-(1.55) and the survival/oscillation probabilities $P_{\ell\ell'}$ Eq. (1.52) for normal hierarchy (blue) and for inverted hierarchy (red).

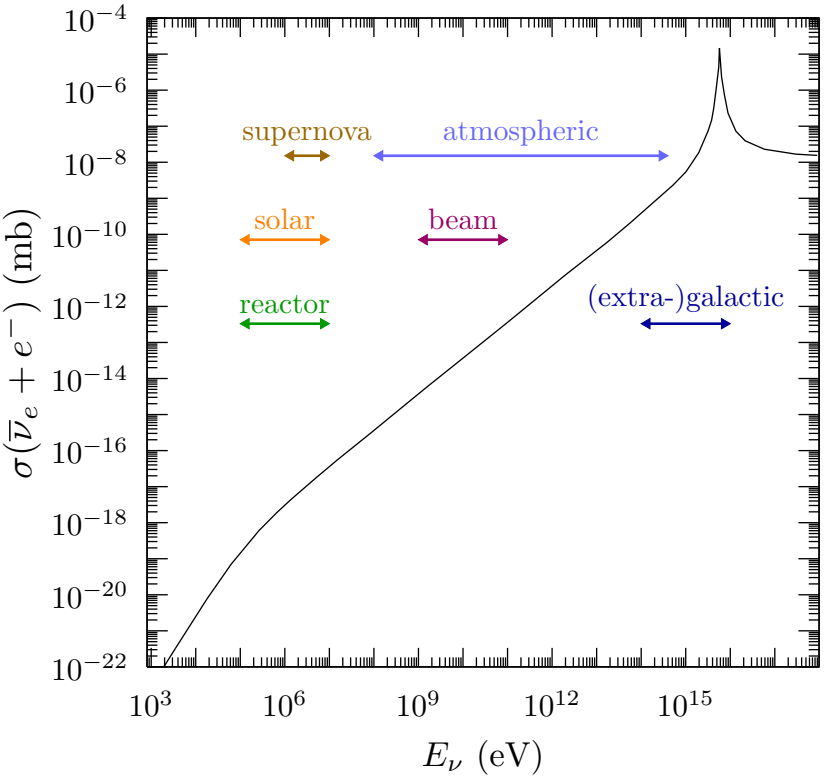

Figure 1.2: $\overline{\nu}_e + e^-$ cross section as a function of the anti-neutrino energy; superimposed are the energy ranges of the commonly treated categories of neutrino - with the exception of relic neutrinos, which are expected to have energies between 10^{-6}–10^{-4} eV.

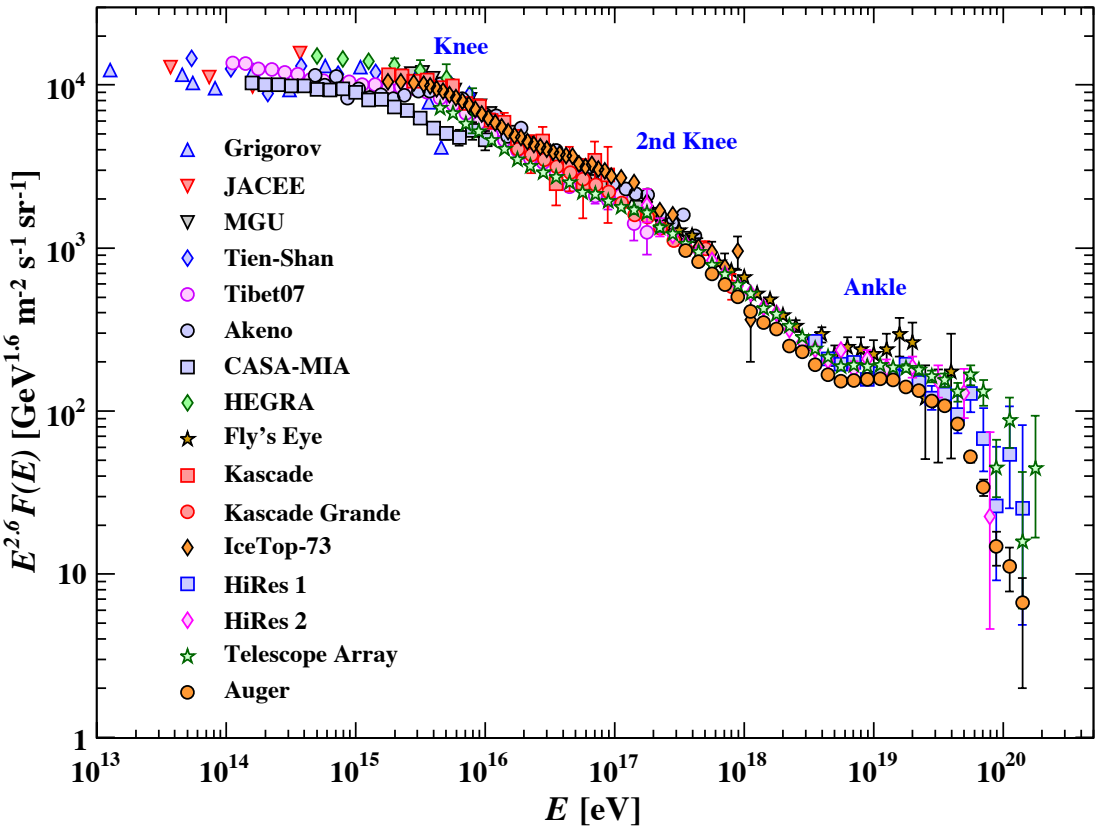

Figure 1.3: The spectrum of cosmic rays, as measured by many experiments over time; plot taken from [44].

2

Solar neutrinos

Hi, I'm Nino the neutrino and I come from the Sun's belly,
where thermonuclear fusion occurs. Now, along with my brothers,
(solar neutrinos like me!) I'm going into outer space.
No one stops us, we're small, evasive, and almost invisible,
and most of us will reach the Earth.
Nino the neutrino

In order to talk about solar neutrinos, we need to start from the Standard Solar Model (SSM), which we will discuss in §2.1, as it is the model that explains how our star burns and also predicts the amount of neutrinos produced in the process.

In §2.2 we will talk about the experimental results concerning Solar neutrinos, going from the first detection of neutrinos with the Homestake experiment to the current and upcoming Solar neutrino experiments, which are currently shedding light on solar physics.

In §2.3 we will present the work, which I contributed to, on the luminosity constraint, i.e. the strict relation between the flux of neutrinos coming from the Sun to the power emitted in photons.

I dedicate this chapter to the memory of Simone Marcocci.

2.1 The Standard Solar Model

Stars burn because of the thermonuclear reactions that fuse their constituents into heavier ones, liberating energy in the process. This is possible due to the fact that the total mass of a nucleus is smaller than the sum of the masses of its nucleons:

$$m(A, Z) = Zm_p + (A - Z)m_n - B(A, Z) \tag{2.1}$$

where $B(A, Z) > 0$ is called *binding energy*.

The modern formulation of stellar nucleosynthesis has been developed by Bethe and Von Weizsäcker in 1939 [54] and others subsequently (see [55] for a review); according to it, the Sun is powered by two groups of thermonuclear reactions, the *pp* chain and the CNO cycle, represented in Figures 2.1 and 2.2.

The electron neutrinos produced in the β^+ reactions in the *pp* chain and in the CNO cycle can be detected on Earth, and provide a unique, practically real-time probe of the Sun interior. Photons, on the other hand, escape the surface of the Sun after suffering some hundred thousand years of scattering in its interior.

For a review on the nuclear physics behind the Standard Solar Model, we refer to [56], as its treatment goes beyond the scope of this thesis.

A Standard Solar Model (SSM) is a "solar model that is constructed with the best available physics and input data" and is "required to fit the observed luminosity and radius of the Sun at the present epoch, as well as the observed heavy-element-to-hydrogen ratio at the surface of the Sun" [57].

Many SSMs have been constructed, as the physical understanding of the Sun, the computation power and the available data improved over time. The first one, which played a major role in neutrino physics, is that developed by Bahcall and collaborators ever since 1962 [58].

From the neutrino standpoint, these efforts culminated in quantitative predictions of the solar neutrino flux at Earth: in particular, the energy spectrum (shape and intensity) of every "kind" of neutrino, which is defined by its production reaction, can be predicted, and is represented[1] in Figure 2.3.

The values of the Solar parameters that SSMs have to reconstruct are listed in Table 2.1, while the current theoretical predictions on the neutrino fluxes

[1]The tabulated spectral shapes obtained by Bahcall are still used, and can be found at the webpage: https://www.sns.ias.edu/~jnb/SNdata/.

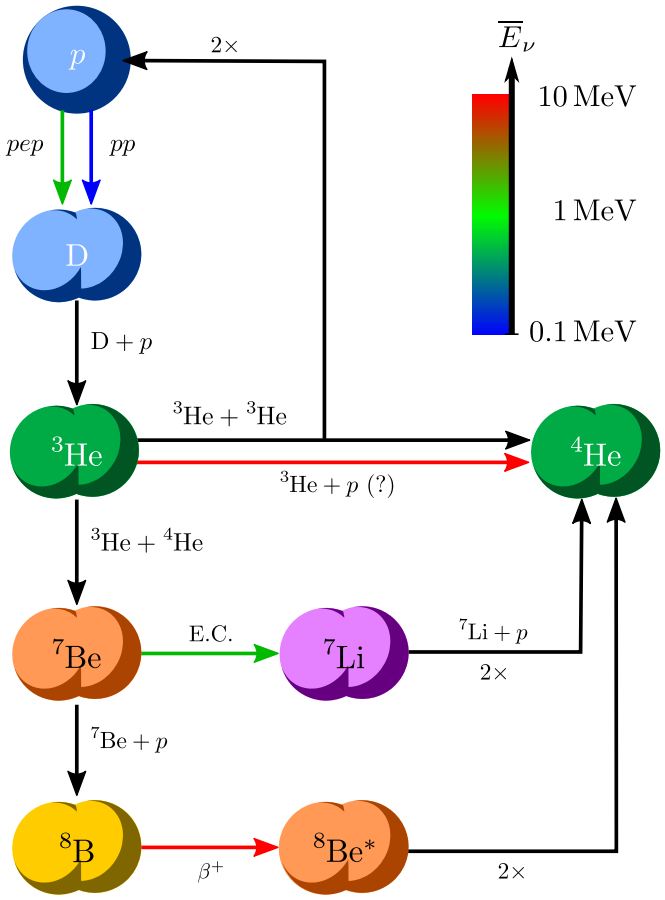

Figure 2.1: Artistic representation of the *pp* chain, the main sequence of reactions operating in the Sun. The colored arrows indicate the production of an electron neutrino, the average energy of which is approximately indicated in the $\overline{E}_\nu$ gradient.

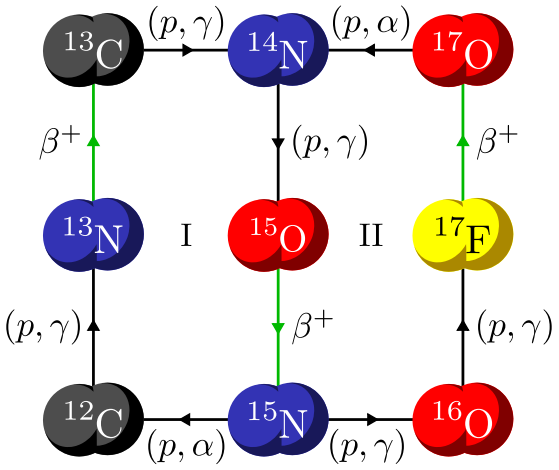

Figure 2.2: Artistic representation of the CNO cycle, the main sequence of reactions operating in massive stars and, supposedly, operating in the Sun as well. The green arrows indicate the production of an electron neutrino, which has average energy of 1 MeV.

Parameter	Value
$M_\odot$	$1.989 \times 10^{33}\,\mathrm{g}$
$R_\odot$	$6.9598 \times 10^{10}\,\mathrm{cm}$
$L_\odot$	$3.8275 \times 10^{33}\,\mathrm{erg\,s^{-1}}$

Table 2.1: The input parameters that SSMs have to reconstruct. The solar radius and mass are taken from [61], while the luminosity is taken from [62].

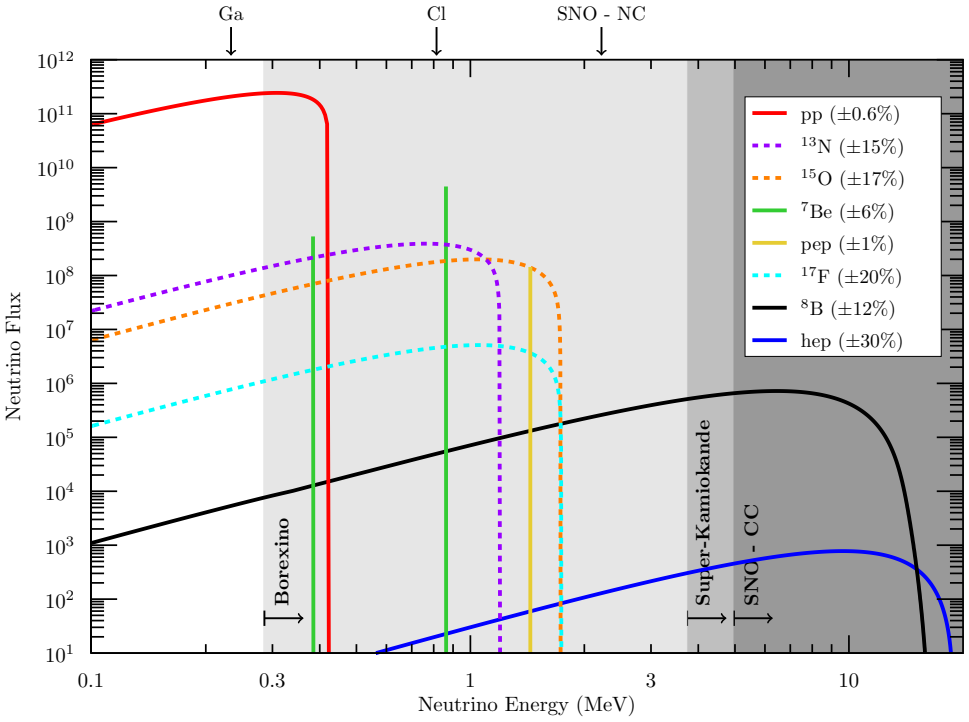

Figure 2.3: Energy dependence of the neutrino fluxes produced by the different nuclear processes in the Sun, according to the B16-GS98 Standard Solar Model [59]. The y axis is in units of $\mathrm{cm}^{-2}\,\mathrm{s}^{-1}\,\mathrm{MeV}^{-1}$ for continuous spectra and $\mathrm{cm}^{-2}\,\mathrm{s}^{-1}$ for monochromatic ones (Beryllium and *pep* neutrinos). The neutrino energy threshold for detection is indicated with a vertical arrow for the experiments which do not reconstruct the neutrino energy (those based on gallium, as GALLEX/GNO and SAGE, on chlorine, as Homestake, or on neutral current ν-D interactions, as SNO) and with a horizontal arrow for those which reconstruct the neutrino energy (those based on elastic scattering, as Borexino and Super-Kamiokande, and on charged current ν-D interactions, as SNO). The dashed lines highlight the CNO-cycle contribution to the solar neutrino flux. The energy distribution of the neutrino fluxes has been taken from https://www.sns.ias.edu/~jnb/SNdata/, while their normalisation is from [59]; figure taken from [60].

Flux	B16-GS98	B16-AGSS09met
Φ_{pp}	$5.98(1 \pm 0.006)$	$6.03(1 \pm 0.005)$
Φ_{pep}	$1.44(1 \pm 0.01)$	$1.46(1 \pm 0.009)$
Φ_{hep}	$7.98(1 \pm 0.30)$	$8.25(1 \pm 0.30)$
Φ_{Be}	$4.93(1 \pm 0.06)$	$4.50(1 \pm 0.06)$
Φ_{B}	$5.46(1 \pm 0.12)$	$4.50(1 \pm 0.12)$
Φ_{N}	$2.78(1 \pm 0.15)$	$2.04(1 \pm 0.14)$
Φ_{O}	$2.05(1 \pm 0.17)$	$1.44(1 \pm 0.16)$
Φ_{F}	$5.29(1 \pm 0.20)$	$3.26(1 \pm 0.18)$

Table 2.2: Theoretical predictions for the solar neutrino fluxes adopting the "Barcelona 2016" (B16, introduced in [59]) SSM with two different metallicity models by Grevesse & Sauval (GS98) [63] and Asplund et al. (AGGS09met) [64]. The units are $10^{10}\,\mathrm{cm}^{-2}\,\mathrm{s}^{-1}$ for *pp* neutrinos, $10^{9}\,\mathrm{cm}^{-2}\,\mathrm{s}^{-1}$ for Be neutrinos, $10^{8}\,\mathrm{cm}^{-2}\,\mathrm{s}^{-1}$ for *pep*, N, and O neutrinos, $10^{6}\,\mathrm{cm}^{-2}\,\mathrm{s}^{-1}$ for B and F neutrinos, and $10^{3}\,\mathrm{cm}^{-2}\,\mathrm{s}^{-1}$ for *hep* neutrinos. Table taken from [59].

are listed in Table 2.2, taken from [59]. In [59] there is also a discussion on the various sources of theoretical uncertainties on the neutrino fluxes, among which the solar "metallicity". In astronomical gergon, the solar metallicity is the fraction of heavier-than-Helium elements in the Sun, and remains a source of uncertainty as it is not well known yet. From Table 2.2 it is easy to note that the CNO neutrino fluxes, i.e. those coming from the decay of Nitrogen, Oxygen and Fluorine, for one metallicity model are in tension with the ones predicted with the other metallicity model. This reflects the fact that the debate on the solar metallicity is still open; it sparked with the measurement of systematically lower values of the lighter metals (C, N, O, Ne, and Ar) abundances than those that had been used in SSMs before 2000 (see [65, 66] and references therein) As the amount of CNO neutrinos is directly connected to the amount of such metals, solar neutrino measurements could prove to be crucial to solve this problem. More on this will follow in the later sections, but first we need to address the experimental techniques and results obtained in the field of solar neutrino physics.

2.2 Looking at the Sun from underground

In this chapter we are going to discuss the experiments that measure solar neutrinos. Due to the very small neutrino interaction cross section, these experiment are all located underground, so as to reduce the otherwise overwhelming cosmic contamination, mainly in mines or deep under mountains. The resulting shielding is measured in mwe, i.e. meter water equivalent, in order to consistently quantify the cosmic-ray (meant both as primaries and as secondaries) attenuation in such underground facilities regardless of the density and shape of the overburden material.

There is, however, another unavoidable source of background, represented by the natural radioactivity of the surrounding environment and of the instruments themselves. Since the signal of solar neutrinos cannot be turned off, the only countermeasure to these sources of background consists in using the purest materials available and in measuring as accurately as possible the local environmental radioactivity.

There are three main kinds of solar neutrino experiments, based on the reaction used for detection:

1. radiochemical experiments: they rely on the neutrino capture by some nucleus, which undergoes an inverse-β nuclear decay, as in the Homestake experiment (which we are going to discuss right after);

2. water Cherenkov experiments: they rely on the observation of the tracks of the ultrarelativistic charged leptons produced by neutrino interactions;

3. scintillator experiments: they rely on the collection of the light emitted by the de-excitation of certain molecules after their electrons received energy from an impinging neutrino.

The use of neutrino absorption as detection reaction implies the existence of an energy threshold, i.e. a minimum energy for neutrinos to produce a signal, but also the impossibility to reconstruct the energy of the impinging neutrino. This, as well as the sensitivity to electron neutrinos only, is the disadvantage of radiochemical experiments, as already noted in figure 2.3.

On the other hand, also scintillator and Cherenkov experiments have a threshold, but in this case it depends on the radiopurity of the experimental setup, on

the sensitivity of the devices used to collect the scintillation light emitted by the electrons and on the level of knowledge of the detector response.

Let us now treat the main experiments and results in the field of solar neutrinos, starting from their first detection by the Homestake experiment. After that, we present a selection of some of the most important experiments in solar neutrino physics. The goal is to cover the main results, some of which will be used in the next section, and complete the overview, from the experimental side, of solar neutrinos.

2.2.1 The first detection and the solar neutrino problem

As said before, the Homestake experiment [67] was the first one to measure solar neutrinos: this was realised using the inverse β-decay reaction

$$\nu_e + {}^{37}\mathrm{Cl} \rightarrow {}^{37}\mathrm{Ar} + e^-$$

which has a neutrino energy threshold of 0.814 MeV. As visible from Figure 2.3, such threshold implies that it was sensitive mostly to Boron and Beryllium neutrinos.

The Homestake Solar Neutrino Observatory was located 1478 m below the surface, in South Dakota, USA, at a depth of about 4200 mwe. The detector consisted in a steel tank of 6×10^5 l containing 2.16×10^{30} atoms of ^{37}Cl in the form of 615 tons of C_2Cl_4.

It was technically very demanding to count the ^{37}Ar atoms produced from Chlorine, but the joint efforts of the Homestake collaboration (see the historical paper [68]) resulted in the average solar neutrino rate:

$$R = 2.56 \pm 0.23\,\mathrm{SNU} \tag{2.2}$$

where 1 SNU is one solar neutrino unit, corresponding to 10^{36} captures per atom per second. Such a large uncertainty is due to the difficulty extract individual Argon atoms.

This flux corresponds to about one third of that predicted by the SSM, which gave birth to the so-called solar neutrino problem (SNP). Thanks to the experimental results that we will discuss in the next section, we now know that this deficit is due to the fact that neutrinos oscillate, as we have already seen in §1.2.2.

2.2.2 Kamiokande and Super-Kamiokande

Kamiokande is an underground water Cherenkov detector, originally built to search for proton decay. It is located in the Kamioka mine in Japan, with an overburden of 2600 mwe; a detailed description of the Kamiokande experiment can be found in [69].

The detector consisted, in its first phase (Kamiokande-I, 1983-1986), in a cylindrical steel tank of 15.6 meters of diameter and 16 meter high containing 3000 tons of water, which was monitored by an array of 1000 photomultipliers (PMTs). The fiducial volume was of about 1 kton of water, equipped to search for proton decay events with an energy of about 1 GeV.

From 1986 it was upgraded to Kamiokande-II, so as to detect events induced by Boron neutrinos [70], which have an energy around 10 MeV. To lower the energy threshold with respect to the former phase, which searched for more energetic events, the water was purified and the detector was divided in order to use its outer part as an anti-coincident active shield. Moreover, the fiducial volume was defined in different ways for different measurements; for solar neutrino detection it consisted in 680 m^3 of water within the inner detector.

The Kamiokande experiment was upgraded further to its third phase, lasted from 1990 until 1996. The neutrino energy thresholds during the three phases of Kamiokande were 9.0, 7.2 and 6.7 MeV. As said before, water Cherenkov experiments measure the solar neutrino flux through the elastic scattering reaction

$$\nu + e^- \rightarrow \nu + e^-$$

which is mainly sensitive to electron neutrinos, as they have also access to charged-current interactions with electrons. Since the recoil electron has a sharp forward peak, solar neutrino events are distinguishable from the isotropic background as the direction of the recoil electron is correlated to that of the Sun.

The Boron neutrino flux, as measured from January 1987 to February 1995 (2079 days) by Kamiokande is [71]:

$$\Phi_B^{Kam} = (2.80 \pm 0.19 \pm 0.33) \times 10^6 \, cm^{-2} \, s^{-1}$$

In this result, it is assumed that the detector measures electron neutrinos.

The Super-Kamiokande (SK) experiment [72], shown in Figure 2.4, is a 50 kton water Cherenkov detector located in the Kamioka mine, close to the cavity that

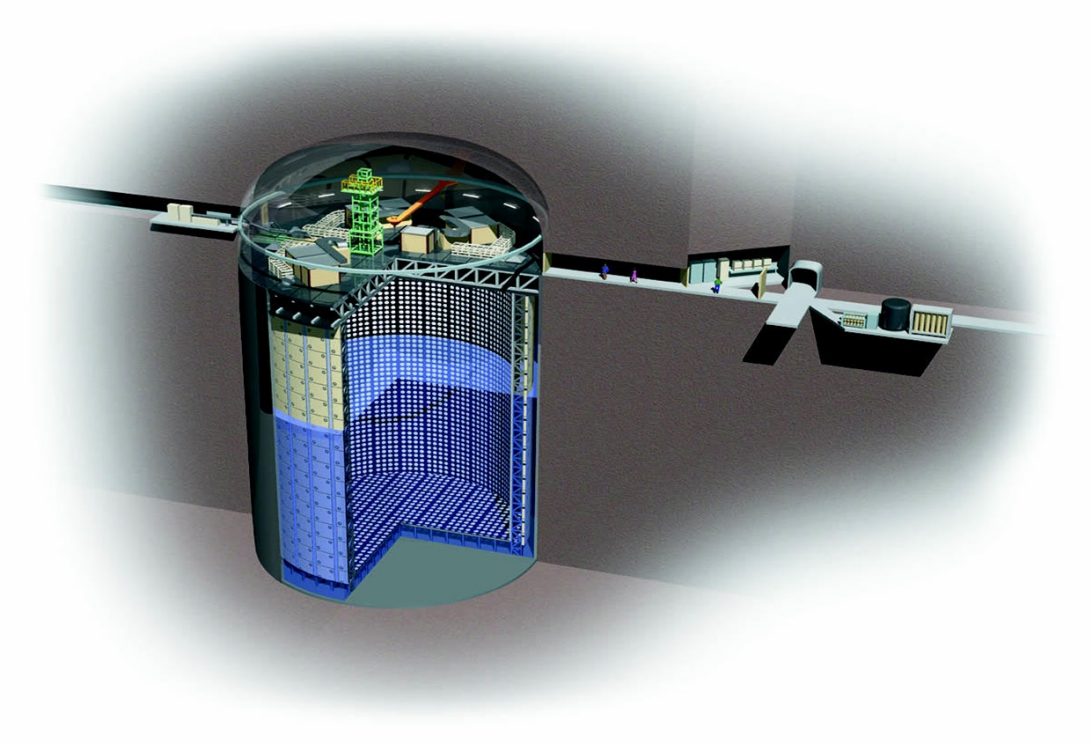

Figure 2.4: Schematic view of the Super-Kamiokande detector. Picture taken from the webpage: https://t2k-experiment.org/supporting-material-for-t2k-press-release-19-7-2013/.

once hosted the Kamiokande detector[2]. SK consists of two concentric, optically separated, water Cherenkov detectors contained in a cylindrical steel tank; the inner detector has a diameter of 33.8 meters and a height of 36.2 meters, and is equipped with 11 146 PMTs.

The Super-Kamiokande experiment has been active for four phases, as of today [74, 75, 76, 77]; hereafter, we are going to report their combined results. In the assumption of no oscillations (ν_e only), the combined Boron neutrino flux measured by the four phases of Super-Kamiokande is:

$$\Phi_{\mathrm{B}}^{\mathrm{SK}} = (2.345 \pm 0.014 \pm 0.036) \times 10^6\,\mathrm{cm}^{-2}\,\mathrm{s}^{-1}$$

for neutrino energies between 3.49 and 19.5 MeV. This result is more precise than the corresponding theoretical prediction [59].

Super-Kamiokande also claims to have found evidence for a day-night asymmetry in the neutrino flux, due to the Earth matter effect on solar neutrinos during the night. The combined day-night asymmetry measured by Super-Kamiokande is:

$$\mathcal{A}_{\text{d-n}}^{\mathrm{SK}} := \frac{\Phi_{\mathrm{day}} - \Phi_{\mathrm{night}}}{(\Phi_{\mathrm{day}} + \Phi_{\mathrm{night}})/2} = (-3.3 \pm 1.0 \pm 0.5)\%$$

2.2.3 GALLEX/GNO and SAGE

These experiments have been grouped due to the reaction they all used to detect neutrinos, i.e.:

$$\nu_e + {}^{71}\mathrm{Ga} \to {}^{71}\mathrm{Ge} + e^-$$

which has a threshold of $E_\nu^{\mathrm{th}} = 0.233\,\mathrm{MeV}$. The neutrino-induced Germanium forms a volatile compound in the detector, which is extracted and converted into GeH_4; this compound is then introduced into a dedicated counter in order to determine the number of ^{71}Ge atoms by observing their radioactive decay, which has a half-life of 11.43 d.

GALLEX was located in the Laboratori Nazionali del Gran Sasso (LNGS), Italy, at a depth of 3300 mwe, and consisted in 101 ton of a liquid $GaCl_3-HCl$ solution containing 30.3 tons of Gallium. It operated between 1991 and 1997 as

[2]Kamiokande was replaced by the KamLAND experiment [73], a very long-baseline (140 to 215 km) reactor experiment.

GALLEX, and was then upgraded to GNO for a second phase of measurements between 1998 and 2003. In [73] a reanalysis of all the acquired data is presented, which yields a rate of neutrino events of:

$$R_{^{71}\mathrm{Ga}}^{\mathrm{GX/GNO}} = 67.6 \pm 4.0 \pm 3.2\,\mathrm{SNU}$$

for the combined GALLEX/GNO periods.

The Soviet-American Gallium Experiment (SAGE) is located in the Baksan Neutrino Observatory (BNO) in the northern Caucasus mountains, with a shielding of about 4700 mwe. The measured best-fit capture rate in the SAGE experiment is [78]:

$$R_{^{71}\mathrm{Ge}}^{\mathrm{SAGE}} = 65.4^{+3.1}_{-3.0}(\mathrm{stat})^{+2.6}_{-2.8}(\mathrm{syst})\ \mathrm{SNU}$$

The combination of this result with those of GALLEX/GNO yields:

$$R_{^{71}\mathrm{Ge}}^{\mathrm{exp}} = 66.1 \pm 3.1\,\mathrm{SNU}$$

where statistical and systematic uncertainties have been summed in quadrature. Such rate is half of the prediction by the SSM in the case of no oscillations, [57]:

$$R_{^{71}\mathrm{Ge}}^{\mathrm{no\ osc}} = 128^{+9}_{-7}\ \mathrm{SNU}$$

with a discrepancy of more than 5σ. Considering oscillations, the expected rate from the SSM is 66.3 SNU for high solar metallicity and 63.2 SNU for low solar metallicity, with a $\sim 4\%$ uncertainty on both estimates.

2.2.4 SNO

The idea, presented in [80], behind the Sudbury Neutrino Observatory (SNO) was to measure the total neutrino flux from the Sun exploiting the neutral-current interaction channel, as shown below.

SNO, shown in Figure 2.5, is a real-time heavy-water Cherenkov detector located in the Creighton mine near Sudbury, Canada, at a depth of 6010 mwe. The detector consists of a 12 m-diameter acrylic vessel filled with one kiloton of isotopically-pure heavy water, D_2O. The Cherenkov light is collected by 9456 PMTs mounted on a spherical stainless steel geodesic structure of 18 m of diameter. The vessel and the geodesic sphere are immersed in ultrapure water, which

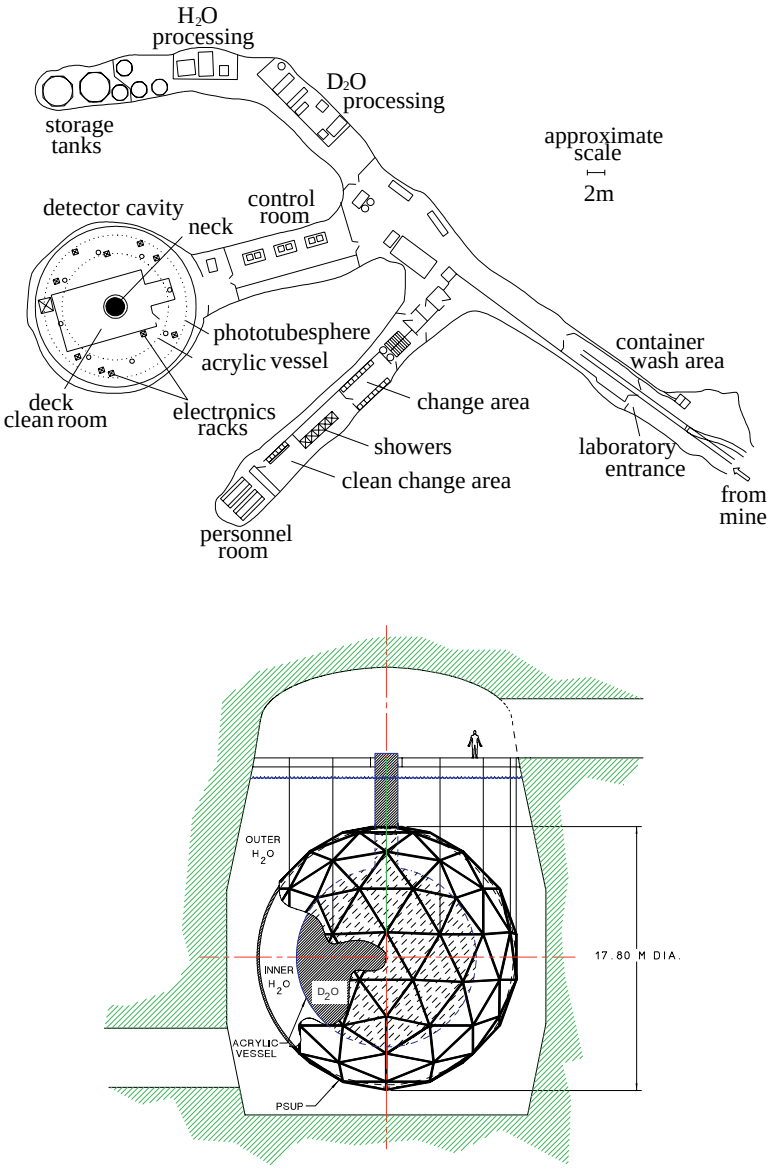

Figure 2.5: Above: layout of the SNO laboratory. Below: the SNO detector. Images taken from [79].

serves as a shield against the radioactive background coming from the structure and the surrounding rock.

The SNO experiments detects solar neutrinos through the three reactions:

$$\begin{aligned} &\text{CC:} && \nu_e + d \to p + p + e^- \\ &\text{NC:} && \nu_\ell + d \to p + n + \nu_\ell \\ &\text{ES:} && \nu_\ell + e^- \to \nu_\ell + e^- \end{aligned}$$

with $\ell = e, \mu, \tau$.

The CC reaction is used to find the energy spectrum of ν_e above the energy threshold $E_\nu^{\text{th,CC}} = 2m_p + m_e - m_d = 1.442\,\text{MeV}$ by measuring the kinetic energy of the final electron, given by $E_\nu - E_\nu^{\text{th,CC}}$. Due to the presence of background, the SNO CC reaction is sensitive to neutrinos of energy larger than 5 MeV, i.e. neutrinos from ^{8}B.

The NC reaction on deuterium can test for neutrino oscillations, as it is equally sensitive to all neutrino flavours, but could not reconstruct the neutrino energy. It has an energy threshold of $E_\nu^{\text{th,NC}} = m_p + m_n - m_d = 2.224\,\text{MeV}$, so that it is also sensitive to Boron neutrinos only.

Since for the ES reaction the electron recoil energy threshold is the same as the one for the CC reaction, the neutrino energy threshold is the same, so that the ES reaction is sensitive to all neutrino flavours of energy larger than 5 MeV.

The SNO collaboration has presented a combined analysis from the three phases of the experiment [81]. The last two phases were characterised, respectively, by the introduction in the heavy water of salt ("salt phase"), and of a grid with three hundred ^{3}He proportional counter tubes (third phase).

Salt helps the detection of neutrons through the reaction

$$n + {}^{35}\text{Cl} \to {}^{36}\text{Cl} + \text{many } \gamma$$

which produces light isotropically, unlike Cherenkov emission, and also allowes to perform more precise measurements well above the low-energy radioactive background, as these photons have an energy of 8.57 MeV.

Helium-3 has a very large cross-section for the capture of thermal neutrons, which produces an energetic proton-triton pair, which in turn results in an electrical pulse in the counter wire.

In the first phase, SNO confirmed the previously observed deficit of solar electron neutrinos [82].

During the salt phase, SNO measured the flux of ^{8}B neutrinos [83]:

$$\Phi_{\mathrm{CC}}^{\mathrm{SNO}} = (1.68 \pm 0.06^{+0.08}_{-0.09}) \times 10^6\,\mathrm{cm}^{-2}\,\mathrm{s}^{-1}$$
$$\Phi_{\mathrm{NC}}^{\mathrm{SNO}} = (4.94 \pm 0.21^{+0.38}_{-0.34}) \times 10^6\,\mathrm{cm}^{-2}\,\mathrm{s}^{-1}$$
$$\Phi_{\mathrm{ES}}^{\mathrm{SNO}} = (2.35 \pm 0.22 \pm 0.15) \times 10^6\,\mathrm{cm}^{-2}\,\mathrm{s}^{-1}$$

with the three reactions presented above. They are clearly not compatible with each other, as the CC flux, corresponding to Φ_{ν_e}, is about 1/3 of the NC one.

The combined fit to the three phases results in a ^{8}B neutrino flux of [81]:

$$\Phi_{^8\mathrm{B}}^{\mathrm{SNO}} = (5.25 \pm 0.16^{+0.11}_{-0.13}) \times 10^6\,\mathrm{cm}^{-2}\,\mathrm{s}^{-1}$$

which is compatible with, and more precise than, the theoretical predictions [59]. A three-flavour neutrino oscillation analysis, combining also results from all other neutrino experiments and KamLAND resulted in:

$$\Delta m^2_{12} = (7.41^{+0.21}_{-0.19}) \times 10^{-5}\,\mathrm{eV}^2$$
$$\tan^2\theta_{12} = 0.446^{+0.030}_{-0.029}$$
$$\sin^2\theta_{13} = (2.5^{+1.8}_{-1.5}) \times 10^{-2}$$

At the time of writing SNO, is currently operating in its SNO+ phase; the experimental setup for their most recent analysis [84] is very similar to that of SNO, with the exception that the acrylic vessel has been filled with normal water H_2O ("water phase"), instead of heavy water, and part of the trigger and the readout system has been upgraded. The resulting ES flux (i.e. the electron neutrino flux) and overall ^{8}B neutrino flux measured by SNO+ after 114.7 days of data are:

$$\Phi_{\nu_e}^{\mathrm{SNO+}} = (2.53^{+0.31}_{-0.28}(\mathrm{stat})^{+0.13}_{-0.10}(\mathrm{syst})) \times 10^6\,\mathrm{cm}^{-2}\,\mathrm{s}^{-1}$$
$$\Phi_{^8\mathrm{B}}^{\mathrm{SNO+}} = (5.95^{+0.75}_{-0.71}(\mathrm{stat})^{+0.28}_{-0.30}(\mathrm{syst})) \times 10^6\,\mathrm{cm}^{-2}\,\mathrm{s}^{-1}$$

which are consistent with the ES results of Super-Kamiokande and with the ^{8}B neutrino flux measured by SNO.

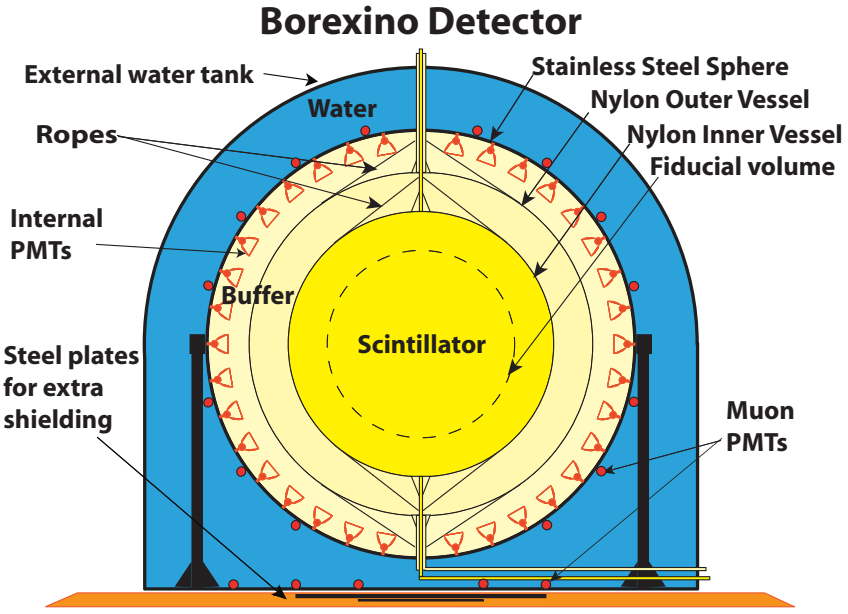

Figure 2.6: Schematic view of the Borexino detector. Figure taken from [85].

2.2.5 Borexino

The Borexino detector [85], schematically shown in Figure 2.6, is a liquid scintillator detector located in the Laboratori Nazionali del Gran Sasso. Its inner part is a stainless steel sphere (SSS), which serves as the container of the scintillator and as the support of the 2212 PMTs. The scintillator volume is then subdivided into in three shells of radii 4.25 m, 5.50 m and 6.85 m, the latter being the radius of the SSS itself. The inner nylon vessel (IV) contains the liquid scintillator solution: pseudocumene (PC, 1,2,4-trimethylbenzene $C_6H_3(CH_3)_3$) as a solvent and the fluor PPO (2,5-diphenyloxazole, $C_{15}H_{11}NO$) as a solute at a concentration of $1.5\,g\,l^{-1}$ The second and the third shell contain PC with a small amount ($5\,g\,l^{-1}$) of DMP (dimethylphthalate, $C_6H_4(COOCH_3)_2$), that is added as a light quencher in order to further reduce the scintillation yield of pure PC. The SSS is immersed in a water tank (WT), which serves both as a powerful shielding against the external background due to γ rays and neutrons from the rock, and as a Cherenkov muon counter and muon tracker thanks to 208 PMTs. The PC/PPO solution provides a high scintillation yield (about 10^4 photons per MeV), a large mean free path for light (about 8 meters) and a fast decay time (about 3 nanoseconds), which are ideal characteristics for energy resolution, precise spatial reconstruction and good $\alpha - \beta$ discrimination.

It appears clear from Figure 2.3 that Borexino is the only experiment that is both able to reconstruct the neutrino energy while being sensitive to the lower end of the solar neutrino spectrum.

Borexino proved to be able to first detect ^{7}Be neutrinos [86, 87], study their day/night asymmetry [88] and their seasonal modulation [89]. In particular, the results from Borexino on the lack of day/night asymmetry of ^{7}Be neutrinos, on their interaction rate [87] and the measurement of ^{8}B neutrinos [90], allowed to restrict the MSW neutrino oscillations to the large mixing angle (LMA) solution at a 90% confidence level.

The data acquisition of Borexino is divided in two phases, I [91] (2007-2010) and II [92] (2011-2016), separated by the purification campaign of the scintillator liquid. Remarkably, the Borexino collaboration has been able to perform the first-ever measurement of *pp*, *pep* and ^{7}Be neutrinos in the energy range 0.19-

2.93 MeV, as well as to set the tightest upper bounds on CNO neutrino [92]:

$$\Phi^{\mathrm{BX}}_{pp} = (6.1 \pm 0.5^{+0.3}_{-0.5}) \times 10^{10}\,\mathrm{cm}^{-2}\,\mathrm{s}^{-1}$$
$$\Phi^{\mathrm{BX}}_{^7\mathrm{Be}} = (4.99 \pm 0.11^{+0.06}_{-0.08}) \times 10^{9}\,\mathrm{cm}^{-2}\,\mathrm{s}^{-1}$$
$$\Phi^{\mathrm{BX}}_{pep,\mathrm{HZ}} = (1.27 \pm 0.19^{+0.08}_{-0.12}) \times 10^{8}\,\mathrm{cm}^{-2}\,\mathrm{s}^{-1}$$
$$\Phi^{\mathrm{BX}}_{pep,\mathrm{LZ}} = (1.39 \pm 0.19^{+0.08}_{-0.13}) \times 10^{8}\,\mathrm{cm}^{-2}\,\mathrm{s}^{-1}$$
$$\Phi^{\mathrm{BX}}_{\mathrm{CNO},95\%\ \mathrm{CL}} < 7.9 \times 10^{8}\,\mathrm{cm}^{-2}\,\mathrm{s}^{-1}$$

for which the MSW-LMA oscillation parameters [93] have been assumed. In this context HZ and LZ refer to a SSM with, respectively, high metallicity and low metallicity. The upper limit on CNO is obtained by setting in the fit a constraint on the ratio of *pp* to *pep* events, which depends on the metallicity hypothesis. More on this will follow in §2.3.

The precision on the Beryllium neutrino flux is better than that of the theoretical prediction of [59].

During phase II, the Borexino collaboration also improved their previous ^{8}B neutrino flux measurement [94]:

$$\Phi^{\mathrm{BX}}_{^8\mathrm{B}} = (2.55^{+0.17}_{-0.19} \pm 0.07) \times 10^{6}\,\mathrm{cm}^{-2}\,\mathrm{s}^{-1}$$

in the case of no flavour conversion. This result is compatible to, even if less precise, the high-precision measurements by Super-Kamiokande.

2.2.6 Future experiments (also) regarding solar neutrinos

Two notable experiments which will regard also the physics of solar neutrinos are the Jiangmen Underground Neutrino Observatory (JUNO), and Hyper-Kamiokande. As these experiments have not collected any data yet, we just provide the interested reader with the relevant design reports and future measurement prospects [95, 96].

JUNO is a multi-purpose underground facility, with a detector consisting a 20 kton liquid scintillator, submerged in a water-Cherenkov detector, on top of which there is a muon tracker. Its main physics goal is to assess the neutrino mass hierarchy, but it is also going to be capable of observing neutrinos from terrestrial and extraterrestrial sources, including supernova burst neutrinos, diffuse supernova neutrino background, geoneutrinos, atmospheric neutrinos, solar

neutrinos, as well as exotic searches such as nucleon decays, dark matter, sterile neutrinos, and so on.

Hyper-Kamiokande is going to be located in the Tochibora mine, 8 km south of Super-Kamiokande, which will host the largest underground water Cherenkov detector. It will employ a ring-imaging water Cherenkov detector technique to detect the neutrino interactions and the possible spontaneous decay of protons and bound neutrons. The highly purified water employed in the detector serves as both target material for the neutrinos coming from the J-PARC proton accelerator and source of nucleons to decay. Apart from nucleon decay and beam neutrino measurements, Hyper-Kamiokande will measure with the highest precision leptonic CP violation and will determine the neutrino mass hierarchy with atmospheric neutrino measurements, probing the standard paradigm for neutrino oscillations in the process.

2.3 The (updated) luminosity constraint

As we have already seen, the theoretical description of the Sun is little more than fifty years old and is still evolving. The first measurements of the neutrinos that correspond directly to sunlight have been obtained only very recently: we refer to the *pp* neutrinos observed by the Borexino collaboration [97]. While the theoretical expectations for the *pp* chain have been verified, the observations of neutrinos coming from the CNO cycle are still missing, and also the relevant theoretical expectations are more uncertain [59]. Observing such neutrinos could clarify persistent doubts about our models of the Sun, and solidify the role of the CNO cycle for stars more massive than the Sun.

The Borexino experiment is currently attempting to detect CNO neutrinos for the first time. An important experimental problem is the background due to beta decays from ^{210}Bi; this problem can be addressed by quantifying the rate of decay of other nuclear species related to ^{210}Bi [98]. The collaboration is, at the time of writing, at work to make this measurement possible [99].

Another equally important difficulty of the measurement is that *pep* neutrinos, which are not precisely known, produce events right in the energy region where neutrinos from the CNO cycle could be observed (see Figure 7 of [92]). An approach to this second problem is based on the knowledge of the connection

$\Phi_i = \varphi_i \times 10^{\alpha_i}$ cm^{-2} s^{-1}	The *pp* chain					The CNO cycle		
i	*pp*	Be	*pep*	B	*hep*	N	O	F
α_i	10	9	8	6	3	8	8	6
GS98	5.99	4.73	1.42	5.38	8.10	2.82	2.06	5.33
PLJ14	6.01	4.53	1.43	4.91	8.23	2.54	1.81	3.93

Table 2.3: Theoretical predictions for the solar neutrino fluxes as in Eq. (2.3) for the two computed SSMs (see §2.3.2 and §2.3.4).

between light and neutrinos, which allows to measure with great precision a linear combination of *pp* and CNO neutrinos, as well as to quantify the *pep* neutrinos.

As various authors have argued (see [100], [101] and references therein) this connection - called the *luminosity constraint* - does not require a detailed model of the Sun. Given the importance of such statement, of some inaccuracies in the expression of the luminosity constraint that have recently emerged [102], and of the current needs of solar neutrino observatories, we examined the constraint anew and in great detail. In particular:

1. we update the values of the physical parameters involved in the discussion;

2. we clarify and verify the hypotheses behind the derivation of the luminosity constraint;

3. we provide an updated and simple analytical expression, for the sake of the experiments in search of neutrinos from the CNO cycle.

2.3.1 The luminosity constraint

The Standard Solar Model (SSM) has proved to be the best tool to understand how the Sun works, and it still is the frontier of helioseismology and solar neutrino physics.

We are particularly interested in it as a way to compute the solar neutrino

fluxes at Earth, which can be expressed as:

$$\Phi_i = \varphi_i \times 10^{\alpha_i} \text{ cm}^{-2}\,\text{s}^{-1} \tag{2.3}$$

where the fluxes are labelled with $i = pp, pep$, Be, B, *hep*, N, O, F according to their production mechanism.

Not surprisingly, the α_i exponents have been stable over time, while the adimensional φ_i factors have been improved and tested with experiments. In Table 2.3 we show the values of φ_i and α_i for the two SSMs presented in this work (see §2.3.2 and §2.3.4). Each model assumes a different solar metallicity which directly influence the prediction for *pep* and CNO neutrinos [92].

After the results of Borexino Phase-II and Super-Kamiokande, discussed in the previous section, we are entering an era of precise solar neutrino measurements, in that the experimental errors are getting close to (and even smaller than, in the case of neutrinos from ^{7}Be and ^{8}B) the theoretical ones.

The experimental uncertainty on the *pp* neutrino flux is, however, still very large, sitting at around 10% [92]. Here the luminosity constraint comes into play, as it allows to link the sum of the fluxes of solar neutrinos to the luminosity in photons of the Sun, which is very well known [62]:

$$L_\odot = 3.8275\,(1 \pm 0.0004) \times 10^{33}\,\text{erg}\,\text{s}^{-1} \tag{2.4}$$

The outstandingly small uncertainty on the solar luminosity compels us to question which approximations are appropriate in deriving a solid luminosity constraint suitable for solar neutrino data analyses.

It is predicted that the Sun burns protons to produce Helium through the *pp* chain, in small measure through the CNO-I cycle, and, to a negligible extent, through the CNO-II cycle. It is important to note that in each of these sets of nuclear reactions the hypothesis of local kinetic equilibrium is just an (excellent) approximation [101]: in fact, the total abundance of certain isotopes, other than ^{4}He, slowly increases over time.

The lifetime of ^{3}He in the solar core is $\gtrsim 10^5$ yr and increases rapidly in the outer parts of the Sun, determining a departure from the local kinetic equilibrium. In the inner region of the Sun, where the kinetic equilibrium with the *pp* chain holds, ^{3}He is burnt to create ^{4}He, while in the outer regions the temperature is too low for such conversion to be effective (see Figure 2.7).

On the other hand, the slow rate of the ^{14}N(p,γ)^{15}O reaction does not allow to close the CNO-cycle and, as a consequence, ^{14}N tends to accumulate (see Figure 2.8), while the abundance of Oxygen is almost constant. As a matter of fact, both ^{3}He and ^{14}N total abundances increase with time (see Figure 2.9).

In addition, in deriving the luminosity constraint, it is also common to assume that the Sun is *stationary*, meaning that the release of energy is due to nuclear reactions only. Relaxing the condition of time independence requires to consider the global change of the total energy E.

The numerical implementation of a SSM already includes all these *out-of-equilibrium* terms in the energy conservation equation, but it is computationally expensive and depends on many physical inputs (e.g. nuclear reaction rates, the solar luminosity, the solar age, heavy-element abundances, radiative opacities) and effects (e.g. Helium and heavy-element diffusion) [103]. In this sense, the luminosity constraint offers a unique tool to pursue a model-independent analysis of the solar neutrino fluxes.

We updated the luminosity constraint to allow for the contribution of the aforementioned out-of-equilibrium terms in a general way, starting from the principles of energy and lepton number conservation.

The fusion of four protons to form a Helium nucleus implies the production of neutrinos and positrons according to:

$$4p \to \alpha + 2\nu_e + 2e^+ \tag{2.5}$$

and releases an amount of heat $Q_\odot \simeq 26.1\,\mathrm{MeV}$. This reaction is atomically equivalent to the fusion of four ^{1}H nuclei into one ^{4}He nucleus, producing two electron neutrinos and liberating an amount of energy equal to:

$$Q_4 := 4M_1 - M_4 = 26.731\,\mathrm{MeV}. \tag{2.6}$$

Such energy goes into photons and neutrinos, so that the solar luminosity can be written as:

$$L = L_\odot + L_\nu \tag{2.7}$$

where $L_\odot$ is the solar luminosity emitted in photons and L_ν is the one emitted in neutrinos, i.e.:

$$L_\nu = 4\pi\,\mathrm{au}^2 \sum_i \langle E_i \rangle\, \Phi_i \tag{2.8}$$

where $\langle E_i \rangle$ is the average energy of the neutrinos resulting from a certain reaction and 1 au is the average Earth-Sun distance.

In order to obtain the luminosity constraint as in [101] only three hypotheses are necessary:

1. energy conservation: all energy that goes into neutrinos and photons comes from the synthesis of one (or more) nuclear species;

2. lepton number conservation: the nuclear fusion processes operating in the Sun inevitably produce neutrinos, which can be used to "tag" such reactions;

3. no element apart from ^{4}He is produced in the Sun.

In §2.3.2 we will relax the last assumption to obtain a general form of the luminosity constraint, which we will then use to compute the contributions to the solar luminosity due to the accumulation of ^{3}He and ^{14}N.

Considering only ^{4}He as accumulating element, the conservation of energy reads:

$$L_\odot + L_\nu = Q_4 \dot{N}(^4\mathrm{He}) \tag{2.9}$$

where $N(^4\mathrm{He})$ is the total number of ^{4}He nuclei in the Sun and $\dot{N}(^4\mathrm{He})$ is its time derivative. As the synthesis of ^{4}He from ^{1}H requires the transformation of four protons into two protons and two neutrons, two neutrinos must be produced in the ensuing β^+ processes. We can then write the corresponding lepton number conservation relation as:

$$4\pi\,\mathrm{au}^2 \sum_i \Phi_i = 2\dot{N}(^4\mathrm{He}) \tag{2.10}$$

as the rate of neutrino production is twice the of ^{4}He production, or, in other words, two neutrinos are produced per ^{4}He nucleus. Substituting Eq. (2.10) in Eq. (2.9), we have that:

$$L_\odot + 4\pi\,\mathrm{au}^2 \sum_i \langle E_i \rangle\, \Phi_i = \frac{Q_4}{2}\, 4\pi\,\mathrm{au}^2 \sum_i \Phi_i \tag{2.11}$$

so that we obtain the standard luminosity constraint:

$$\frac{L_\odot}{4\pi\,\mathrm{au}^2} = \sum_i \left(\frac{Q_4}{2} - \langle E_i \rangle \right) \Phi_i \tag{2.12}$$

Notice that only when substituting the numerical values of Q_4, $\langle E_i \rangle$ (on which we assume negligible uncertainty) as well as choosing which "kind" of neutrinos are produced, the nuclear physics details are needed. We will adopt the values for $\langle E_i \rangle$ provided in Table 2 of [102].

To give an idea of the power of the luminosity constraint, let us assume that only *pp* neutrinos are produced in the Sun: we would then have

$$13.10\,\mathrm{MeV} \times \Phi_{pp} = L_\odot / 4\pi\,\mathrm{au}^2$$

which would yield a *pp* neutrino flux of:

$$\Phi_{pp} = 6.485\,(1 \pm 0.0004) \times 10^{10}\,\mathrm{cm}^{-2}\,\mathrm{s}^{-1}$$

which directly gets the relative error from the solar luminosity.

Including now all the other solar neutrino components, and dividing both sides of Eq. (2.12) by $L_\odot/(4\pi\,\mathrm{au}^2) = 8.4946 \times 10^{11}\,\mathrm{MeV\,cm^{-2}\,s^{-1}}$ we obtain:

$$(1.0000 \pm 0.0004) = \frac{1}{8.4946 \times 10^{11}} \sum_i k_i \varphi_i. \tag{2.13}$$

where the k_i coefficients are,

$$k_i = \left(\frac{Q_4}{2} - \langle E_i \rangle \right) 10^{\alpha_i} \tag{2.14}$$

Their values in units of $\mathrm{MeV\,cm^{-2}\,s^{-1}}$ are listed in Table 2.4.

From the argument above if follows that the luminosity constraint effectively links, within a very small 0.04% uncertainty, the *pp*, Be, *pep*, N and O neutrinos, the other kinds of neutrinos give a negligible contribution.

2.3.2 Tests and refinements

Due to the importance and power of the luminosity constraint, we find it is interesting and useful to accurately test the hypotheses on which it is based. It is possible to allow for the inclusion of other out-of-equilibrium elements simply by adding new terms to Eq. (2.9) and by weighing them according to the amount on the corresponding neutrinos. We will also estimate the effect of the non-nuclear processes of energy production; with these two ingredients, we will obtain an even more refined version of the luminosity constraint.

i	k_i
pp	1.310×10^{11}
Be	1.255×10^{10}
pep	1.192×10^{9}
B	6.630×10^{6}
hep	3.735×10^{3}
N	1.266×10^{9}
O	1.237×10^{9}
F	1.237×10^{7}

Table 2.4: The k_i factors as defined in Eq. (2.14), in units of $\mathrm{MeV\,cm^{-2}\,s^{-1}}$.

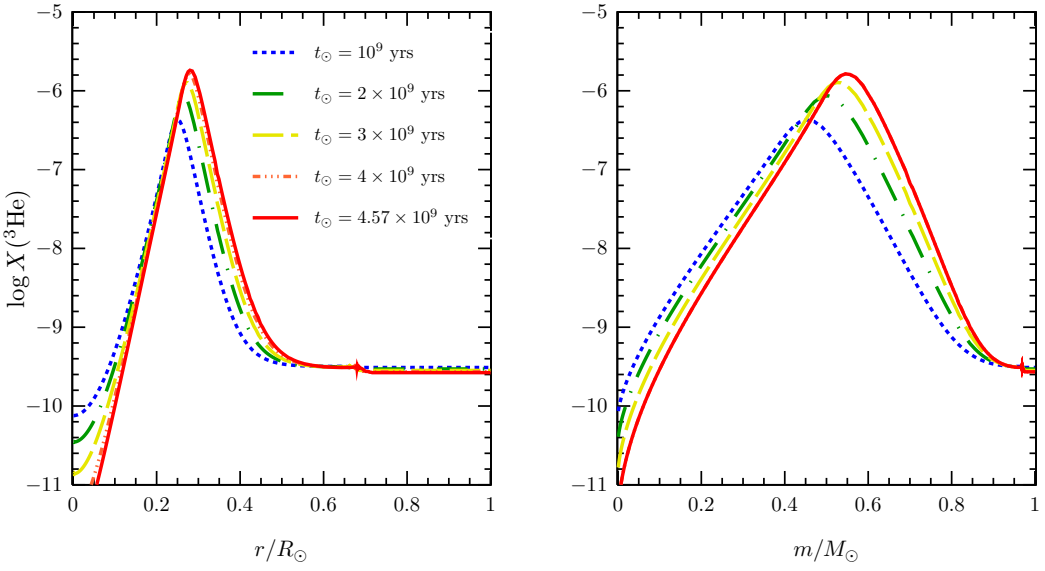

Figure 2.7: ^{3}He mass fraction dependence on the fractional solar radius (left) and mass (right) for 5 different ages of the Sun, adopting the GS98 solar composition. The color code suggests the rise of temperature over time.

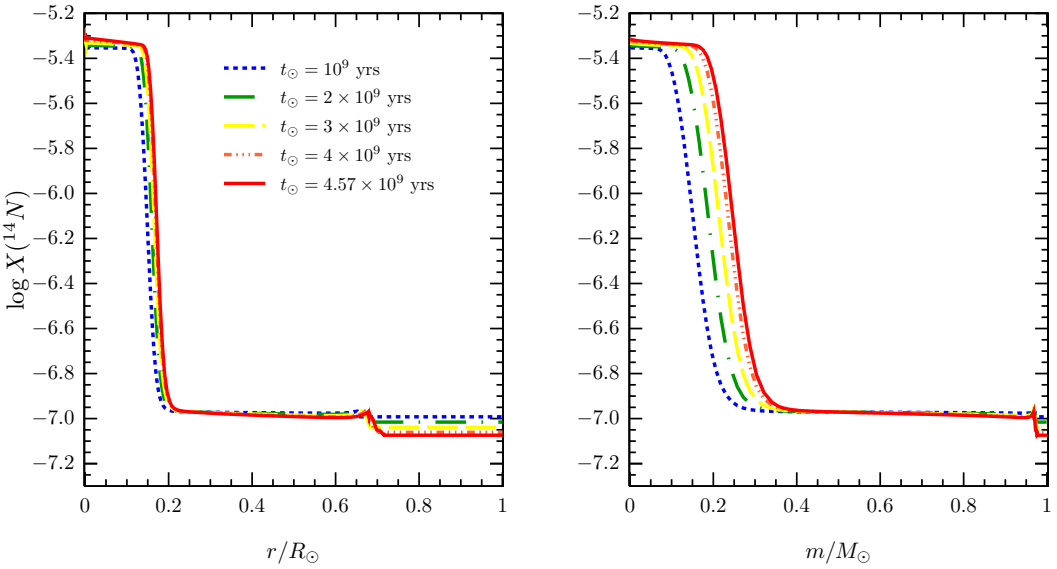

Figure 2.8: Same as Figure 2.7, but relative to the ^{14}N mass fraction.

Formalism In the case of more accumulating elements, taken into account by $N(j)$, the lepton number conservation reads:

$$4\pi \,\mathrm{au}^2 \sum_i \Phi_i = \sum_j c_j \dot{N}(j) \tag{2.15}$$

where c_j counts for the number of electron neutrinos emitted in the production of a nucleus j; for example, as seen before, $c_{^4\mathrm{He}} = 2$. The energy conservation equation (2.9) becomes:

$$L_\odot + L_\nu = \sum_j Q_j \dot{N}(j), \tag{2.16}$$

as now we have allowed for the production of more elements. As before, we can isolate $\dot{N}(^4\mathrm{He})$ from Eq. (2.15) and substitute it into Eq. (2.16), so that:

$$L_\odot + 4\pi \,\mathrm{au}^2 \sum_i \langle E_i \rangle \, \Phi_i = \frac{Q_4}{2} \left[4\pi \,\mathrm{au}^2 \sum_i \Phi_i - \sum_{j \neq ^4\mathrm{He}} c_j \dot{N}(j) \right] + \sum_{j \neq ^4\mathrm{He}} Q_j \dot{N}(j) \tag{2.17}$$

which results in:

$$\frac{1}{4\pi\,\mathrm{au}^2}\left(L_\odot + \sum_{j\neq{}^4\mathrm{He}} L_j\right) = \sum_i \left(\frac{Q_4}{2} - \langle E_i\rangle\right)\Phi_i \tag{2.18}$$

where we have defined:

$$L_j := \left(\frac{c_j Q_4}{2} - Q_j\right)\dot{N}(j). \tag{2.19}$$

In the following, we show that both the *pp* chain and the CNO cycle can be naturally broken into two sub-processes, both leading to the production of one intermediate nuclear species and one neutrino - i.e., $c_j = 1$. Therefore, the sign of L_j depends upon the amount of energy released per neutrino; in particular, it is positive if Q_j/c_j is smaller than $Q_4/c_{^4\mathrm{He}}$ - assuming that the intermediate species accumulates over time, i.e. $\dot{N}(j) > 0$.

Nuclear species that accumulate in the Sun While in the innermost part of the Sun the reactions are in kinetic equilibrium, this is not so in the external, colder regions: there are zones of out-of-equilibrium nuclear fusion, that can lead to accumulation of certain nuclear species besides ^{4}He.

In order to identify which are the other elements that accumulate, we have to refer to the nuclear fusion processes in the Sun. In the *pp* chain, ^{3}He is the bottleneck of the chain, and we argue that this specie is currently accumulating; in the CNO cycle, instead, it is ^{14}N that accumulates, due to the slowness of the subsequent proton capture reaction, that separates the CNO-I cycle in two sub-cycles. For a quantitative statement, we need to know the production rate of these elements, i.e. the time derivative of their number abundances $\dot{N}(j)$. The generic $\dot{N}(j)$ can be expressed as:

$$\dot{N}(j) = \frac{\mathrm{d}N(j)}{\mathrm{d}t} = \frac{1}{A_j}\frac{\mathrm{d}X(j)}{\mathrm{d}t} N_A M_\odot \tag{2.20}$$

where N_A is the Avogadro number, $X(j) = M_j/M_\odot$ is the mass fraction of the j-nucleus, and $A(j)$ the relative atomic mass number.

We computed the number abundances of ^{3}He and ^{14}N using two different SSMs, adopting both the GS98 [104] and the PLJ14 [105] solar models in the

Model	$\dot{N}(^3\mathrm{He})$ [s^{-1}]	$\dot{N}(^{14}\mathrm{N})$ [s^{-1}]	$L_{^3\mathrm{He}}$[erg s^{-1}]	$L_{^{14}\mathrm{N}}$[erg s^{-1}]	L_{g} [erg s^{-1}]
GS98	2.47×10^{35}	2.19×10^{35}	2.55×10^{30}	5.78×10^{29}	2.48×10^{30}
PLJ14	1.96×10^{35}	2.12×10^{35}	2.02×10^{30}	5.62×10^{29}	3.13×10^{30}

Table 2.5: The accumulation rates of ^{3}He, ^{14}N, their corresponding luminosities Eq. (2.19) and the luminosity connected to the gravitational effects of the Sun. These are the most relevant quantities involved in the formulation of the revised luminosity constraint, and they are reported both for the GS98 and the PLJ14 models.

run of the FUNS stellar evolutionary code [106, 61]. We used the same input physics as in [61], except for the solar luminosity, which has been taken from [62]. In Table 2.5 we show the ensuing predictions for $\dot{N}(^3\mathrm{He})$ and $\dot{N}(^{14}\mathrm{N})$.

In order to calculate the contribution of these elements to the luminosity constraint, as described by Eq. (2.18), we also need to quantify the energy released in the production of such nuclei, i.e.,

$$Q_3 := M_3 - 3M_1 = 6.936\,\mathrm{MeV}$$
$$Q_{14} := M_{12} + 2M_1 - M_{14} = 11.71\,\mathrm{MeV}$$

Finally, as the production of ^{3}He and ^{14}N is always accompanied by the emission of one electron neutrino, their c_j factors are both equal to 1. In Tab. 2.5 we also show the corrective terms to the luminosity constraint due to the accumulation of ^{3}He, ^{14}N according to Eq. (2.19). We find that the corrections to the luminosity constraint are important, being larger than the present uncertainty on the solar luminosity.

Cross-check of the effect of ^{14}N accumulation Note that the correction to the solar luminosity due to the accumulation of ^{14}N can be computed according to the connection among $\dot{N}(^{14}\mathrm{N})$, Φ_{O} and Φ_{N}, in the assumption that the $^{12}\mathrm{C} \to {}^{14}\mathrm{N}$ and $^{15}\mathrm{O} \to {}^{12}\mathrm{C}$ branches of the CNO-I cycle proceed fast. In fact, the emission of a Nitrogen neutrino in the reaction $^{13}\mathrm{N}(\mathrm{e}^+\,\nu_e)^{13}\mathrm{C}$ precedes the production of ^{14}N; in the same way, every time that a ^{14}N nucleus is destroyed, an "Oxygen neutrino" is emitted in the reaction $^{15}\mathrm{O}(\mathrm{e}^+\,\nu_e)^{15}\mathrm{N}$. This means that the flux

difference $\Phi_{\rm N} - \Phi_{\rm O}$ keeps track of the accumulation of ^{14}N as

$$\dot{N}(^{14}\mathrm{N}) \simeq 4\pi\,\mathrm{au}^2(\Phi_{\rm N} - \Phi_{\rm O}) = 2.12 \times 10^{35}\,\mathrm{s}^{-1}, \tag{2.21}$$

which is sufficiently close to the value reported above, considering the 15%-20% uncertainties on these neutrino fluxes [102].

It is possible to improve this argument by considering also the presence of the CNO-II cycle, which would be tagged by the neutrinos produced in the process $^{17}\mathrm{F}(\mathrm{e}^+\,\nu_e)^{17}\mathrm{O}$, i.e. by the Fluorine neutrinos $\Phi_{\rm F}$; since also this process precedes the production of ^{14}N, we can write that

$$\dot{N}(^{14}\mathrm{N}) \simeq 4\pi\,\mathrm{au}^2(\Phi_{\rm N} + \Phi_{\rm F} - \Phi_{\rm O}) = 2.27 \times 10^{35}\,\mathrm{s}^{-1} \tag{2.22}$$

This means that a possible test of out-of-equilibrium processes in the Sun is to look for a non-zero value of $\Phi_{\rm N} + \Phi_{\rm F} - \Phi_{\rm O}$; this is a very demanding task as it requires very high precision, considering that the spectra of $\Phi_{\rm F}$ and $\Phi_{\rm O}$ are almost identical.

Non-stationary luminosity constraint It is common, in deriving the luminosity constraint, to assume that the Sun is stationary and in thermal equilibrium, and that the nuclear fusion reactions are responsible for the production of energy. This is in general an excellent approximation, as the gravitational luminosity, i.e. the amount of power related to the expansion of the Sun over time, is $L_{\rm g} = \text{few} \times 10^{-4} L_\odot$ [107, 108]. In light of the small uncertainty on the new estimate of the solar luminosity [62] we can refine Eq. (2.16) by including the amount of energy $L_{\rm g}$ lost by gravitational expansion as well:

$$L_\odot + L_\nu = \sum_j Q_j \dot{N}(j) - L_{\rm g} \tag{2.23}$$

For a star evolving in time, $L_{\rm g}$ simply represents the negative time derivative of the total energy of the star $-\partial E/\partial t$, which can be computed within the SSM.

We found that, in our models, $L_{\rm g}$ and $-\partial E/\partial t$ deviate by $\sim 10^{-7} L_\odot$, a value safely below the uncertainty of the present solar luminosity (i.e. 0.04%). For this reason we adopted the derived values for $L_{\rm g}$ (see Table 2.5), for both GS98 and

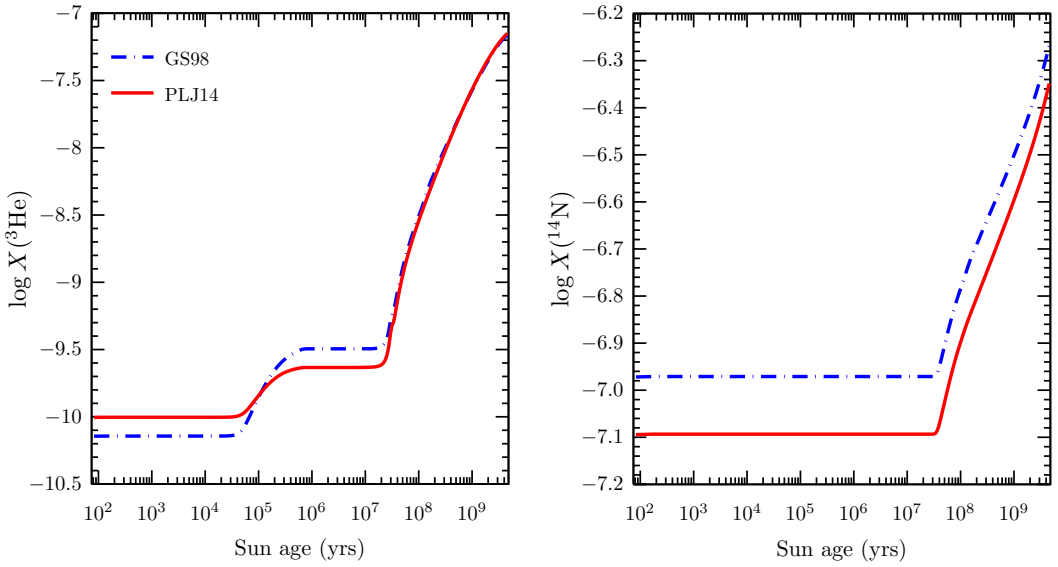

Figure 2.9: Temporal evolution of the total ^{3}He (left) and ^{14}N (right) mass fractions, adopting both GS98 (blue, dash-dotted line) and PLJ14 (red, solid line) solar compositions.

PLJ14 models, in computing the revised luminosity constraint. Comparing the values of Table 2.5, one can conservatively fix the value of $L_{\rm g}$ to:

$$L_{\rm g} = (2.805 \pm 0.325) \times 10^{30}\,{\rm erg\,s^{-1}}$$

which corresponds to $(7.33 \pm 0.85) \times 10^{-4} L_\odot$.

Summary We are now ready to include in the luminosity constraint the effects of the accumulation of ^{14}N and ^{3}He, as well as that due to gravitational expansion. From Eq. (2.23) and Eq. (2.18) we get:

$$\frac{1}{4\pi\,{\rm au}^2}\left(L_\odot + L_{^3{\rm He}} + L_{^{14}{\rm N}} + L_{\rm g}\right) = \sum_i \left(\frac{Q_4}{2} - \langle E_i\rangle\right)\Phi_i \qquad (2.24)$$

The values of the new quantities that appear in the equation above are given in Table 2.5 for the two SSMs considered in this work.

Before proceeding, and in order to recap, let us discuss the various terms in Eq. (2.24). The reason for the sign of the first two terms after $L_\odot$ has been already explained after Eq. (2.19) - note that in the case of ^{14}N, the $Q_4/2 - \langle E_{\rm N}\rangle$ term is particularly small, as the production of ^{14}N releases an amount of energy slightly smaller than $Q_4/2$.

Next, we have the term due to gravitational energy. The Sun is steadily increasing its inner temperature and luminosity; the gravitational energy of the Sun is gained at the expense of nuclear energy, and so the same amount of nuclear reactions (and thus of neutrinos) would correspond to a photon luminosity diminished by $L_{\rm g}$. Now, since the solar luminosity is fixed by observations, and the three new terms are all positive, this means that their net effect is to increase the number of expected neutrinos.

The net result of these new terms can be recast in the same form of Eq. (2.13), namely

$$(1.0000 \pm \sigma) = \frac{1}{8.5072 \times 10^{11}} \sum_i k_i \varphi_i. \qquad (2.25)$$

where the values of the k_i is still the one given in Table 2.4.

The relative error σ in the previous equation can be evaluated with different procedures; hereafter we discuss the least and most conservative ones.

The least conservative approach would be considering that the values of $L_{^3\mathrm{He}} + L_{^{14}\mathrm{N}} + L_{\mathrm{g}}$ for the two SSMs agree so well that the value $\sigma = 0.0004$ remains unaffected.

The most conservative procedure is to say that the absolute error on such sum is itself, i.e. $\delta L = L_{^3\mathrm{He}} + L_{^{14}\mathrm{N}} + L_{\mathrm{g}}$; in this case $\sigma = 0.0015$, that is, it increases by about 4 times.

In any case, σ in Eq. (2.25) is very small when compared to the current needs, so that we can conclude that the luminosity constraint provides us with a very useful and precise tool for the study of the solar neutrino fluxes.

2.3.3 Comparison with the literature

In this section we compare our methodology to the two main previous approaches to the luminosity constraint; we highlight where steps forward were taken and where our updates are relevant.

The first benchmark work on the luminosity constraint is, in our opinion, Bahcall's [101], in which he states:

> If nuclear fusion reactions among light elements are responsible for the solar luminosity, then a specific linear combination of solar neutrino fluxes must equal the solar constant [...]
>
> $$\frac{L_\odot}{4\pi\,\mathrm{au}^2} = \sum_i \left(\frac{\alpha_i}{10\,\mathrm{MeV}}\right) \Phi_i$$
>
> where $L_\odot$ is the solar luminosity measured at the earth's surface and 1 au is the average Earth-Sun distance. The coefficient α_i is the amount of energy provided to the star by nuclear fusion reactions associated with each of the important solar neutrino fluxes, Φ_i.

In his work he divides, as we do in Eq. (2.13), the equation above by the left-hand side:

$$1 = \frac{4\pi\mathrm{au}^2}{L_\odot} \sum_i \left(\frac{\alpha_i}{10\,\mathrm{MeV}}\right) \Phi_i$$

The analogous factors to Bahcall's α_i are:

$$\alpha_i = 10^{-\gamma_i - 1} k_i$$

i	α_i [101]	$10^{-\gamma_i-1}k_i$ (this work)
pp	1.309 87	1.309 87
pep	1.191 93	1.192 05
hep	0.373 70	0.373 55
Be	1.260 08	1.255 25
B	0.663 05	0.663 05

Table 2.6: The matching of Bahcall's formalism from [101] (α_i column) to ours.

where the $\gamma_i + 1$ comes from the 10 MeV the α_i factors are divided by.

It should be noted that this correspondence does not hold for $i \in \{\text{C, N, O}\}$ as Bahcall's definitions are:

$$\alpha_{\text{N}} = \frac{M_{12} + M_1 - M_{13} - \langle E_{\text{N}} \rangle}{10\,\text{MeV}} = 0.345\,77 \tag{2.26}$$

$$\alpha_{\text{O}} = \frac{3M_1 + M_{13} - M_4 - M_{12} - \langle E_{\text{O}} \rangle}{10\,\text{MeV}} = 2.157\,06 \tag{2.27}$$

$$\alpha_{\text{F}} = \frac{M_{16} + M_1 - M_{17} - \langle E_{\text{F}} \rangle}{10\,\text{MeV}} = 0.2363 \tag{2.28}$$

α_{N}, α_{O}, α_{F} would be respectively 0.345 70, 2.157 and 0.2361 with the use of the modern values of the atomic masses. The matching of our formalism and his is shown in Tab. 2.6, from which it is evident that the factors are very close to each other. There is, though, a notable exception, i.e. that of α_{Be}: in the computation of that factor, Bahcall states:

> [...] one must average over the two ^{7}Be neutrino lines with the appropriate weighting *and include the γ-ray energy from the 10.3% of the decays that go to the first excited state of ^{7}Li.*

We believe that this procedure leads to double counting the largest neutrino energy can have in such decay, as first noted in [102].

The second benchmark work we compare our results to is [102]. There is perfect agreement with the values we use and list in the rightmost column of

Tab. 2.6 with those from [102]. However, also in [102] the treatment of CNO neutrinos has been different from that in the present work: in it, the CNO cycle is seen as a sequence of two sub-cycles from the start, due to the slowness of the reaction $^{14}\mathrm{N}(p,\gamma)^{15}\mathrm{O}$. In this way, the author considered immediately the accumulation of $^{14}\mathrm{N}$, which we introduced only in a second moment. In [102] a different value for the solar luminosity has been used, which is $L_\odot = 3.8418\,(1 \pm 0.004) \times 10^{33}\,\mathrm{erg\,s^{-1}}$, to be compared with the one that we used here $L_\odot = 3.8275\,(1 \pm 0.0004) \times 10^{33}\,\mathrm{erg\,s^{-1}}$

In order to compare our result with that of [102], we restart from Eq. (2.34):

$$\Phi_{pp} + 1.646\,\Phi_{\mathrm{N}} = 6.007\,(1 \pm 0.2\%) \times 10^{10}\,\mathrm{cm^{-2}\,s^{-1}}$$

which is the analogous of

$$\Phi_{pp} + 0.93\Phi_{\mathrm{CNO}} = 6.02\,(1 \pm 0.5\%) \times 10^{10}\,\mathrm{cm^{-2}\,s^{-1}}$$

in [102]. We can try to match the two formalisms considering that in [102]:

$$\Phi_{\mathrm{CNO}} = \Phi_{\mathrm{N}} + \Phi_{\mathrm{F}} + \Phi_{\mathrm{O}} \approx (1 + 0.72)\Phi_{\mathrm{N}} \tag{2.29}$$

$$\delta\Phi_{\mathrm{CNO}} = \Phi_{\mathrm{N}} + \Phi_{\mathrm{F}} - \Phi_{\mathrm{O}} \approx (1 - 0.72)\Phi_{\mathrm{N}} \tag{2.30}$$

$$\sum_i \left(1 - \frac{2\,\langle E_i \rangle}{Q_4}\right) \Phi_i - 0.123\,\delta\Phi_{\mathrm{CNO}} = \frac{2L_\odot}{4\pi\,\mathrm{au}^2} \tag{2.31}$$

which would then result into:

$$\Phi_{pp} + 0.937\Phi_{\mathrm{CNO}} = 6.007\,(1 \pm 0.2\%) \times 10^{10}\,\mathrm{cm^{-2}\,s^{-1}}$$

The difference in the coefficient in front of Φ_{CNO} is most likely due to roundoff.

From these comparisons we can state that our derivation is the simplest, despite sharing the same fundamental hypotheses as [101]. We believe that the way we include the accumulation of $^{14}\mathrm{N}$ is less model dependent and more transparent with respect to the one in [102], which, however, retains important physical insight.

2.3.4 An application to the search for CNO neutrinos

In the view of the experimental state-of-the-art of solar neutrino measurements, it is timely and useful to illustrate the use of the luminosity constraint to improve the search for CNO neutrinos.

From Tab. 2.4 it is clear that neutrinos from CNO, in particular N and O neutrinos, play an important role in the determination of φ_{pp} in the context of the luminosity constraint, which helps connecting φ_{pp} and φ_{CNO}. In fact, the luminosity constraint by itself is not enough to improve our knowledge on these neutrino fluxes: however, when further theoretical information on the Φ_{pep}/Φ_{pp} and on the $\Phi_{\mathrm{O}}/\Phi_{\mathrm{N}}$ ratios is provided, then a stringent relation between the *pp* and CNO fluxes can be obtained.

At first glance, the use of this theoretical input would seem to introduce model dependence to the application of the luminosity constraint, but this is not the case. The ratio of the *pp* and *pep* reaction rates is fixed by nuclear physics [56], and such ratio is assumed also for the *pp* and *pep* neutrino fluxes, which, a priori, could be different due to the impact of the whole ensemble of processes, nuclear and hydrodynamical, occurring in the Sun. Comparing how the *pep* to *pp* neutrino fluxes change with different metallicities, we get:

$$\Phi_{pep}/\Phi_{pp}|_{\mathrm{GS98}} = 2.367 \times 10^{-3}$$
$$\Phi_{pep}/\Phi_{pp}|_{\mathrm{PLJ14}} = 2.376 \times 10^{-3}$$

The relative difference of $\delta = -0.38\%$ shows that there is no significant model dependence is introduced with such hypothesis.

Regarding the ratio of N and O neutrinos, if we assume that only ^{4}He accumulates, its value is exactly 1, due to the kinetic equilibrium of all elements in the CNO cycles. In the experimental analyses, however, the ratio $\Phi_{\mathrm{O}}/\Phi_{\mathrm{N}}$ is fixed to be different from 1, which means that there must be accumulation of some element between ^{13}C and ^{15}N, in amounts dependent upon the adopted Solar Model. In the two cases that we calculated, the ratios are:

$$\Phi_{\mathrm{O}}/\Phi_{\mathrm{N}}|_{\mathrm{GS98}} = 0.732$$
$$\Phi_{\mathrm{O}}/\Phi_{\mathrm{N}}|_{\mathrm{PLJ14}} = 0.713$$

which result in a relative difference of $\delta = 2.76\%$. This affects the luminosity constraint so slightly (less than 0.02%) that model dependence is not a significant issue also in this regard.

We can then safely fix such ratios of neutrino fluxes to:

$$\Phi_{pep}/\Phi_{pp} = 2.37 \times 10^{-3}$$
$$\Phi_{\mathrm{O}}/\Phi_{\mathrm{N}} = 0.72$$

Moreover, after Borexino phase-II [92], the ^{7}Be neutrinos flux is known with a precision better than that of the theoretical prediction, so that we can fix:

$$\Phi_{^7\mathrm{Be}} = (4.99 \pm 0.11^{+0.06}_{-0.08}) \times 10^9\,\mathrm{cm}^{-2}\,\mathrm{s}^{-1}$$

We are finally ready to put everything together, starting by writing Eq. (2.13) with a highlight on all relevant terms:

$$(1 \pm 0.0004) = 0.1542\,\varphi_{pp} + 0.0148\,\varphi_{\mathrm{Be}} + 0.0014\,\varphi_{pep} + 0.0015\,\varphi_{\mathrm{N}} + 0.0015\,\varphi_{\mathrm{O}}$$

introducing the ratios discussed above, we have:

$$(1 \pm 0.0004) = 0.1542\,\varphi_{pp} + 0.0148\,\varphi_{\mathrm{Be}} + 0.0025\,\varphi_{\mathrm{N}} \tag{2.32}$$

and now we can subtract the Beryllium contribution:

$$(0.926 \pm 0.002) = 0.1542\,\varphi_{pp} + 0.0025\,\varphi_{\mathrm{N}} \tag{2.33}$$

so that, isolating Φ_{pp}:

$$\Phi_{pp} + 1.646\,\Phi_{\mathrm{N}} = 6.007\,(1 \pm 0.2\%) \times 10^{10}\,\mathrm{cm}^{-2}\,\mathrm{s}^{-1} \tag{2.34}$$

In order to include the refinements described in §2.3.2, it is sufficient to replace the central value of the right-hand side of Eq. (2.34) with the values given in Table 2.7. If one prefers to treat the errors conservatively, as discussed after Eq. (2.25), it is enough to replace the errors 0.2% with 0.25%.

out of equilibrium corrections	GS98	PLJ14
none	6.007	6.007
^{3}He	6.011	6.010
^{3}He + ^{14}N	6.012	6.011
^{3}He + ^{14}N + $L_{\rm g}$	6.016	6.017

Table 2.7: The central value, in units of $10^{10}\,{\rm cm}^{-2}\,{\rm s}^{-1}$, of the luminosity that constrains with 0.2% (0.25% in the more conservative approach) precision the linear combination of $\Phi_{pp} + 1.646\,\Phi_{\rm N}$ in all the cases covered in this work.

3

Atmospheric neutrinos

"What are those huge round things?" said Nino to the photon.
"Those are the atoms of the atmosphere; you neutrinos will just whiz by without even noticing, but they can mean a lot of trouble for us, and especially for the protons" answered the photon.
Nino the neutrino

In section 3.1 we are going to review the theoretical expectations about atmospheric neutrinos, both in terms of production, which is tightly connected to cosmic rays, and oscillation through the atmosphere.

In section 3.2 we will talk about the experiments that obtained the most important results in this field, and finally, in section 3.3 we will present the work, which is my original contribution, on the connection between the cosmic-ray knee and the flux of atmospheric neutrinos.

The articles I worked on and that are relevant for this chapter are [3, 4].

3.1 Theoretical expectations

Here we present an overview, based on [6, 45], of the atmospheric neutrino phenomenology.

3.1.1 The components of the atmospheric neutrino spectrum

Atmospheric neutrinos had not been studied above 1 TeV before IceCube, but they can be predicted, within uncertainties linearly increasing from $\lesssim 10\%$ at 100 GeV to about 30% at 1 PeV, from the observed flux of cosmic rays and the theory of strong interactions. These numbers refer to our particular computations, used in [3, 4], which feature a fixed hadron interaction model, which is another source of uncertainty (around 10% at 100 GeV up to $30-40\%$ at 100 TeV [109]).

Atmospheric neutrinos are produced in the collisions of the cosmic rays, which thus take the name of primaries, on the nuclei in the atmosphere. Cosmic rays are mainly (90%) protons and (9%) helium nuclei, but also heavier nuclear species are present. As mentioned in 1.3.3, these collisions create numerous particles, named secondaries, among which mesons, like pions and kaons; these mainly[1] decay into muons, according to:

$$\pi^{\pm} \to \mu^{\pm} + \nu_{\mu}(\overline{\nu}_{\mu}) \sim 100\% \qquad K^{\pm} \to \mu^{\pm} + \nu_{\mu}(\overline{\nu}_{\mu}) \sim 63.5\%$$

The neutrinos produced in the decay of pions and kaons constitute the *conventional* component of the atmospheric neutrino spectrum. The other component of the atmospheric neutrino spectrum, yet to be measured, is the *prompt* one, which is supposed to be produced in the decay of heavy, charmed particles. The most relevant parents for prompt neutrinos are $D^{\pm}$, D^0, D_s and Λ_C; prompt tau neutrinos are mostly produced in the decay of τ leptons.

There are other good reasons to distinguish these two components, as we will now see: their spectrum, angular distribution, and flavor composition are different, and thus experimentally distinguishable - in principle.

Conventional neutrinos If the muon produced by the pion or kaon decay has sufficiently low energy, it decays in the atmosphere and produces neutrinos according to:

$$\mu^+ \to e^+ + \nu_e + \overline{\nu}_{\mu} \qquad \mu^- \to e^- + \overline{\nu}_e + \nu_{\mu}$$

[1] Kaons have a 5% probability of decaying into $\pi^0 + e + \nu_e$, and there is also the $K_L^0 \to \pi + e + \nu_e$ contribution.

This happens when the muon decay length is smaller than its typical production height ($\sim$ 15 km), i.e. for $E_\mu \lesssim 2.5\,\text{GeV}$. The (unoscillated) flavour ratios at Earth for $E_\mu \lesssim 2.5\,\text{GeV}$ would then be:

$$(\mathcal{F}_{\nu_e} : \mathcal{F}_{\nu_\mu} : \mathcal{F}_{\nu_\tau}) = (1 : 2 : 0) \tag{3.1}$$

where $\mathcal{F}_x$ is the sum of the flux of the neutrinos and antineutrinos of a certain flavour. For higher muon energies, muons do not decay in the atmosphere, and thus it is expected that $\mathcal{F}_{\nu_\mu} \gg \mathcal{F}_{\nu_e}$. In the conventional component of the atmospheric neutrino spectrum there are no tau neutrinos at production.

The two-body pion and kaon decays produce muons and neutrinos with average energies given by:

$$\frac{\langle E_\mu \rangle}{E_\pi} = 0.79 \qquad \frac{\langle E_\nu \rangle}{E_\pi} = 0.21$$

$$\frac{\langle E_\mu \rangle}{E_K} = 0.52 \qquad \frac{\langle E_\nu \rangle}{E_K} = 0.48$$

due to the fact that the muon mass is 105.7 MeV, i.e. very close to the pion mass of 139.6 MeV, and thus gets most of the energy in the decay. Kaons, on the other hand, are much heavier, with a mass of 493.7 MeV, and thus allow for a more even distribution of the energy in the two-body decay.

If $\gamma = -2.7$ is the slope of the cosmic-ray spectrum in the energy range relevant for atmospheric neutrinos, the expected slope of the conventional component is $\propto E^{\gamma-1} = E^{-3.7}$, due to the fact that the higher the pion/kaon energy, the larger the probability that it interacts and loses energy before decaying. The discrimination between the interaction-dominated regime and the decay-dominated one is done comparing the typical lengths, which are introduced in Eq. (3.3) - the smaller the relative length, the more important the process. For pions interactions are more relevant than decay for $E\cos\theta \gtrsim \epsilon_\pi = 115\,\text{GeV}$[2], while for kaons this happens for $E\cos\theta \gtrsim \epsilon_K = 850\,\text{GeV}$ [45]; for this reason, conventional neutrinos mainly come from kaons at higher energies.

[2]The cosine of the azimuthal angle is indicative of the importance of the trajectory of the particles, as down-going pions or kaons are less likely to have time decay than horizontal-going ones; it is not meant to be analytically accurate.

Due to the long lifetime of pions and kaons ($\tau_{\text{rest}} \sim 10^{-8}\,\text{s}$), the more atmosphere is traversed, the larger the flux of conventional neutrinos: this is why the conventional neutrino angular distribution goes roughly like $|\cos\theta|^{-1}$, where θ is the azimuthal angle, i.e. $\theta = 0$ for the upward direction and $\theta = \pi$ for the downward one - more on this will follow in the later sections.

Prompt neutrinos This component of the atmospheric neutrino flux comes mainly from the decay of heavy mesons $D^{\pm}$, D^0, D_s, Λ_C, and of the τ lepton, which is the main producer of prompt tau neutrino. Their lifetime at rest is about $10^{-12}\,\text{s}$ and $10^{-13}\,\text{s}$ for the tau lepton, which causes such particles to decay almost immediately (hence the name prompt) and produce neutrinos. This is why the spectrum of prompt neutrinos is predicted to closely resemble that of cosmic rays, which is $\propto E^{-2.7}$ in the energy range relevant for prompt neutrinos.

Also due to the fact that the parent mesons decay almost immediately, the prompt neutrino flux is expected to be isotropic, except above hundreds of TeV, when the absorption of neutrinos in the Earth becomes relevant. For recent observations on this, see [110] and references therein.

Finally, its flavour ratio at production is expected to be about $(\mathcal{F}_{\nu_e} : \mathcal{F}_{\nu_\mu} : \mathcal{F}_{\nu_\tau}) = (1 : 1 : 0.1)$, as tau leptons are rarer than heavy mesons, which in turn decay in almost equal amounts in ν_e and ν_μ.

3.1.2 Cosmic rays and their collisions on the atmosphere

A few words about the cosmic ray (CR) spectrum, shown in figure 3.1, are now necessary, given their "parental role" in the context of atmospheric neutrinos.

The cosmic-ray spectrum Cosmic rays are charged nuclei which come from outside of the solar system, with the exception of very low energy cosmic rays coming from solar flares. This first statement is based on the fact that they are observed isotropically and reach energies which require a much more powerful accelerator than the Sun. The Sun, however, has an impact on their flux, as its wind modulates the CR flux below about 10 GeV proportionally to its 11-year cyclical activity. Above a few GeV, the CR flux can be described with a series of

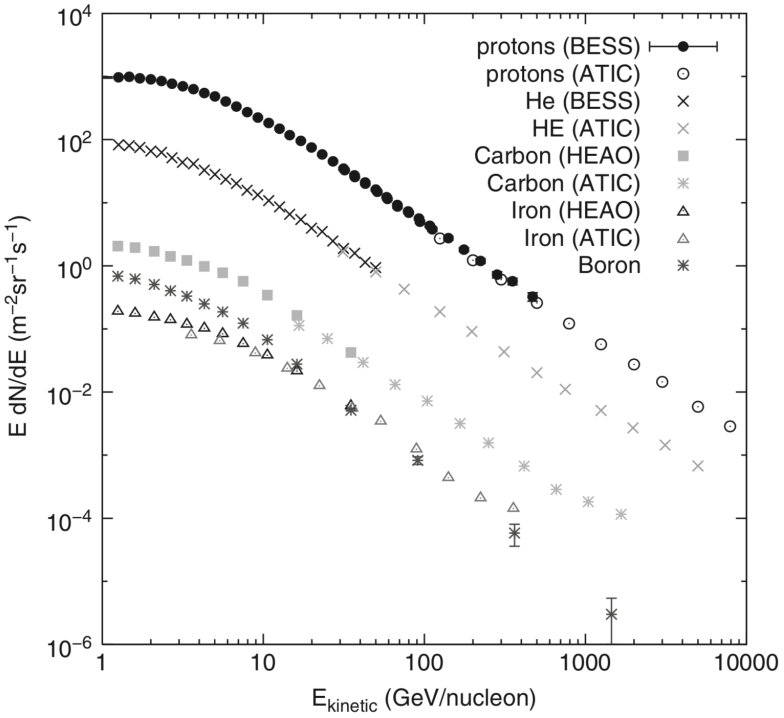

Figure 3.1: The energy spectra of several components of the cosmic rays. For energies smaller than 10 GeV/nucleon the solar wind causes a modulation in the flux. Figure taken from [45].

power laws[3]:

$$\frac{\mathrm{d}N}{\mathrm{d}E} \propto \begin{cases} E^{-2.7} & 10^{10}\,\mathrm{eV} \lesssim E \lesssim 10^{15}\,\mathrm{eV} \\ E^{-3.1} & 10^{15}\,\mathrm{eV} \lesssim E \lesssim 10^{18}\,\mathrm{eV} \\ E^{-2.6} & 10^{18}\,\mathrm{eV} \lesssim E \lesssim 10^{20}\,\mathrm{eV} \end{cases}$$

At $10^{20}\,\mathrm{eV}$ the CR spectrum apparently cuts off, which may be an indication of the predicted Greisen-Zatsepin-Kuzmin (GZK) effect [112], i.e. the resonant interaction of CR protons with the CMB photons ($E_{\gamma,\mathrm{CMB}} \simeq 0.235\,\mathrm{meV}$). In this reaction protons either lose energy or are disintegrated according to:

$$p + \gamma_{\mathrm{CMB}} \to \Delta^+ \to \begin{cases} p + \pi^0 \\ n + \pi^+ \end{cases} \qquad E_{p,\mathrm{th}} \approx 5 \times 10^{19}\,\mathrm{eV}$$

GZK neutrinos are expected to be produced in the decay of the eventual final-state π^+ [113].

The transition regions are known as the "knee", around few PeV, and the "ankle", around few EeV, as visible from figure 1.3. They are usually interpreted respectively as the end of the spectrum of galactic accelerators and the emergence of extragalactic particles, but this picture is not final.

Before moving on, we find it necessary to clarify that even if up to now we have been referring to energy, the more relevant quantity for cosmic rays, at least in the case of acceleration and propagation through magnetic fields, is the rigidity $R := E/Z$. The knee is the "envelope" of the change of slope in the *energy* spectrum of the various elemental components of the CR spectrum, for which the change of slope in the *rigidity* spectrum occurs at the same value of R.

Now we find it useful to cover the formalism of cascade equations, which is used to compute the flux of secondary particles produced in the atmosphere by the impinging cosmic rays.

Cascade equations The interaction of CRs entering the Earth atmosphere induces the generation of hadronic showers, accompanied by the production of

[3]The extremely high-energy behavior is even more complex than here reported, which serves as a general introduction; we refer to [111] for the latest details.

neutrinos. Following [45], the development of the cascade of particles of type i in the atmosphere is described by solving the transport equation:

$$\frac{\mathrm{d}N_i(E_i,X)}{\mathrm{d}X} = -\frac{N_i(E_i,X)}{\lambda_i} - \frac{N_i(E_i,X)}{d_i} + \sum_j \int_E^\infty \mathrm{d}E_j \, \frac{F_{ji}(E_i,E_j)}{E_i} \frac{N_j(E_j,X)}{\lambda_j} \quad (3.2)$$

where $N_i(E_i,X)\mathrm{d}E_i$ is the flux of particles i at slant depth X in the atmosphere, with energy in the interval $[E_i, E_i + \mathrm{d}E_i]$.

The index j labels i's parent particles, λ_i is the interaction length of particles of type i in the atmosphere, and d_i is the decay length, namely:

$$\lambda_i = \frac{Am_p}{\sigma_{i+\mathrm{air}}} \qquad d_i = \rho\gamma c\tau_i, \quad (3.3)$$

so that they both are in units of $\mathrm{g\,cm^{-2}}$; A is the mean mass of target nuclei in the atmosphere and ρ is the air density, which is a function of the altitude h. The grammage corresponding to the height h can be written as

$$X(h) = \int_0^h \mathrm{d}\ell \, \rho(h(\ell)) \qquad \ell = \text{particle trajectory}. \quad (3.4)$$

The functions F_{ji} are the dimensionless particle yields for the production of a particle i with energy E_i in a collision of a particle j with energy E_j on air. They can be defined as:

$$F_{ji}(E_i,E_j) = E_i \, \frac{1}{\sigma_{j+\mathrm{air}}} \frac{\mathrm{d}\sigma_{j+\mathrm{air}\to i}}{\mathrm{d}E_i},$$

where E_i and E_j are defined in the laboratory frame. This term can be suitably written to include the production of particles of type i from the decay of their parent particle of type j.

While this set of coupled equations can be solved analytically in some simplified cases, such an approach would force the assumption that the spectrum of CR species is a power law (as in [45]). In order to solve these equations with a more realistic CR spectrum than a single power law, a numerical approach is needed, which also requires some model for hadronic interactions at energies higher than measured at accelerators. More on this will follow later, when discussing the original work resulted in [3].

3.1.3 Atmospheric neutrino oscillations

Atmospheric neutrinos are produced practically uniformly around the globe above a few GeV, when the geomagnetic field of the Earth does not affect anymore the flux of cosmic ray primaries and the secondaries they produce. In the absence of oscillations, then, one would have the same flux of neutrinos coming from θ and $\pi - \theta$, neglecting absorption in the Earth, i.e. below several tens of TeV. This means that neutrino oscillations can be detected in a model-independent way by comparing the upgoing and downgoing fluxes of high[4] energy neutrinos of a certain flavour. In fact, downgoing neutrinos travel some tens of kilometres in air, while Earth-traversing (upgoing) neutrinos go through additional several thousand of kilometres of matter, which could affect flavour oscillations for neutrinos of energy between several and tens of GeV[5]. Such up-down asymmetry is quantified by the ratio:

$$\mathcal{A}_\ell = \left(\frac{\phi_{\text{up}} - \phi_{\text{down}}}{\phi_{\text{up}} + \phi_{\text{down}}} \right)_\ell \tag{3.5}$$

or the up-down ratio:

$$R_\ell = \left(\frac{\phi_{\text{up}}}{\phi_{\text{down}}} \right)_\ell \tag{3.6}$$

As reported in table 1.3, oscillations can be probed with atmospheric neutrinos in the energy range from 0.1 to 100 GeV with $\Delta m^2 \simeq 10^{-3}\,\text{eV}^2$. The oscillation length $L_{\text{osc}} \approx 2E/\Delta m^2$ (with E in GeV, L in km, and Δm^2 in eV^2) in fact must be in the range 10 - 10^4 km in order to observe oscillations either in down- or in upgoing atmospheric neutrinos; this happens for the lowest energy range for detectable atmospheric neutrinos, i.e. 0.1 - 100 GeV and only for the largest value of the squared mass difference, i.e. $\Delta m^2 \approx \Delta m^2_{23} \approx 10^{-3}\,\text{eV}^2$. The corresponding mixing parameter is $\sin^2\theta_{23} \approx 0.5$, corresponding to close-to-maximal mixing. In the next chapter we will cover how such measurements are performed.

[4] With the proviso that for neutrino energies of several TeV the Earth becomes opaque.

[5] So far this energy region is not yet accurately studied, as it is the end of Kamiokande and before the beginning of IceCube. It is currently being considered for future observation.

3.2 Experimental results on atmospheric neutrinos

Hereafter we are going to cover the atmospheric neutrino experiments which obtained the most important results in the context of neutrino oscillations as well as those that are currently probing the most energetic part of their spectrum.

The typical reaction that is used to measure the atmospheric neutrino fluxes is the charged-current neutrino-nucleon collision:

$$\nu_\ell + N \to X + \ell^- \qquad \ell = e, \mu, \tau$$

as well as its charge-conjugated variant. Detecting the so-produced charged lepton allows for the detection of the corresponding (anti-)neutrino. Due to the lack of a magnetic field in the experimental apparati, charge discrimination has not been implemented in atmospheric neutrino experiments. Tau neutrino identification is very difficult due to the very short lifetime of the tau lepton, which makes the signal very similar to that produced in the case of a charged-current event due to any other flavour of neutrino.

The data are usually divided into classes, according to the topology of the signals. Such classes are:

- **contained events**, i.e. events produced by neutrino-nucleon interaction *inside* the detector and such that the tracks of all the produced particles are fully contained in the detector;

- **stopping muons**, i.e. tracks of muons originating outside the detector that stop inside the detector;

- **through-going muons**, i.e. tracks of muons originating outside the detector that do not stop inside the detector.

In experiments with an inner part of the detector which is particularly clean, called fiducial volume (FV), an additional subdivision is used to distinguish contained events which are *fully contained* in the FV from those which are *partially contained*.

Kamiokande The Kamiokande experiment has been described before in the context of solar neutrinos. It has a FV of 2142 ton of purified water surrounded by a shield and anticounter of 1500 ton of water.

A first indication of atmospheric neutrino oscillations was found in 1988 by measuring the ratio of muon to electron neutrinos in two energy ranges, *sub-GeV* (visible energy below 1.33 GeV) and *multi-GeV* (visible energy above 1.33 GeV), and comparing that ratio to the Monte Carlo simulations. The final results are:

$$\mathcal{R}_{e/\mu} := \frac{(N_{\mu\text{-like}}/N_{e\text{-like}})_{\text{data}}}{(N_{\mu\text{-like}}/N_{e\text{-like}})_{\text{MC}}} = \begin{cases} 0.60^{+0.07}_{-0.06} \pm 0.05 & \text{sub-GeV [114]} \\ 0.57^{+0.08}_{-0.07} \pm 0.07 & \text{multi-GeV [115]} \end{cases} \tag{3.7}$$

Such discrepancies with respect to the Monte Carlo simulations, which did not include oscillation effects, have been interpreted as ν_μ disappearance due to oscillations.

Kamiokande also found a zenith angle dependence of upward through-going muons, which supported the interpretation of the contained events anomaly as a signature of neutrino oscillations [116].

IMB The Irvine-Michigan-Brookhaven detector was a tank of roughly 8000 ton of water, 3300 ton of which constituted the fiducial mass [117]. It was located in the Morton Thiokol salt mine in Ohio, USA, at a depth of about 1570 mwe (meter water equivalent), and it has taken data during three phases from 1982 to 1991.

Also IMB measured a flavour ratio of sub-GeV contained events different from the Monte Carlo expectation [118]:

$$\mathcal{R}_{\mu/e}^{\text{sub-GeV}} = 0.54 \pm 0.05 \pm 0.11$$

which is in agreement with the results from Kamiokande.

No zenith-dependent anomaly was found in the upward-going muon data.

Super-Kamiokande The Super-Kamiokande experiment has been described before in the context of solar neutrinos; it has a fiducial mass for neutrino detection of 22.5 ktons.

The Super-Kamiokande (SK) collaboration measured an up-down asymmetry, as defined in Eq. (3.5), of muon neutrinos of [52]:

$$\mathcal{A}_\mu = -0.296 \pm 0.048 \pm 0.01$$

for multi-GeV, partially contained μ-like events, while it was consistent zero for the corresponding electron up-down asymmetry.

The muon asymmetry is most likely due to neutrino oscillations, as the source-detector distance for upward-going neutrinos is much larger than that for down-going neutrinos. This explanation is supported by the distribution of the observed number of μ-like events as a function of L/E, shown in Figure 3.2. One can see from it that for $L/E \lesssim 10^2\,\mathrm{km\,GeV^{-1}}$ the experimental results agree with the Monte Carlo calculation, i.e. neutrinos did not have enough time to oscillate as their oscillation phase was too small. For larger L/E, however, the deficit is evident, as the oscillation phase of the neutrinos became large enough to generate a transition.

The absence of any anomaly in the electron-like data disfavours the oscillation $\nu_\mu \leftrightarrow \nu_e$, so that the relevant flavour oscillations is $\nu_\mu \to \nu_\tau$[6].

The up-down ratio of multi-GeV, partially contained μ-like events confirms the presence of neutrino oscillations with a statistical significance of 12σ, as for these events:

$$R_\mu^{\text{up-down}} = 0.551^{+0.035}_{-0.033} \pm 0.004$$

The latest results of Super-Kamiokande, included in [30], have been presented in [119]; in the case of the favoured normal hierarchy, they are:

$$\begin{aligned} \Delta m^2_{32} &= 2.5 \times 10^{-3}\,\mathrm{eV}^2 \\ \sin^2\theta_{23} &= 0.587 \\ \delta_{\mathrm{CP}} &= 4.189 \end{aligned}$$

[6]The oscillation $\nu_\mu \to \nu_s$, where ν_s is a sterile neutrino is ruled out due to the lack of matter effects for neutrinos traversing the Earth (ν_s does not interact with matter, while ν_μ and ν_τ suffer the same matter effect) and by the up-down symmetry of a sample of events with a considerable neutral-current fraction.

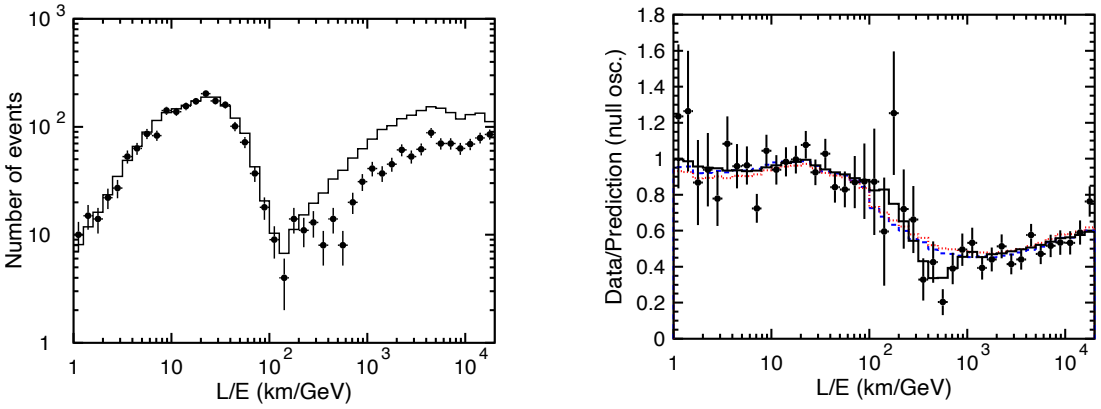

Figure 3.2: Left: number of μ-like events in Super-Kamiokande as a function of L/E (points) compared to the Monte Carlo prediction without oscillations (histogram). Right: ratio of the data and the Monte Carlo prediction without oscillations for the number of μ-like events in Super-Kamiokande as a function of L/E (points). The solid histogram shows the best-fit expectation for $\nu_\mu \to \nu_\tau$ oscillations ($\sin^2 2\theta = 1$, $\Delta m^2 = 2.4 \times 10^{-3}\,\mathrm{eV}^2$), with statistical-only error bars. For more details we refer to [120], where these figures are taken from.

MACRO The Monopole Astrophysics and Cosmic Ray Observatory was a $76.6 \times 12 \times 9.3\,\mathrm{m}^3$ scintillator detector that operated in the Laboratori Nazionali del Gran Sasso, Italy, between 1989 and 2000. Detecting the flight of upward-going muons, it measured [121] a deviation in their zenith-angle distribution with respect to the Monte Carlo expectation without neutrino oscillations. Their results are compatible with those of Super-Kamiokande, with a best fit of $\sin^2 2\theta_{23} \simeq 1$ and $\Delta m^2_{23} \simeq 2.5 \times 10^{-3}\,\mathrm{eV}^2$ in the case of $\nu_\mu \to \nu_\tau$ oscillations.

IceCube IceCube is the first kilometre-scale detector ever built by man. As of now, it consists of 86 vertical strings, along each of which 60 Digital Optical Modules (DOMs) are deployed with an inter-DOM separation of 17 m, between 1450 and 2450 m of depth inside the Antarctic ice. The DOMs collect the Cherenkov light produced by the charged particles moving faster than light in ice, so as to reconstruct their energy and trajectory.

On the surface, near the top of each string, there is a pair of tanks, separated from each other by 10 m and with two DOMs in each tank, so as to form a

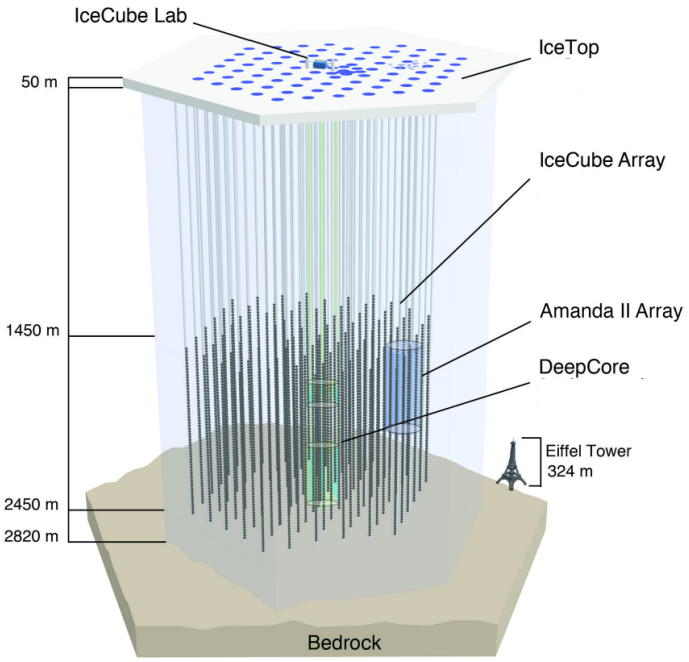

Figure 3.3: The architecture of the IceCube observatory in its current state. Figure taken from [122].

km^2-scale air shower array, IceTop.

For a review of its construction and early results, see [123, 124]; for a more recent discussion, see [122, 125]. Many of the most exciting results obtained by IceCube will be the subject of deeper discussion later in this work. In Figure 3.3 the current layout of the IceCube observatory is shown.

Most of the events that IceCube detects are due to atmospheric muons, which leave a track-like signature in the detector, due to the stochastic losses of this very penetrating particle. Such tracks can also be due to muons produced in charged-current interactions of muon neutrinos.

The other main topology of events is shower-like, produced by neutral-current interactions of all flavours of neutrinos, and by charged-current interactions of electron and tau neutrinos.

A special event topology is that of "double bangs", i.e. two consecutive showers produced by the charged-current interactions $\nu_\tau \to \tau \to \nu_\tau$. This topology, however, is distinguishable from the single-shower one only at energies high enough that either the mean free path of the tau lepton is larger than the inter-string distance, or its Lorentz-boosted lifetime is larger than the temporal window for single-shower acceptance of the DOMs, which would then see two clearly distinct pulses. More on this will follow in 4.4.1.

The presence of IceTop allows to select the atmospheric contributions to the IceCube events. Atmospheric neutrinos can be tagged by coincident muons, provided that the muon Lorentz-boosted lifetime allows them to reach the detector; this is known as the self-veto.

IceCube measured the spectra of atmospheric electron and muon neutrinos in the range 10^2 - 10^6 GeV [126, 127, 128, 129, 130], and tested neutrino oscillations [131, 132] and sterile neutrino mixing [133] in the high-energy interval 6-56 GeV. In the same energy range they are going to test for the mass ordering [134] of neutrinos. The IceCube investigation on neutrino mixing yields:

$$\Delta m^2_{32} = 2.31^{+0.11}_{-0.13} \times 10^{-3}\,\mathrm{eV}^2 \qquad \sin^2\theta_{23} = 0.51^{+0.02}_{-0.09}$$

in the assumption of the (preferred) normal mass ordering; these results are compatible with, and of similar precision to those of Super-Kamiokande, IMB, as well as the other accelerator and reactor-based experiments. IceCube also excluded the absence of tau neutrino oscillations at a significance of 3.2σ for charged-current and neutral-current interactions.

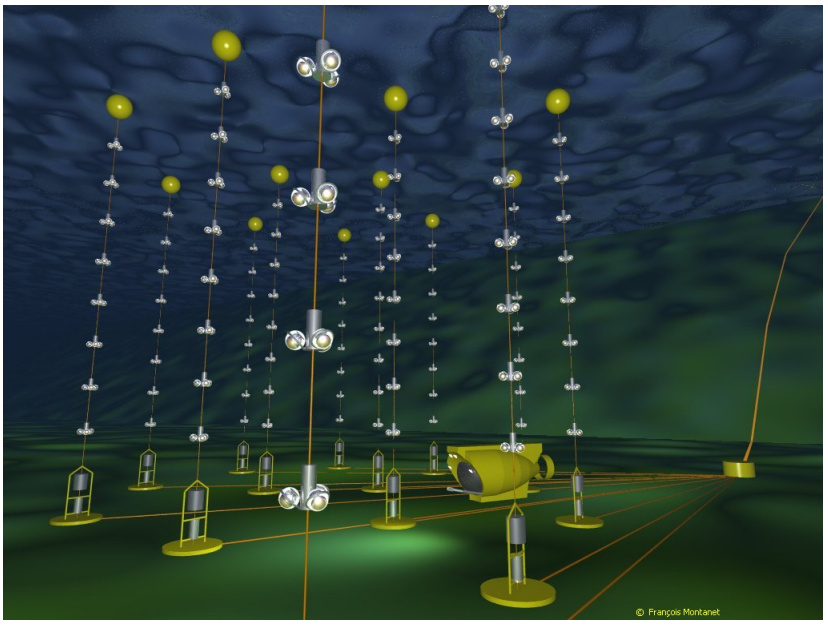

Figure 3.4: An artistic view of the ANTARES detector; picture taken from http://antares.in2p3.fr/Gallery/.

The IceCube collaboration has proposed an upgrade to the already existing facility, with the aim of performing much more precise measurements on the fundamental properties of neutrinos. PINGU (the Precision IceCube Next Generation Upgrade) is the proposed low-energy in-fill extension to the already existing detector, which will allow to have sensitivity down to neutrino energies of few GeV - see [135] for more details on this.

As we will see in much more detail later, the results on the atmospheric neutrino spectrum agree with the theoretical expectations, except for the elusive, yet undetected prompt component.

ANTARES The ANTARES neutrino telescope [136] is located in the Mediterranean Sea, 40 km off the coast of Toulon, France, at a mooring depth of about 2475 m. It has been working since 2008, and it consists of 12 detection strings with 25 storeys of 3 optical modules (OMs) each, for a total of 885 OMs (line 12 only has 25 storeys). The horizontal spacing of the strings is of about 60 meters,

while the vertical separation between the storeys is 14.5 meters.

Its concept is very similar to that of IceCube, with the important differences that ANTARES is in water, it is smaller, and is located in the Northern hemisphere.

The fact that it is in water allows for a better angular reconstruction of the events, as in ice the presence of dust can be, and is, a source of additional uncertainty. It also means that additional sources of background, on top of energetic atmospheric muons, are constituted by the decay products of ^{40}K, naturally present in sea water, and by the light emitted through bioluminescence by living organisms.

The smaller size of ANTARES ($0.01\,\mathrm{km}^3$), with respect to that of IceCube, means that less energy can be contained in the detector, and thus it cannot probe the same energy range of IceCube; more on this will be discussed in the following chapter. This is why a larger and improved version of ANTARES, called KM3NeT, has been proposed and is in the process of realisation and first data acquisition [137, 138].

Being in the Northern hemisphere, ANTARES can probe the Galactic centre using events coming from below, the advantage of which will be widely discussed later on.

Also the ANTARES collaboration has measured the muon neutrino atmospheric flux at high energy ($10^2 - 2 \times 10^5\,\mathrm{GeV}$) [139], measured the mixing parameters and probed the 3+1 neutrino model with 10 years worth of data [140] between 1 and 100 GeV. The muon neutrino flux they measure is compatible with that of IceCube, and the mixing parameters they obtain are compatible with those already established in literature:

$$\Delta m^2_{32} = 2.0^{+0.4}_{-0.3}\,\mathrm{eV}^2 \qquad \sin^2\theta_{23} = 0.50^{+0.19}_{-0.18}$$

ANTARES rejects the non-oscillation hypothesis with a significance of 4.6σ; it also constrained values of the parameter space of the 3+1 neutrino model never probed before.

The ANTARES detector will be upgraded to KM3NeT [137], a distributed infrastructure comprising two facilities, ARCA and ORCA. Of the two, the most relevant for atmospheric neutrinos is ORCA (Oscillation Research with Cosmic in the Abyss), which will be located at a depth of about 2500 m offshore Toulon (France). ORCA will be optimised for neutrino energies between 1 and 100 GeV

in order to study fundamental neutrino properties; this is possible for the closer spacing of the strings, of about 20 m, as well as the vertical spacing of the DOMs, of about 9 m.

3.3 The connection between the CR knee and atmospheric neutrinos

For the sake of convenience, let us show again the spectrum of cosmic rays shown in Fig. 1.3, as taken by [44]:

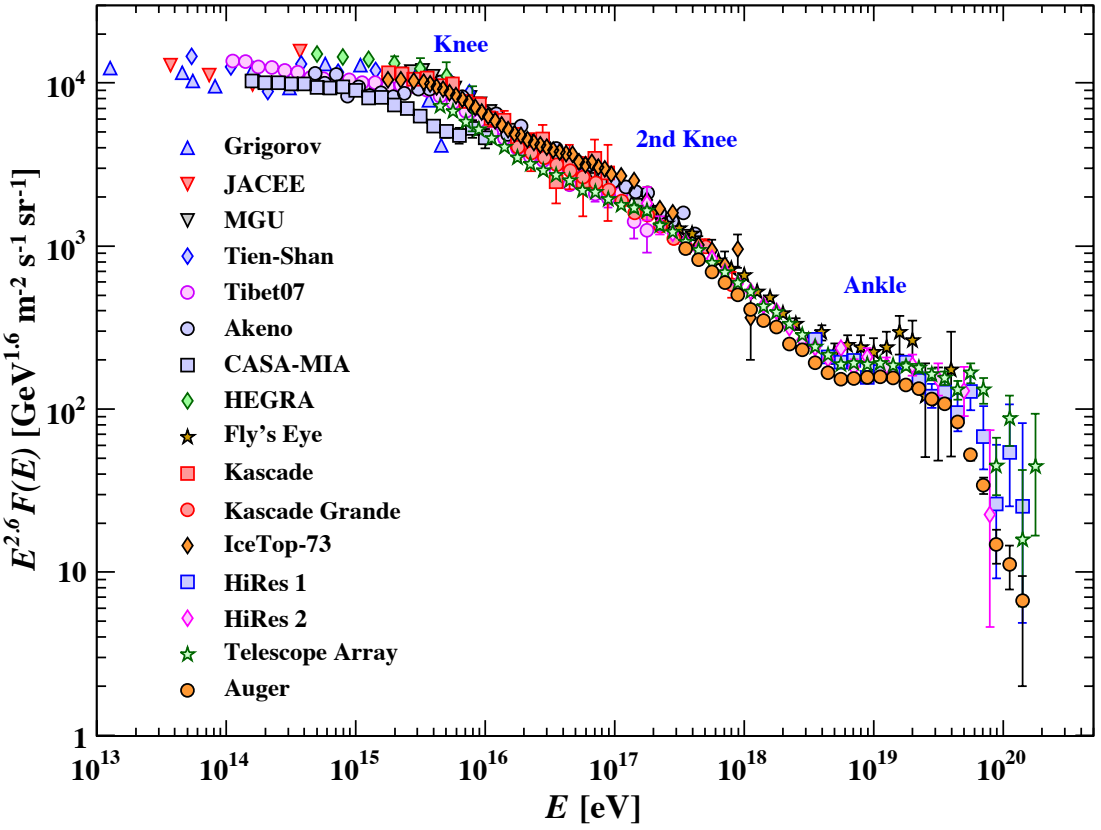

Despite decades of investigation on the nature of the most prominent feature in the cosmic ray (CR) spectrum, the knee remains poorly understood: a change

of mass composition would suggest that the knee is due to the overlap of the contributions of accelerators running out of steam in a rigidity dependent manner, a picture that became solid after KASCADE data [141]. On the other hand, recent measurements of the spectrum of individual elements by the ARGO collaboration suggest the existence of a knee in the light component of the cosmic ray spectrum (H+He) around ~ 700 GV [142]. This would imply that the knee (at few PeV) is shaped by intermediate mass elements (CNO), quite at odds with the common wisdom that associates the knee to a steepening of the spectrum of light elements. The implications of this finding for the understanding of the transition from Galactic to extragalactic CRs are also worth being mentioned. One should keep in mind the possibility that the knee might not be due to the maximum rigidity dependence in the accelerator, but rather to a change of regime in the propagation of cosmic rays through the Galaxy [143]. This scenario implies that the maximum energy in the accelerators should be much higher than PeV, thereby increasing the tension with theoretical models of CR acceleration that have serious problems explaining how to reach even PeV energies [144]. These different possibilities, though potentially equivalent from the point of view of the all-particle cosmic ray spectrum that they result in, may lead to different predictions in terms of the spectrum of atmospheric neutrinos, which is most sensitive to the maximum energy of the light component in cosmic rays.

In a rather qualitative way one can see that if the spectrum of Galactic CR protons were sharply cut off at energy $E_{\rm max}$, the corresponding neutrino spectrum of atmospheric origin would fall at energy $\sim \xi E_{\rm max}$, where $\xi \sim 0.05$. Due to either the rigidity dependence of acceleration or Galactic transport, the spectrum of He would then steepen at $2E_{\rm max}$, but the corresponding neutrino spectrum would be terminated at energy $\sim \xi E_{\rm max}/2$, as determined by the energy per nucleon. The same conclusion applies to all nuclei heavier than helium (assuming a mean $A/Z \sim 2$). This simple exercise shows that the end of the spectrum of atmospheric neutrinos is mainly shaped by the parent protons rather than by heavier elements. Moreover, the flux of such heavier elements is numerically smaller, thereby making the argument above more solid. Hence, the two scenarios in which $E_{\rm max} \sim$ few PeV (standard model for the knee) and the one with a maximum rigidity $R_{\rm max} \sim 700$ GV may result in substantially different spectra of atmospheric neutrinos in the energy region $\gtrsim 50$ TeV.

In addition to this basic picture, one should keep in mind other aspects of

the problem: 1) the knees in the spectra of individual species are not necessarily exponential, in that particle acceleration in some types of supernova remnants could lead to a spectrum of CRs with a steepening at $E_{\rm max}$ rather than an exponential drop [145, 146]; 2) the knee in the all-particle spectrum of CRs, as mentioned above, might be due to a change in the propagation regime, rather than to a rigidity dependence of the spectra of species with different mass [143]. All these aspects are expected to affect, to different extents, the shape of the spectrum of atmospheric neutrinos in the high energy region.

Here we calculate the atmospheric neutrino flux that follows from different assumptions on the mass composition and models of the knee and discuss the possibility to discriminate among such models by accurate measurements of the atmospheric neutrino flux, taking into account the uncertainties deriving from interaction models of CRs in the atmosphere. We also discuss the implications of a low $R_{\rm max}$ (light component of CRs) in terms of the onset of astrophysical neutrinos.

The present discussion is organized as follows: in §3.1.2 we outline the "Matrix Cascade Equation" (MCEq) [147] code that we use in the present work. In §3.3.2 we present the results obtained by modelling the knee as a cutoff and as a change of slope of the galactic CR component, and different assumptions on $R_{\rm max}$. In §3.3.3 we discuss the role of uncertainties in modelling CR interactions in the atmosphere. The predictions are then compared with the IceCube measured neutrino flux [128] and angular distribution of the events [129]. The impact of the uncertainty in $R_{\rm max}$ upon the onset of the astrophysical neutrino flux is discussed in §3.3.4.

3.3.1 Equations for cascades in the atmosphere

As said before, while the set of coupled equations (3.2) can be solved analytically in some simplified cases, such an approach would force us to assume that the spectrum of CR species is a power law (as in [45]) and would not be suitable for the investigation of the dependence of the atmospheric neutrino flux on the interaction models. In order to consider realistic spectra of parent CR nuclei (with a cutoff or a break at high rigidity) and to study the dependence of the results upon the physics of particle interactions in the atmosphere, we used "Matrix Cascade Equations" (MCEq) [147] to compute the atmospheric neutrino fluxes at

Earth. MCEq is a publicly available package which allows us to adopt different CR primary spectra as well as different interaction models and compute particle cascading.

This code also features tabulated atmospheric data (e.g. from satellites) and numerical codes, such as NRLMSISE-00 [148], which we used in order to account for seasonal atmospheric variations and to average the neutrino fluxes over the zenith angle.

In the following we adopt SIBYLL-2.3c [149] as our benchmark model to describe interactions in the atmosphere, while in §3.3.3 we discuss the dependence of our results on the interaction model.

3.3.2 The flux of primary CRs and the rigidity of the knee

The main difficulty in making physical predictions concerning the knee is that while there are very good direct measurements of individual CR species at energies ~ 10 TeV, our data in the energy range around the knee are rather poor. In fact, different measurements suggest rather different scenarios: the CR spectrum based upon reconstruction of KASCADE data [141] hinted at a knee dominated by the light component (protons and He nuclei), though with a rather strong dependence of this conclusion upon the choice of the model for the description of CR interactions in the atmosphere. A tentative confirmation of this picture comes from the KASCADE-Grande detection of a knee feature in the heavy CR component [150] at energy ~ 26 times higher than the knee in the light component. Recent measurements by the ARGO experiment show a flux suppression (a knee) in the spectrum of light CR nuclei at energies ~ 700 TeV [151], well below the energy of the knee in the all-particle spectrum. The Tibet III Collaboration also reported on the detection of a light-component knee at about 500 TeV[7]. This latter conclusion appears to confirm a tentative trend, based on older experiments as well, to locate the proton knee at somewhat lower energies for experiments at altitude closer to the maximum of the shower induced by CRs in the atmosphere (see Ref. [152] for a recent review). This is also expected to make the dependence of the results on the adopted hadronic model weaker than for experiments at sea level. However, the interpretation of these results

[7]See the talk by J. Huang on behalf of the Tibet ASγ collaboration given at ISVHECRI2018, Nagoya, Japan.

should take into account that, due to the very different systematics of the various experiments, their comparison is non-trivial.

In order to check the implications of these different scenarios for the knee, we first need to make some assumptions on the shape of the elemental spectra below the knee. The recent measurements by PAMELA and AMS-02 showed that both the spectra of protons and helium manifest a change of slope (spectral break) at the same rigidity, about 300 GV [153, 154, 155]. Hence we first fit the slope and normalization of the proton and helium spectra to the AMS-02 fluxes[8] above the spectral break, at $\sim$ 300 GV, sufficiently far from the knee region that the assumption of power law may be considered reliable.

In terms of the total energy E, we adopt the following parametrization for the power law portion of the spectrum:

$$\frac{\mathrm{d}N_i}{\mathrm{d}E} = a_i \left(\frac{E}{10\,\mathrm{TeV}}\right)^{-\gamma_i} \times 10^{-7}\,\mathrm{GeV}^{-1}\,\mathrm{m}^{-2}\,\mathrm{s}^{-1}\,\mathrm{sr}^{-1} \qquad i = p,\ \mathrm{He} \tag{3.8}$$

The results of the fit for protons and helium nuclei are shown in table 3.1.

	protons	Helium
a_i	1.5 ± 0.2	1.5 ± 0.1
γ_i	2.71 ± 0.04	2.64 ± 0.03

Table 3.1: Normalization and spectral index for protons and helium, as in Eq. (3.8), as to fit AMS-02 fluxes [154, 155]. The reduced χ^2 is 0.1 and 0.2 for the fit to protons ($N_{\mathrm{dof}} = 4$) and Helium ($N_{\mathrm{dof}} = 5$) respectively.

The shape of the knee in the individual components is harder to model due to the lack of detailed measurements. Earlier measurements of the proton and helium spectra carried out by KASCADE [141] were inconclusive in terms of locating the energy of the proton and helium knees, due to the strong dependence of the results upon the model of CR interactions in the atmosphere. It is probably more reliable to use the total spectrum of the light component as a constraint on the location and shape of the knee in the individual elements. Hence we

[8] Publicly made available on the website https://lpsc.in2p3.fr/cosmic-rays-db/ [156]

tried to model the spectrum of light CRs at the Earth as power laws (with slope and normalization taken from fitting AMS-02 data) and a knee (modelled in two different ways) fitted to the recent ARGO and KASCADE-Grande data respectively. An exponential suppression at the knee does not provide a good fit to either set of data because of the spectral sharpness observed at the knee, hence we explored two other possibilities, namely that of an "exponential-square" cutoff:

$$\frac{\mathrm{d}N_i}{\mathrm{d}E} = a_i \left(\frac{E}{10\,\mathrm{TeV}}\right)^{-\gamma_i} \exp\left[-\left(\frac{E}{Z_i\overline{R}}\right)^2\right] \times 10^{-7}\,\mathrm{GeV}^{-1}\,\mathrm{m}^{-2}\,\mathrm{s}^{-1}\,\mathrm{sr}^{-1} \tag{3.9}$$

and that of a change of slope:

$$\frac{\mathrm{d}N_i}{\mathrm{d}E} = \begin{cases} a_i \left(\dfrac{E}{10\,\mathrm{TeV}}\right)^{-\gamma_i} \times 10^{-7}\,\mathrm{GeV}^{-1}\,\mathrm{m}^{-2}\,\mathrm{s}^{-1}\,\mathrm{sr}^{-1} & E \leq Z_i\overline{R} \\ b_i \left(\dfrac{E}{10\,\mathrm{TeV}}\right)^{-\gamma_i+\delta-2} \times 10^{-7}\,\mathrm{GeV}^{-1}\,\mathrm{m}^{-2}\,\mathrm{s}^{-1}\,\mathrm{sr}^{-1} & E > Z_i\overline{R} \end{cases} \tag{3.10}$$

where the parameters of the fit are found using the data of KASCADE-Grande [150] and ARGO-YBJ [151] respectively. The main physical motivation for the change of slope written in the form above is that at some rigidity $\bar{R}$ it is expected that the diffusion coefficient changes its dependence on energy from $D(R) \propto R^\delta$ to $D(R) \propto R^2$. The transition occurs when the CR Larmor radius equals the largest scale in the turbulence L that is responsible for particle scattering [157]. For magnetic fields in the galaxy of order $\sim \mu G$ and $L \sim 10$ pc, this reflects in $\overline{R} \sim 3$ PeV. Smaller values of L lead to correspondingly smaller values of $\overline{R}$. This change of slope in $D(R)$ reflects in a steepening in the CR spectrum from a slope $\gamma_i = \alpha + \delta$ (α is the slope of the injection spectrum) to $\alpha + 2 = \gamma_i - \delta + 2$. This possibility has recently been discussed in [143]. However it is worth keeping in mind that a similar change of slope might be associated to the spectrum of CRs injected by individual supernova remnants, as discussed in [145, 146]. We notice that in Eq. (3.10), as in Eq. (3.9), the only free parameter is $\overline{R}$, since b_i is fixed by requiring continuity at $R = \overline{R}$. For the case of a change of slope, we adopt $\delta = 1/3$, but we checked that a good fit can also be obtained for $\delta = 1/2$.

In our model for primary CRs we also included an extragalactic light component, as was measured by KASCADE-Grande [150], with fixed slope $\gamma_{\mathrm{eg}} = 2.7$

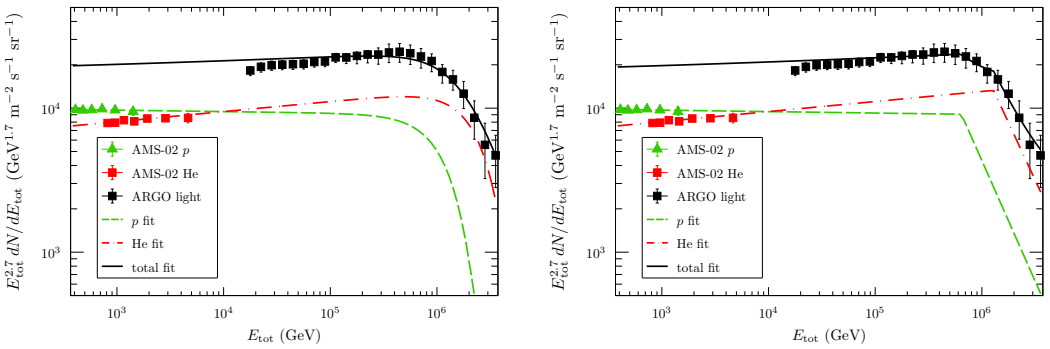

Figure 3.5: Fits to the ARGO-YBJ [151] data points with the knee modelled according to Eq. (3.9) (left panel) and Eq. (3.10) (right panel). The low-energy part ($E \lesssim 10\,\text{TeV}$) derives from the independent power-law fit to the AMS-02 data on the spectrum of protons and helium separately, also shown in the plot.

and normalization to be determined by fitting the data of KASCADE-Grande:

$$\frac{\mathrm{d}N_{\rm eg}}{\mathrm{d}E} = a_{\rm eg} \left(\frac{E}{100\,\text{PeV}} \right)^{-2.7} \times 10^{-19}\,\text{GeV}^{-1}\,\text{m}^{-2}\,\text{s}^{-1}\,\text{sr}^{-1}. \tag{3.11}$$

From the fit to the KASCADE-Grande data we obtain:

$$a_{\rm eg} = \begin{cases} 6.0 \pm 0.2 & \text{using (3.9)} \\ 5.0 \pm 0.5 & \text{using (3.10)} \end{cases} \qquad \overline{R} = \begin{cases} 15.1 \pm 0.7\,\text{PV} & \text{using (3.9)} \\ 5.8 \pm 0.6\,\text{PV} & \text{using (3.10).} \end{cases} \tag{3.12}$$

The fit to the light-component data of ARGO-YBJ provides the following results:

$$\overline{R} = \begin{cases} 1.3 \pm 0.1\,\text{PV} & \text{using (3.9)} \\ 640 \pm 50\,\text{TV} & \text{using (3.10).} \end{cases} \tag{3.13}$$

The results of the fits can be seen in Fig. 3.5 superimposed on ARGO data and in Fig. 3.6 for the KASCADE-Grande data. In both figures we also show the AMS-02 data points and the proton, helium and total (i.e. proton + helium + extragalactic) fluxes. The two models of knee in the individual elements provide a reasonable fit to the data, with a slight preference for the model involving a

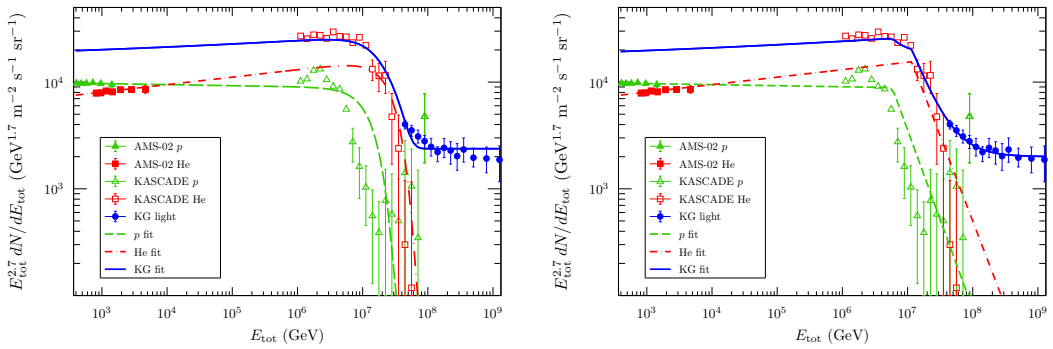

Figure 3.6: Fits to the KASCADE-Grande [150] datapoints with the knee modelled according to Eqs. (3.9) (left panel) and (3.10) (right panel). The low-energy part ($E < 10\,\text{TeV}$) derives from the independent power-law fit to the AMS-02 data. We also show the fits to the proton, helium and total (proton + helium + extragalactic) spectra. Also shown are the fluxes of protons and helium measured by KASCADE [141], obtained using QGSJET as a model for CR interactions in the atmosphere.

change of slope[9] when KASCADE-Grande data are used. In Fig. 3.6 we also show the proton and helium fluxes as originally derived by KASCADE [141] using QGSJET as a model for CR interactions in the atmosphere. It is clear that data reconstructed with QGSJET are inconsistent with power-law extrapolations from the current measurements of the proton and helium spectra as measured by AMS-02 at lower energies. The same consideration applies to reconstruction with SIBYLL. It is important to realize that these codes for CR interactions in the atmosphere are not up-to-date and it would be interesting to see the KASCADE reconstructed spectra if modern versions of these interaction codes were used for the reconstruction. Some preliminary work in this direction was presented in Ref. [158]. Based on these considerations, we stand by our decision to fit the shape of the knees to the recent measurements of the light component (p+He) as carried out with ARGO and KASCADE-Grande respectively.

[9]The change of slope fit results in a reduced χ^2 of 0.1 and 0.7 for KG ($N_{\rm dof} = 11$) and ARGO ($N_{\rm dof} = 23$) respectively, while the exponential-square fit results in a reduced χ^2 of 0.8 and 1.1.

3.3.3 The atmospheric muon neutrino flux

The flux of neutrinos of atmospheric origin is sensitive to the spectrum of parent cosmic rays. In this subsection we test the possibility to discriminate among different scenarios for the origin of the knee by using neutrino data.

Dependence on the spectrum parametrization After fitting the primary cosmic ray flux to the data, as described in the previous subsection, we computed the corresponding atmospheric muon neutrino flux expected in IceCube.

Clearly all mass components of cosmic rays contribute to the neutrino flux. However, protons and helium fluxes dominate the production of neutrinos. In order to demonstrate this point we compare the flux of neutrinos obtained with the protons and helium as parametrized above with the one obtained using the so-called "H3a" model of Hillas and Gaisser [159], which comprises three different populations of five groups of nuclei each, namely:

$$\frac{\mathrm{d}N_i}{\mathrm{d}E} = \sum_{j=1}^{3} \mathcal{N}_{i,j} E^{-\gamma_{i,j}} \exp\left(-\frac{E}{Z_i \overline{R}_j}\right) \qquad i = p, \mathrm{He}, \mathrm{CNO}, \mathrm{Mg\text{-}Si}, \mathrm{Fe}, \tag{3.14}$$

where the values of the free parameters are taken from Table 1 of Ref. [160]. In the "H3a" model the knee of the light component is in the PeV region, as suggested by KASCADE observations, hence one can expect that the flux of atmospheric neutrinos in this model is closer to what we calculate for the case in which the flux of light elements is fitted to KASCADE-Grande data.

We computed the total atmospheric muon neutrino flux at the IceCube observatory height using the MCEq code, averaging uniformly over $\cos\theta$ ($\theta \equiv$ zenith angle) and over the conditions of the atmosphere as described by the `MSIS00_IC` model [148] for the South Pole in January and July. We adopted SIBYLL-2.3c [149] as hadronic interaction model, unless otherwise indicated.

In Fig. 3.7 we show the atmospheric muon neutrino flux resulting from the primary spectrum as in Eq. (3.9) and for the values of $\overline{R}$ obtained from fitting the data of KASCADE-Grande (dashed red line) and ARGO (solid blue line). We compared the resulting fluxes to that obtained with the use of the H3a primary spectra (dotted brown line). Fig. 3.7 confirms that the flux of atmospheric neutrinos is dominated by the light CR component (p+He) for a given value of

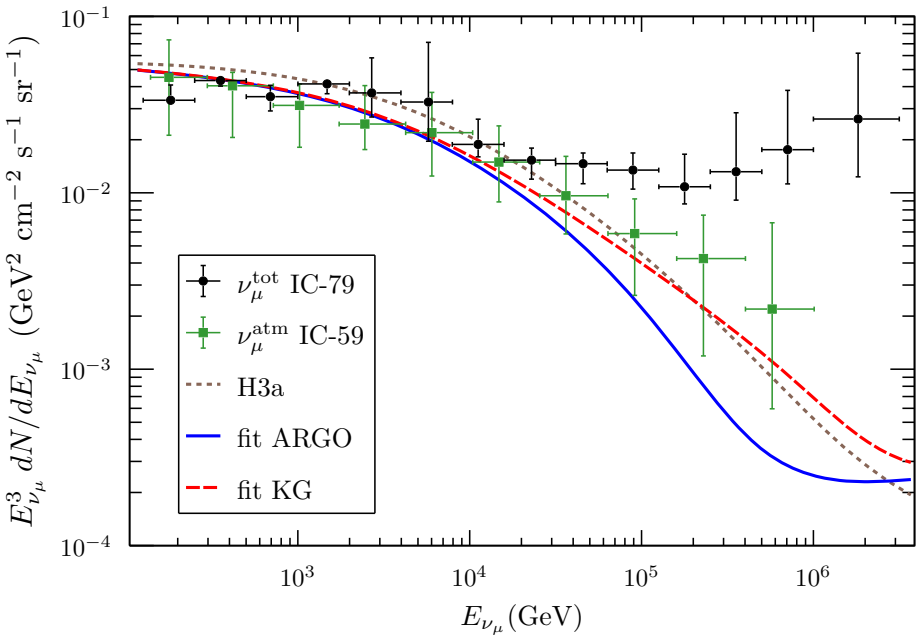

Figure 3.7: Muon neutrino fluxes resulting from the parametrizations of the primary spectrum of Eq. (3.9). Our spectra are compared to those resulting from the "H3a" [160] primary flux model and to the IceCube unfolded atmospheric ν_μ spectrum [127] and the total ν_μ spectrum [128]. The vertical error bars are the the quadratic sum of the statistical and systematic uncertainties.

the knee rigidity. In Fig. 3.7 we also show the neutrino spectra as obtained by IceCube-59 [127] and IceCube-79 [128]. Given the smaller statistics of events, the former data points are expected to trace only the atmospheric contribution to the total neutrino flux in the high energy regime. The comparison between the solid and dashed lines show that the expected atmospheric neutrino flux is sensitive to the rigidity of the knee in the individual elements for energies above 50 TeV, while at lower energies all predictions provide an equally satisfactory description of the data. Although one might be tempted to express a slight preference for the primary model inspired to KASCADE-Grande data, rather than an ARGO-like model in which the knee rigidity is lower, current experimental uncertainties do

not allow to draw firm conclusions.

Theoretical uncertainties There are two types of theoretical uncertainties that affect the calculation of the muon neutrino flux, namely uncertainties in the parameters describing the flux of primary CRs (see table 3.1) and uncertainties deriving from the choice of the hadronic interaction model.

The former can be quantified by calculating the minimum and maximum flux of atmospheric neutrinos obtained by changing the parameters describing the fluxes of primary protons and helium (with different assumptions on the shape of the knees). The result of this calculation is illustrated in Fig. 3.8 for the case of ARGO-like and KASCADE-Grande-like knee. The shaded bands illustrate the uncertainties deriving from the shape of the spectrum at low energy and the shape of the knees. Given such uncertainties, it appears that a separation between the low rigidity and high rigidity cases is possible for neutrino energies above ~ 100 TeV, although in that energy region the current statistics of events is rather low and the contribution of astrophysical neutrinos to the total flux is important. With all these caveats, we computed the average residual of the IC-59 [127] data with respect to the top of the KG and ARGO band for the 5 most energetic datapoints: we obtain 0.9 for KG and 1.5 for ARGO, which shows some weak preference for the case with high rigidity knee in the light CR component.

In order to quantify the dependence of our results on the interaction model, we computed the muon neutrino fluxes employing four hadronic interaction models available in MCEq, namely SIBYLL-2.3c [149], EPOS-LHC [161], QGSJET-II-04 [162] and DPMJET-III-17.1 [163]. Our results are shown in Fig. 3.9, together with the IC-59 and IC-79 data points. The difference in the theoretical predictions at energies $\gtrsim 100$ TeV are due to that fact that QGSJET and EPOS do not include the contribution of prompt neutrinos.

We assumed a primary spectrum like Eq. (3.10), fitted to the ARGO data, and with normalization $a_i + \delta a_i$ and slope $\gamma_i - \delta\gamma_i$ in order to maximize the atmospheric neutrino flux in the case of a fit to the ARGO data. The aim of this exercise is to check the extent to which the difference between KASCADE-Grande and ARGO fits to light primary CR can be masked by the uncertainties in the interaction models. It appears that the uncertainties due to the fit to primaries and those deriving from interaction models are comparable.

Another source of uncertainty in the atmospheric neutrino flux is the contri-

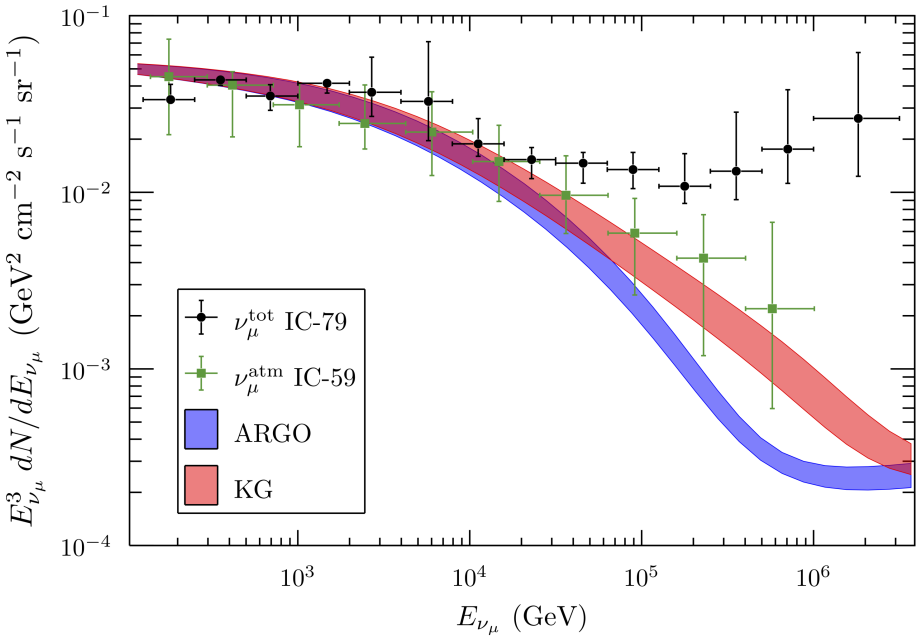

Figure 3.8: The atmospheric muon neutrino flux uncertainty due to that on the primary cosmic ray flux parameters and on its functional form: the bands are delimited by the largest and the smallest fluxes obtained by choosing $(a_i + \delta a_i; \gamma_i - \delta\gamma_i;$ exp-square-knee) and $(a_i - \delta a_i; \gamma_i + \delta\gamma_i; \Delta\gamma -$knee) respectively. These fluxes are compared to the IceCube unfolded ν_μ spectrum [128] and to the unfolded atmospheric ν_μ spectrum [127].

bution of the prompt component, namely neutrinos due to the decay of charmed mesons produced in cosmic rays collisions on the atmosphere, which is yet to be measured. Many (semi-)analytical computations [164, 165, 166, 167, 168, 169] have been carried out, adopting different primary CR spectra and hadronic interaction models. Our predictions based on using MCEq, adopting the primary CR fluxes as defined in Sec. 3.3.2 and adopting SYBILL-2.3c as interaction model, agree with the most recent of these computations. As can be seen from Fig. 3.9, the level of uncertainty due to the prompt component becomes somewhat of a concern at $\gtrsim 300$ TeV, so that it is not expected to affect in any significant way our conclusions on the position of the knee in the light component.

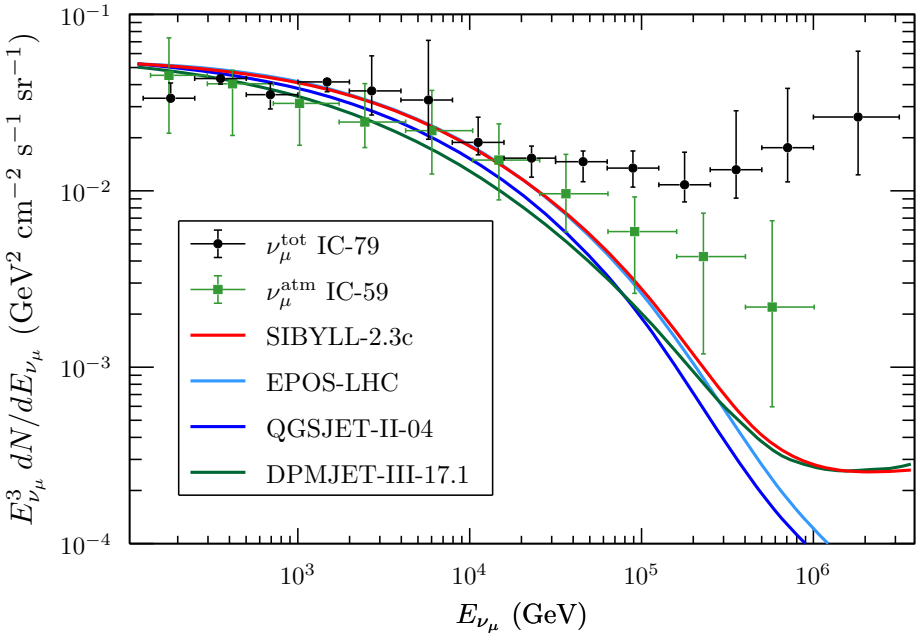

Figure 3.9: Muon neutrino fluxes resulting from four interaction models available in MCEq [149, 161, 162, 163]. As primary spectrum we used Eq. (3.10) fitted to the ARGO datapoints with normalization $a_i + \delta a_i$ and slope $\gamma - \delta\gamma_i$ in order to obtain the largest muon neutrino flux possible according to the ARGO data. These fluxes are compared to the IceCube unfolded ν_μ spectrum [128] and to the unfolded atmospheric ν_μ spectrum [127].

Angular distribution expectations A safe discrimination between different models of the knee in the individual light elements requires neutrinos with energies above a few hundred TeV and a clear tagging of atmospheric neutrinos, perhaps based upon the angular distribution of the signal. In fact neutrinos of astrophysical origin are expected to show a quasi-isotropic angular distribution. Such isotropy may either reflect the homogeneity of the universe on cosmological scales (the pathlength of neutrinos at the energies of interest is larger than the size of the universe), if the sources have a cosmological spatial distribution (see for instance [122] and references therein), or the presence of a large emission

region around our own Galaxy, as would be the case in some models [170, 171].

Some information on the observed angular distribution of neutrinos was recently presented in Ref. [129] for IC-86; unfortunately in the highest energy bin used in the analysis, around 100 TeV, the expected effect is still rather marginal. This is clearly visible in Fig. 3.10, where we show the data of IC-86 [129] compared with our predictions for a low and high rigidity model of the knee in the light component. Notice that here an astrophysical neutrino flux was added to the atmospheric contribution (including prompt neutrinos) so that the total flux is a good fit to the preliminary IC-86 data points. We will comment below on such an astrophysical component. Visual inspection of Fig. 3.10 clearly shows that data on the angular distribution of the events do not have much discrimination power between different models of the knee, at least at the energies considered so far.

3.3.4 Astrophysical neutrinos

The difference between the neutrino flux measured by IC-79 and the expected atmospheric neutrino flux (including prompt neutrinos) provides evidence for an additional component that is naturally interpreted to be of astrophysical origin. From the discussion above it is clear that the modelling of the shape and position of the knees in the light CR component affects the inferred spectrum of neutrinos of astrophysical origin, which makes the motivation for accurate understanding of atmospheric neutrinos even stronger.

For the model in which the knee is at higher energy (motivated by KASCADE-Grande data) our best fit to the differential spectrum of the additional component can be written as

$$\frac{\mathrm{d}\Phi_\nu}{\mathrm{d}E_\nu} = (7 \pm 3) \times 10^{-18} \left(\frac{E_\nu}{100\,\mathrm{TeV}}\right)^{-2.6\pm0.2} \mathrm{GeV}^{-1}\,\mathrm{cm}^{-2}\,\mathrm{s}^{-1}\,\mathrm{sr}^{-1}, \qquad (3.15)$$

while for a lower energy knee of the light component (ARGO-like) the best fit that we obtain is

$$\frac{\mathrm{d}\Phi_\nu}{\mathrm{d}E_\nu} = (10 \pm 3) \times 10^{-18} \left(\frac{E_\nu}{100\,\mathrm{TeV}}\right)^{-2.9\pm0.2} \mathrm{GeV}^{-1}\,\mathrm{cm}^{-2}\,\mathrm{s}^{-1}\,\mathrm{sr}^{-1}. \qquad (3.16)$$

with reduced χ^2 of 0.06 in both cases ($N_{\mathrm{dof}} = 3$). It is easy to understand that in the latter case the atmospheric component is suppressed at lower energies, so

that the inferred astrophysical neutrino spectrum needs to be steeper than in the former case and with a higher normalization at 100 TeV.

The IceCube collaboration has released the results of different analyses revealing the detection of an astrophysical component of the neutrino flux. The dataset based on muon tracks has been fitted to the expression [172]:

$$\frac{\mathrm{d}\Phi_\nu^{\mathrm{tracks}}}{\mathrm{d}E_\nu} = (0.9^{+0.30}_{-0.27}) \times 10^{-18} \left(\frac{E_\nu}{100\,\mathrm{TeV}}\right)^{-2.13\pm0.13} \mathrm{GeV}^{-1}\,\mathrm{cm}^{-2}\,\mathrm{s}^{-1}\,\mathrm{sr}^{-1}, \quad (3.17)$$

while high energy starting events (HESE) selected with energies $\gtrsim 60$ TeV in the last six years appear to have a substantially steeper spectrum [173]:

$$\frac{\mathrm{d}\Phi_\nu^{\mathrm{HESE}}}{\mathrm{d}E_\nu} = (2.46\pm0.8)\times10^{-18} \left(\frac{E_\nu}{100\,\mathrm{TeV}}\right)^{-2.92^{+0.33}_{-0.29}} \mathrm{GeV}^{-1}\,\mathrm{cm}^{-2}\,\mathrm{s}^{-1}\,\mathrm{sr}^{-1}. \quad (3.18)$$

In both cases the adopted atmospheric neutrino flux is expected to be close to the one derived in our scenario with a higher energy knee in the light CR component. Yet, the inferred flux of astrophysical neutrinos at 100 TeV in IceCube turns out to be a factor $\sim 2-3$ below the one inferred above and based on our calculated atmospheric neutrino flux, which is in good agreement with other calculations present in the literature, as the conventional atmospheric best fit in Ref. [172]. In part this discrepancy may be due to the anomalously large neutrino flux in IC-79 (about a factor 2 above average for a reconstructed muon energy $\gtrsim 100$ TeV, but still compatible within statistical fluctuations). On the other hand, it seems likely that the atmospheric neutrino flux adopted in the IceCube analyses may be somewhat different from that typically used in the literature. This type of details may be difficult to assess with a scrutiny from outside the collaboration, hence we argue that more details on this point might in fact be useful to the community to make an independent assessment of the actual flux of neutrinos having a non-atmospheric origin.

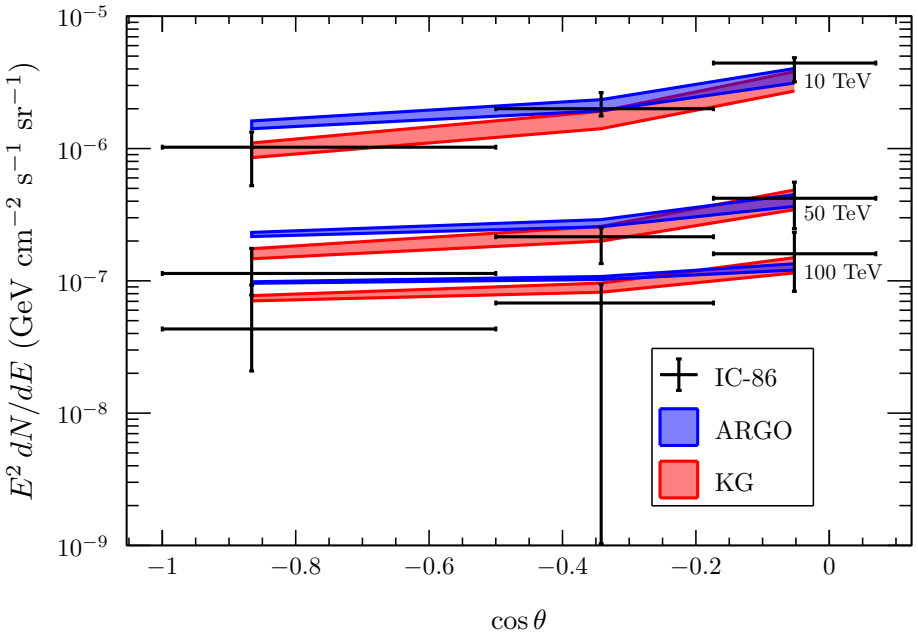

Figure 3.10: The muon neutrino fluxes as a function of the zenith angle θ for $E_\nu = 10, 50, 100$ TeV resulting from the primary models fitted to the KASCADE-Grande (KG) and ARGO datapoints compared to the measured flux of [129] (IC-86). We averaged our neutrino fluxes in the same angular bins for which the data are reported in [129]. The theoretical uncertainties on the primary spectrum are shown (shaded areas). An astrophysical neutrino flux has been added to the atmospheric contribution in order to fit the total IC-86 preliminary flux.

4

Cosmic neutrinos

These neutrino observations are so exciting and significant that I think we're about to see the birth of an entirely new branch of astronomy: neutrino astronomy. Supernova explosions that are invisible to us because of dust clouds may occur in our galaxy as often as once every 10 years, and neutrino bursts could give us a way to study them.
John N. Bahcall

In this chapter we are going to discuss the rather recent branch of physics that goes under the name of neutrino astronomy.

In §4.1 we are going to contextualise the search for astrophysical neutrinos in the state-of-the-art theoretical framework.

In §4.2 we will cover the experiments that are currently online for astrophysical neutrinos, as well as their results.

In §4.3 we are going to discuss the compatibility of the measurements of the astrophysical neutrino spectrum with the current set of assumptions. I treated this topic with a few collaborators in [1].

In §4.4 we highlight the crucial role of astrophysical tau neutrino observations in the current framework of neutrino astrophysics, which has been one of the article [2] I wrote during the PhD thesis.

Finally, in §4.5, we will discuss the role of prompt neutrinos in the interpretation of the measurements obtained by IceCube. Section 4.5 is mostly taken from

the article [4].

4.1 Astronomy with high-energy neutrinos

With high-energy for neutrinos we mean $E > 10\,\mathrm{TeV}$. We can date the origin of observational neutrino astronomy back to 2013 with the first evidence [17] and then the definitive discovery, in 2014 [174], that neutrinos arrive to us from extragalactic sources.

Due to their charge neutrality and a huge mean free path, compared to photons, neutrinos have a great potential in the context of multi-messenger astronomy [175]. On top of this, the detection of a neutrino source is most plausibly linked to the detection of a source of cosmic rays as well; this is yet to be observed, even though there is already some interesting evidence, as we will see in the next section.

Let us now present the state-of-the-art phenomenological framework for astrophysical neutrinos, i.e. the set of assumptions and interpretations relevant for the experimental research.

4.1.1 The production mechanism of cosmic neutrinos

As prefaced in §1.3.3, the most energetic neutrinos that we can detect come either from proton-proton[1] interactions:

$$p_{\mathrm{CR}} + p_{\mathrm{gas}} \to X + \pi^+ + \pi^- + \pi^0$$

or from proton-photon interactions[2]:

$$p_{\mathrm{CR}} + \gamma_{\mathrm{bckgr}} \to X + \pi^+ + \pi^0$$

as the decay of charged pions produces muon and electron neutrinos. Since also neutral pions are present in the final state of such reactions, gamma rays are expected to be produced along with neutrinos, but the converse is not true; since

[1] Or nucleus-proton interactions.

[2] This kind of reaction usually produces more π^+ and π^0 than π^-, which is what this equation is meant to stress - it does not mean that π^- cannot be produced in $p + \gamma$ interactions.

gamma rays are also produced in pure leptonic environments (i.e. by electrons, positrons and their interaction with magnetic fields), they do not provide an evidence for cosmic-ray acceleration.

The neutrino-photon connection for hadronic production The connection between photon and neutrino fluxes produced by hadronic processes is particularly strict. This can be very useful for observations: in the case that the photons from a certain production site can be detected on Earth[3], so that it is possible to estimate the corresponding neutrino flux. These observations resulted in a work has been presented in [176] and that has been updated in [4], to which I contributed.

The formalism developed in [177, 176] connects the photon and the neutrino spectrum at the source in a linear way, through the introduction of kernels:

$$\frac{\mathrm{d}\Phi_\nu(E_\nu)}{\mathrm{d}E_\nu} = \int_{E_\nu}^{\infty} \frac{\mathrm{d}E}{E}\, \tilde{K}_\nu(E_\nu, E)\, \frac{\mathrm{d}\Phi_\gamma(E)}{\mathrm{d}E} \tag{4.1}$$

where $\tilde{K}_\nu$ is a kernel which accounts also for ν oscillations (as we will see in the next paragraph). Eq. (4.1) can be rewritten as

$$\frac{\mathrm{d}\Phi_\nu(E_\nu)}{\mathrm{d}E_\nu} = \int_{0}^{1} \frac{\mathrm{d}x}{x}\, \tilde{K}(x)\, \frac{\mathrm{d}\Phi_\gamma(x/E_\nu)}{dE} \tag{4.2}$$

The original contribution in this context has been to update the oscillation parameters, to provide the kernels related to electron neutrinos and antineutrinos, as well as to explicitly report the "unoscillated" kernels linking neutrinos to photons, as in Eq. (4.77). The "unoscillated" kernels are useful due to the fact that the survival/oscillation probabilities change over time due to the improvement of the experiments and analyses about neutrino mixing. The oscillated kernels, which we denote with a $\sim$, are easily obtained from the non-oscillated ones:

$$\tilde{K}_{\nu_\ell} = \sum_{\ell'=e,\mu} P_{\ell\ell'} K_{\nu_{\ell'}} \qquad \ell = e, \mu, \tau$$

[3]This happens for Galactic, transparent sources, so that photons do not get absorbed. For cosmic distances, photons above 100 GeV suffer from absorption.

ν	α_π	α_K	β_0	β_1	χ_0	χ_1	χ_2	χ_3	δ_0	δ_1
ν_e	0	0	18.611	−84.173	−0.0070	0.4579	8.6140	−11.426	−5.7189	18.921
$\overline{\nu}_e$	0	0	13.257	−58.739	−0.0048	0.3170	6.3360	−8.3753	−4.1830	13.823
ν_μ	0.4541	0.0347	47.980	−103.75	0.0442	0.4579	12.802	−14.218	−3.4151	23.528
$\overline{\nu}_\mu$	0.3322	0.0241	55.343	−86.796	0.0692	0.3170	12.049	−12.184	−1.0295	20.129

Table 4.1: The updated parameters for the non-oscillated kernels.

while the generic form of the non-oscillated kernels is the following:

$$K_{\nu_\ell}(x) = \alpha_\pi \delta\left(z - (1 - r_\pi)\right) + \alpha_K \delta\left(z - (1 - r_K)\right) + \begin{cases} z^2(\beta_0 + \beta_1 z) & z \leq r_K \\ \displaystyle\sum_{n=0}^{3} \chi_n z^n & r_K < z < r_\pi \\ (1-z)^2(\delta_0 + \delta_1 x) & z \geq r_\pi \end{cases}$$

and their parameters are listed in table 4.1, while $r_i = (m_\mu/m_i)^2$.

The flavour ratio at the source A theoretical aspect that we can treat before discussing the possible neutrino sources is the one regarding the flavour ratio of neutrinos at the source and at Earth. Let us consider some extreme cases which can allow us to explore the possible neutrino production scenarios:

- in the case of hadronic interactions, π^+, π^-, π^0 are produced in very similar amounts; the decay of charged pions results into $\nu_\mu, \overline{\nu}_\mu$ and either a ν_e (π^+) or $\overline{\nu}_e$ (π^-). In this case the flavour ratio at the source is $(\nu_e : \nu_\mu : \nu_\tau) \simeq (1 : 2 : 0)$;
- in the case of the "damped muon" scenario, muons interact before decaying, losing most of their energy in some other way than neutrinos. Correspondingly, the flavour ratio for high-energy cosmic neutrinos would be $(\nu_e : \nu_\mu : \nu_\tau) \simeq (0 : 1 : 0)$;
- in the case of neutrinos coming from neutron decays, such as in the case of Supernovae, the neutrino flavour ratio at the source is: $(\nu_e : \nu_\mu : \nu_\tau) \simeq (1 : 0 : 0)$.

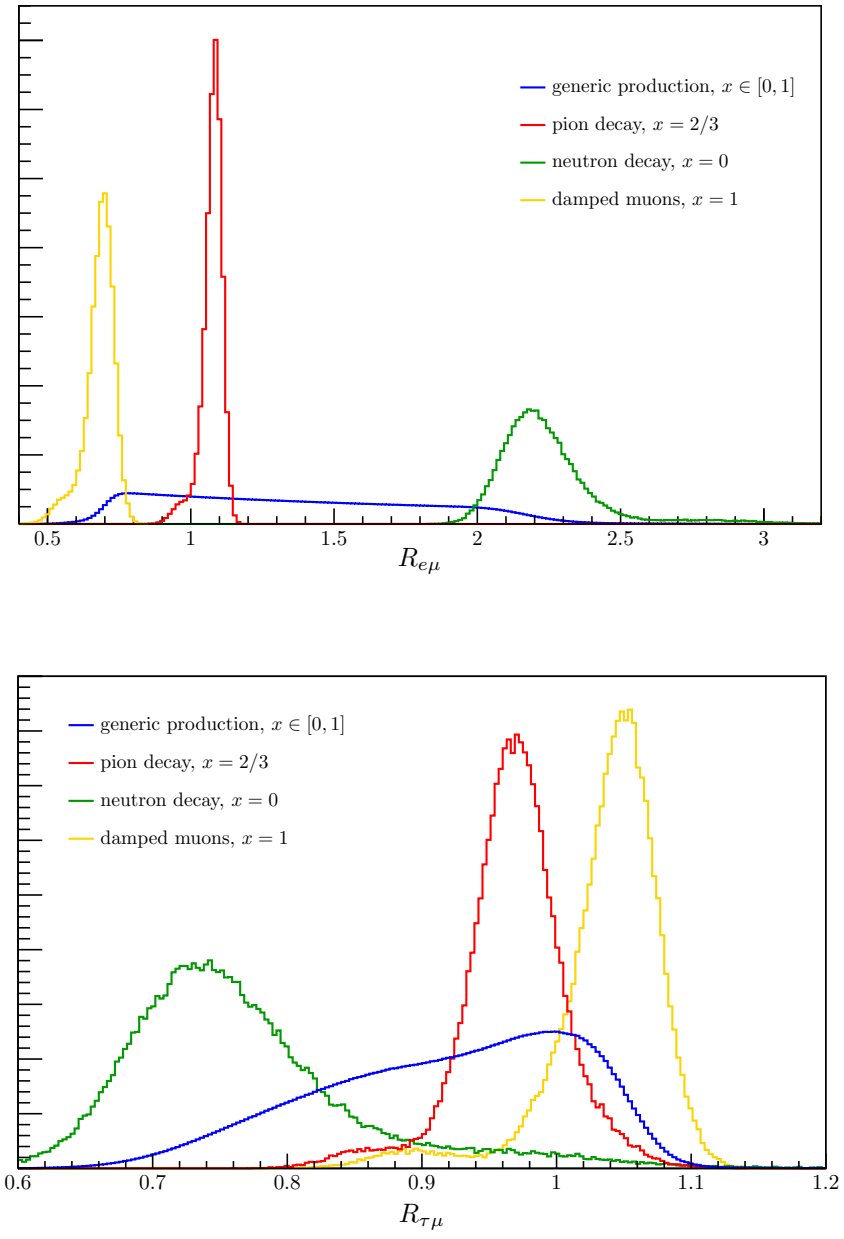

Figure 4.1: The distributions of the $R_{\ell\mu}$ factors, as defined in Eqs. (4.4), (4.5), for the most interesting cases of neutrino production mechanisms. These distributions have been obtained sampling the oscillation/survival probabilities $P_{\ell\ell'}$ according to their distributions, shown in Fig. 1.1, and, in the case of the generic mechanism of production, uniformly sampling $x \in [0,1]$ - x is defined in Eq. (4.3).

We just listed the most common expectations, but there is a rather simple way to make the prediction on the flavour ratio at Earth more independent from the expectations about the production site. Tau neutrinos at production are usually neglected, as they can result from the decay of heavy mesons as well as tau leptons (see the discussion on prompt neutrinos in §3.1), and, even in that case, their amount is much smaller (1/10) of that of electron and muon neutrinos. One can then parametrise the flavour ratio at the source with:

$$(\nu_e : \nu_\mu : \nu_\tau) = (1 - x : x : 0) \qquad x \in [0, 1] \tag{4.3}$$

and compute the distributions of the ratios $R_{\ell\mu}$ ($\ell \neq \mu$) at Earth defined as[4]:

$$R_{e\mu} = \frac{(1-x)P_{ee} + xP_{\mu e}}{(1-x)P_{e\mu} + xP_{\mu\mu}} \tag{4.4}$$

$$R_{\tau\mu} = \frac{(1-x)P_{e\tau} + xP_{\mu\tau}}{(1-x)P_{e\mu} + xP_{\mu\mu}} \tag{4.5}$$

sampling x uniformly in $[0, 1]$ and $P_{\ell\ell'}$ according to their distributions, shown in Fig. 1.1. In figure 4.1, we provided also the distributions of $R_{\ell\mu}$ in the other cases considered above, and in table 4.2 we list the relevant central values and 68% C.L. intervals. The results in table 4.2 show that for pion decay the neutrino flavour ratio at Earth is very close to $(1 : 1 : 1)$, while in the other cases some deviation from $(1 : 1 : 1)$ is possible.

4.1.2 Candidate sources of astrophysical neutrinos

Energy-wise, as we have already covered in §3.3, we expect the astrophysical component of the neutrino spectrum to start dominating at about 100 TeV on the atmospheric one - much more detail on this will follow in §4.5.

Predicting the astrophysical neutrino flux requires modelling the acceleration of the cosmic rays in the source, which is far from trivial, as it depends upon the conditions of the magnetic field turbulence and of the gas in the surrounding environment, as well as upon an efficient mechanism to energise particles. Also

[4]The form of these ratios is based only on the assumption of standard three-flavour neutrino oscillations across cosmic distances.

Production mechanism	$R_{e\mu}$	$R_{\tau\mu}$
generic	$0.78^{+0.57}_{-0.07}$	$1.00^{+0.05}_{-0.15}$
pion decay	$1.09^{+0.03}_{-0.04}$	$0.97^{+0.03}_{-0.04}$
neutron decay	$2.18^{+0.13}_{-0.11}$	0.74 ± 0.07
damped muon	$0.70^{+0.04}_{-0.05}$	1.05 ± 0.03

Table 4.2: The central values and 68% C.L. intervals of the $R_{\ell\mu}$ factors defined in Eqs. (4.4), (4.5) and shown in Fig. 4.1.

the collisions of CRs at energies high enough to produce the observed flux of cosmic neutrinos need some modelling, as man-made accelerators do not cover the corresponding kinematical ranges of such interactions. On top of this, there are bounds imposed by the associated production of gamma rays and the connection of neutrinos to cosmic rays [178]. However, these bounds may be avoided in dependence of the amount of gamma-ray absorption [179]. The hypothesis of neutrinos from very heavy (100 TeV - 1 PeV) dark matter particles has also been discussed [180]; in this thesis, however, we will focus on the astrophysical scenarios for their production.

It is not surprising, then, that the debate about the sources of cosmic neutrinos is still open. The most popular candidates include:

- blazars (see, for example, [181]), i.e. Active Galactic Nuclei which emit a variable and very powerful jet which points toward the Earth;
- gamma-ray bursts (GRBs) (see, for example, [182] and references therein), some of the most energetic transient phenomena in the Universe, dominating the gamma-ray sky over their existence.
- starburst Galaxies [183, 184, 185], i.e. Galaxies in which the rate of star formation is more than 10 times as large as that in our Galaxy.

Normal Galaxies, like ours, are also expected to be filled with cosmic rays, which produce neutrinos and gamma rays in the collisions with the interstellar medium; other possibilities have been recently considered, e.g. [186] .

The simplest and most popular hypothesis is that cosmic neutrinos are distributed as $E_\nu^{-\gamma}$ with $\gamma \sim 2$, at least in the range of energies where they become observable. A corresponding, plausible physical picture is that cosmic neutrinos are produced in collisions between the accelerated cosmic rays and the gas surrounding the accelerators. In the diffusive shock acceleration (DSA) picture, the cosmic-ray spectrum is a power-law $\propto E^{-2}$; due to the "scaling", a characteristic feature of hadronic collisions, also the gamma-ray and neutrino spectra at the source[5] will be power laws $\propto E^{-2}$. This setup can be regarded as an extension of what it is commonly supposed for the Galactic cosmic rays. The postulated abundance of target hadrons points to some dusty environment; this could be compatible with the site of intense stellar formation, say, starburst and/or star-forming Galaxies.

In the next section we will present a selection of the experiments that are currently (and soon to be) online in the field of cosmic neutrinos, accompanied by their results.

4.2 The search for extraterrestrial neutrinos

Having covered the general astrophysical picture about cosmic neutrinos, we pass to review the exciting and unexpected observational results in this very young field. The idea of their detection dates back to the '60s [187, 188], which in the beginning relied on scintillators. Presently, Cherenkov emission in transparent media (ice and water) is the main detection technique, but also other types of detector are at work in this field.

These discoveries have been performed by IceCube, with subsequent contributions by ANTARES. Recent upper limits on the ultra-high-energy neutrino flux have been obtained by detectors which detect them via their Askaryan emission, such as ARIANNA, ANITA and ARA. Also Auger is competitive in the search for neutrinos of ultra-high energy. In the following we will present the detectors, their main results and future upgrades.

Focussing on the important case of Cherenkov cosmic neutrino detectors, the event topologies that are most relevant are mainly subdivided in showers and tracks:

[5] The neutrino spectrum is supposed to be unaltered even far from the source.

- shower-like events are produced in charged-current interactions of electron and tau neutrinos, as well as in neutral-current interactions of all neutrino flavours: in the former case, the resulting charged lepton interacts (or decays, in the case of the tau lepton) in the close vicinity of the interaction vertex, producing light in the process;

- track-like events are produced in charged-current interactions of muon neutrinos, which result in a muon that loses energy quite sporadically and stochastically along its way, leaving a straight track of light behind.

Another important class of event is double cascades: with this term we mean two showers, which are produced in the CC interaction of a tau neutrino and in the subsequent decay of the tau lepton. Just like tracks, this kind of event is peculiar of one neutrino flavour, but it is very difficult to detect due to the fact, as we will se in §4.4, the tau lepton must be very energetic in order to distinguish the two showers.

It useful to preface this section by showing the reason why km^3-scale detectors have been built to detect cosmic neutrinos; after this, we will present an experimental overview of astrophysical neutrinos.

Why a cubic kilometre detector? Let us assume, for the sake of convenience, a fluence of neutrinos given by:

$$F = \Delta T \int_{100\,\mathrm{TeV}}^{\infty} \mathrm{d}E\, 4\pi\, \frac{\mathrm{d}\Phi_{\mathrm{WB}}}{\mathrm{d}E}$$

where $\Delta T = 1\,\mathrm{yr}$ and $\mathrm{d}\Phi_{\mathrm{WB}}/\mathrm{d}E$ is the Waxmann-Bahcall neutrino flux limit from [178]:

$$\frac{\mathrm{d}\Phi_{\mathrm{WB}}}{\mathrm{d}E} = 5 \times 10^{-18} \left(\frac{E}{100\,\mathrm{TeV}}\right)^{-2} \mathrm{GeV}^{-1}\,\mathrm{cm}^{-2}\,\mathrm{s}^{-1}\,\mathrm{sr}^{-1}$$

Computing the integral, we have:

$$F \simeq 2 \times 10^{-4}\,\mathrm{cm}^{-2}\,\mathrm{yr}^{-1}$$

The number of events per year can be computed as:

$$R = F\,\sigma\,\frac{\rho V}{m_N}$$

where the deep-inelastic scattering (DIS) cross-section at 100 TeV is $\sigma \approx 10^{-34}\,\mathrm{cm}^2$ [189] and

$$\frac{\rho V}{m_N} \approx 6 \times 10^{38} \left(\frac{V}{\mathrm{km}^3}\right)$$

R turns out to be of the order of 10 events per year. Note that this is a very optimistic calculation as:

- we used an upper limit for the astrophysical neutrino flux;
- we considered perfect response of the detector at all energies above 100 TeV.

The conclusion is that a km^3 detector is the minimum requirement for cosmic neutrino detection.

4.2.1 IceCube

The main result of IceCube is the discovery of the astrophysical component of the neutrino flux, in 2013 [17]. From that moment on, its main goals have been the characterisation, in terms of flavour content, normalisation and shape, of the astrophysical neutrino spectrum, as well as the search for neutrino sources.

Before covering the results obtained by the IceCube collaboration, it is necessary to present the kinds of events which they use for their analyses.[6]

The IceCube datasets There are two main datasets:

1. the **high-energy starting events** (HESE) dataset, which comprises track- and shower-like events which have the first interaction vertex inside the detector itself;

[6] The IceCube setup has already been presented in the context of atmospheric neutrinos in §3.2.

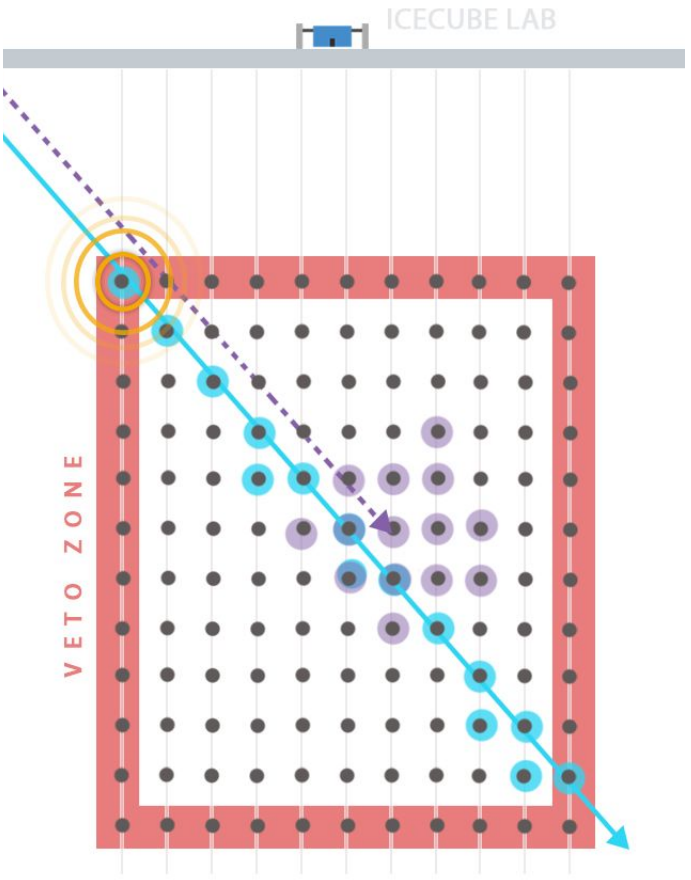

Figure 4.2: Schematic representation of the veto for HESE events in IceCube. The solid blue track represents an atmospheric muon, which deposits energy also in the outer parts of the detector area, and is thus discarded for astrophysical neutrino analyses. The dashed purple track represents a neutrino which could pass the veto, as its interaction vertex is contained in the fiducial volume of the detector. If the two events are coincident and down-going, it probably means that the neutrino has been produced with the muon, i.e. it is an atmospheric neutrino, and is discarder as well. In this figure we can also appreciate the track-like topology of muon-induced events, and the shower-like topology of NC interactions of all neutrinos and CC interactions of all neutrinos but ν_μ. Figure taken from [190] - seee the corresponding slides https://www.icrc2019.org/uploads/1/1/9/0/119067782/nu4b_schneider.pdf.

2. the **through-going muons** dataset, which comprises upward-going track-like events generated by ν_μ-induced muons.

The HESE dataset can be further divided in a track-like sample and a shower-like sample, so as to separate the contribution of CC ν_μ from the rest.

The DOMs at the boundaries of the IceCube detector are used as a veto for the HESE dataset, as represented in figure 4.2. Due to the important presence of atmospheric background (muons, atmospheric neutrinos), especially for down-going events, the HESE analyses use a threshold at 60 TeV of deposited energy inside the detector [190] in order to search for the high-energy cosmic neutrino component.

For the through-going muons dataset the atmospheric contribution is expected to be smaller, as the Earth efficiently filters muons; however, up-going tracks could be due also to muons generated by atmospheric ν_μ. For this reason, the selected events currently have a muon energy proxy above about 100 TeV (it was 200 TeV for [172]).

HESE events are usually better known energy-wise (about 10-15%) than through-going muons events; the latter kind of events are not fully contained in the detector, which makes it impossible to precisely reconstruct the energy proxy. On the other hand, through-going muons events are characterised by a better angular reconstruction (about 1° with respect to about 10°), thanks to their track-like topology and high energy. In particular, the angular reconstruction of the events in IceCube is hindered by the uncertainties on light scattering in ice as well as the presence of dust in the Antarctic ice [191, 192, 193].

The IceCube effective areas In the analyses, it is of paramount importance to understand the detector response as a function of energy and zenith angle. This response is parametrised by the so-called *effective areas*: these are functions which have the physical dimension of a surface and allow to compute the expected number of events according to:

$$N = \Delta T \int \mathrm{d}\Omega \int_{E_{\min}}^{E_{\max}} \mathrm{d}E \, A_{\mathrm{eff}}(E, \theta, \varphi) \, \frac{\mathrm{d}\Phi}{\mathrm{d}E}$$

where $\mathrm{d}\Phi/\mathrm{d}E$ is the flux relevant for the analysis and $E_{\min,\max}$ is the energy range for which the effective area can be used like so. In the case of our interest, the

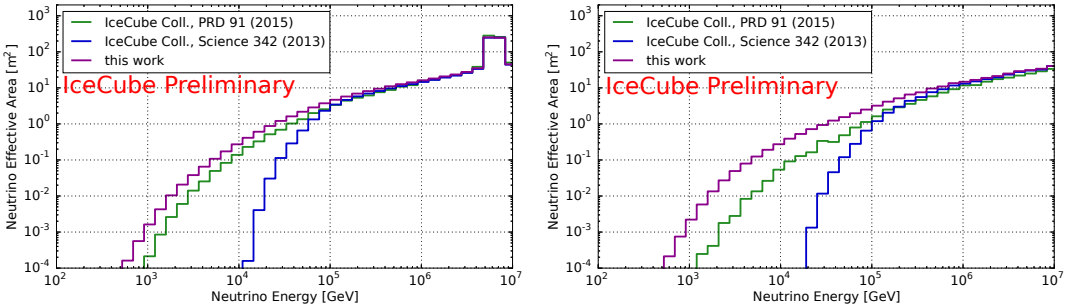

Figure 4.3: The IceCube effective areas, averaged over the solid angle, for starting events due to ν_e (left) and ν_μ (right), compared to previous IceCube analyses. The effective areas are averaged over neutrinos and antineutrinos. The effective area for ν_τ is similar to that of ν_e except for the lack of the resonance feature at several PeV. Figure taken from [194].

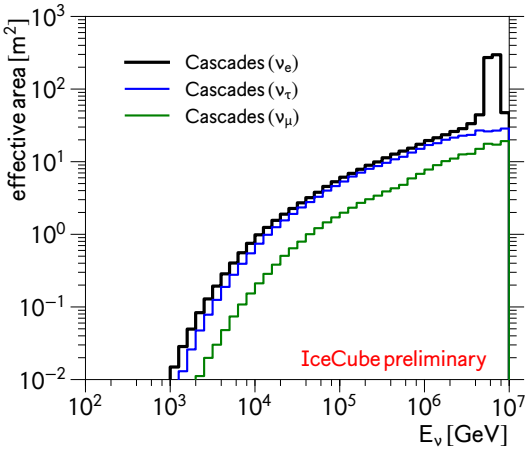

Figure 4.4: The IceCube effective areas, averaged over the solid angle, for cascade events. The effective areas are averaged over neutrinos and antineutrinos. Figure taken from [195].

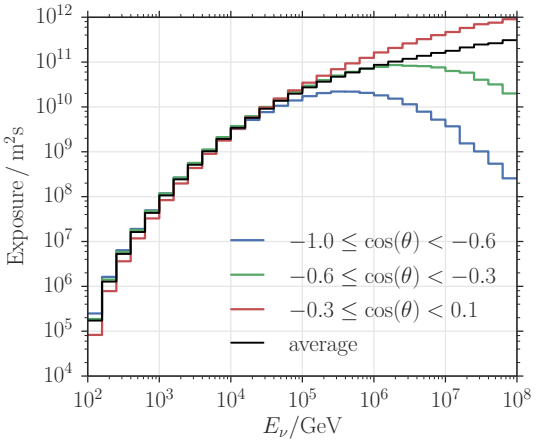

Figure 4.5: The IceCube exposures (i.e. the effective areas integrated over time) for the through-going muons analysis [172] for different zenith ranges. The exposures are averaged over neutrinos and antineutrinos and refer to 2060 days of data. Figure taken from [172].

effective area depends only on the cosine of the azimuthal angle. Such effective areas can be expressed as:

$$A_{\text{eff}}(E, \cos\theta) = [N \times \sigma(E) \times f(E, \cos\theta)]\, \epsilon(E, \cos\theta)$$

in which:

- as seen before, N is the amount of targets for interaction;
- $\sigma(E)$ is the cross-section of the interaction used for detection;
- $f(E, \cos\theta)$ is a function which parametrises physical effects due to the trajectory of neutrinos, e.g. Earth absorption, or the presence of a veto;
- $\epsilon(E, \cos\theta)$ describes the ratio of the effective detector volume with respect to that of an ideal one, and it is a function of energy and azimuthal angle.

We find it useful to report in figures 4.3, 4.4, and 4.5 the effective areas for the event topologies as well as neutrino flavours in IceCube, complemented by their

Event type	figure	$\mathcal{N}$	α	β	γ	E range
ν_e-cascade	4.4	5	0.25	6	2/5	10^3-10^7 GeV
ν_μ-cascade	4.4	1.072	0.34	6.929	2/5	10^3-10^7 GeV
ν_τ-cascade	4.4	32.87	0.045	8.387	3/10	10^3-10^7 GeV
through-going μ	4.5	561.8	0.14	7.2	0.265	10^2-10^8 GeV

Table 4.3: The parameters for the IceCube effective areas of figures 4.4, 4.5 and the energy range for which they can be used. These parameters refer to the analytical approximation of the effective areas as in Eqs. (4.6), (4.7), which do not have the pretence of capturing the physics underlying such quantities. The effective area relevant for the through-going μ events has been obtained from the zenith-averaged exposure in figure 4.5, which has been rescaled by the data-taking time of 2060 days. It is worth mentioning that during that data-taking period the detector was updated, as the number of strings increased, and the analysis procedure changed accordingly.

analytic approximations in equation (4.6) and table 4.3.

$$A_{\text{eff}}(E) \simeq \mathcal{N} \left(\frac{E}{1\,\text{TeV}}\right)^{\alpha} \exp\left[-\beta \left(\frac{E}{1\,\text{TeV}}\right)^{-\gamma}\right] \text{ m}^2 \tag{4.6}$$

In the case of electron antineutrinos, the effective area reflects the presence of the Glashow resonance, as can be seen from figures 4.3 and 4.4: in this case, the approximate effective area (averaged over neutrinos and antineutrinos) is:

$$A_{\text{eff},\nu_e}(E) \simeq A_{\text{eff}}(E) + \theta(E - 1\,\text{PeV}) \left\{ 75\,\text{m}^2 \frac{\gamma^2}{\pi\gamma[\log_{10}^2(E/6.32\,\text{PeV}) + \gamma^2]} \right\} \tag{4.7}$$

where $\theta(x)$ is Heaviside' step function and $\gamma = 1/100$.

The results of IceCube concern the spectrum of atmospheric and astrophysical neutrinos, neutrino oscillations and the search for the sources of cosmic neutrinos. We already talked about atmospheric neutrino and the oscillation measurements performed by IceCube in §3.2. From now on we will talk about the investigation of astrophysical neutrinos by IceCube.

Dataset	main flavour(s)	ref	year	$\min E_\nu$	Φ_{100}	γ
HESE	all	[173]†	2017	60 TeV	2.46 ± 0.8	$2.92^{+0.33}_{-0.29}$
		[190]†	2019		$2.15^{+0.49}_{-0.15}$	$2.89^{+0.20}_{-0.19}$
starting tracks	ν_μ	[197]	2019	3.5 TeV	$1.6^{+1.6}_{-1.0}$	$2.43^{+0.28}_{-0.30}$
cascades	ν_e, ν_τ	[197]	2019	3.5 TeV	$2.2^{+0.6}_{-0.5}$	2.62 ± 0.08
		[196]	2020	16 TeV	$1.66^{+0.25}_{-0.27}$	2.53 ± 0.07
through-going μ	ν_μ	[172]	2016	194 TeV	$0.90^{+0.30}_{-0.27}$	2.13 ± 0.13
		[198]†	2019	40 TeV	$1.44^{+0.25}_{-0.24}$	$2.28^{+0.08}_{-0.09}$
all combined	all	[199]	2015	25 TeV	$2.23^{+0.37}_{-0.40}$	2.50 ± 0.09

Table 4.4: The parameters of the astrophysical neutrino spectra, as parametrised in Eq. (4.8), fitted from the different IceCube analyses. We indicated with † preliminary results; the analysis in [197] refers to contained events.

Astrophysical neutrinos The IceCube detector published the first evidence for cosmic neutrinos in [17], which was connected mainly to an excess of high-energy, contained, shower-like events collected between 2010 and 2012. At the time of writing, the two main kinds of analyses from which the spectrum of cosmic neutrinos is fitted are the HESE and the through-going muons dataset. It is also interesting, however, to consider the two subsets of the HESE dataset, which are the starting track and cascade samples, as they add more depth to the data collected by IceCube. As for through-going muons, the starting track subset of HESE is due to muon (anti-)neutrinos, whereas the cascade subset is mainly (90% [196]) due to electron and tau (anti-)neutrinos.

In table 4.4 we list the published results, as well as the more recent, even if preliminary, ones. We show the normalisation and slope of the per-flavour astrophysical neutrino spectrum, which is assumed to be isotropic and described by an unbroken power law:

$$\frac{\mathrm{d}\Phi_\nu}{\mathrm{d}E_\nu} = \Phi_{100} \times 10^{-18} \left(\frac{E_\nu}{100\,\mathrm{TeV}}\right)^{-\gamma} \mathrm{GeV}^{-1}\,\mathrm{cm}^{-2}\,\mathrm{s}^{-1}\,\mathrm{sr}^{-1} \tag{4.8}$$

In table 4.4 we also indicated the minimum energy for the fit; we find it relevant to take it into consideration recalling that the atmospheric contribution may

still be important below 100 TeV. We also recall that the through-going muons dataset contains mostly up-going events, i.e. those coming from the Northern Sky, whereas with the HESE dataset IceCube mainly "sees" the Southern Sky, but is also sensible to the Northern Sky.
Critical discussions of these results will follow in §4.3 and §4.5.

All these results show compatibility with a $(1:1:1)$ flavour ratio at Earth, and no deviation from the standard three-flavour neutrino oscillations has been observed. It is worth mentioning that the first double cascade events have likely been observed, as preliminarily presented at the last ICRC [200]. This measurement could prove the existence of astrophysical tau neutrinos, i.e. tau neutrinos with so much energy that the resulting τ lepton decays far/later enough that the DOMs can distinguish two subsequent cascades - the first ν_τ interaction and the τ decay. Ultrarelativistic τ's cover a Lorentz-boosted distance of about

$$d_\tau \simeq 50\,\mathrm{m}\left(\frac{E}{1\,\mathrm{PeV}}\right)$$

which has to be compared with the inter-DOM separation of 17 m and the average inter-string separation of 125 m. The importance of this observation, or the lack thereof, is discussed in §4.4.

A first candidate event due to the Glashow resonance has been presented in [201], even though this event belongs to a new kind of high energy cascade sample, which is at the limit of the IceCube sensitivity. Glashow events will be discussed further in §4.3.

IceCube-gen2 The IceCube collaboration proposed an upgrade to the current facility, named IceCube-gen2 [202]: this consists in the enlargement of the already existing facility, in order to reach an instrumented volume of about $10\,\mathrm{km}^3$ with the aim of significantly increasing the astrophysical neutrino detection rate. This will probably result in the identification of hot spots, by collecting multiple events pointing to the same point in the sky, which will conduce to the discovery of sources.

This increase in the detection rate is going to be accompanied by an improvement in the angular and energy resolution; this upgrade will allow for discoveries in the larger-than-PeV energy band and in unexplored wavelengths where most of the universe is opaque to high-energy photons.

With such a large size, the IceCube-gen2 detector will collect significant samples of ν_τ-induced double cascade events and even, possibly, of cosmogenic neutrinos and Glashow resonances. It will also allow to probe neutrino interactions at 100 TeV of centre-of-mass energy, testing electroweak physics at energies beyond the reach of terrestrial accelerators.

For more details and prospects, see [202]; the IceCube-gen2 effective area will be discussed later, in §4.4.3.

The search for neutrino sources: the TXS 0506+056 case At the time of writing the search for point-like and extended sources has not resulted in any firm candidate, even combining the efforts of IceCube and ANTARES [203]; this comes from the fact that no significant excess of neutrinos (neither localised nor diffuse) has been found.

On the other hand, a high-energy (about 290 TeV) ν_μ-induced event, called "IceCube-170922A", has been detected by IceCube in coincidence with the brightest state of a known blazar, TXS 0506+056, during its gamma ray flare, which was observed by many gamma-ray experiments [18]. According to [18], the neutrino event has a 56.5% estimated probability to be of astrophysical origin, and a chance coincidence with the flaring state of TXS 0506+056 is excluded at 3.5σ. After detecting this event, the IceCube collaboration looked for neutrino emission from said source in 9.5 yr worth of data, finding an excess at 3.5σ of 13 ± 5 events with respect to the atmospheric background [204].

These two papers prompted the phenomenological community to model such source in order to allow for the emission of IceCube-170922A as well as the 13 events prior to it. As summarised in [47] and further explained in its references, the interpretation of the gamma-ray emission from TXS 0506+056 as of purely leptonic origin - i.e. without hadrons and, thus, neutrinos - is the simplest and most satisfactory from a statistical standpoint. According to [47], it is possible to accommodate for the emission of a neutrino during the flaring state of TXS 0506+056; concerning the other 13 excess events, the phenomenological models can reproduce up to 5 events.

There may not be further progress about TXS 0506+056 and IceCube-170922A, but this piece of evidence for a neutrino, and thus a cosmic-ray, source has surely started the era of multi-messenger physics with high-energy neutrinos. Moreover, with time and upgrades IceCube will most likely be able to find significant,

localised excesses of events, which may lead us to unequivocally finding the first source of neutrinos.

4.2.2 ANTARES and KM3NeT

The ANTARES setup has already been presented in §3.2 in the context of atmospheric neutrinos. Due to the relatively small volume ($0.01\,\mathrm{km}^3$) of ANTARES, the energy that neutrino-induced particles can deposit in the detector is too small to allow for competitive cosmic neutrino analyses. At the time of writing, the best sensitivity of ANTARES is in the range 1-300 TeV [205].

With 9 year worth of all-flavour data, the ANTARES collaboration reported the observation of a 1.8σ excess of events over the atmospheric background, excluding the null-cosmic contribution in their high-energy sample at 90% C.L. [206]. The energy spectrum fit to the data yields:

$$\frac{\mathrm{d}\Phi_\nu}{\mathrm{d}E} = (1.5 \pm 1.0) \times 10^{-18} \left(\frac{E}{100\,\mathrm{TeV}}\right)^{-2.3\pm0.4} \mathrm{GeV}^{-1}\,\mathrm{cm}^{-2}\,\mathrm{s}^{-1}\,\mathrm{sr}^{-1}$$

They also report individual fits to the track-like sample:

$$\left.\frac{\mathrm{d}\Phi_\nu}{\mathrm{d}E}\right|_{\mathrm{tracks}} = (0.8^{+0.5}_{-0.6}) \times 10^{-18} \left(\frac{E}{100\,\mathrm{TeV}}\right)^{-2.0^{+0.8}_{-0.4}} \mathrm{GeV}^{-1}\,\mathrm{cm}^{-2}\,\mathrm{s}^{-1}\,\mathrm{sr}^{-1}$$

and to the shower-like one:

$$\left.\frac{\mathrm{d}\Phi_\nu}{\mathrm{d}E}\right|_{\mathrm{showers}} = (2.1 \pm 0.8) \times 10^{-18} \left(\frac{E}{100\,\mathrm{TeV}}\right)^{-2.4\pm0.4} \mathrm{GeV}^{-1}\,\mathrm{cm}^{-2}\,\mathrm{s}^{-1}\,\mathrm{sr}^{-1}$$

Interestingly, these results are compatible with those of IceCube. The differences in normalisation and spectral index are attributable to different results for the atmospheric components in the separate fits. In particular, the atmospheric component resulting from the fit to the track-like sample is 30% higher than the theoretical predictions, while it is compatible with predictions in the case of the shower-like one.

Unfortunately, the limited energy acceptance hinders the potential of ANTARES in the search of sources, in which it can boast a very good angular resolution, better than 0.4° above 10 TeV [207]. In [207], the ANTARES collaboration presents

a search for astrophysical neutrino sources using 11 years of data. They looked for excesses correlating to different catalogs of sources, but no significant result has been found.

The Mediterranean Sea offers an optimal location for the observation of the Southern sky, where the Galactic centre and most of the Galactic plane are located, with through-going muons tracks. This is why KM3NeT [137] has been proposed as an upgrade to ANTARES. KM3NeT will be a distributed infrastructure, meaning that it will comprise two telescopes: ARCA (Astroparticle Research with Cosmic in the Abyss), located at a depth of about 3500 m off the coast of Capo Passero (Italy), and ORCA (Oscillation Research with Cosmic in the Abyss), located at a depth of about 2500 m offshore Toulon (France) [205]. ARCA will focus on the high-energy neutrino astrophysics, as it is optimised for neutrino energies between 100 GeV and 100 PeV, with a total volume of about $1\,\mathrm{km}^3$ and horizontal (vertical) DOM spacing of about 90 m (36 m). ORCA will be optimised for neutrino energies between 1 and 100 GeV in order to study fundamental neutrino properties; this is possible for the closer spacing of the strings, of about 20 m, as well as the vertical spacing of the DOMs, of about 9 m.

We will further discuss KM3NeT-ARCA and its effective area in §4.4.3; for a more complete review of the last results from ANTARES and KM3NeT, we refer to [205] and references therein.

4.2.3 Radio detectors

Neutrinos of energy above 10 PeV can be most efficiently detected with the radio technique [208]. Radio signals are produced via the Askaryan effect [209]: a charge excess develops at the front of the neutrino-induced shower as it accumulates electrons from the surrounding medium. The propagation of this charge asymmetry in a dielectric medium results in radio emission of Cherenkov light and of transition radiation, which occurs when charged particles pass through a boundary between two dielectrically different media [210]. For wavelengths much larger than the shower dimensions, the radio emission is coherent, meaning that the radiated power is proportional to N_e^2, where N_e is the number of excess electrons, versus a linear dependence typical of incoherent emission. Such radio emission is produced in the MHz - GHz frequency range, to which the Antarctic ice is transparent and its attenuation length is about 1 km, depending on the

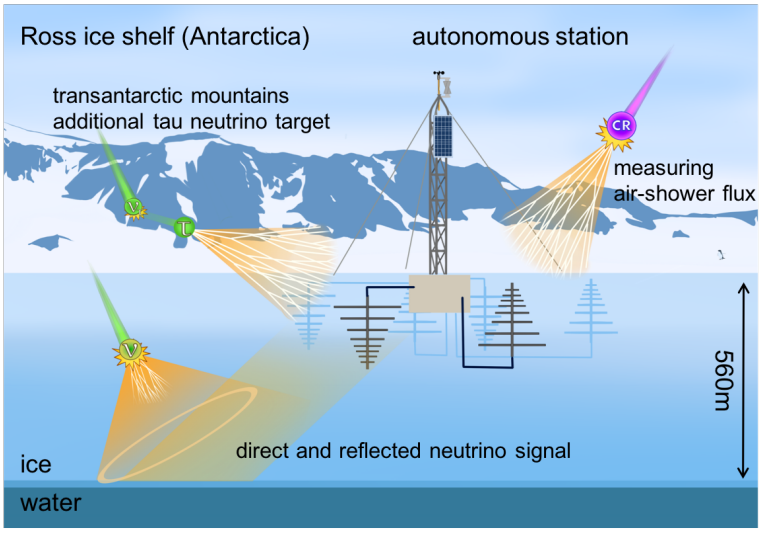

Figure 4.6: Sketch of the ARIANNA detector at the Ross Ice Shelf. Figure taken from [212].

temperature and the frequency [211].

Let us now briefly review the results of the experiments which currently use this detection technique.

ARIANNA The ARIANNA detector [212] consists of autonomous detector stations located slightly below the Antarctic ice surface; the station layout is shown in figure 4.6. Autonomous means that the information of one station is sufficient to measure a neutrino event, without the need of multi-station coincidences. This allows for quick deployment of large antennas, called log periodic dipole antennas (LPDAs), with different orientations, so as to precisely measure:

1. the polarisation of the signal, which, in turn, allows to reconstruct the neutrino direction;

2. the frequency spectrum of the signal, required to determine the neutrino energy.

The vicinity to the surface allows dipole antennas to measure also the Askaryan radio pulse which is reflected off the ice surface for almost all events, helping

thus unambiguous neutrino identification. Each station comprises two pairs of downward facing LPDAs with orthogonal orientation and are spatially separated by 6 m. In the second generation of ARIANNA stations, the downward facing LPDAs for neutrino detection are complemented by two pairs of upward pointing LPDAs for cosmic-ray detection and vetoing.

The main part of the ARIANNA pilot array is the hexagonal radio array (HRA) [213]. It consists of seven 4-channel stations and has been installed at the Moore's Bay site. All stations have been operating successfully since their deployment (the first stations were deployed in 2012), demonstrating the stability of the ARIANNA hardware in Antarctic conditions. The pilot array of a large scale neutrino detector (the future ARIA) consists in 7 HRA stations with 4 downward facing LDPAs each. For more technical details on ARIANNA, we refer to [212]; see [214] for a discussion on the energy and direction reconstruction capabilities of Askaryan detectors.

The ARIANNA collaboration recently presented some preliminary results from a combined analysis of 4.5 years of data acquired by the pilot array [215]. The neutrino search yielded no candidate events, and they provided an upper limit for the diffuse ultra-high energy (UHE) neutrino flux of:

$$E^2\Phi \leq 1.7 \times 10^{-6}\,\mathrm{GeV\,cm^{-2}\,s^{-1}\,sr^{-1}}$$

at $E_\nu = 10^3\,\mathrm{PeV}$.

ARA The Askaryan Radio Array (ARA) consists of a five-station array of radio antennas, located a few kilometres grid-west of the geographic South Pole in Antarctica [216]. A single station consists of 16 antennas, along with signal conditioning and data acquisition electronics. The antennas are deployed down holes 200 m deep on four "measurement strings", roughly forming a cubical lattice of side length 20 m; each antenna is sensitive to 100-750 MHz radiation.

In [216], the ARA collaboration presented constraints on the flux of neutrinos between 10 and 10^6 PeV from four years of data acquired by two stations. They place an upper limit on the diffuse neutrino flux at 10^3 PeV of:

$$E^2\Phi \leq 3.9 \times 10^{-7}\,\mathrm{GeV\,cm^{-2}\,s^{-1}\,sr^{-1}}$$

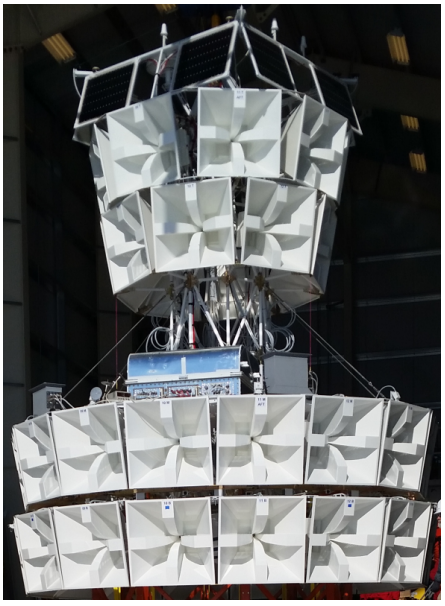

Figure 4.7: The ANITA-IV payload. ANITA is about 8 m tall, and each horn antenna is roughly 0.95 m edge to edge. Figure taken from [217].

ANITA The ANtarctic Impulsive Transient Antenna (ANITA) (see [217] and references therein) instrument is primarily designed for the detection of the UHE cosmogenic neutrino flux via the Askaryan effect in ice, but is also able to trigger on a wide variety of different impulsive radio sources, such as geomagnetic emission from extensive air showers (EAS) induced by cosmic rays or other particles. It consists in a long-duration balloon payload, featuring 48 high-gain, dual-polarisation antennas, and flies at a height of about 40 km above the Antarctic surface. At the time of writing, ANITA has acquired data during four flights; we will cover the results of the last [217] and touch on the anomalies seen during the first and third flight [218].

ANITA's fourth flight lasted 28 days, during which it recorded over 90×10^6 triggers, of which about 99% are thermal noise. The majority of the remaining events are anthropogenic transient, continuous-wave (CW) emission and occasional impulsive emission believed to be electromagnetic interference that escapes ANITA's Faraday enclosure, thus named *payload blasts*. Askaryan neutrino signals are expected to be predominantly vertically polarised, in the Standard Model. As such, horizontally-polarised events are not in the Askaryan neutrino signal region, but they provide a useful cross-check on the analyses. Within the horizontally-polarised sideband region are any EAS events from cosmic rays as well as a sub-class of cosmic-ray-like events with opposite polarity (as CRs are down-going the signal of their induced shower can reach ANITA after reflection on the ice) and are compared to EAS induced by cosmic rays, as found in the two previous ANITA flights.

During the fourth flight of ANITA [217], one event was identified in the Askaryan neutrino signal region, and 30 in the horizontally-polarised EAS region. One Askaryan neutrino event is consistent with the background estimates, while the numbers of EAS-like events is consistent with the estimated analysis efficiencies. The ANITA collaboration set a 90% integral flux limit on a pure E^{-2} neutrino spectrum of:

$$E^2\Phi \leq 2.2 \times 10^{-7}\,\mathrm{GeV\,cm^{-2}\,s^{-1}\,sr^{-1}}$$

for energies between 10^3 and 10^6 PeV.

In the first flight of ANITA one UHECR-like event was observed with characteristics similar to the direct, horizontal cosmic rays, but from a direction well below the horizon and without the phase inversion due to a reflection [219], and

with an estimated background of $\leq 10^{-3}$ events. To explain this event, it was suggested that it originated from a high-energy ν_τ CC interaction in the ice, leading to a τ lepton decay in an upward-going air shower. However, a possible anthropogenic origin for this event could not be ruled out at sufficient confidence to be conclusive.

The third flight [218] was disturbed by continuous-wave interference due to geosynchronous satellites, so that the effective full-payload exposure was about 7 days. Despite this loss of sensitivity, 20 radio-detected UHECR events were identified, one of which had a clearly non-inverted polarity, inconsistent with a reflection, but in all other ways consistent with UHECR origin. The collaboration claims that there was no known physical background remotely close to explaining this event. The potential ν_τ origin proposed for the similar event during the first flight fails to the fact that the Earth is opaque to such energetic neutrinos, according to the Standard Model, even including ν_τ regeneration [220]. For a technical discussion on this, see [218].

4.2.4 Auger and POEMMA

Hereafter we review the contributions of two other experiments, Auger and POEMMA, to the search for ultra-high energy neutrinos. We grouped them separately due to the fact that they are not specifically built for neutrino detection, but are still able to contribute to UHE neutrino searches due to the fact that they can detect neutrino-induced showers.

Auger The Pierre Auger Observatory is located in the province of Mendoza, Argentina, at a mean altitude of 1400 m above sea level. It was primarily designed to measure extensive air showers induced by UHECRs, and has been running and taking data since its construction started in 2004. For that purpose, a surface detector (SD) samples the front of shower particles at the ground level with an array of water-Cherenkov detectors, named stations, each filled with 12 tonnes of water. A complete description of the Auger telescope is beyond the scope of this section, so that we refer the interested reader to [221].

Auger can also identify UHE neutrinos, detecting the showers they induce; for example, tau neutrinos can undergo CC interactions and produce a tau lepton in the Earth crust, which then decays in the atmosphere producing an "Earth-

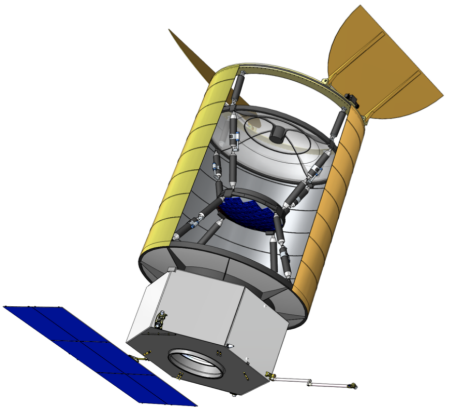

Figure 4.8: Schematic view of a POEMMA satellite. Figure taken from [223].

skimming" (ES) upward-going shower. Neutrino-induced showers are different from CR-induced ones in their electromagnetic component, as inclined (zenith angle $\theta > 60°$) CR-induced showers are rather poor in electromagnetic component, as it is immediately absorbed in the case of CR-initiated showers, and produce signals in the SD characterised by large peaks spread over small time intervals. Conversely, neutrinos can generate "young" (rich in electromagnetic component) showers quite deep in the atmosphere. Auger' strategy to detect neutrinos is thus to look for inclined showers (divided in down-going: $60° < \theta < 90°$, and Earth-skimming: $90° < \theta < 95°$) that exhibit a broad time structure in the signals induced in the SD stations [222]. Such signals are indicative of an early stage of development of the shower. No neutrino-induced shower has been found in 14.5 years of data-acquisition; see [222] for a thorough presentation of the relevant analysis.

The Auger collaboration also set an upper limit to the UHE neutrino flux; assuming an E^{-2} spectral shape, the single-flavor 90% C.L. integrated limit is:

$$E^2\Phi \leq 4.4 \times 10^{-9}\,\mathrm{GeV\,cm^{-2}\,s^{-1}\,sr^{-1}}$$

in the energy interval 100-25 000 PeV [222].

POEMMA Developed as a NASA Astrophysics Probe mission concept study, the Probe Of Extreme Multi-Messenger Astrophysics (POEMMA [223]) science

goals are to identify the sources of ultra-high energy cosmic rays and to observe cosmic neutrinos above 20 PeV. POEMMA consists of two satellites, schematically shown in figure 4.8 flying in loose formation at 525 km of altitude. A novel focal plane design is optimised to observe the UV air fluorescence signal from extensive air showers (EASs) in a stereoscopic UHECR observation mode and the Cherenkov signals from EASs from UHECRs and neutrino-induced τ-leptons in an Earth-limb viewing mode. POEMMA is designed to achieve full-sky coverage and significantly higher sensitivity to the highest energy cosmic messengers compared to what have been achieved so far by ground-based experiments. It will also have sensitivity to cosmic neutrinos by observing the upward-moving air showers induced from tau neutrino interactions in the Earth. POEMMA will also be able to re-orient to a target-of-opportunity neutrino mode to view transient astrophysical sources with unique sensitivity. For a technical description of the satellites, we redirect the interest reader to [223].

POEMMA has two science operation modes, the stereo UHECR one and the neutrino one. We are interested in the latter, in which the two satellites are separated by about 50 km and are tilted 47° away from nadir to observe the limb of the Earth, in an almost monocular configuration. In this operation mode, POEMMA can detect the Cherenkov light from decays of Earth-emerging tau leptons sourced from tau neutrino interactions in the Earth. POEMMA is a promising experiment, both in UHECR and cosmic neutrino measurements. For more details on the expectations about POEMMA's performances, we refer to [223, 224] and references therein.

In the following sections, we will present the original work that I have contributed to concerning astrophysical neutrinos. Such work resulted in three refereed papers, which are phenomenological in nature, as they offer an interpretation and a critical discussion on the experimental results in the field - which are mainly due to the IceCube collaboration. Hereafter we presented almost *verbatim* the contents of these articles, except where otherwise noted. The first of these works discusses the IceCube results on the astrophysical neutrino flux and assesses their compatibility with the assumptions of an unbroken power-law spectrum. An alternative model for the astrophysical spectrum is proposed and used to compute the expected rate of events induced by tau neutrinos and by Glashow resonances.

4.3 What is the IceCube spectrum?

IceCube observed a new quasi-isotropic component of the neutrino spectrum, that exceeds the atmospheric neutrino flux above few hundreds TeV. This new component extends, at least, up to few PeV and it has an intensity close to the Waxman-Bahcall upper bound [178].

This is one of the most exciting recent results in neutrino physics, even though we do not know which are the sources of these neutrinos. The energy spectrum displays non trivial and even unexpected features, such that the aim of the present work is to propose a global investigation of the IceCube findings in terms of a universal spectrum.

We base our analysis on a minimal set of hypotheses, namely:

1. the spectrum is continuous and regular, which is not only a simple mathematical requirement but also a reasonable assumption, as the existence of major discontinuities would require some specific motivation, that we do not have currently;

2. the cosmic neutrinos are subject to three-flavor neutrino oscillations, as recently proved by terrestrial experiments and observations;

3. the new population of cosmic neutrinos derives from some unspecified astrophysical mechanisms of production, where ν_e ($\overline{\nu}_e$) and ν_μ ($\overline{\nu}_\mu$) are created at the source.

Moreover, we consider the most recent datasets[7] obtained by IceCube, discussing the relevant backgrounds.

These hypotheses restrict significantly the overall shape of the spectrum. The hard power-law spectrum, that describes the induced muons up to a few PeV, can be extended to low energy either by assuming a piecewise functional form or by adding a softer power-law component, but there is no tangible difference, as the resulting flux is quite constrained. This has direct implications for the physics

[7]The work presented here, and published in [1] (2017), is based on somewhat obsolete results. Now the new, *preliminary* results on the fit to the through-going muons sample seems to be softer, while that to the cascade and HESE datasets seem to be harder, as presented in §4.2.1. However, the discussions on the sources of background are still valid.

of muon neutrinos events – HESE tracks or through-going events. Neutrino oscillations allow us to derive the electron and tau neutrino spectra. Possible deviation from the standard pion decay scenario are analyzed. We show that there is a hint of a slight excess of electron neutrinos and antineutrinos, but this is not significant. Several tests of the ensuing physical picture are discussed, including tau neutrino events (that are detectable), Glashow resonance events, examining their relation to the specific dataset or range of the neutrino spectrum. We examine the dependence of the predictions upon the specific dataset and upon the energy range of the universal spectrum.

4.3.1 The IceCube dataset

In this subsection we present two recent datasets provided by the IceCube collaboration after 6 years of data taking: the through-going muons dataset and the high energy starting events (HESE) dataset.

Notation: from here on we denote by ϕ_ℓ the flux of ν_ℓ and of $\overline{\nu}_\ell$. Whenever we are only interested to the flux of neutrinos (or antineutrinos), we denote it by ϕ_{ν_ℓ} (or $\phi_{\overline{\nu}_\ell}$). When the subscript is not present (ϕ), the all-flavor flux is considered.

through-going muons The IceCube collaboration acquired data from 2009 to 2015, collecting a sample of charged current events due to upgoing muon neutrinos; due to the position of IceCube, the field of view, for this class of events, is restricted to the Northern hemisphere [172]. The highest energy sample (with reconstructed energy above ~ 200 TeV) corresponds to 29 events of this type; a purely atmospheric origin of them is excluded at more than 5σ of significance. The most energetic event corresponds to a reconstructed muon energy equal to 4.5 PeV.

The corresponding cosmic muon flavour (neutrino and antineutrino) flux was obtained with a power-law fit to the data:

$$\frac{d\phi_\mu^{\rm data}}{dE} = F_\mu \left(\frac{E}{100\ {\rm TeV}}\right)^{-\alpha} \times 10^{-18}\,{\rm GeV}^{-1}\,{\rm cm}^{-2}\,{\rm s}^{-1}\,{\rm sr}^{-1} \tag{4.9}$$

The parameters are $F_\mu = 0.90^{+0.30}_{-0.27}$ and $\alpha = 2.13 \pm 0.13$. This analysis is sensitive only to muon neutrinos and antineutrinos. No correlation with known γ-ray

sources was found by analyzing the arrival directions of these 29 events [172, 225].

High Energy Starting Events The most recent data concern 2078 days (5.7 years) of detection. This dataset includes 82 HESE [173]: they have been classified in 22 tracks and 58 showers (2 of them are not classified being coincident events). These events are characterized by a deposited energy larger than 30 TeV, and the most energetic HESE deposited an energy of 2 PeV into the detector.

The flux attributed to astrophysical neutrinos is described, in first approximation, by an isotropic distribution and a power-law spectrum. The all-flavor flux is:

$$\frac{d\phi^{\text{data}}}{dE} = F \left(\frac{E}{100 \text{ TeV}} \right)^{-\alpha} \times 10^{-18} \, \text{GeV}^{-1} \, \text{cm}^{-2} \, \text{s}^{-1} \, \text{sr}^{-1} \tag{4.10}$$

with $F = 2.5 \pm 0.8$ and $\alpha = 2.92^{+0.33}_{-0.29}$ [173]. We denote by F the normalization of the all-flavor flux.

Although the bulk of HESE coming from the Southern sky suggests a power-law spectrum with spectral index $\alpha \approx 2.9$, the subset of highest energy (above 200 TeV) HESE is in agreement with a much harder spectrum and, more precisely, follows the same distribution suggested by the through-going muons: see figure 6 of [226] and figure 5 of [172], and discussions therein. In other words, the flux of the highest energy HESE observed from the Southern sky is compatible with the same hard spectrum, $\alpha \approx 2$, suggested by through-going muons.

4.3.2 Atmospheric background of HESE

Before continuing the discussion, it is important to recall what are the backgrounds for high energy neutrinos. A precise knowledge of the different background sources is relevant for the correct identification of the astrophysical signal, that we perform in section 4.3.3.

When cosmic rays collide with the terrestrial atmosphere, lots of mesons are produced: from pion decay (and from kaon decay, in smaller amounts) muons and neutrinos are produced, constituting the main source of background for high energy neutrino detection. We call these two sources of background as atmospheric muons and conventional neutrino background.

Another contribution to the background is given by the decay of heavy, charmed mesons: the neutrinos which come from these decays are called "prompt neutrinos".

Atmospheric muons Atmospheric muons, mainly generated by pion decay, have an energy spectrum $\propto E^{-3.7}$. This is due to the fact that, with increasing energy, the probability that pions interact before decaying grows linearly with E. Since muons come from pion decay, their spectrum is steeper than the $E^{-2.7}$ spectrum of primary cosmic rays. This is an unavoidable source of background for the HESE analysis; on the other hand, it does not affect the througohgoing muon analysis, since atmospheric muons are absorbed crossing the Earth. It has been estimated by the IceCube collaboration that the the number of atmospheric muons, contributing to HESE background after 5.7 years of exposure, is:

$$b_\mu = 25.2 \pm 7.3 \tag{4.11}$$

According to table 4 of [174], 90% of them (23.0 ± 7.3) are identified as track-like events and 10% (2.2 ± 0.7) as shower-like events. This is due to the fact that a certain misidentification of tracks is possible from an experimental point of view.

Prompt neutrinos Prompt neutrinos are produced in the decay of heavy mesons, which contain the charm quark (charmed mesons). These particles are highly unstable and decay before interacting, following the same $E^{-2.7}$ spectrum of primary cosmic rays.

To date, the contribution of prompt neutrinos to the IceCube dataset has not been yet identified, although it is expected to exist: see e.g. [165, 227, 168]. An upper limit has been set by the IceCube collaboration [174], while Palladino et al. [228] have calculated that their contribution to HESE is smaller than 3.5 events, in 4 years of exposure, at 90% confidence level (CL). Scaling such estimate with the present exposure, we obtain that the contribution of prompt neutrinos is expected to be smaller than 5 HESE, at 90% CL.

Since at the time of the writing the best fit value of prompt neutrino events is 0, the probability density function (PDF) of prompt neutrinos can be reasonably approximated by an exponential function:

$$\mathcal{L}_p(b_p) = \frac{1}{b_p^0} \exp\left(-\frac{b_p}{b_p^0}\right) \tag{4.12}$$

with $b_p^0 = 2.17$.

According to table 4 of [174] about 20% of prompt neutrinos produce track-like events, whereas about 80% of them produce shower-like events.

Conventional background Neutrinos produced in the decay of pions (and kaons, in smaller amounts) constitute the so called conventional background. These neutrinos follow an $E^{-3.7}$ energy spectrum, for the same reason discussed in the case of atmospheric muons.

The IceCube collaboration [173] has estimated that the contribution of atmospheric neutrinos (conventional plus prompt) to the HESE background is equal to:

$$b_{\pi k} + b_p = 15.6^{+11.4}_{-3.9} \tag{4.13}$$

In order to isolate the contribution of conventional neutrinos, we have built the likelihood function $\mathcal{L}_{\pi k+p}(b)$ that reproduces the best fit value and the 68% CL asymmetric interval. We obtain the PDF of conventional neutrinos marginalizing over b_p:

$$\mathcal{L}_{\pi k}(b_{\pi k}) = \int_0^\infty \mathrm{d}b_p \, \mathcal{L}_{\pi k+p}(b_{\pi k} + b_p)\mathcal{L}_p(b_p) \tag{4.14}$$

Following this procedure, the expected background from conventional neutrinos is equal to:

$$b_{\pi k} = 14.7^{+10.8}_{-5.1} \tag{4.15}$$

where we quote the best fit value and the 68% CL interval obtained as described in §1.2.3, i.e. using the condition that the integral of the normalized likelihood function is equal to 0.68 between b_m and b_M and $\mathcal{L}(b_m) = \mathcal{L}(b_M)$. This is a general procedure that we use for every asymmetric function from here on. We have verified that the same result is obtained performing a Monte Carlo extraction for the total background and for prompt neutrinos.

According to table 4 of [174], 70% of them ($10.3^{+9.1}_{-4.7}$) contribute to track-like events, whereas 30% of them ($4.4^{+4.2}_{-2.0}$) contribute to shower-like events. The uncertainties on the expected number of showers and tracks reproduce the total uncertainty when summed in quadrature.

Summary of backgrounds We summarize the backgrounds relevant to the HESE analysis in table 4.5.

The expected number of background tracks in the HESE dataset is equal to $34.3^{+12.3}_{-8.7}$, as reported in table 4.5. This number is larger than the observed 22 tracks. Moreover, we expect that also $\sim 20\%$ of cosmic neutrinos produce tracks in the HESE dataset, according to table 4 of [174]. On the other hand, as discussed in [173], the misidentification of some tracks, that could be identified as showers, could play an important role for this kind of analysis. In conclusion, since the track-like subset is supposedly dominated by the atmospheric background rather than by the signal, *it is quite hard to extract useful information on ϕ_μ from HESE, and this is the reason why we do note use this subset of data in our analysis.*

On the contrary, we include the tracks contained into the through-going muons dataset, since they are affected by the atmospheric background at the level of 30%, as estimated in [225]. Moreover, we repeat that this kind of analysis is free from atmospheric muons, since they are absorbed into Earth.

As a final remark, let us consider that the atmospheric background affects shower-like events, in the HESE dataset, at the level of 15%. Indeed the expected number of showers, due to atmospheric background, is

$$b_s = 8.8^{+4.0}_{-3.0} \tag{4.16}$$

We denote by $\mathcal{L}_s(b_s)$ the distribution function of this background. This number has been obtained using a Monte Carlo simulation and combining the showers expected from atmospheric muons, conventional neutrinos and prompt neutrinos.

It is reasonable, therefore, to consider through-going muons and shower-like HESE in our analysis, due to their small atmospheric background. On the other hand, it is cautious to neglect track-like HESE in the rest of the analysis, due to the huge atmospheric background, that does not allow to extract useful information on the astrophysical signal.

4.3.3 The neutrino spectrum

In subsection 4.3.3 we define the "universal" spectrum, starting from the muon neutrino spectrum. This kind of spectrum reconciles all the recent IceCube measurements. In subsection 4.3.3 we evaluate the spectrum of tau neutrinos, show-

	b_μ	$b_{\pi k}$	b_p	Sum
Tot. events	25.2 ± 7.3	$14.7^{+10.8}_{-5.1}$	< 5.0 at 90% CL	$43.1^{+12.9}_{-9.2}$
Tracks	23.0 ± 7.3	$10.3^{+9.9}_{-4.7}$	< 1.0	$34.3^{+12.3}_{-8.7}$
Showers	2.2 ± 0.7	$4.4^{+4.2}_{-2.0}$	< 4.0	$8.8^{+4.0}_{-3.0}$

Table 4.5: Summary of the backgrounds expected in HESE analysis after 5.7 years of exposure.

ing that neutrino oscillations are sufficient to strongly constrain it. In subsection 4.3.3 we evaluate the spectrum of electron neutrinos and electron antineutrinos. In this case we analyze ν_e and $\overline{\nu}_e$ separately, since they produce different signals in the detector and, as a consequence, they are distinguishable.

The shape of muon neutrino spectrum

Combining all the information provided by the IceCube collaboration with their different analyses, it is evident that the assumption of a single power-law model is not the best choice to explain the present data. In several papers [226, 228, 229, 230, 231, 232, 233] this aspect has been emphasized, invoking the presence of at least two populations of high energy neutrinos with different energy spectra.

In this paper we test the compatibility of a two power-law spectrum with the observations (HESE showers, double pulses, resonant events) and with the standard production mechanisms of high energy neutrinos, expected to occur in astrophysical environments.

Above 200 TeV we can rely on the through-going muons analysis (green band in figure 4.9), while below 200 TeV we rely on the HESE analysis (blue band in figure 4.9), for the reasons discussed in the previous section. In order to proceed, we define the broken power-law flux in the following manner:

$$\frac{d\phi_{br}}{dE} = \frac{N_\mu^{br} \times 10^{-18}}{\text{GeV cm}^2 \text{ s sr}} \begin{cases} E_{200}^{-2.13} \text{ for } E \geq 200 \text{ TeV} \\ E_{200}^{-2.92} \text{ for } E < 200 \text{ TeV} \end{cases} \tag{4.17}$$

where $E_{200} = E/200$ TeV and the normalization at 200 TeV is $N_\mu^{br} = 0.206$ (in units of equation (4.17)); this value corresponds to the normalization of the

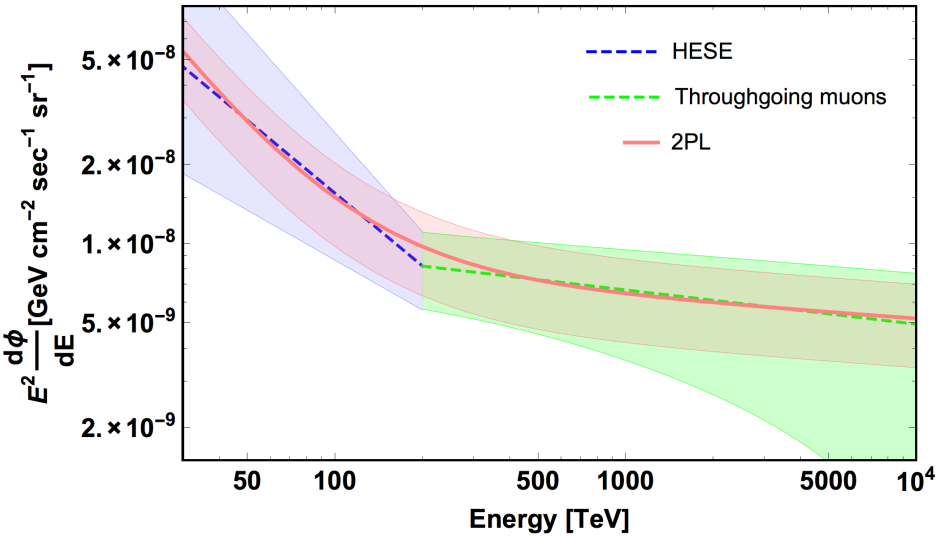

Figure 4.9: The two power-law benchmark spectrum (2PL) as defined by Eqs. (4.18), (4.20), (4.21), compared with the through-going muons flux (green band) and a flux with the slope suggested by HESE below 200 TeV (blue band)–compare with equation (4.17).

through-going muons flux at 200 TeV, using the best fit values. The choice of the break at 200 TeV represents:

- the minimal modification that reconciles the through-going muons and the HESE dataset;
- the most conservative choice, since the energy threshold of the through-going muons analysis is about 200 TeV.

Now, we define our "benchmark" two power-law flux ϕ_μ for the muon neutrino plus antineutrino spectrum as follows:

$$\frac{d\phi_\mu}{dE} = \frac{N_\mu}{2} \frac{10^{-18}}{\text{GeV cm}^2 \text{ s sr}} \left(E_{100}^{-\alpha} + E_{100}^{-\beta} \right) \tag{4.18}$$

where $E_{100} = E/100\,\text{TeV}$. Thanks to the prefactor $N_\mu/2$, the normalization N_μ denotes directly the normalization of the two power-law flux at 100 TeV. The

choice of the normalization at 100 TeV reproduces, reasonably well, the behavior of the broken power-law flux. The value can be slightly different but we have verified that choosing 150 TeV or 200 TeV the analyses proposed in the next sections are not affected appreciably.

In order to determine the parameters N_μ, α, β of equation (4.18), we define a "distance" between this benchmark flux and the broken power-law flux ϕ_{br}, i.e. the flux suggested by the data. The distance between the two functions is defined as follows:

$$d(N_\mu, \alpha, \beta) = \int_{30\,\mathrm{TeV}}^{10\,\mathrm{PeV}} \frac{|\phi_\mu(E, N_\mu, \alpha, \beta) - \phi_{br}(E)|}{\phi_{br}(E)}\, d\log E \tag{4.19}$$

Such distance is minimized by the following set of values:

$$N_\mu = 1.5 \quad \alpha = 2.08 \quad \beta = 3.5 \tag{4.20}$$

Since the normalization of the through-going muons flux is known with an uncertainty of about 30%, we take it into account considering that

$$N_\mu = 1.5 \pm 0.5 \tag{4.21}$$

The two descriptions of the fluxes are presented in figure 4.9.

Let us recall that assuming three flavour neutrino oscillations and the same mechanism of production for all cosmic neutrinos, we expect that the shape of neutrino spectra is the same for all flavors, and only their normalization is expected to be different. For this reason, we refer to assumption with the terminology: universal spectrum of neutrinos.

In figure 4.9 we see that the sum of the two power-law fluxes (pink band), with spectral indexes $\alpha = 2.08$ and $\beta = 3.50$, reproduces well the $\sim E^{-2.92}$ behavior at low energy and the $\sim E^{-2.13}$ behavior at high energy, within the uncertainties on the spectral index and on the normalization.

It is important to remark that we assume the shape of the spectrum suggested by the low energy HESE data, but we do not yet use the normalization suggested by the same data. In fact, HESE data refer to an all-flavor analysis, but the flavour partition of the neutrinos is dictated by the mechanism of production, that to date is unknown. Therefore, we include the information on HESE in the analysis by adopting the following procedure:

- we start from the measured flux of through-going muons;
- we extrapolate this flux at low energy with the shape suggested by the HESE data;
- we adopt the smooth spectrum of equation (4.18). In this manner we determine the "universal" cosmic neutrinos spectrum.
- we use the universal spectrum, neutrino oscillations and experimental constraints to predict the flux ϕ_τ and ϕ_e.

The last step of this procedure concerns the following two sections. In other words, we are going to test whether *for some production mechanisms* the assumption of a universal spectrum agrees with HESE.

The flux of ν_τ

The most plausible mechanism of high energy neutrino production is the pion decay scenario, that yields $\phi_e \simeq \phi_\tau \simeq \phi_\mu$.

Despite the popularity of this hypothesis, in the following we choose to adopt a more conservative and unbiased position, i.e. we assume that the mechanism of production is unknown. Therefore, we perform a test on the flavour composition to verify what is the astrophysical scenario that is in better agreement with the observations.

To begin with, let us discuss the general constraints that come from theoretical and experimental considerations.

Constraints from neutrino oscillations The assumption of this paragraph is just that:

"We believe in three-flavor neutrino oscillations"

The only expectation we have on the production mechanism of neutrinos is that no ν_τ are produced at the source. This applies to any reasonable astrophysical scenario. Therefore, the flavour composition at the source, defined as $\xi^0_\ell = \phi^0_\ell/\phi^0$ (where ϕ^0 denotes the all-flavor neutrino flux at the source), is given by:

$$(\xi^0_e : \xi^0_\mu : \xi^0_\tau) = (x : 1-x : 0) \qquad x \in [0,1] \tag{4.22}$$

We do not distinguish between neutrinos and antineutrinos for the moment; we just consider the total flux for each flavour ℓ. Using this notation we have that:

- $x = 1$ denotes the neutron decay scenario;
- $x = 1/3$ denotes the pion decay scenario;
- $x = 0$ denotes the damped muon scenario, in which muons, produced by pion decay, interact before decaying. Therefore only ν_μ (or $\overline{\nu}_\mu$ or both) are produced.

Since in subsection 4.3.3 we have defined the two power-law spectrum of muon neutrinos, it is interesting to compute the ratio between the flux ϕ_τ and the flux ϕ_μ after neutrino oscillations. The ratio is given by the following expression:

$$R_{\tau\mu} = \frac{P_{e\tau}x + P_{\mu\tau}(1-x)}{P_{e\mu}x + P_{\mu\mu}(1-x)} \tag{4.23}$$

that using the natural parametrization becomes:

$$R_{\tau\mu} = \frac{2 + 3P_0(1-3x) - 6P_1x - 6P_2(1-x)}{2 + 3P_0(1-3x) - 6P_1(1-2x) + 6P_2(1-x)} \tag{4.24}$$

Since P_1, P_2 are small, this ratio is equal to:

$$R_{\tau\mu} \simeq 1 + \mathcal{O}(P_1) + \mathcal{O}(P_2) \tag{4.25}$$

for every mechanism of production.

Randomly sampling x in $[0, 1]$ according to a uniform distribution, so as to consider also mixed mechanisms of production, we obtain the distribution of $R_{\tau\mu}$ represented in figure 4.10 by orange bars. The ratio between the flux of ν_τ and the flux of ν_μ is, in good approximation, a Gaussian function. The best fit value and the 68% CL interval are:

$$R_{\tau\mu} = 1.08 \pm 0.05 \tag{4.26}$$

Therefore, the amount of cosmic ν_τ is the same of ν_μ, to a very good approximation. This result takes into account also the uncertainties on neutrino oscillations.

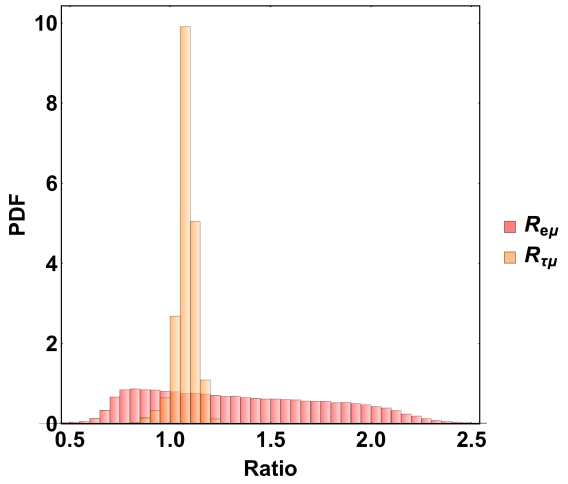

Figure 4.10: The distributions of $R_{\tau\mu}$ (yellow) and of $R_{e\mu}$ (red) obtained from all neutrino production mechanisms (uniformly weighted) which neglect tau (anti-)neutrinos at the source.

Combining equation (4.26) with the normalization of ϕ_μ (see equation (4.21)), we find:

$$N_\tau^{\text{th}} = 1.62 \pm 0.51 \tag{4.27}$$

This means that the theory it is sufficient to firmly constrain the flux of tau neutrinos and antineutrinos.

In the next subsection we analyze whether it is possible to improve the knowledge of ϕ_τ, using informations provided by the observations.

Constraints from observations: double pulses As we have seen in the previous subsection, tau neutrino production at the source is neglected in any plausible neutrino production scenario, but, thanks to neutrino oscillations, we expect the $\nu_\tau(\overline{\nu}_\tau)$ flux to be approximately equal to the flux of $\nu_\mu(\overline{\nu}_\mu)$, regardless of the mechanism of production of high energy neutrinos (see equation (4.26)).

Unfortunately, it is quite hard to measure the flux of ν_τ directly because, until some hundreds of TeV, tau neutrinos do not produce a peculiar signature in neutrino telescopes. With increasing energy the possibility to tag a ν_τ increases, since the first vertex of interaction, in which the τ is created, and the second

vertex of interaction, in which the τ decays, become distinguishable. This process has been proposed by the IceCube collaboration in [234] and it is called "double pulse".

In [235] Palladino et al. derived accurate parametrizations of various effective areas relevant for the analysis. The effective area of double pulse is given by:

$$A_\tau^{\mathrm{2P}} = \bar{A}_{\mathrm{2P}} \left(\frac{E_\nu}{1\ \mathrm{PeV}} \right)^\beta \ \exp\left(-\frac{E_{\mathrm{min}}}{E_\nu} \right) \tag{4.28}$$

with

$$\begin{cases} \bar{A}_{\mathrm{2P}} = 2.33\,\mathrm{m}^2 \\ \beta = 0.455 \\ E_{\mathrm{min}} = 0.5\,\mathrm{PeV} \end{cases}$$

This analytical parametrization reproduces well the effective area of double pulses provided by the IceCube collaboration in [234].

Using our benchmark flux reported in equation (4.18), the expected number of double pulse events can be estimated as:

$$\mathcal{R}_{\mathrm{2P}} = 4\pi \mathrm{T} \int_0^\infty \frac{d\phi_\tau}{dE}\ A_\tau^{\mathrm{2P}}\ dE \tag{4.29}$$

where T is the exposure time. Considering 5.7 years of exposure the expected number of events is:

$$\mathcal{R}_{\mathrm{2P}}(N_\tau) = 0.44 \times N_\tau \tag{4.30}$$

Up to now no double pulse events have been observed by the IceCube collaboration; it is then possible to associate a probability to the normalization N_τ, given by the lack of observations. Using Poissonian statistics, the probability to observe zero events is given by:

$$\mathcal{L}_\tau^{obs} \propto \exp\left[-\mathcal{R}_{\mathrm{2P}}(N_\tau) \right] \tag{4.31}$$

Theory and observations Combining theoretical expectations, due to neutrino oscillations, with the most recent measurements of the flux of ν_μ and with the absence of double pulse events, it is possible to put a strong constraint on the expected flux of ν_τ with cosmic origin.

The likelihood of ϕ_τ, apart from a normalization factor, is obtained using equations (4.24) and (4.31) as follows:

$$\mathcal{L}_\tau(N_\tau) \propto N_\tau \int_0^\infty R_{\tau\mu}\left(\frac{N_\tau}{N_\mu}\right)\ \mathcal{L}_\tau^{obs}(N_\tau)\ \mathcal{L}_\mu(N_\mu)\ \frac{dN_\mu}{N_\mu^2} \tag{4.32}$$

where $\mathcal{L}_\mu(N_\mu)$ is a Gaussian function with mean value equal to 1.5 and standard deviation equal to 0.5 (see equation (4.21)). Note the Jacobian $R_{\tau\mu}(y)dy = R_{\tau\mu}(N_\tau/N_\mu)N_\tau\, dN_\mu/N_\mu^2$ in the previous integral. The resulting function $\mathcal{L}_\tau(N_\tau)$ is, in good approximation, a Gaussian function, with:

$$N_\tau = 1.48 \pm 0.54 \tag{4.33}$$

This result is very similar to the one of equation (4.27). This means that:

> *neutrino oscillations* ***alone*** *are sufficient to constrain the flux of tau neutrinos, given the flux of muon neutrinos.*

It is important to remark that the above results *do not depend upon the mechanism of production*, since we take into account a generic mechanism in the computation of the function $R_{\tau\mu}$.

The flux of ν_e and $\overline{\nu}_e$

As already done for tau neutrinos, we can consider theoretical and experimental constraints for the flux of ν_e and $\overline{\nu}_e$ separately. Let us remark that the flux of $\overline{\nu}_e$ is constrained by the non observation of resonant events, which we discuss in section 4.3.3.

Constraints from neutrino oscillations We follow the same procedure adopted in section 4.3.3 also for electron neutrinos and antineutrinos. In this case the ratio between ϕ_e and ϕ_μ is given by:

$$R_{e\mu} = \frac{P_{ee}x + P_{e\mu}(1-x)}{P_{e\mu}x + P_{\mu\mu}(1-x)} \tag{4.34}$$

Using the natural parametrization it becomes equal to:

$$R_{e\mu} = \frac{2 - 6P_0(1-3x) + 6P_1(1-x)}{2 + 3P_0(1-3x) - 6P_1(1-2x) + 6P_2(1-x)} \tag{4.35}$$

Also in this case we consider a generic mechanism of production, performing a uniform extraction of x between 0 and 1. The resulting distribution of $R_{e\mu}$ is non Gaussian, as it can be noticed from figure 4.10 (red bars). The mode and the 68% CL interval are given by:

$$R_{e\mu} = 0.81^{+0.85}_{-0.10} \tag{4.36}$$

Combining the last result with equation (4.21) we find

$$N_e^{\text{th}} = 1.46^{+1.18}_{-0.62} \tag{4.37}$$

The uncertainty on N_e^{th} is quite large; therefore neutrino oscillations alone are not sufficient to constrain accurately ϕ_e. This is due to the fact that, unlike the ratio $R_{\tau\mu}$, the ratio $R_{e\mu}$ strongly depends upon the mechanism of production.

In order to constrain ϕ_e we can rely on the existing data:

1. the showers observed in HESE dataset;
2. the lack of resonant events.

Let us emphasize that only at this point, i.e. when we consider these two experimental ingredients, we can obtain indications on the mechanism of cosmic neutrino production.

Flux of $\overline{\nu}_e$: Glashow resonance The process:

$$\overline{\nu}_e + e^- \to W^- \tag{4.38}$$

is called "Glashow resonance" [236] and happens for electron antineutrinos with an energy of 6.32 PeV (resonance). Assuming that the flux of neutrinos has no energy cutoff below 6.32 PeV, the resonant events, produced in the interaction of $\overline{\nu}_e$ with the electrons in the ice, must be observed. In several papers [27, 235, 237, 238, 239] the possibility to discriminate the production mechanisms of high

energy neutrinos using the resonant events has been investigated, since different production mechanisms produce a different amount of $\overline{\nu}_e$.

The Glashow resonance cross section is given by:

$$\sigma_{\mathrm{G}}^{\mathrm{hadr}}(E) = \frac{G_{\mathrm{F}}^2\ (\hbar c)^2\ M_{\mathrm{W}}^2}{3\pi} \frac{E \times \overline{\mathrm{BR}}}{E_{\mathrm{G}} \left[\left(\frac{E}{E_{\mathrm{G}}} - 1 \right)^2 + \left(\frac{\Gamma_{\mathrm{W}}}{m_{\mathrm{G}}} \right)^2 \right]}$$

where G_{F} is the Fermi constant, $M_{\mathrm{W}} \simeq 80\,\mathrm{GeV}$ is the mass of the W^- boson, $\Gamma_{\mathrm{W}} = 2.085\,\mathrm{GeV}$ is its FWHM, and $E_{\mathrm{G}} = M_{\mathrm{W}}^2/2M_e \simeq 6.32\,\mathrm{PeV}$ is the energy at which the cross section is largest. The coefficient $\overline{\mathrm{BR}} \simeq 20/3$ denotes the ratio between the branching ratio of the hadronic channel and the branching ratio of $W^- \to \overline{\nu}_\mu + \mu^-$. Here we consider the hadronic channels only, that produce a distinguishable signal in the detector (for a discussion of the leptonic ones see [235]).

The expected number of events can be computed using the following general formula:

$$\mathcal{R}_\ell = 4\pi \mathrm{T} \int_0^\infty \frac{d\phi_\ell}{dE}\ A_\ell\ dE \tag{4.39}$$

where A_ℓ is the effective area for each flavor, T is the exposure time (fixed to 5.7 years) and the flux is given by equation (4.18). For the specific case of resonant events we use the flux of $\overline{\nu}_e$. A useful approximation of the hadronic Glashow resonance effective area is obtained using the Dirac δ function, as follows:

$$A_{\overline{\nu}_e}^{\mathrm{G}}(E) = 1.15 \times 10^6 \times \delta \left(\frac{E}{1\,\mathrm{TeV}} - 6320 \right) \mathrm{m}^2 \tag{4.40}$$

Using the benchmark flux defined in equation (4.18), the expected number of resonant events, after 5.7 years of exposure, is equal to:

$$\mathcal{R}_{\mathrm{G}}(N_e, \epsilon) = 2.3\ N_e \times \epsilon \tag{4.41}$$

where the parameter that quantify the asymmetry between electron neutrinos and antineutrinos is simply:

$$\epsilon = \frac{\phi_{\overline{\nu}_e}}{\phi_{\overline{\nu}_e} + \phi_{\nu_e}}, \qquad 0 \leq \epsilon \leq 1 \tag{4.42}$$

The quantity ϵ is related to the mechanism of production and provides complementary information with respect to the parameter x (see equation (4.22)). Let us summarize:

- $\epsilon = 1$ derives from neutron decay scenario, because only $\overline{\nu}_e$ are produced in this mechanism;
- $\epsilon \simeq 1/2$ comes from the proton-proton interaction, in which an about equal amount of ν_e and $\overline{\nu}_e$ is produced;
- $\epsilon \simeq 1/4$ comes from the ideal $p\gamma$ mechanism (δ approximation, i.e. only the Δ^+ resonance is produced). In more realistic scenarios, analyzed in [239, 240], ϵ is larger that $1/4$, due to the production of π^-;
- $\epsilon = 0$ is obtained in extreme scenarios, in which there are no antineutrinos at the source at all. This happens when only π^+ are produced and only the first decay ($\pi^+ \to \mu^+ + \nu_\mu$) is allowed. For example, it could happen in an ideal $p\gamma$ mechanism, in which muons interact before decaying (damped muons scenario).

Since no resonant events have been detected by IceCube up to now [173], it is possible to associate a prior distribution to the normalization of the $\overline{\nu}_e$ flux, i.e. to $N_e \times \epsilon$, related to the non observation of resonant events. Using Poissonian statistics the likelihood is given by:

$$\mathcal{L}_{\overline{\nu}_e}(N_e \times \epsilon) \propto \exp\left[-\mathcal{R}_{\mathrm{G}}(N_e, \epsilon)\right] \tag{4.43}$$

with the condition $\epsilon \in [0, 1]$.

Finally, just as for double pulse events, we remark that the assumption on the low energy part of the spectrum does not affect the result, since only very high energy neutrinos contribute to the resonant events; the broken power law or the double power laws are equivalent for the purpose of estimating the number of Glashow resonance events.

The flux of $\boldsymbol{\nu_e + \overline{\nu}_e}$: HESE and theory The strongest constraint on the normalization of the ϕ_e flux comes from the number of showers observed with contained events (HESE). In fact, the ϕ_μ flux gives a negligible contribution

to the showers, whereas the flux of ϕ_τ is fixed (within the uncertainty) by the theoretical and experimental constraints analyzed in section 4.3.3. This means that the degrees of freedom needed to reproduce the observed number of showers are N_e and ϵ.[8]

We use the effective areas of HESE, reported in [17] and on the IceCube website, to evaluate the expected number of events for each neutrino flavor. We compute these expectations using equation (4.39).

Using the benchmark flux given in equation (4.18), the expected numbers of showers for each neutrino flavour are given by:

$$\begin{aligned} \mathcal{R}_e &= N_e[k_{\nu_e}(1-\epsilon) + k_{\overline{\nu}_e}\epsilon] \\ \mathcal{R}_\mu &= N_\mu k_\mu \\ \mathcal{R}_\tau &= N_\tau k_\tau \end{aligned}$$

where the coefficients k_ℓ are equal to:

$$k_{\nu_e} = 14.7; \quad k_{\overline{\nu}_e} = 17.8; \quad k_\mu = 1.3; \quad k_\tau = 9.3 \tag{4.44}$$

For $\mathcal{R}_e$ we need to distinguish between the contribution of ν_e and $\overline{\nu}_e$, since only $\overline{\nu}_e$ can produce resonant events. Let us notice that

$$k_{\overline{\nu}_e} - k_{\nu_e} > 2.3, \text{ see equation (4.41)} \tag{4.45}$$

because in the effective areas also the leptonic channels are included, which give showers below 6.32 PeV, which are not distinguishable from those produced by deep inelastic scattering [235]. For $\mathcal{R}_\mu$ we take into account that only 20% of events produced by muon neutrino plus antineutrinos are shower-like events, as discussed in [241].

Using the previous coefficients k_ℓ, we define the likelihood $\mathcal{L}_{\text{HESE}}$ as follows, taking into account that the observed number of showers is $\mathcal{R}_s = 58$:

$$\mathcal{L}_{\text{HESE}}(N_e, \epsilon) \propto [b_s + N_\mu(k_\mu + k_\tau) + \mathcal{R}_e(N_e, \epsilon)]^{\mathcal{R}_s} \exp[-(b_s + N_\mu(k_\mu + k_\tau) + \mathcal{R}_e(N_e, \epsilon)] \tag{4.46}$$

[8] Let us clarify that we are assuming that all ν_τ are detected as showers. This assumption is not completely true but, even if about 20% of tau neutrinos would produce tracks, it would affect our result at level of $0.2k_\tau/49 \simeq 3.8\%$, where 49 denotes the average number of showers with a plausible astrophysical origin, after subtracting the atmospherical background given in equation (4.16).

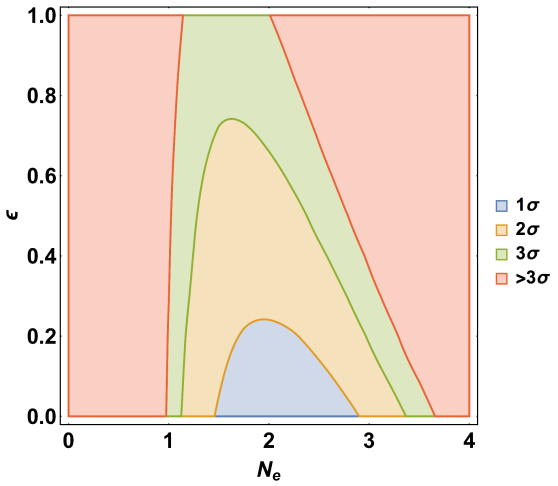

Figure 4.11: The likelihood of N_e as a function of the normalization of ϕ_e and of ϵ, the fraction of electron antineutrinos.

Adding the prior distribution $R_{e\mu}$ (4.35), $\mathcal{L}_{\overline{\nu}_e}$ (4.43), $\mathcal{L}_\mu$ (4.21), $\mathcal{L}_s$ (4.16), we compute the complete likelihood function of N_e and ϵ as follows:

$$\mathcal{L}_e(N_e,\epsilon) = N_e \int_0^\infty \frac{dN_\mu}{N_\mu^2} \int_0^\infty db_s \; \mathcal{L}_{\text{HESE}}(N_e,\epsilon) R_{e\mu}\left(\frac{N_e}{N_\mu}\right) \; \mathcal{L}_{\overline{\nu}_e}(N_e,\epsilon) \; \mathcal{L}_\mu(N_\mu) \; \mathcal{L}_s(b_s) \tag{4.47}$$

In the previous expression we are using $N_\mu \simeq N_\tau$ (see equation (4.33)), in order to simplify the calculation.

The results are illustrated in figure 4.11. The regions are defined using the Gaussian 2-dimensional approximation:

$$(1-\text{CL}_1) \times \mathcal{L}_e^{max} \leq \mathcal{L}_e \leq (1-\text{CL}_2) \times \mathcal{L}_e^{max} \tag{4.48}$$

Marginalizing the 2-dimensional likelihood we obtain, separately, an estimate for N_e and ϵ:

$$\begin{aligned} N_e &= 1.83 \pm 0.44 \\ \epsilon &< 0.52 \text{ at } 90\% \text{ CL} \end{aligned} \tag{4.49}$$

We have checked that the choice between the spectrum given in equation (4.18) and the spectrum given in equation (4.17) affects the previous analysis at level

of few %. The same consideration applies considering a different normalization point (within a factor 2) in the flux defined in equation (4.18). This demonstrates the robustness of the analyses proposed in this paper.

In table 4.6 we summarize the results obtained in this subsection. With these results on normalization factors of the neutrino fluxes N_ℓ ($\ell = e, \mu, \tau$) and on ϵ, we have concluded the definition of our model for universal spectrum of the cosmic neutrinos given in equation (4.18).

N_e	N_μ	N_τ	ϵ (68-90% C.L.)
1.98 ± 0.45	1.50 ± 0.50	1.48 ± 0.54	$< 0.25 - < 0.52$

Table 4.6: Summary of the normalizations of the high energy neutrino flux at Earth defined in equation (4.18), divided per flavor. The parameter ϵ given in equation (4.42) is the fraction of electron antineutrinos with respect to the ϕ_e flux.

Before discussing the predictions, it is useful to see again figure 4.11 keeping in mind table 4.6. It can be noticed that $N_e \simeq N_\mu \simeq N_\tau$ (expected from π production) is contained into the 1σ region; moreover, a small value for ϵ is preferable.

4.3.4 Predictions and critical aspects of the model

Having introduced and described our model, we can assess the expectations. We will discuss in the following three specific instances: 1) we examine in section 4.3.4 the flavour composition of the universal spectrum defined above and compare it with some important cases; 2) we discuss in section 4.3.4 the expected number of double pulse and Glashow resonance events, examining the uncertainties and showing their relevance; 3) we consider in section 4.3.4 the angular distribution of the events and emphasize the critical importance of testing it for the low energy part of the spectrum, possibly, using new detectors in the Northern hemisphere.

Flavor composition at Earth

First of all, we discuss what flavour composition of the universal spectrum we obtain from our model and compare it with the theoretical expectations from some specific models for cosmic neutrino production.

Theory: using the natural parametrization described in the first section it is trivial to compute the flavour composition expected from a theoretical standpoint for different mechanisms of production. For a generic mechanism, with initial flavour composition

$$(\xi_e^0 : \xi_\mu^0 : \xi_\tau^0) = (x : 1-x : 0) \tag{4.50}$$

the fraction ξ_e of $\nu_e + \bar{\nu}_e$ after neutrino oscillations is equal to:

$$\xi_e(x) = x\left(\frac{1}{3} + 2P_0\right) + (1-x)\left(\frac{1}{3} - P_0 + P_1\right) \tag{4.51}$$

where $x = 1$ denotes the neutron decay scenario, $x = 1/3$ the pion decay scenario and $x = 0$ the damped muon scenario, as already discussed in section 4.3.3. This flavour ratio is useful because it allows a clear discrimination of the different theoretical predictions, due to the fact that $P_{e\mu} \simeq P_{e\tau} \approx P_{ee}/2$, i.e. ν_e is the neutrino that mixes the least with other neutrinos.

Observations: using the fluxes reported in table 4.6, we compute the flavour composition. The normalization of the total flux (a pure number, see equation (4.18)) is given by:

$$N_{\rm tot} = N_e + N_\mu + N_\tau = 4.96 \pm 0.86 \tag{4.52}$$

where the uncertainty is obtained summing in quadrature the uncertainties on the different normalizations. The observed flavour ratio of $\nu_e + \bar{\nu}_e$ is thus equal to:

$$\xi_e^{\rm obs} = \frac{N_e}{N_e + N_\mu + N_\tau} = 0.40 \pm 0.11 \tag{4.53}$$

where the uncertainty is, as usual, given by:

$$\Delta\xi_e^{\rm obs} = \sqrt{\left(\frac{\Delta N_e}{N_e}\right)^2 + \left(\frac{\Delta N_{\rm tot}}{N_{\rm tot}}\right)^2} \tag{4.54}$$

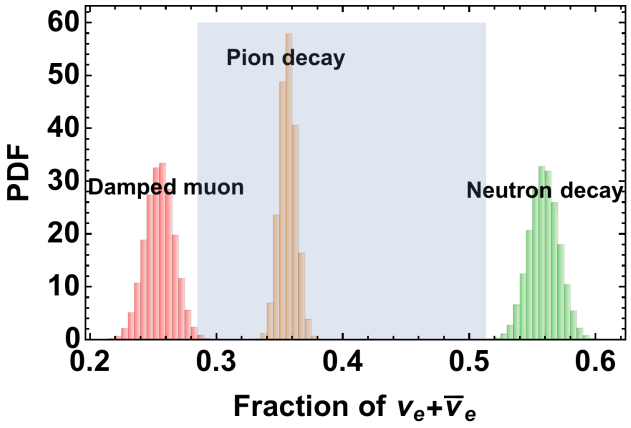

Figure 4.12: Comparison between the theoretical flavour ratio expected from different mechanisms of production (colored histograms) and the observed one (shaded area).

The three histograms represent the predictions due to oscillations, while the gray vertical band covers the range given in equation (4.53).

Comparison: The comparison between theoretical expectations (equation (4.51)) and the observed flavour ratio (equation (4.53)) is shown in figure 4.12. This indicates compatibility with the pion decay scenario, that is also the most plausible mechanism of production from a theoretical point of view. The neutron decay scenario is excluded at about 2σ, but a stronger constraint is given by the fact that $\epsilon = 1$ (i.e. the neutron decay scenario) is excluded at least at 3σ (see figure 4.11). On the other hand, the damped muon scenario is still compatible with the expectations within 1.5σ.

Taking simultaneously into account the flavour ratio ξ_e and the preference for small ϵ, we conclude that, under the hypothesis that no energy cutoff is present below $\sim 7 - 8\,\mathrm{PeV}$, there is an hint for $p\gamma$ as mechanism of production. In this scenario high energy neutrinos are likely to be produced in the decay of π^+ and, in smaller amount, in the decay of π^-. As a consequence, the flux of ν_e is larger than the flux of $\bar{\nu}_e$.

Observable high energy events of new type

Only the high energy part of the spectrum is relevant for the computation of double pulse events and Glashow resonance events: these events are related to the $\propto E^{-2.1}$ part of the spectrum. There is thus no difference in expectations when we use the spectrum suggested by through-going muons, or the broken power-law spectrum of equation (4.17), or the two power-law spectrum of equation (4.18). Let us proceed to evaluate the expectations assuming T = 5.7 years of exposure.

Double pulse events In subsection 4.3.3 we have seen that $\phi_\tau \simeq \phi_\mu$, due to neutrino oscillations. We remark that it is always true for a generic production mechanism, not only for the pion decay scenario.

This result gives rise to an important theoretical prediction. Combining equations (4.33) and (4.30) (or similarly equations (4.27) and (4.30)), we find that the expected number of double pulse events after T = 5.7 years of exposure is:

$$\mathcal{R}^{\rm th}_{\rm 2P} = 0.65 \pm 0.24 \tag{4.55}$$

if we assume there is no energy cutoff. About this expectation, we find it important to remark that:

1. the IceCube collaboration used a E^{-2} spectrum for the calculation of double pulse events [234]; our expectations are in excellent agreement with [234] and also with [235];

2. even more importantly, half of the expected double pulse events are produced by neutrinos with an initial energy of 2 PeV, i.e. neutrinos which have been already observed by IceCube. As a consequence, tau neutrinos *must be observed* in the future: it is only a matter of exposure.

The last consideration is very remarkable, because the observation of tau neutrinos would be the definitive proof that cosmic neutrinos have been detected.
However, we have to consider that the presence of an energy cutoff could reduce the possibility to observe a double pulse event. An energy cutoff at 2 PeV, 5 PeV and 10 PeV would reduce the previous expectation to 55%, 70% and 85%, respectively.

Glashow resonance events Let us use the best fit value of N_e, reported in equation (4.49), with the expected number of resonant events given by equation (4.41) and assuming pion decay as mechanism of production (as suggested by the result of section 4.3.4).

The number of events depends upon ϵ. Assuming $\epsilon = 1/2$, namely for pp production, this is:

$$\mathcal{R}_{\mathrm{G}}^{(\mathrm{pp})} = 2.28 \pm 0.52 \tag{4.56}$$

while in the case $\epsilon = 1/4$, that is the idealized case of $p\gamma$ production (or minimum value expected) this is:

$$\mathcal{R}_{\mathrm{G}}^{(\mathrm{p}\gamma)} = 1.14 \pm 0.26 \tag{4.57}$$

These consideration show that, if the baseline model is correct and, in particular, the spectrum does not have a cutoff for energies much smaller than 6.32 PeV, Glashow resonance events should be seen in the future years.
Note that the preference for small values for ϵ, visible from figure 4.11 and the relevant discussion, derives just from the non observation of resonant events in the current IceCube dataset. The presence of an energy cutoff much smaller than 6.32 PeV diminishes or inhibits the possibility to separate the contribution of ν_e and $\bar{\nu}_e$ and, as a consequence, to extract useful information on the parameter ϵ. (On the contrary, the constraint on N_e can be calculated also when a cutoff is present, and we have checked that its impact is negligible with respect to the result obtained in this paper.) We mention in passing speculative scenarios for the production of the neutrinos, with major deviations from the previous standard cases: considering the value $\epsilon = 1$ for the neutron decay and $\epsilon = 0$ for the damped muon scenario with only π^+ at the source, the expected number of resonant events would become 4.2 and 0, respectively.

The angular distribution of the flux

The diffuse flux of high energy neutrinos detected by IceCube is compatible with the isotropy. On the contrary, if we assume isotropy also for the low energy part, there is tension between the HESE analysis [173] and the through-going muons analysis [172], as remarked in [228] (even if, strictly speaking, a direct comparison is not possible, since the energy threshold of HESE is 30 TeV [173] whereas the through-going muons analysis, at low energy, concerns neutrinos with energy of few TeV or less [172]). Let us recall the argument.

The analysis of the through-going muons at TeV energy has been performed to identify prompt neutrinos, that are expected to follow an $E^{-2.7}$ spectrum and to be isotropically distributed. An astrophysical isotropic component with an $E^{-2.9}$ spectrum (as suggested by HESE) or a two power-law flux $E^{-3.5} + E^{-2.08}$ (as suggested by our model) would produce a larger excess at low energy than the one expected from prompt neutrinos [228]. On the contrary, the through-going muons analysis did not observe any significant excess over the conventional background at low energy and an upper limit on the prompt neutrino flux has been placed. In view of neutrino oscillations, the same bound apply to tau neutrinos and similar bounds apply to electron neutrinos. This remarks is worth of consideration and can be regarded as an issue. It could be due to:

- the presence of an additional component of high energy neutrinos, observed mostly or only from the Southern hemisphere, as already suggested in [226, 228]. The multi-component model proposed in [228], that predicts a Galactic contribution between 10% and 20%, is still compatible with the most recent experimental constraints concerning the Galactic flux, provided by ANTARES [242] and IceCube [243]. However, a Galactic flux $E^{-\alpha}$, with $\alpha \in [2.4, 2.7]$ is no more sufficient to explain alone the very steep spectrum suggested by the last HESE dataset [173] that behave as $E^{-2.9}$;

- the different backgrounds contributing to the dataset. In fact, only prompt neutrinos (discussed in subsection 4.3.2) are relevant for the through-going muons analysis above 200 TeV whereas conventional neutrinos, prompt neutrinos and penetrating muons (see section 4.3.2), are relevant for the HESE analysis, and some of them are prominent in the Southern hemisphere;

- a larger contamination of conventional atmospheric background than expected, that could be related to an efficiency of the IceCube veto smaller than expected. This is a kind of speculative scenario that would be in agreement with the $E^{-3.5}$ component of our two power-law model, since the conventional atmospheric background (both muons and neutrinos) follows an $E^{-3.7}$ spectrum;

- another change of slope between 1 TeV and 30 TeV, although it is quite hard to imagine a physical motivation that could produce this effect.

4.4 The importance of observing astrophysical tau neutrinos

The work presented hereafter has been published in [2], and it is based on the simple expectation of astrophysical tau neutrinos, as discussed in §4.1.1. Quantitative predictions of the ν_τ-induced events in the most relevant detectors are presented, as well as the impact of their non-observation.

4.4.1 Theoretical overview

Non-zero neutrino masses have been considered seriously since the neutrino was proposed (Pauli, Fermi, Perrin) and allow us to explain a wide set of phenomena. While they imply modifications of the accepted standard model of elementary particles, these modifications fit well the conventional three family picture. Neutrino masses emerge quite naturally [244, 245]; if we describe them with effective operators [245], neither the gauge group nor the particle content should be modified. This position is completely consistent with the currently available data and maintains predictive power. E.g., a transition magnetic moment is predicted to exist, even if it is expected to be small $\mu_\nu \sim 10^{-24}\mu_\mathrm{B}$ [246] (the adimensional constant $\sim 3G_F m_e m_\nu/(16\sqrt{2}\pi^2)(m_\tau/m_W)^2$ is evaluated with $m_\nu \sim \sqrt{\Delta m^2} = 50$ meV, where $\Delta m^2 = 2.5 \times 10^{-3}$ eV^2). On the contrary, we do not have convincing theoretical indications in favour of other light neutrinos besides the usual three.[9]

The observed phenomenology of oscillations (see [249, 250, 251, 252, 253, 254, 255, 256, 257] for an incomplete list) can be explained with three massive neutrino states with different masses, which imply two different frequencies of oscillation in vacuum: these have been measured, testing the oscillation phases $\varphi_{ij} = (E_{\nu_i} - E_{\nu_j})t/\hbar$ with $E_{\nu_i} = \sqrt{\mathbf{p}^2 + m_{\nu_i}^2}$. Solar neutrinos offer evidence for another effect for neutrinos that propagate in ordinary matter [258], which

[9] The same is largely true for the known phenomenology [247, 248]. There are several anomalies that could be explained individually invoking new oscillations, however the overall picture lacks of consistency. Conversely, Z-width measurements rule out other interacting neutrinos species; big-bang nucleosynthesis is consistent with three neutrino species; the study of the anisotropies of the microwave distribution at cosmic scales indicates the same and together with cosmological measurements at smaller scales yields a tight bound on neutrino masses.

implies an additional frequency of oscillation associated to the energy $E'_{\nu_e} - E'_{\nu_\mu} = E'_{\nu_e} - E'_{\nu_\tau} = \sqrt{2} G_F\, n_e$, where n_e is the electronic number density.

The importance of neutrino oscillations for cosmic neutrinos has been generally appreciated after [259], even if their relevance and implications have been discussed even much in advance, see, e.g., [260, 25]. The conventional formalism is the simplest one, namely averaged vacuum oscillations [25]. A particularly convenient parametrization of the effects of vacuum oscillations was discussed in [27]. Before passing to the quantitative considerations, we assess the reliability of the above theoretical setup.

Possible deviations from the minimal assumption The distances traveled by cosmic neutrinos are much larger than those explored directly and, moreover, the corresponding energies are very small, $\Delta m^2_{\rm atm}\, L/(2E^\star_\nu) = 6 \times 10^{-17}$ eV for $\Delta m^2_{\rm atm} = 2.5 \times 10^{-3}\,{\rm eV}^2$ and $E^\star_\nu = 50$ TeV. These considerations suggest that new physics could play a role. Therefore, we examined a number of concrete possibilities:

1. The matter effect [258] could be relevant if neutrinos are produced in a dense medium. This was studied in [261], finding that some effects exist for energies $\ll E^\star_\nu$, smaller than those of our interest.

2. If neutrinos are produced near a neutron star, the neutrino magnetic energy, $\delta H = -\boldsymbol{\mu}_\nu \cdot \mathbf{B}$ is of the same size as the vacuum term $\Delta m^2_{\rm atm}\, L/(2E^\star_\nu)$ for extreme parameters $B = 10^{11}$ T and $\mu_\nu = 4 \times 10^{-24} \mu_{\rm B}$. However, neutrino leave the star at velocity c, and the accumulated phase $\delta\varphi = T\,\delta H \sim 10^{-5}$ is very small.

3. Suppose that different neutrinos propagate differently in gravitational fields [262] having peculiar dispersion relations such as $E^2_{\nu_i} = \mathbf{p}^2 + m^2_{\nu_i} + \eta_{\nu_i} \mathbf{p}^4/M^2_{\rm Pl}$ (where $M_{\rm Pl} = 1.2 \times 10^9\,{\rm GeV}$ is the Planck mass and η_{ν_i} are i-dependent coefficients) see for a recent discussion [263].

   This would imply an effect for energies above $E^\star_\nu$ if $\eta_i - \eta_j \geq 1/20$; however, the theoretical motivations and the completeness of the modeling seems to be weak.

4. Certain models for sterile neutrinos, which would lead to new effect on cosmic scales, have slightly stronger theoretical bases. These include the model with exact mirror symmetry [264] or pseudoDirac neutrinos [265]; in both cases, tau neutrinos have to be produced due to oscillations, just as in the three flavour case.

Assessment of the vacuum oscillation hypothesis The above discussion does not strive to completeness but simply to argue the following position: even if in principle the propagation of cosmic neutrinos could be possibly affected by new effects, as (some of) those examined above or other ones - for instance, those described in [266, 267] - we fail to see any convincing reason at present to assume a deviation from the conventional picture. In particular there is *no such indication from the available data from IceCube, interpreted in terms of cosmic neutrinos*, see e.g., [241, 268, 1]. Conversely, in the most plausible astrophysical situations, the sites of neutrino production are typically almost empty and the simple and assessed picture of neutrino propagation, that includes only three flavour vacuum oscillations, does apply.

As a final observation apropos, we would like to remind that the ratio L/E_ν, relevant for the vacuum oscillations phase of high energy neutrinos, is similar to other L/E_ν ratios that have been already probed with low energy neutrino astronomy.

In view of these reasons, we will proceed with a detailed quantitative exploration of the minimal hypothesis that concerns the propagation of cosmic neutrinos, namely, we will assume the occurrence of three-flavor vacuum oscillations and no other phenomena.

Oscillation and survival probabilities The distances and the energies for several interesting cases, relevant for vacuum neutrino oscillation studies, are resumed in Fig. 4.13.

In the case in which we are interested (ordinary three flavour neutrinos) the phases of propagation are very large. Therefore, the values of the three-flavor oscillation/survival probabilities can be written as Eq. (1.36) [25]:

$$P_{\ell\ell'} = \sum_{i=1}^{3} |U_{\ell i}|^2 |U_{\ell' i}|^2 \qquad \ell, \ell' = e, \mu, \tau$$

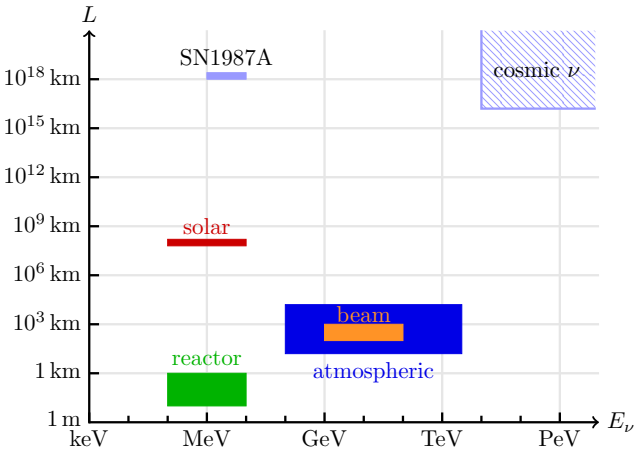

Figure 4.13: The regions of the L and E_ν space relevant for experiments on neutrino oscillations (red, blue, orange and green rectangles), for SN1987 (light blue rectangle) and for the neutrinos that can be detected in IceCube (light blue shaded rectangle).

As already reported in §1.2.3, we computed the distributions of $P_{\ell\ell'}$ starting from the best fit to the neutrino oscillation experiments by [30]. Sampling the oscillation parameters distributions of Fig. 1 of [30], we obtained the distributions for the $P_{\ell\ell'}$, which we show in Fig. 4.14.

4.4.2 Tau neutrinos from neutrino oscillations

Tau neutrinos are assumed not to be produced in standard astrophysical mechanisms of high energy neutrino production. On the other hand, tau neutrinos are always expected at Earth due to standard neutrino oscillations, as shown in Fig. 4.15.

As shown in Fig. 4.15 (discussed below) and consistently with [1], the observation of an astrophysical muon neutrino flux [17, 269] by itself would imply a very similar tau neutrino flux at Earth, assuming the validity of standard three-flavor neutrino oscillations up to these energies.

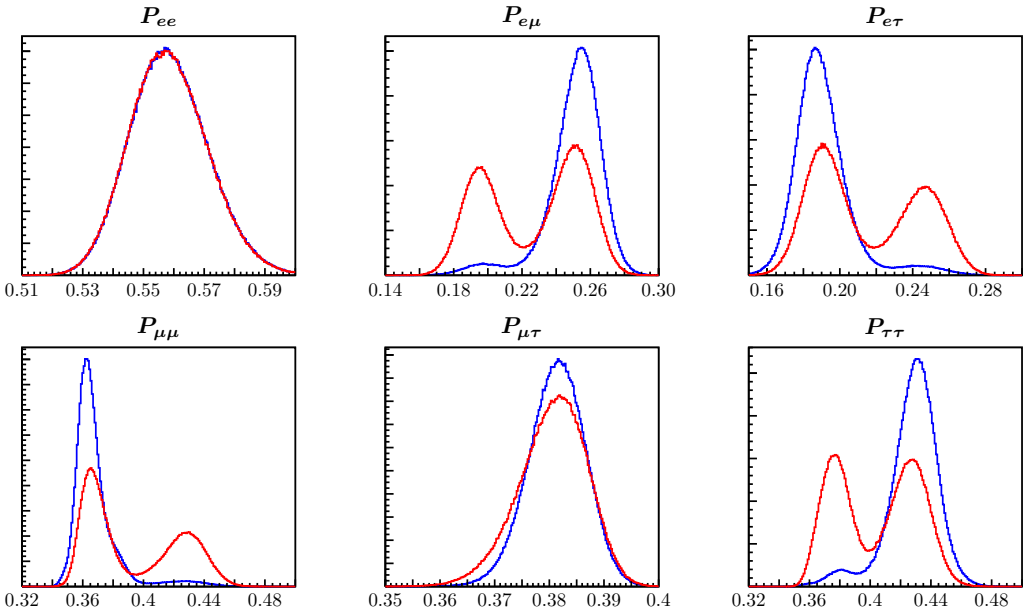

Figure 4.14: The PDFs of the oscillation/survival probabilities $P_{\ell\ell'}$ in the case of normal ordering (blue) and inverse ordering (red), in the average regime.

By considering the flavour fractions before and after oscillations,

$$\xi_\ell = \frac{\Phi_{\nu_\ell}}{\Phi_{\nu_e} + \Phi_{\nu_\mu} + \Phi_{\nu_\tau}} \ , \ \xi^0_\ell = \frac{\Phi^0_{\nu_\ell}}{\Phi_{\nu_e} + \Phi_{\nu_\mu} + \Phi_{\nu_\tau}}$$

where $0 \leq \xi_\ell \leq 1$, $0 \leq \xi^0_\ell \leq 1$ and $\ell = e, \mu, \tau$, we obtain the astrophysical neutrino flux fraction at Earth after oscillations

$$\xi_\ell = P_{\ell e}(1 - \xi^0_\mu - \xi^0_\tau) + P_{\ell\mu}\xi^0_\mu + P_{\ell\tau}\xi^0_\tau \tag{4.58}$$

where the generic mechanism of production at the source is described by two parameters,

$$(\nu_e : \nu_\mu : \nu_\tau) = (1 - \xi^0_\mu - \xi^0_\tau : \xi^0_\mu : \xi^0_\tau)$$

subject to the condition $0 \leq 1 - \xi^0_\mu - \xi^0_\tau \leq 1$. Starting from this general flavour composition at the source, it is possible to evaluate the ratio between the flux of ν_τ and the flux of ν_μ at Earth, that we call $R_{\tau\mu}$. This quantity is particularly

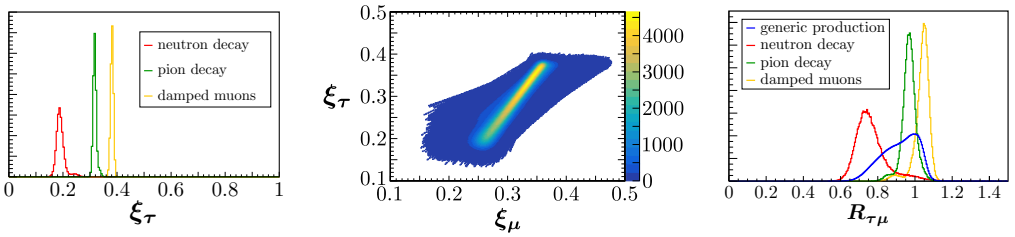

Figure 4.15: Left panel: the PDFs of the fraction of tau neutrinos at Earth expected from standard production mechanisms of high energy neutrinos, after neutrino oscillations. Central panel: the astrophysical tau neutrino flux fraction at Earth ξ_τ vs. the astrophysical muon neutrino flux fraction at Earth ξ_μ. The color bar indicates how many times (out of 10^7) a certain bin has been filled. Right panel: the PDFs of the ratio between the flux of tau neutrinos and flux of muon neutrinos (at Earth) for different production mechanisms and for a generic situation (blue line). These plots have been obtained sampling the survival/oscillation probabilities according to their distribution about 10^5 times for each ξ_μ^0, which has been picked uniformly between 0 and 1. For these three plots, and from now on, we assume normal ordering.

interesting since the flux of ν_μ is measured by means of the through-going muons flux. The function $R_{\tau\mu}$ is given by the following expression:

$$R_{\tau\mu} = \frac{P_{e\tau} + \xi_\mu^0(P_{\mu\tau} - P_{e\tau}) + \xi_\tau^0(P_{\tau\tau} - P_{e\tau})}{P_{e\mu} + \xi_\mu^0(P_{\mu\mu} - P_{e\mu}) + \xi_\tau^0(P_{\mu\tau} - P_{e\mu})}$$

In standard astrophysical environments tau neutrinos are not produced at the source, that motivates us to assume $\xi_\tau^0 = 0$. If a small fraction of ν_τ is present at the source, the flux of ν_τ at Earth would slightly increase.

Under this assumption the previous equation becomes simpler:

$$R_{\tau\mu} = \frac{P_{e\tau} + \xi_\mu^0(P_{\mu\tau} - P_{e\tau})}{P_{e\mu} + \xi_\mu^0(P_{\mu\mu} - P_{e\mu})} \tag{4.59}$$

In the rest of this work, we will consider the expression for $R_{\tau\mu}$ given in Eq. (4.59); now, we proceed to quantify its value.

In the left panel of Fig. 4.15, we show the expected fraction of ν_τ at Earth, using Eq. (4.58) and taking into account the uncertainties on neutrino oscillations. The production mechanisms at the source that are considered are the following:

- $(\xi_e^0 : \xi_\mu^0 : \xi_\tau^0) = (1 : 0 : 0)$, neutron decay;
- $(\xi_e^0 : \xi_\mu^0 : \xi_\tau^0) = (1/3 : 2/3 : 0)$, pion decay;
- $(\xi_e^0 : \xi_\mu^0 : \xi_\tau^0) = (0 : 1 : 0)$, damped muons.

The second is the most plausible one (possibly, with minor variants), and the other two are introduced mostly for the purpose of comparison.

Sampling ξ_μ^0 uniformly in $[0, 1]$ and sampling the oscillation parameters $P_{\ell\ell'}$ according to their distribution (see Fig. 4.14), we obtain the second panel of Fig. 4.15, while the quantity relevant for the rightmost panel of Fig. 4.15 is the ratio of the tau neutrino flux to the muon neutrino flux at Earth, defined in Eq. (4.59). Using the normal hierarchy in the case of $\xi_\mu^0 \in [0, 1]$, we obtain

$$R_{\tau\mu}^{\mathrm{NH}} = 1.00^{+0.05}_{-0.15}$$

and its distribution is represented by the blue line in the rightmost panel of Fig. 4.15.

We notice that the flux of ν_τ is strictly related to the flux of ν_μ:

$$\phi_\tau \geq 0.78\,\phi_\mu \quad \text{within } 90\% \text{ C.L.}$$

This means that once ϕ_μ is measured, ϕ_τ is very strongly constrained, if standard neutrino oscillations hold. This consideration is relevant, since ϕ_μ is measured in IceCube by means of the through-going muons signal, i.e. the flux of muons generated by ν_μ coming from the hemisphere opposite to the one in which the neutrino telescope is located. In the case of IceCube the through-going muons come from the Northern hemisphere [269], whereas for the upcoming KM3NeT they will come mostly from the Southern hemisphere.

The previous results are obtained using the normal hierarchy, that is favoured at approximately 2σ by [30]. Using the inverted hierarchy in the case of $\xi_\mu^0 \in [0, 1]$, we obtain

$$R_{\tau\mu}^{\mathrm{IH}} = 1.02^{+0.04}_{-0.15}$$

The quantity $R_{\tau\mu}$ is relevant, since it will be used in Sec. 4.4.4 to predict the expected number of double cascades in different detectors.

4.4.3 Double pulse and double bang: the effective areas

As stated in the introduction, a tau neutrino usually produces a shower-like event and it cannot be distinguished from other neutrinos: in fact, a ν_e that interacts via charged current interaction, or whatever neutrino that interacts via neutral current interaction, would produce the same shower-like event.

A tau neutrino can be unequivocally identified when two vertices of interaction become visible, and this happens in the so-called double bangs and double pulses. Before discussing this kind of events we need to introduce some concepts related to the detector. The neutrino telescopes are characterized by several digital optical modules (DOMs) enclosed in strings. There are 86 DOMs for each string in IceCube, but this number can be different for other experiments. The separation between the strings is a peculiar feature of the detector and it is 120 meters in IceCube [17], 240 meters in IceCube-gen2 [202] and 90 meters in KM3NeT [137].

Now we can explain the difference between double pulse and double bang:

- a double bang consists in the observation of two vertices of interaction in two different strings, which are separated by ~ 100 meters in the neutrino telescopes of our concern. This kind of events can be produced only by tau neutrinos having multi-PeV energy. This was the historical method proposed in the past to observe directly a ν_τ [259];

- a double pulse event corresponds to the detection of two subsequent signals in the same DOM. In this case the tau lepton has to travel few tens of meters in order to produce two distinguishable vertices of interaction. For this reason, only tau neutrinos of few hundreds of TeV are capable to produce such an event [234].

In both cases the vertices of interaction must be contained into the detector, therefore double bangs and double pulses are subclasses of the so-called "High Energy Starting Events" (HESE), where "Starting" means that the vertex of interaction is contained into the detector. On the contrary, the case of ν_μ that interact via charged current outside the detector is called "through-going muon"; we will also refer to this class of events in the following of this work, since this class of events can provide important information on the flux at very high energy (above 200 TeV).

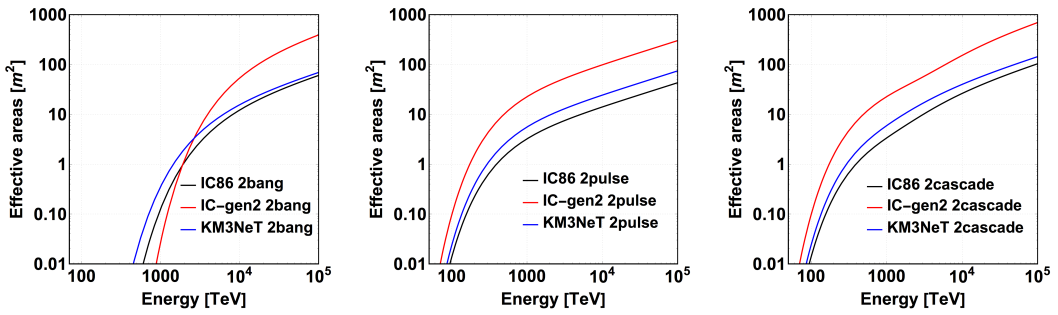

Figure 4.16: Simulated effective areas of double bang, double pulse and double cascade (double pulse + double bang) events for present and future neutrino telescopes.

From here on we will also use the generic term "double cascade" when we consider the two processes together. A general parametrization for the double cascade effective area, which is appropriate for our purposes and that it is based on the analytical expression proposed in [235], is given by the following formula:

$$A_{\rm eff}(E_\nu, E_{\rm min}) = \frac{\rho V}{m_n} \frac{1 + S(E_\nu)}{2} \times {\rm BR} \times \sigma_{\rm cc}(E_\nu) \exp\left(-\frac{E_{\rm min}}{E_\nu}\right) \qquad (4.60)$$

where ρ is the density of the material, V the volume of the detector, m_n the nucleon mass. The function $S(E_\nu)$ is the probability for neutrinos to cross the Earth, namely 0.91, 0.66, 0.37 and 0.18 at 10, 100, 1000 and 10000 TeV [235]. The parameter BR $\simeq 80\%$ denotes the branching ratio of the hadronic decay modes of the tau, which allow the second cascade to be visible (basically it excludes the channel in which a tau lepton decays into a muon [270]). The function $\sigma_{\rm cc}(E_\nu)$ is the charged current cross section [189] (averaged for neutrinos and antineutrinos) and $E_{\rm min}$ is the minimum energy required to observe two vertices of interactions. As stated before, this energy is order of sub-PeV for double pulses and multi-PeV for double bangs; for this reason, double pulse events are intrinsically more likely to detected than double bang events.

Double bangs

In this subsection we examine the first method that was proposed to observe tau neutrinos, i.e. the so called double bang [259], showing how it is possible to obtain

an estimation of the effective area starting from theoretical considerations of the relevant physics. (Before proceeding, note that at the energies of interest for the current IceCube dataset, ν_τ and τ energy losses are negligible, see footnote 12 for a discussion.)

It is possible to estimate the minimum energy required for a ν_τ in order to produce two distinguishable signals in two different strings. In order to do that we take into account the lifetime of the ν_τ. It is easy to verify that a tau neutrino of 1 PeV travels ~ 50 meters before decaying. Moreover, the energy of the tau lepton is about 3/4 the energy of the primary ν_τ. Combining these conditions, we can compute the (average) minimum energy as a function of the required minimum length as follows:

$$E_{\min} = \frac{4}{3}\left(\frac{d}{50\ \mathrm{m}}\right)\ \mathrm{PeV} \tag{4.61}$$

where d is the distance between the strings. Therefore, the minimum energy is equal to 2.4 PeV, 3.2 PeV, and 6.4 PeV for KM3NeT, IceCube and IceCube-gen2, respectively.

The effective area of double bang events is not published, but it is possible to estimate it starting from the effective area of tau neutrinos given in [17]. Comparing our parametrization given in Eq. (4.60) (including also the neutral current cross section, that is included in the total effective area of ν_τ reported in [17]) we found that, far above the 30 TeV energy threshold, the effective area of ν_τ is well reproduced (with coefficient of determination $R^2 = 0.99$) using an effective volume $V = 0.97\ \mathrm{km}^3$ and a minimum energy of 100 TeV.[10] This means that the effective volume is similar to the physical volume of the detector for tau neutrinos.

[10]The meaning of this minimum energy is not relevant for the treatment of double bangs and double pulses. Anyway, in order to check the plausibility of this calculation, let us recall that the energy threshold of IceCube High Energy Starting Events (whose the effective area of ν_τ is connected) is 30 TeV of deposited energy. The deposited energy of a tau neutrinos is about 70%-80% in charged current interaction and 25% in neutral current interaction (see [271] in which the connection between the deposited energy and the reconstructed energy is discussed). Therefore, a minimum incident energy of 100 TeV would correspond to a deposited energy between 20-80 TeV, that is reasonably in agreement with the energy threshold of 30 TeV, that characterizes the high energy starting events (HESE).

In order to estimate the double bang effective area we need to consider the minimum energies described before, in order to cover the distance between two strings. Moreover, we have to consider that the path necessary to reach the second string is a function of the incident angle of neutrinos. In fact, the distance between two different strings is equal to $d/\cos\theta$, where θ denotes the angle between the neutrino's direction and the plane perpendicular to the strings. Therefore the minimum energy required for a ν_τ will be greater than $E_{\rm min}$ for $\theta \neq 0$, namely $E_{\rm min}/\cos\theta$ following (4.61). Taking into account this aspect, we obtain the general parametrization of the double bang effective area as follows:

$$A_{\rm eff}^{\rm 2bang}(E_\nu, E_{\rm min}) = \frac{1}{\pi} \int_{-\pi/2}^{\pi/2} A_{\rm eff}\left(E_\nu, \frac{E_{\rm min}}{\cos\theta}\right) d\theta \tag{4.62}$$

The previous formula is valid for an isotropic flux of neutrinos, as expected from cosmic neutrinos. In the left panel of Fig. 4.16 we report the simulated effective areas for double bangs for the three different neutrino telescopes that we have considered. We denote the three experiments with the name IC86 (IceCube), IC-gen2 (IceCube generation 2) and KM3NeT. The parameters used to obtain them are reported in Tab. 4.7. For IC-gen2 we consider that the new detector will have a sensitivity about 7 times larger than the present IceCube [202], therefore the effective volume for the double bang detection would be $V = 6.8$ km^3. For KM3NeT, instead, we limit our analysis to the ideal scenario of $V = 1$ km^3, since there is still no information available for this process in this future neutrino telescope. In view of the fact that the effective volume of double bang for IceCube is close to 1 km^3, we believe that our approximation is adequate.

Double pulses

In this subsection we focus on double pulses, i.e. the processes in which the two vertices of interaction are identified in the same optical module. Comparing (4.60) with the IceCube double pulse effective area given in [234], as already done in [235], we found that it is well reproduced (within an average uncertainty of 5% between 100 TeV and 10 PeV) by the set of parameters $V = 0.28$ km^3 $E_{\rm min} = 0.5$ PeV. This means that the effective volume for this kind of event is a factor 3.5 smaller than the physical volume of the detector. Let us recall that in [234]

Detector	Event type	ρ ($\mathrm{g\,cm^{-3}}$)	V ($\mathrm{km^3}$)	E_{min} (PeV)	d (m)
IC86	Double pulse	0.917	0.63	0.58	22
IC86	Double bang	0.917	0.97	3.2	120
IC-gen2	Double pulse	0.917	4.4	0.58	22
IC-gen2	Double bang	0.917	6.8	6.4	240
KM3NeT	Double pulse	1	1	0.58	22
KM3NeT	Double bang	1	1	2.4	90

Table 4.7: Table of the parameters related to the double pulse and double bang effective areas for IceCube, IceCube-gen2 and KM3NeT. The parameters for IceCube are based on the present detector whereas the parameters for IceCube-gen2 and KM3NeT are estimated.

the expected number of double pulses in 4 years was ~ 0.5 events, assuming an E^{-2} spectrum.

Recently IceCube has presented an updated (preliminary) analysis of the double cascade events expected in 6 years in [272]. The expected number of identifiable astrophysical tau neutrinos is claimed to be equal to:

$$N_{\mathrm{2p}}^{\mathrm{IC86}} = 2.318^{+0.038}_{-0.029}$$

after 6 years of exposure, considering an $E^{-2.3}$ spectrum, with normalization at 100 TeV of $1.5 \times 10^{-18}\,\mathrm{GeV^{-1}cm^{-2}sec^{-1}sr^{-1}}$. We denote this flux by $d\phi/dE_\nu$. In this case the effective area has not been released, so that the best we can do is to use the same minimum energy of the previous analysis, changing the effective volume in order to reproduce the expected number of events.

The expected number of events can be computed using the following formula:

$$N_{\mathrm{2p}}(E_{\mathrm{min}}) = 4\pi \mathrm{T} \int_0^\infty \frac{d\phi}{dE_\nu} A_{\mathrm{eff}}(E_\nu, E_{\mathrm{min}})\, dE_\nu$$

Assuming that the expectations reported in [272] are related to double cascade events (double pulse + double bang), in order to be in agreement with them the

effective volume of Eq. (4.60) must be equal to $V = 0.63$ km^3, fixing $E_{\rm min} = 0.5$ PeV, as in the previous analysis (this value, in fact, depends on the features of the process, not on the optimization of the analysis). Under this assumption[11], a fraction of the expected number of events is provided by double bangs.

In our understanding, this conclusion means that IceCube has performed an optimization of the analysis dedicated to the research of tau neutrinos, gaining more than a factor 2 in the expected number of events when compared to the previous analysis [234]. Summarizing, the effective area for double pulse events is exactly given by the same formula of Eq. (4.60). In Fig. 4.16 we report the simulated effective areas for the future neutrino telescopes, obtained with the parameters reported in Tab. 4.7.

The search for tau neutrinos with energies larger than the maximum currently observed in IceCube, ~ 5 PeV, is also regarded with interest: this adds further motivation for the present study. However, at ultra-high energies the detection principle has to change, since we are dealing with distances that exceed the size of any conceivable detector:

$$\ell_\tau = c\gamma_\tau\tau_\tau^0 \approx 10 \text{ km} \times \frac{E_\tau}{0.2 \text{ EeV}}$$

Let us consider tau neutrinos of similar ultra-high energies, that interact inside the Earth and decay outside of it. These could be observed by a detector devoted to monitor the circular region *below* its own horizon [273, 274, 275]; the recent efforts to achieve this goal using a satellite are documented in [276]. Note that for energies $\gtrsim 0.1$ EeV the tau particles interact significantly[12] with the matter in which they propagate, see [277] for a recent study.

[11] Let us remark that it is a conservative hypothesis, because the assumption that 2.3 events are created only by double pulses would increase the expected number of total double cascade events, when also the contribution of the double bang events is taken into account. This would make our conclusions even stronger.

[12] The range in water is $x \sim x_* \log[(1+E_\tau^{\rm in}/\varepsilon)/(1+E_\tau^{\rm fin}/\varepsilon)]$ with $x_* \sim 50$ km and $\varepsilon \sim 10$ TeV, much more than the decay length ℓ_τ till 0.1 EeV. In fact, we have roughly $dE_\tau/dx = -(\alpha+\beta E_\tau)$, where α is almost the same as for the muon while $x_* = 1/\beta$ (mainly due to pair production and to photonuclear interaction) and $\varepsilon = \alpha/\beta$ scale roughly as m_τ/m_μ.

4.4.4 Results

Parent function

The flux of high energy neutrinos, that is relevant for double pulse and double bang events, is the flux above few hundreds of TeV. This can be clearly seen looking at Fig. 4.17, where the parent functions of double cascade events are represented for different spectral indices. The parent function is defined as follows:

$$P(E_\nu, \alpha) = \frac{\int_0^{E_\nu} E^{-\alpha}\, A_{\text{eff}}(E_\nu) dE_\nu}{\int_0^{\infty} E^{-\alpha}\, A_{\text{eff}}(E_\nu) dE_\nu} \tag{4.63}$$

The plots in Fig. 4.17 clearly show that, whatever is the spectral index of the neutrino spectrum, double cascades are mostly generated by neutrinos with energy above few hundreds of TeV. Therefore, when we generally discuss "double cascade"events, we can say that

> the low energy part of the cosmic neutrino spectrum (below 200 TeV)
> is irrelevant for the prediction of the τ event rate.

The previous consideration permits us to use directly the through-going muons flux [269], avoiding all the discussion related to the tension between this spectrum and the HESE spectrum [199], that shows a different behavior below 200 TeV.

Moreover, it is important to stress that tau neutrinos *must* be observed assuming standard oscillations, and that even the presence of a possible energy cutoff is not expected to modify this conclusion strongly. This statement is based on the fact that one 4.5 PeV track event has already been observed; this most likely means that there is no energy cutoff below this energy. In Fig. 4.17 we notice that a considerable fraction of double pulse events is produced by neutrinos below 4.5 PeV; namely, between 60% and 90% going from an hard spectrum to a soft spectrum. Moreover, a 4.5 PeV track requires a more energetic neutrino to be produced, around 10 PeV or above (with large uncertainties, see [271] where the energy reconstruction is widely discussed).

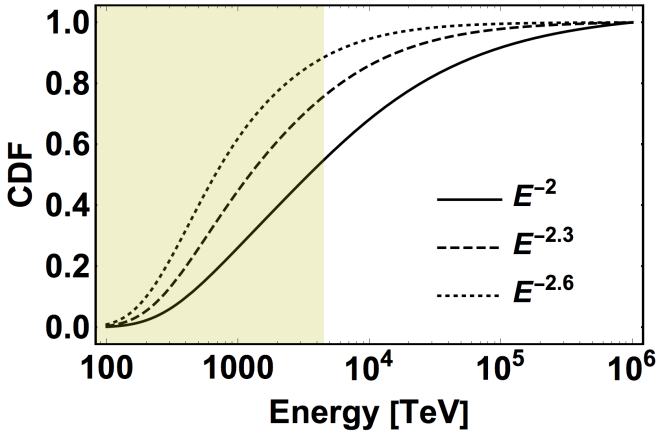

Figure 4.17: Parent function of double cascade events (as defined in Eq. (4.63)), assuming power law spectra $E^{-\alpha}$, with $\alpha = 2, 2.3, 2.6$, without any energy cutoff. The shaded region is the one currently explored by IceCube.

Expected number of events in the pion decay scenario

In this section we use the measured flux of through-going muons [269] to evaluate the expected number of double cascades in the three detectors as a function of the spectral index. We perform the calculation in two different ways:

1. in this section we calculate the expectation for a particular case, i.e. the pion decay, in which the approximation $\phi_\tau = \phi_\mu$ is valid. Moreover, we show the expectations as a function of the spectral index;

2. in the next section we show the general result, taking into account the uncertainties given by the normalization, the spectral index and the production mechanism.

The normalization at 100 TeV, that we denote by $F(\alpha)$, changes with the spectral index, as reported in Fig. 6 of [269]. Namely, the normalization assumes the values 0.65, 0.8, 1, 1.25, 1.5, 1.75 (in the usual units of $10^{-18}\,\mathrm{GeV}^{-1}\,\mathrm{cm}^{-2}\,\mathrm{s}^{-1}\,\mathrm{sr}^{-1}$) for spectral indices $2, 2.1, \ldots, 2.5$ respectively.

We can use this information to evaluate the expected number of events per

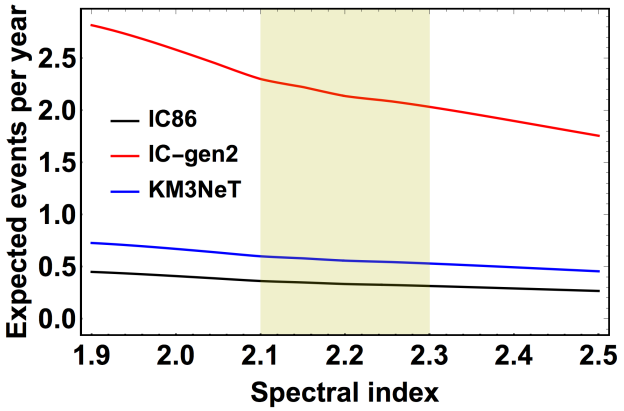

Figure 4.18: Expected number of double cascades in the three detectors considering different spectral indices. The shaded region brackets spectral indices favoured by the analysis of the through-going muons events within 1σ. The shallow dip seen in the curves around $\alpha = 2.1$ is due to the fact that the number of events does not decrease linearly for increasing spectral index. This behavior is related to the low energy threshold of the effective areas of double bang and double pulse; this effect can be also appreciated by looking at Fig. 4.17.

year as a function of the spectral index, using the usual formula:

$$N^i_{\rm 2casc}(\alpha) = 4\pi {\rm T} \int_0^\infty F(\alpha)\, E_\nu^{-\alpha}\, A^i_{\rm eff,2casc}(E_\nu)\, dE_\nu$$

where T is the exposure time and $A^i_{\rm eff,2casc}(E_\nu)$ is the effective area of the i-th experiment. The results are reported in Fig. 4.18, where the 3σ interval of the spectral index is shown, i.e. $1.9 < \alpha < 2.5$. In the same figure also the 1σ band (in yellow) of the spectral index is shown. Within the 1σ region the expected rate is roughly 0.35, 0.55 and 2.15 events per year in IceCube, KM3NeT and IceCube-gen2 respectively. The expectation changes of few % within the 1σ band and of about 40%-50% in the extreme intervals of the 3σ band.

Expected number of events: general case

In this section we present the expectations, in the three different detectors, in the most general way. More specifically:

- we do not assume any spectral index, as we just use its probability distribution function $P(\alpha)$, that is a Gaussian function, being $\alpha = 2.19 \pm 0.1$;
- we do not assume any specific production mechanism, using the distribution $R_{\tau\mu}$ defined in subsection 4.4.2.

Under these hypotheses the expected number of events is given by the following formula:

$$\langle N^i_{\rm 2casc} \rangle = 4\pi {\rm T} \int_0^\infty dE_\nu \int_0^\infty d\alpha \int_0^\infty dr\, r F(\alpha)\, E_\nu^{-\alpha}\, A^i_{\rm eff,2casc}(E_\nu)\, P(\alpha)\, \frac{d\rho}{dr}(r) \quad (4.64)$$

where $\phi_\tau(E_\nu) = rF(\alpha)E_\nu^{-\alpha}$ is the flux of tau neutrino, and we indicate ϕ_τ/ϕ_μ as r, rather than $R_{\tau\mu}$ as in Eq. (4.59), to shorten the notation. The function $d\rho/dr$ is the normalized distribution of $R_{\tau\mu}$, shown in the rightmost in Fig. 4.15. The meaning of the integral in α and r is that, in absence of more precise information on these parameter, we take into account the current uncertainty on the slope of the neutrino distribution and on the flavour ratio, weighting the parameters in the most unbiased manner[13]. $A^i_{\rm eff,2casc}(E_\nu)$ is the effective area for double cascades (i.e. double pulses + double bangs) for the detector i-th, T is the exposure time, $P(\alpha)$ is the PDF of the spectral index and $R_{\tau\mu}(r)$ is the distribution of the ratio between ϕ_τ/ϕ_μ in the case of a generic production mechanism at the source, see the rightmost panel of Fig. 4.15.

The expected yearly rates of double cascades for IceCube, IceCube-gen2 and KM3NeT are, respectively, 0.32, 2.07 and 0.54. Other details are reported in Tab. 4.8.

The ratio between double pulse and double bang events is 4:1 in IceCube and KM3NeT, whereas it becomes 6:1 in IceCube-gen2, as the larger distance between the strings disfavours the double bang detection.

The uncertainties produced by the spectral index and by the production mechanism can be computed using the following formula:

$$\langle \Delta N^i_{\rm 2casc} \rangle = \left(\int_0^\infty d\alpha \int_0^\infty dr\, r \left[N^i_{\rm 2casc}(\alpha) - \langle N^i_{\rm 2casc} \rangle \right]^2 P(\alpha)\, \frac{d\rho}{dr}(r) \right)^{1/2} \quad (4.65)$$

[13] With improved experimental and/or theoretical knowledge, this information should be updated.

Experiment	$N_{2\text{bang}}$	$N_{2\text{p}}$	$N_{2\text{casc}}$	$T_{\text{year}}^{\text{P}>90\%}$	$T_{\text{year}}^{\text{P}>99\%}$	$T_{\text{year}}^{\text{P}>5\sigma}$
IC86	0.07	0.25	0.32	5.1	10.1	31.7
IC-gen2	0.29	1.78	2.07	0.8	1.6	5.0
KM3NeT	0.10	0.44	0.54	3.1	6.1	19.1

Table 4.8: In the columns from 2nd to 4th, the expected yearly rates of tau neutrino events, obtained integrating over the spectral index distribution and over the production mechanisms. The uncertainties associated to these expectation are 30%. In the column from 5th to 7th the number of years required to observe at least one double cascade with a certain probability, namely 90%, 99% or 99.9999% (5σ). In this calculation we consider that the background is equal to the 40% of the signal, as plausibly expected from the information contained in [272].

where $N_{\text{ev}}^{i}(\alpha)$ are the expected number of double cascade events for an $F(\alpha)E^{-\alpha}$ spectrum, evaluated in Sec. 4.4.4. The uncertainties due to the spectral index and the production mechanism amount to $\sim 10\%$, therefore the global uncertainty is dominated by that on the spectrum normalization ($\sim 25\%$ [269, 272]), and it is equal to 30%, summing the uncertainties in quadrature.

Expected number of background events

At this point a clarification is necessary. The flux of ν_τ produced in atmosphere is very low compared to the astrophysical flux of ν_τ, because atmospheric tau neutrinos are produced in the decay of the rare meson D_s. Following [278], the flux of atmospheric tau neutrinos is approximately equal to:

$$E^2\phi_{\nu_\tau}^{\text{atmo}} \simeq 2 \times 10^{-10} \left(\frac{E}{100\ \text{TeV}}\right)^{-0.7} \text{GeV}\,\text{cm}^{-2}\,\text{s}^{-1}\,\text{sr}^{-1}$$

Using the usual effective area for double cascade events, we find that the expected rate of double cascades produced by atmospheric ν_τ is 1/200 of the rate due to astrophysical neutrinos. Therefore this source of background is totally negligible.

On the contrary an important source of background is represented by the misidentified events, classified as double cascades. At present, it is not trivial to evaluate this aspect, since the number of misidentified double cascades is not

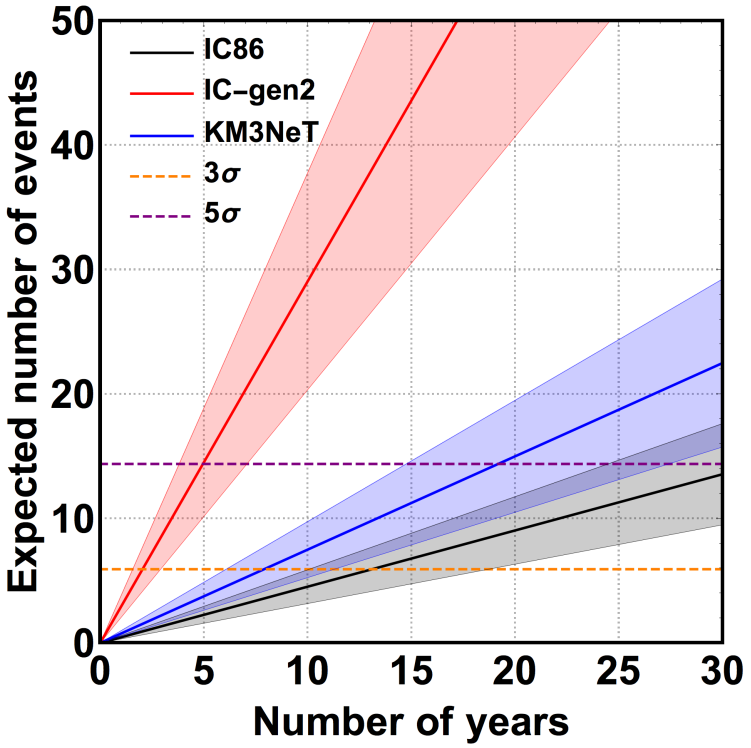

Figure 4.19: The expected number of double cascade events in the three detectors, assuming that the background is equal to the 40% of the signal. The colored bands represent the global uncertainties (spectral index + normalization + production mechanism).

linearly related to other measured atmospheric backgrounds, but it also depends on experimental details connected to the technology used to detect high energy neutrinos. The best that we can do is to use the available informations presented in [272], where the misidentified double cascades are expected to be not negligible and roughly equal to the $\sim 40\%$ of the number of double cascades produced by astrophysical neutrinos.

In Fig. 4.19 we show the expected number of events as a function of the number of years, showing also the associated global uncertainties with the colored bands. These predictions are obtained assuming that the background is 40% of the signal, as supported by the informations contained in [272]. Let us discuss how many

years are required to observe at least 1 event with a certain probability:

- the present IceCube should be close to identify a tau neutrino with a probability of 90%, since an exposure of 5.1 years is required and 6 years of HESE have been already collected. On the other hand, if IceCube does not observe any ν_τ in the next years, this would be still compatible within 5σ with the theory, until ~ 30 years of exposure;

- the situation is totally different in IceCube-gen2, where a ν_τ should be identified in ~ 1 year with a probability of 99%. The non observation of any double cascade would contradict the theory at the level of 5σ, after only 5 years;

- the future KM3NeT should have slightly better performance than IceCube, due to the fact that the strings are separated by 90 meters and water is $\sim 10\%$ denser than ice. This experiment should observe a tau neutrino in about 3 years with a probability of 90%. On the other hand, as for the present IceCube, the non observation of double cascades would represent an issue at 5σ only after an exposure of ~ 20 years.

In conclusion, for both IceCube and KM3NeT some tens of years worth of data have to be collected, before being in contradiction with the theory if no tau neutrinos will be observed. For these reasons the role of IceCube-gen2 is crucial for the observation of this kind of events, since it is expected to observe 2 double cascade events per year in the most general scenario. All these results are summarized in Tab. 4.8.

The non observation of tau neutrinos would have dramatic consequences for the neutrino physics, such as:

- the fraction of ν_τ is much smaller than what expected. Therefore ϕ_τ is not connected to the flux of ϕ_μ, which would mean that neutrino oscillations are violated. This scenario would imply evidence of new physics.

- tau neutrinos are not observed because neutrino telescopes are observing mostly atmospheric background, in which tau neutrinos are not present. This would mean that cosmic neutrinos have not been observed.

For these reasons the direct observation of tau neutrinos is a crucial point for neutrino physics, and their eventual non observation cannot be overlooked in the next years.

Discrimination between signal and misidentified double cascades

In the previous sections we computed the expected number of double cascades produced by astrophysical neutrinos. We have estimated and taken into account the background events resulting from atmospheric ν_τ, that, as discussed, are very few, fewer than 1% of the signal events. We also discussed that the most important source of background is related to the misidentified events. The misidentified events, classified as double cascades, become relevant when we want to know how many years are required to extract the astrophysical signal from the sample of observed events. This will become the most important task, once a sufficient sample of double cascade events will be detected.

As in the previous section and as quoted in [272], the background rate, which exists for sure, corresponds to about 40% of the signal one, i.e. $N_b \approx 0.13\ \mathrm{yr}^{-1}$ for the present IceCube. If we use this value, it is evident that it is not possible yet to discriminate the signal and the background in IceCube and KM3NeT, since, as indicated in Tab. 4.8, the rate of data collection is expected to be very low. On the other hand, the separation between the double cascades produced by astrophysical neutrinos and those due to misidentification is achievable in IceCube-gen2.

In order to test whether the (future) data are consistent with the background, which we call hypothesis H_0, or instead indicate the presence of a signal along with the background, which we call hypothesis H_1, it is useful to define the following test statistic:

$$\mathrm{TS} = \frac{\mathcal{P}(n|H_0)}{\mathcal{P}(n|H_0) + \mathcal{P}(n|H_1)} \tag{4.66}$$

where $\mathcal{P}(n|H_i)$ is the conditional probability of observing n events assuming the hypothesis H_i. For us the yearly rate of signal events is $0.32\ \mathrm{yr}^{-1}$, and the background rate is 40% of that, i.e. $0.13\ \mathrm{yr}^{-1}$: the expected number of events after an exposure time t is thus $\mu_0 = 0.13\, t/\mathrm{yr}$ in the case of background only, and $\mu_1 = 0.32\, t/\mathrm{yr}$ in the case of signal and background. We assume Poissonian

distributions for $\mathcal{P}(n|H_i)$, i.e.:

$$\mathcal{P}(n|H_i) = \frac{\mu_i^n}{n!} e^{-\mu_i}$$

At present ($t = 5.7$ yr) no events are seen ($n = 0$) while we expect $5.7\,\text{year} \times 0.45\,\text{events/year} = 2.6$ events[14] and thus,

$$\text{TS}|_{\text{today}} = \left(1 + e^{-0.45\,t/\text{yr}}\right)^{-1} = 93\%$$

This is not worrisome at all, as this value for the TS corresponds to a 1.8σ-level evidence of background only, but we think the community should be aware of how fast this could change with IceCube-gen2. In order to estimate the exposure needed to accept the hypothesis H_0 or to reject the hypothesis H_1 at a certain confidence level, it is convenient to assume two cases:

1. over time data accumulate as expected in the case of background only;
2. also the signal is present.

These cases are described by the assumption:

$$n(t) = \begin{cases} [N_b\, t + 1/2] & \text{background only} \\ [(N_b + N_s)\, t + 1/2] & \text{also signal} \end{cases} \tag{4.67}$$

where $[x]$ denotes the integer part of x. The result for the test statistics is shown in Fig. 4.20, which concerns IceCube-gen2 [202].

From this figure we see that if the signal is actually present and it is correctly described, it will take 10 years to confirm it at 5σ, while it will take 15 years to establish the most pessimistic scenario, when the signal is absent.[15] The meaning of this result is the following:

[14] Note that this prediction is based on the through-going muons spectrum (see also Tab.4.7) and for this reason slightly differs from the prediction of [272] where an $E^{-2.5}$ spectrum is considered.

[15] A different and simpler take on this matter is the following. We can obtain a similar result by comparing the expected number of background events with an under-fluctuation of the expectations in the case when the signal is also present. If N_b and N_s are the background and signal rates respectively, we obtain that the condition

$$N_{\text{b}} t < (N_{\text{s}} + N_{\text{b}})t - 5\sqrt{(N_{\text{s}} + N_{\text{b}})t}$$

which corresponds roughly to the 5σ criterion, is satisfied after 17 years.

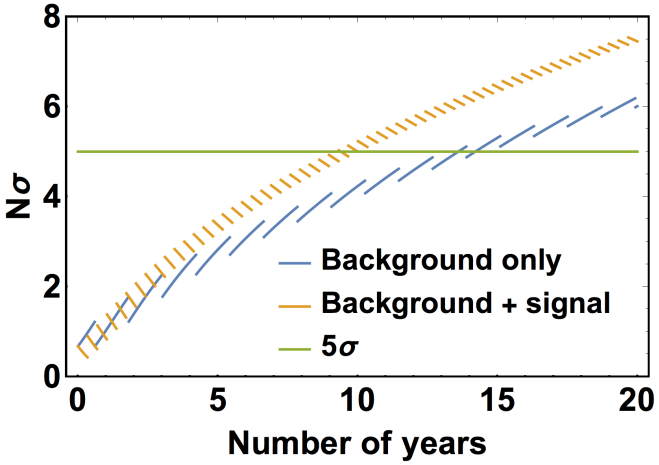

Figure 4.20: In this plot we represent the function TS, defined in Eq. 4.66, for the following cases: *i)* background only (blue line), *ii)* background + signal (orange line). The broken curves follow formally from the function 'integer part' in Eq. (4.67), that describes the fact that, as the time goes by, new individual events are expected to accumulate according to the specified hypothesis.

> once double cascade events will be detected, in order to claim with great confidence that cosmic tau neutrinos have been observed, an important exposure will be required.

On the other hand, as discussed in the previous sections, the non observations of any double bang in IceCube-gen2 could become an issue since the occurrence of double cascade events are expected with a probability of 99% already after 2 years.

Let us remark that the results presented in this section have the character of estimation and might improve by subsequent experimental work and systematic analysis: a significant reduction of the expected misidentified events will be important to decrease the required exposure.

In the upcoming section we present the work that has been published in [4]. The atmospheric and cosmic components of the neutrino spectrum have been modelled in order to evaluate the possible contribution of prompt neutrinos to the astrophysical neutrino analyses. A promising dataset for the extraction of the prompt neutrino signal has been identified and quantitative predictions for

the rates of all components of the neutrino spectrum in such datasets have been computed and discussed.

4.5 The role of prompt neutrinos for the interpretation of the IceCube signals

After almost ten years of operation, the IceCube detector has provided unique and most important observations of neutrino events with energies ranging between 100 GeV and 10 PeV, which resulted in the detection of an astrophysical component of neutrinos [279, 172] and in the measurement of the atmospheric components of the electron and muon neutrino spectrum [126, 127]. The prompt component of the atmospheric neutrino spectrum, which is expected to be produced in the decay of charmed mesons in the atmosphere, has not been measured yet.

On the other hand, some missing pieces of the high-energy neutrino jigsaw puzzle seem to be finally appearing: one notable astronomical coincidence [18] may hint that we are close to detecting the source of cosmic neutrinos. Moreover, two double cascade events attributable to astrophysical tau neutrinos and one candidate Glashow resonance event have been recently observed[16].

The accepted set of assumptions on the astrophysical component, that are adopted for the interpretation of these findings, includes:

1. isotropy
2. standard three-flavor oscillations
3. an unbroken power law for the energy spectrum of the new component.

However, the cosmic neutrino spectrum resulting from the HESE analysis [280] is different from that obtained in the through-going muons analysis [172], as argued, for example, in [228, 1]. Moreover, if the spectrum from HESE were extrapolated down to energies lower than 100 TeV, it would overshoot the gamma-ray diffuse measurements [281].

[16] see the talk by H. Niederhausen, on behalf of the IceCube Collaboration, at the XVIII International Workshop on Neutrino Telescopes (Venice, March 2019).

In this situation, we find it necessary to rely on theoretical guidance. In this work a primary cosmic-ray flux, fitted to the data of AMS-02 [154, 155] and KASCADE-Grande [150], is defined to numerically compute both conventional and prompt components of the atmospheric neutrino spectrum. The cosmic neutrino flux is modeled as a single-population power law, assuming *pp* collisions in dense sources as the production mechanism. The ensuing expectations from theory are combined to the through-going muons analysis to make the astrophysical muon flux phenomenologically precise. The same muon neutrino flux is also used to predict the electron and tau cosmic neutrino fluxes. Credible regions are computed for all neutrino fluxes, which are in turn compared to the available measurements.

Finally, we comment on the results and address

1. the compelling issue[17] of the low-energy softness of the HESE spectrum
2. the lack of detection of prompt neutrinos in the currently examined datasets
3. the methodological consistency of independent analyses of the various datasets.

4.5.1 The expected neutrino fluxes

In this section we describe our approach to the study of cosmic neutrinos, based upon theoretical considerations.

In figure 4.21 we anticipate some of our results, with the aim of emphasizing the region from 1 TeV to 1 PeV, where the prompt component is expected to be relevant. This is especially evident in the panels that show the expected electron (and tau) neutrino flux components. The normalization of the astrophysical component is an important ingredient of our model, and will be discussed in subsection 4.5.1.

Atmospheric neutrinos Atmospheric neutrinos had not been studied at the highest energies before IceCube, but they can be predicted, within uncertainties linearly increasing from $\lesssim 10\%$ at 100 GeV to about 30% at 1 PeV, from the

[17] After the preliminary results presented by IceCube at the ICRC of 2019, these issue may not be as compelling.

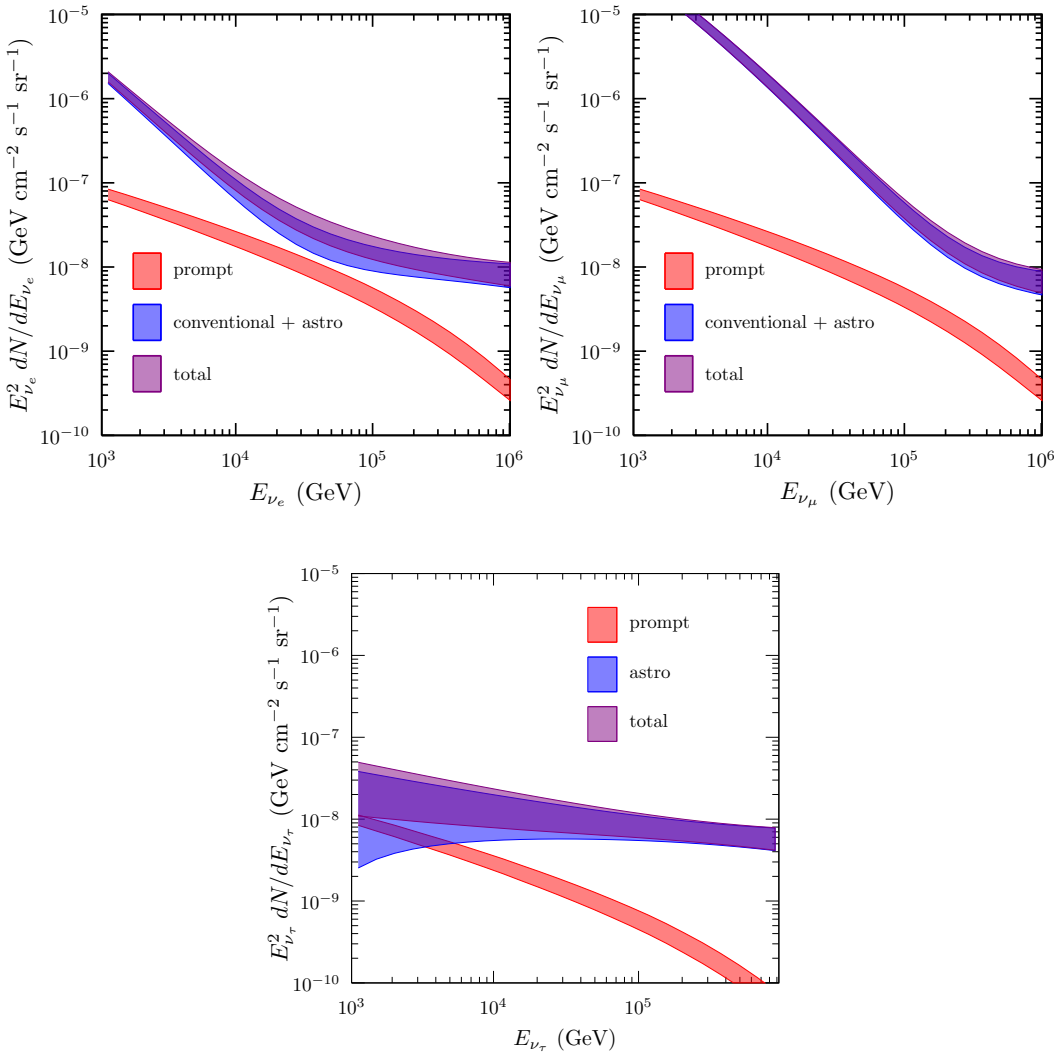

Figure 4.21: The expected electron (top left), muon (top right) and tau (bottom) neutrino flux components in the energy range from 1 TeV to 1 PeV. Particular emphasis is given to prompt neutrinos, which are shown separately and summed to all other components. As in the rest of the paper, the bands corresponding to the sum of two or more fluxes are delimited by the sum of the lower bounds and the sum of the upper bounds of the single fluxes, as our purpose is mostly illustrative when we do not deal with single fluxes.

observed flux of cosmic rays and the theory of strong interactions[18]. Many (semi-)analytical computations [164, 165, 166, 167, 168, 169] have been carried out, adopting different primary cosmic-ray and hadronic interaction models, in order to predict the *conventional component*, which results from the decay of pions, kaons, and unflavored mesons, and the *prompt component*, which comes from charmed meson decays – even though the latter contribution is considerably more uncertain and, moreover, undetected at present. Before proceeding, note that atmospheric neutrinos are occasionally accompanied by observable muons, that are absent in the case of cosmic neutrinos instead; the observation of these coincident atmospheric muons allows us to test the reliability of the predictions for the atmospheric neutrinos, and to veto atmospheric events when looking for astrophysical ones.

There are a few good reasons to distinguish these two components: their spectrum, angular distribution, and flavour composition are different, and thus experimentally distinguishable – in principle.

The conventional component of the atmospheric spectrum is mainly produced in the decay of pions and kaons ($\tau_{\rm rest} \sim 10^{-8}\,{\rm s}$), which are produced when cosmic rays collide with the atmosphere; since these mesons have time to interact and lose energy in the atmosphere before decaying, the spectrum of conventional atmospheric neutrinos is expected to be softer than that of the parent cosmic rays of a factor E^{-1}, i.e. $\propto E^{-3.7}$. Prompt neutrinos are also produced in hadronic collisions of cosmic rays on the atmosphere as a product of the subsequent immediate decay of charmed mesons ($\tau_{\rm rest} \sim 10^{-12}\,{\rm s}$), so that their spectrum is expected to closely reflect that of the parent cosmic rays $\propto E^{-2.7}$.

The bulk of atmospheric neutrinos is due to pions and kaons; the larger the energies of the muon produced in the pion/kaon decay, the smaller the probability it decays, so that the flavour ratio of such component shifts from a $(1:2:0)$ for energies lower than $10\,{\rm GeV}$ to $(0:1:0)$ at higher energies. The conventional component is also anisotropic: the thicker the layer of the atmosphere traversed (with maximum at an azimuthal angle $\theta = \pi/2$, where $\theta = 0$ refers to the upward direction and $\theta = \pi$ to the downward one), the larger the amount of possible targets for cosmic rays.

[18] these numbers refer to our particular computations which feature a fixed hadron interaction model, which is another source of uncertainty (around 10% at 100 GeV up to $30-40\%$ at 100 TeV [109]).

The prompt component is expected, on the contrary, to be isotropic and to follow a flavour ratio of about $(1:1:0.1)$, with the same energy distribution for all flavors. This means that the prompt contribution is the dominant one in the ν_e atmospheric spectrum already at few tens TeV, as we will later show, while, in the case of ν_μ, it reaches the level of the conventional one only at larger-than-PeV energies.

Following [3], we compute the conventional and prompt atmospheric neutrino flux with MCEq [147], adopting the most recent version of SYBILL, the 2.3c release [149], the NRLMSISE-00 [148] model of the atmosphere, and a primary CR flux defined as follows:

- only protons and helium nuclei are considered, because they are the most abundant elemental species, and because nuclei of mass number A and energy E produce neutrinos with average energy $E/(20A)$ when colliding with other nuclei;

- the most important part of the (Galactic) CR flux is a power-law fitted to the AMS-02 [154, 155] low energy (from 100 GeV to 10 TeV) data, and its knee is assumed to be either an "exponential-square" cutoff or a change of slope.

$$\frac{d\Phi_{p,\mathrm{He}}^{\text{exp-square}}}{dE} = N_{p,\mathrm{He}} \left(\frac{E}{10\,\mathrm{TeV}}\right)^{-\gamma_{p,\mathrm{He}}} \exp\left[-\left(\frac{E}{Z_{p,\mathrm{He}} R_{\mathrm{knee}}}\right)^2\right] \tag{4.68}$$

$$\frac{d\Phi_{p,\mathrm{He}}^{\Delta\gamma}}{dE} = N_{p,\mathrm{He}} \left(\frac{E}{10\,\mathrm{TeV}}\right)^{-\gamma_{p,\mathrm{He}}} \times \begin{cases} 1 & E \leq Z_{p,\mathrm{He}} R_{\mathrm{knee}} \\ \left(\dfrac{E}{10\,\mathrm{TeV}}\right)^{-\alpha} & E > Z_{p,\mathrm{He}} R_{\mathrm{knee}} \end{cases} \tag{4.69}$$

  where $\alpha = 2 - \delta$, $\delta = 1/3 \equiv$ slope of the diffusion coefficient, i.e. $D(E) = D_0(E/E_0)^\delta$. The knee is assumed to be rigidity-dependent, and its position is obtained by fitting the overall primary shape of Eq. (4.71) to the KASCADE-Grande data [150];

- an additional, supposedly extra-galactic[19] proton component is added to

[19] In [150] this is the component which onsets after the ankle at $E \approx 10^{17}\,\mathrm{eV}$.

the fitting spectrum

$$\frac{d\Phi_{\rm eg}}{dE} = N_{\rm eg}\left(\frac{E}{100\,{\rm PeV}}\right)^{-2.7} \tag{4.70}$$

with $N_{\rm eg}$ as the only free parameter.

$$\frac{d\Phi^k_{\rm tot}}{dE} = \sum_{i=p,{\rm He}} \frac{d\Phi^k_i}{dE} + \frac{d\Phi_{\rm eg}}{dE} \qquad k = \text{exp-square},\ \Delta\gamma \tag{4.71}$$

The errors on the atmospheric neutrino flux are given by the uncertainty on the shape of the knee and by that on the normalisation and slope resulting from the fits. In table 4.9 we show the results of our fits.

model	$R_{\rm knee}$	N_p	γ_p	$N_{\rm He}$	$\gamma_{\rm He}$	$N_{\rm eg}$
(4.68)	$15.1 \pm 0.7\,{\rm PV}$	1.5 ± 0.2	2.71 ± 0.04	1.5 ± 0.1	2.64 ± 0.03	6.0 ± 0.2
(4.69)	$5.8 \pm 0.6\,{\rm PV}$					5.0 ± 0.5

Table 4.9: the parameters of our primary CR spectrum as resulting from the fit to the KASCADE-Grande data. N_p and $N_{\rm He}$ are given in units of $10^{-7}\,{\rm GeV}^{-1}\,{\rm m}^{-2}\,{\rm s}^{-1}\,{\rm sr}^{-1}$, while $N_{\rm eg}$ is in units of $10^{-19}\,{\rm GeV}^{-1}\,{\rm m}^{-2}\,{\rm s}^{-1}\,{\rm sr}^{-1}$. See [3] for more details on this.

Cosmic neutrinos

The predictions for cosmic neutrinos are much more uncertain and require more discussion. Depending upon the adopted model, the resulting neutrino spectra vary greatly in shape and normalization. One of the few stable expectations is that, according to the observed three flavour oscillation phenomena, cosmic electron, muon and tau neutrinos have to be present in similar amounts. The simplest and most popular hypothesis is that cosmic neutrinos are distributed as $E_\nu^{-\gamma}$ with $\gamma \sim 2$, at least in the range of energies where they become observable. Surely this case is conducive to observation, however it is important to state clearly what are its motivations, what is its extent, what are its implications; this is the aim of the present discussion.

The physical picture that we have in mind is that cosmic neutrinos are produced in collisions between the accelerated cosmic rays and the gas surrounding the accelerators. In the diffusive shock acceleration (DSA) picture, the cosmic-ray spectrum is a power-law $\propto E^{-2}$; due to the scaling associated to hadronic collisions, also the gamma-ray and neutrino spectra at the source[20] will be power laws $\propto E^{-2}$. This setup can be regarded as an extension of what it is commonly supposed for the Galactic cosmic rays, where $E_{\rm max}$ has probably a lower value than $10-100\,\mathrm{PeV}$; however, the slope of the injected cosmic rays might be similar or equal to the Galactic one. The abundance of target hadrons points out instead to some dusty environment; this could the site of intense stellar formation, say, starburst and/or star-forming Galaxies.

As a specific instance, we refer to the theoretical model of Loeb and Waxman [5], according to whom the flux of cosmic neutrinos is:

$$\frac{d\Phi}{dE} = \Phi_{\rm astro} \left(\frac{E}{100\,\mathrm{TeV}} \right)^{-\gamma_{\rm astro}} \tag{4.72}$$

with

$$\Phi_{\rm astro}^{\rm LW} = 2 \times 10^{\pm 0.5} \times 10^{-18}\,\mathrm{GeV^{-1}\,cm^{-2}\,s^{-1}\,sr^{-1}} \qquad \gamma_{\rm astro}^{\rm LW} = 2.15 \pm 0.10$$

in the case (as we know today) of an astrophysical neutrino spectrum extending above 100 TeV. The slope of this spectrum is very close to the one we would expect in the simple case of DSA.

The assumptions above are consistent with the measurements of through-going muons [172] obtained by IceCube above 200 TeV and tested by the HESE dataset [279] in the same energy region, which result in

$$\Phi_{\rm astro}^{{\rm IC},\mu} = 0.90^{+0.30}_{-0.27} \times 10^{-18}\,\mathrm{GeV^{-1}\,cm^{-2}\,s^{-1}\,sr^{-1}} \qquad \gamma_{\rm astro}^{{\rm IC},\mu} = 2.13 \pm 0.13$$

Moreover, as we will show in the following, they do not imply any clash with the measurements of the diffuse gamma-ray emission, obtained at lower energies, even if we assume that the cosmic neutrino spectrum extends well below the observed range.

Assuming *pp*-based sources of neutrinos, we expect pion decay as the main mechanism of neutrino production, thus resulting in a $(\nu_e : \nu_\mu : \nu_\tau) \simeq (1 : 2 : 0)$

[20] the neutrino spectrum is supposed to be unaltered even far from the source.

flavour ratio at the source; due to the impact of standard three-flavor neutrino oscillations, we expect a flavour ratio at Earth of about $(1:1:1)$.

In order to have much more precise predictions, we define our phenomenological muon neutrino flux by combining the through-going muons neutrino flux as observed in [172] and that of Loeb and Waxman of Eq. (4.72). We do this in the following way:

1. we define the combined $\gamma_{\rm astro}$ and $\Phi_{\rm astro}$ - as well as their errors - as the weighted average of those from [5] and [172]; notice that, due to the large error on the normalization from [5], the weighted average on the normalization is very close to that of [172], while $\gamma^{\rm best}_{\rm astro} = 2.14 \pm 0.08$. The resulting combined muon neutrino flux is thus:

$$\frac{d\Phi_{\nu_\mu}}{dE} = 0.90^{+0.30}_{-0.27} \times 10^{-18} \left(\frac{E}{100\,\text{TeV}}\right)^{-2.14\pm0.08} \text{GeV}^{-1}\,\text{cm}^{-2}\,\text{s}^{-1}\,\text{sr}^{-1} \quad (4.73)$$

2. we reproduce, using a Gaussian likelihood, the 68% CL contour in the $\gamma_{\rm astro}$-$\Phi_{\rm astro}$ plane in figure 6 of [172] in order to account for the correlation[21] $\rho \sim 0.6$ between the two parameters:

$$\mathcal{L}(\mathbf{v}) = \frac{1}{2\pi\sqrt{\det\Sigma^2}} \exp\left[-\frac{1}{2}(\mathbf{v}-\mathbf{v}^{\rm best})^T \Sigma^{-2} (\mathbf{v}-\mathbf{v}^{\rm best})\right]$$

where

$$\mathbf{v} = \begin{pmatrix} \Phi_{\rm astro} \\ \gamma_{\rm astro} \end{pmatrix} \qquad \Sigma^2 = \begin{pmatrix} \sigma_\Phi^2 & \rho\sigma_\Phi\sigma_\gamma \\ \rho\sigma_\Phi\sigma_\gamma & \sigma_\gamma^2 \end{pmatrix}$$

and σ_Φ and σ_γ are the errors on the flux normalization at 100 TeV and the slope respectively, as taken from [172], since the correlation of the parameters can be extracted only from the data;

3. we define the best fit astrophysical neutrino flux as the flux averaged using the likelihood defined above:

$$\left\langle \frac{d\Phi}{dE} \right\rangle = \int_{\Phi^{\rm best}_{\rm astro}-5\sigma_\Phi}^{\Phi^{\rm best}_{\rm astro}+5\sigma_\Phi} d\Phi_{\rm astro} \int_{\gamma^{\rm best}_{\rm astro}-5\sigma_\gamma}^{\gamma^{\rm best}_{\rm astro}+5\sigma_\gamma} d\gamma_{\rm astro}\, \mathcal{L}(\Phi_{\rm astro}, \gamma_{\rm astro})\, \frac{d\Phi}{dE} \quad (4.74)$$

[21] shown in figure 3 of the same paper.

and its 1σ uncertainty as:

$$\delta\left(\frac{d\Phi}{dE}\right) = \sqrt{\left\langle\left(\frac{d\Phi}{dE}\right)^2\right\rangle - \left(\left\langle\frac{d\Phi}{dE}\right\rangle\right)^2} \tag{4.75}$$

The resulting cosmic muon neutrino flux is the blue band in figure 4.22. We can obtain the cosmic flux of ν_e and ν_τ simply by multiplying that of muon neutrinos by $R_{e\mu}$ and $R_{\tau\mu}$

$$\frac{d\Phi_{\nu_e}}{dE} = R_{e\mu}\frac{d\Phi_{\nu_\mu}}{dE} \qquad \frac{d\Phi_{\nu_\tau}}{dE} = R_{\tau\mu}\frac{d\Phi_{\nu_\mu}}{dE}$$

In fact, the $R_{\ell\mu}$ factors can be calculated in *two different approximations*. Standard three-flavor oscillations are assumed in both cases, and described by $P_{\ell\ell'}$, the matrix of the survival/oscillation probabilities averaged over cosmic distances (as seen in §1.2.3)

$$P_{\ell\ell'} = \sum_{i=1}^{3} |U_{\ell i}|^2 |U_{\ell' i}|^2$$

where U is the neutrino mixing matrix. The two approaches are the following:

1. the "2 : 1 approximation", in which we define

$$R_{\ell\ell'} = \frac{\sum_{\ell''} P_{\ell\ell''}\xi^0_{\ell''}}{\sum_{\ell''} P_{\ell'\ell''}\xi^0_{\ell''}} \qquad \ell, \ell', \ell'' = e, \mu, \tau$$

   where ξ^0_ℓ is the fraction of $\nu_\ell + \overline{\nu}_\ell$ produced at the source. We compute $R_{\ell\ell'}$ assuming the commonly accepted flavour ratio[22] at production of $\xi^0_\mu = 2/3$ and $\xi^0_\tau = 0$ and sampling $P_{\ell\ell'}$ according to their distributions (see subsection 1.2.3) in the case of normal hierarchy of the neutrino masses. We obtain:

$$R_{e\mu} = 1.09^{+0.03}_{-0.04} \qquad R_{\tau\mu} = 0.97^{+0.03}_{-0.04}$$

[22]Known as the pion decay scenario. Choosing a generic flavour ratio with $\xi^0_\mu = x$, $\xi^0_e = 1 - x$, $\xi^0_\tau = 0$, sampling x uniformly between 0 and 1, we would have $R_{e\mu} = 0.78^{+0.57}_{-0.07}$ and $R_{\tau\mu} = 1.00^{+0.05}_{-0.15}$.

2. the "kernel approach", which relies on a more accurate and physically more comprehensive procedure to fully embrace the consequences of the hadronic production mechanism, namely the strict relationship between gamma rays and neutrinos. As shown in [176], and updated in subsection 4.1.1 with the use of the most recent oscillation parameters from [30], the gamma-ray flux at the production site and the cosmic neutrino flux are linked by the following relation:

$$\frac{d\Phi_\nu(E_\nu)}{dE_\nu} = \int_{E_\nu}^{\infty} \frac{dE}{E}\, \tilde{K}_\nu(E_\nu, E)\, \frac{d\Phi_\gamma(E)}{dE} \tag{4.76}$$

where $\tilde{K}_\nu$ is a kernel which accounts also for ν oscillations (see [176] and subsection 4.1.1 for more on this). Equation (4.76) can be rewritten as

$$\frac{d\Phi_\nu(E_\nu)}{dE_\nu} = \int_0^1 \frac{dx}{x}\, \tilde{K}(x)\, \frac{d\Phi_\gamma(x/E_\nu)}{dE} \tag{4.77}$$

and it can be easily proven that, assuming a power-law gamma-ray flux $\propto E^{-\gamma}$:

$$R_{\ell\ell'} = \frac{\zeta_{\nu_\ell}(\gamma)}{\zeta_{\nu_{\ell'}}(\gamma)} \tag{4.78}$$

where

$$\zeta_{\nu_\ell}(\gamma) = \int_0^1 dx\, x^{\gamma-1} \left[\tilde{K}_{\nu_\ell}(x) + \tilde{K}_{\overline{\nu}_\ell}(x)\right]$$

$R_{\ell\ell'}$ as defined in Eq. (4.78) depend negligibly[23] on γ, and this time we obtained:

$$R_{e\mu} = 1.30 \pm 0.05 \qquad R_{\tau\mu} = 0.92 \pm 0.04$$

We conservatively estimated the impact a 20% variation of the non-oscillated electron (anti-)neutrino kernel variation, which could be due to systematic errors, as neglecting the K_L and K_S contributions [176]: we found out that $R_{e\mu}$ varies of 6%, while $R_{\tau\mu}$ of 1%, which are not important considering the

[23] they change of less than 0.1% in the 3σ range around $\gamma^{\rm best}_{\rm astro} = 2.14$.

30% uncertainty on the astrophysical muon neutrino flux normalization. Moreover, if the electron neutrino and muon neutrino kernels were subject to the same systematic error, the factors $R_{\ell\ell'}$ would not change.

Both procedures yield very similar tau neutrino fluxes, while the electron neutrino flux is larger in the kernel approach than in the $2:1$ approximation. This is due to the fact that in the kernel formalism the presence of neutrinos due to kaons is accounted for, the decay of which results in an electron-neutrino richer flux.

We chose to multiply the flux of muon neutrinos by $R_{\ell\ell'}$ computed with the kernel approach to consider hadronic collisions as the neutrino production mechanism and include the effect of charged kaons, having thus a clear and precise physical picture in mind. Note that the error on the astrophysical ν_μ flux normalization is 30%, much larger that those on $R_{e\mu}$ and $R_{\tau\mu}$, so that the relative error on the cosmic electron and tau neutrino fluxes will be 30% as well.

4.5.2 Results and discussion

The components of the neutrino spectra In figure 4.22 we show the expectations for the various components of the muon neutrino flux, as well as the corresponding measurements by the IceCube Collaboration. We assume isotropy, but note that the IC-59 points and the HESE ones refer to two different kinds of events, namely ν_μ-induced tracks from the Northern sky and all-flavor High-Energy Starting Events from the whole sky respectively.

In figure 4.23 we show the prediction for the cosmic electron neutrino flux and the expectations for the other components of the electron neutrino spectrum, alongside with the relevant measurement by the IceCube Collaboration.

No tau neutrino data is available, also due to the fact that the atmospheric tau neutrino flux consists only in the prompt component, thus we do not show the corresponding plot as it would convey no useful information.

From figure 4.22 and 4.23 a few noteworthy features are noticeable:

1. the conventional atmospheric expectations obtained with MCEq, featuring SYBILL-2.3c and our primary cosmic ray spectrum Eq. (4.71), agree well with the measurements from IceCube;

2. the region where the atmospheric and cosmic components of the muon neutrino spectrum cross is around $250\,\mathrm{TeV} \simeq E_{\mathrm{knee}}/20$;

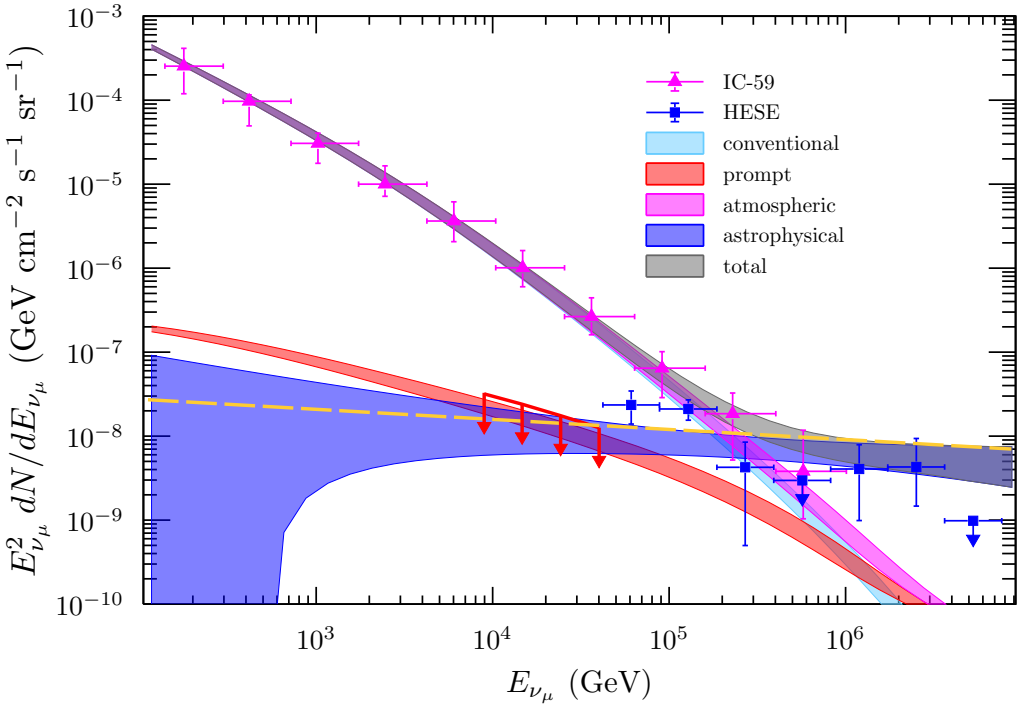

Figure 4.22: The various components of the muon neutrino flux obtained with the model defined in Section 4.5.1. Also shown are the measurement of the atmospheric muon neutrino flux by IceCube [127], that of the cosmic neutrino flux with from the HESE dataset [280], the 68% C.L. upper bound on prompt muon neutrinos in the relevant sensitivity region [172] and the upper flux limit (yellow dashed line) obtained in [281], featuring $\gamma = 2.12$ and the best fit normalization + 1σ as taken from the through-going muons analysis [172].

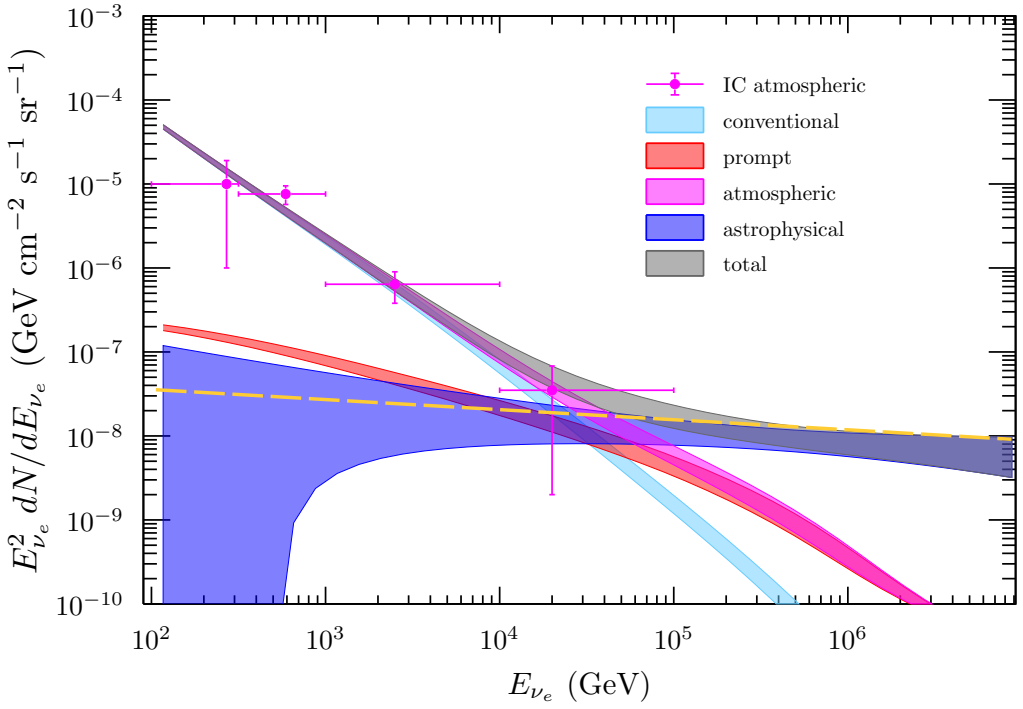

Figure 4.23: The predictions of the various components of the electron neutrino flux obtained with the model defined in Section 4.5.1. Also shown is the measurement of the atmospheric electron neutrino flux by IceCube [126] and the upper flux limit (yellow dashed line) obtained in [281], featuring $\gamma = 2.12$ and the best fit normalization + 1σ as taken from the through-going muons analysis from [172] rescaled by $\zeta_{\nu_e}/\zeta_{\nu_\mu}$.

3. the prompt component is always subdominant in the ν_μ spectrum, so that within our model it is not surprising that no significant evidence for prompt neutrinos has been found in the through-going muons analysis;

4. the conventional atmospheric component is a factor ~ 30 less important for electron neutrinos compared to muon neutrinos, so that the prompt component sizably contributes to the overall flux of ν_e for $E_\nu \geq 10\,\text{TeV}$.Eq. (4.73).

Is it possible to extract the prompt neutrino signal? Our results suggest that the best chance to detect the prompt flux of neutrinos is from electron neutrino atmospheric data for $E \gtrsim 1\,\text{TeV}$, assuming the possibility to somehow discriminate the flavour of the events.

The cascade (or shower) event topology is the most interesting in this regard; it is one of the two kinds of events comprised in the HESE dataset, the remainder being tracks. Track-like events are produced by charged-current muon neutrino interactions, while cascades are produced in all other possible cases. It follows that the cascade sample is the one with the smallest relative contribution of muon neutrinos, which, as already seen in figure 4.22, are very prompt-neutrino poor. Another reason to focus on the cascade subset of the HESE dataset is that the track-like subset is compatible with being due to background events (atmospheric muons and atmospheric muon neutrinos) only [1, 197].

The contributors to the cascade dataset are:

1. atmospheric muons;

2. conventional atmospheric ν_e and ν_μ;

3. prompt atmospheric ν_e, ν_μ and ν_τ;

4. astrophysical ν_e, ν_μ and ν_τ.

Therefore, provided that the contamination due to muons, conventional muon neutrinos and all-flavor astrophysical neutrinos can be subtracted, the cascade sample offers us the chance to detect prompt neutrinos.

In order to quantitatively test our hypothesis we use the effective areas for cascade-like events given in figure 1 of [197] to estimate the yearly rate of cascade-like events due to neutrinos with larger-than-TeV energy. In figure 4.24 we show

the parent distribution of cascade events, dividing them by flavour and component, in order to show the energy ranges which contribute the most to the events of table 4.10. The yearly rates are computed according to[24]:

$$\Gamma_{\nu_\ell} = 1\,\text{year} \times \int \mathrm{d}\Omega \int_{1\,\text{TeV}}^{10\,\text{PeV}} dE\, \mathcal{A}_{\nu_\ell}(E)\, \mathcal{P}_\nu(E, \cos\theta)\, \frac{d\Phi_{\nu_\ell}}{dE} \tag{4.79}$$

where $\mathcal{A}_{\nu_\ell}(E)$ is the effective area for the detection of cascade-like events induced by ν_ℓ and $\overline{\nu}_\ell$, $1\,\text{year} = \pi \times 10^7\,\text{s}$ and $\mathcal{P}_\nu(E, \cos\theta)$ parametrises the effect of the veto for atmospheric neutrinos of flavour ℓ, as in [282]. For cosmic neutrinos, $P_\nu(E, \cos\theta) = 1$ for all energies, angles and flavours; for atmospheric neutrinos, $P_\nu(E, \cos\theta) = 1$ for all energies for $\cos\theta \in [-1, 0.1)$.

The expected rate due to prompt neutrinos is small, less than 3% of the conventional contribution, which is not encouraging for the search of prompt neutrinos. However, the conventional contribution could be somewhat reduced by searching for cascades coming from below and/or by using a higher energy threshold, so as to exclude most of the conventional events.

component	Γ_{ν_e}	Γ_{ν_μ}	Γ_{ν_τ}
conventional	140 – 180	385 – 485	0
prompt	9 – 12	1.4 – 1.8	0.77 – 1.02
cosmic	10 – 40	2 – 6	5 – 20

Table 4.10: 68% CL intervals relative to the yearly rate of cascade-like events in the energy range 1 TeV and 10 PeV in IceCube, as computed with Eq. (4.79), due to the different components of the three neutrino fluxes.

In order to compute the number of events due to atmospheric neutrinos, we had to approximate analitically the atmospheric neutrino spectrum. We find it

[24] This formula has been corrected to include the effect of the self-veto for atmospheric neutrinos, the action of which is shown in figure 4.2 and tabulated in [282]. The results obtained with this formula have been corrected to account for the presence of the veto, even though they did not considerably change. I thank Carlos Argüelles for the useful feedback he provided.

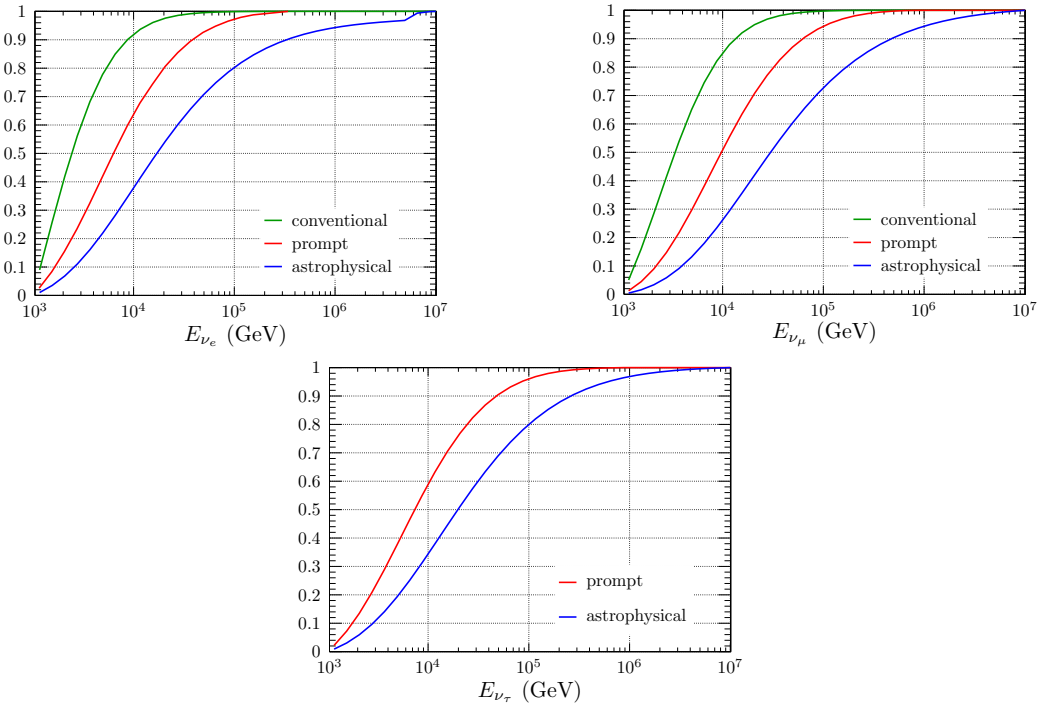

Figure 4.24: The cumulative distributions of cascade events in IceCube in the energy range 1 TeV – 10 PeV, divided by component and flavor.

ν	N_ν^{conv}	N_ν^{prompt}
ν_e	$(0.086 - 0.108) \times 10^{-15}$	$(6.85 - 9.03) \times 10^{-17}$
$\overline{\nu}_e$	$(0.067 - 0.086) \times 10^{-15}$	$(6.70 - 8.86) \times 10^{-17}$
ν_μ	$(2.19 - 2.71) \times 10^{-15}$	$(6.67 - 8.80) \times 10^{-17}$
$\overline{\nu}_\mu$	$(1.30 - 1.66) \times 10^{-15}$	$(6.53 - 8.62) \times 10^{-17}$
ν_τ	-	$(0.89 - 1.18) \times 10^{-17}$
$\overline{\nu}_\tau$	-	$(0.92 - 1.21) \times 10^{-17}$

Table 4.11: The atmospheric neutrino normalisation, assuming Eqs. (4.80), (4.81) as parametrisations of the conventional and prompt spectrum. The reported range corresponds to the value of the relevant atmospheric neutrino flux at 100 TeV and $\cos\theta = 1$ as obtained from the CR flux models Eq. (4.69) (lower value) and Eq. (4.68) (higher value), as discussed in §3.3.2 and §4.5.1. In particular, the lower (higher) value comes from using the smallest (largest) flux within 1σ distance from the best fit parameters of table 4.9.

interesting to provide the reader with the relevant results, which are listed in table 4.11, and presented according to Eqs. (4.80), (4.81).

For conventional atmospheric neutrinos, we used the parametrisation:

$$\frac{\mathrm{d}\Phi_\nu^{\text{conv}}}{\mathrm{d}E\,\mathrm{d}\cos\theta} = \frac{1.1 N_\nu^{\text{conv}}}{|\cos\theta| + 0.1} \left(\frac{E}{100\,\text{TeV}}\right)^{-3.7} \text{GeV}^{-1}\,\text{cm}^{-2}\,\text{s}^{-1}\,\text{sr}^{-1} \tag{4.80}$$

whereas for prompt neutrinos we used:

$$\frac{\mathrm{d}\Phi_\nu^{\text{prompt}}}{\mathrm{d}E\,\mathrm{d}\cos\theta} = N_\nu^{\text{prompt}} \left(\frac{E}{100\,\text{TeV}}\right)^{-2.7} \text{GeV}^{-1}\,\text{cm}^{-2}\,\text{s}^{-1}\,\text{sr}^{-1} \tag{4.81}$$

Is there a spectral anomaly? In [228, 1, 283] the spectral difference between the HESE and the through-going muons spectra is labelled as an anomaly. In fact, if we compare the astrophysical neutrino fits to the cascade and starting track samples, which together constitute the HESE dataset, from [197] to that

from the through-going muons analysis [172] there is an evident difference, as can be appreciated from table 4.12 and from figure 10 of [197].

dataset	$\Phi_{\rm astro}$	$\gamma_{\rm astro}$
C	$2.2^{+0.6}_{-0.5}$	2.62 ± 0.08
ST	$1.6^{+1.6}_{-1.0}$	$2.43^{+0.28}_{-0.30}$
HESE	2.46 ± 0.8	$2.92^{+0.33}_{-0.29}$
TM	$0.90^{+0.30}_{-0.27}$	2.13 ± 0.13

Table 4.12: The flux normalizations, in units of $10^{-18}\,\mathrm{GeV}^{-1}\,\mathrm{cm}^{-2}\,\mathrm{s}^{-1}\,\mathrm{sr}^{-1}$, and slopes deriving from the astrophysical best fits to the cascade (C) and starting tracks (ST) samples from [197], to the 6-years HESE sample from [284] and to the through-going muons (TM) sample from [172]. The numerical values of the flux normalizations for the cascade and starting tracks best fits have been obtained from figure 10 of [197] as they are not explicitly reported in the paper.

Since, as said before, the starting track sample is compatible to be due to background events only, a more accurate and interesting comparison is between the cascade and through-going muons analyses, which, however, still results in a quite evident spectral difference.

Notice that these two datasets give "complementary" indications, as cascades come from the whole sky and are due to all flavours of neutrinos, with likely a preference for electron and tau neutrinos at high energies, while through-going muons are due to muon neutrinos coming from the Northern sky.

From table 4.10 and figure 4.24 a very interesting feature emerges: the number of prompt and cosmic signals in the cascade dataset with $E_\nu^{\rm th} \simeq 1\,\mathrm{TeV}$ are very similar to each other, both in the expected rate of events and in the range of energy in which they contribute. Taking into account also that prompt and cosmic neutrinos are expected to be isotropically distributed in the sky, it appears then difficult[25] to disentangle the prompt component from the astrophysical one between 1 TeV and 100 TeV in the cascade (and thus, HESE) dataset. This is consistent with the idea that the sum of the ($\sim E^{-2.7}$) prompt and the ($\sim E^{-2.13}$)

[25] it is possible when the cascade accompanying prompt neutrinos can be tagged.

astrophysical components could produce the $\sim E^{-2.62}$ spectrum obtained in the cascade analysis. This is demonstrated in figure 4.25, where we show

- the best-fit cosmic neutrino spectrum from the HESE analysis [284]
- the best-fit cosmic neutrino spectrum from the cascade analysis [197]
- the best-fit cosmic neutrino spectrum from the through-going muons analysis [172]
- the sum of the prompt and cosmic components as computed with the model defined in section 4.5.1.

We show only the ν_e flavour contribution in figure 4.25 because it is the most relevant for the cascade dataset due to astrophysical neutrinos, as seen in table 4.10. While the resemblance of the spectral shape due to the sum of cosmic and prompt neutrino fluxes and the astrophysical best fits from [197, 284] is not perfect, the tension between the analyses below 10 TeV seems somewhat alleviated. The spectral shape obviously does not change summing over the flavors, so that this result holds true, but the sum of our prompt and cosmic components would be slightly smaller than three times the best fits from [197, 284]. From this figure, it is evident that:

- the spectra resulting from the through-going muons and the HESE (and cascade) analyses are not compatible at low energy, which gives rise to the "spectral anomaly" of the cosmic neutrino spectrum;
- the theoretical expectations for the sum of prompt and cosmic neutrinos, instead, agrees within 1σ with the best-fit cosmic neutrino flux from the cascade analysis.

We conclude that the cause of the alleged spectral anomaly can be attributed to two factors;

1. a prompt component does contribute to the cascade dataset in the the low-energy region, $\lesssim 100\,\mathrm{TeV}$.

2. a part of the HESE dataset is subject to background contamination due to tracks especially at the lowest energies $\lesssim 10\,\mathrm{TeV}$.

At this point of the discussion, it is useful to bear in mind a couple of important considerations:

(i) the effectiveness of a veto system, based on the presence of muons accompanying the events with a contained vertex [285], is better in the energy range relevant for the search for a cosmic neutrino signal - namely, above several tens of TeV - rather than in the region of lower energies, which is most relevant for the search for prompt neutrinos instead;

(ii) the same analysis that has obtained the cascade dataset [197] has been able to extract also a sample that is highly enriched in muons instead. Its power law description requires a slope of $2.43^{+0.28}_{-0.30}$, whose error is 3-4 times larger than for the cascade dataset and therefore is much less informative[26].

We performed nonetheless the same exercise considering muon neutrinos, i.e. comparing the starting tracks best fit and the sum of prompt and astrophysical muon neutrino flux computed in this work. As can be understood from figure 4.26, no information can be extracted due to the very large uncertainties on the starting tracks sample, which could be due to difficulties in excluding atmospheric contamination.

There are other (non-exclusive) explanations of the low-energy discrepancy between the cosmic neutrino spectrum as resulting from HESE analysis and from the through-going muons analysis: a part of the low-energy soft spectrum of HESE could be due to neutrinos from the Galactic plane, and in this case one would expect a peculiar angular distribution [286, 287, 229, 288, 289] (which to

[26]This is not surprising since the conventional atmospheric component, to be subtracted, is much larger for muon neutrinos - see figure 4.21 - and therefore, it is harder to identify new components in the track dataset.

date is not seen [290]); a priori, there could be other sources of extraterrestrial neutrinos which could cause such effect (but this would be at odds with the null search of prompt neutrinos [172]). Note that our proposal, concerning the role of prompt neutrinos in the cascade dataset, does not require the inclusion of hypothetical physical ingredients, and in this sense can be considered minimal.

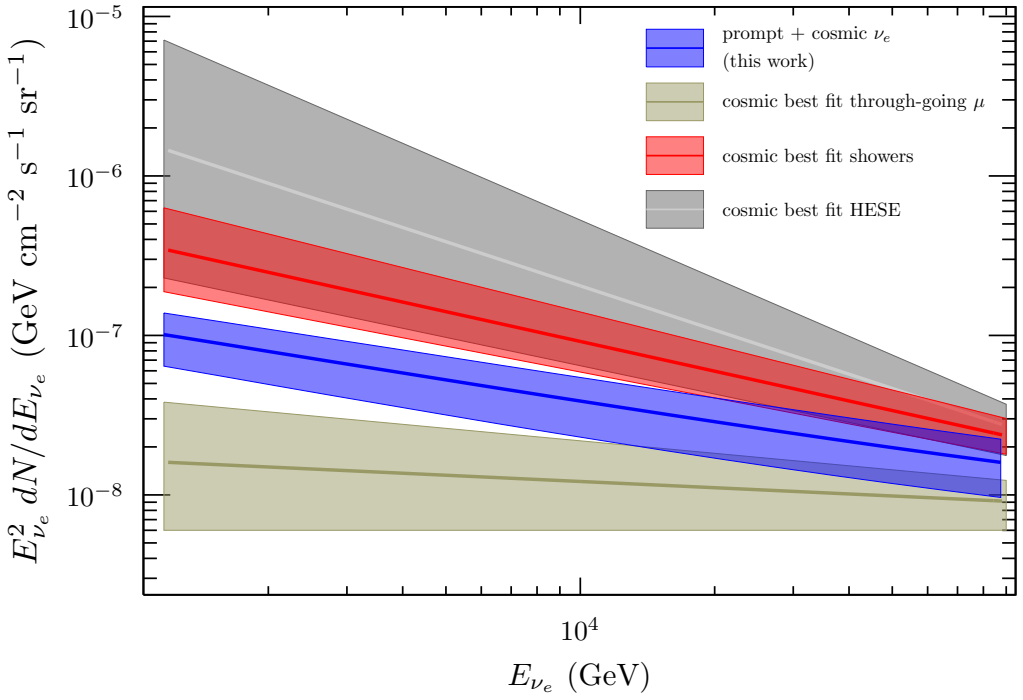

Figure 4.25: The sum of the prompt and cosmic components of the ν_e spectrum as computed in this work (blue band) confronted to the astrophysical neutrino fluxes resulting from fitting the cascade sample [197] (red band), from the 6-year through-going muons analysis [172] (brown band), and from the 6-year HESE analysis [284] (grey band). The grey and red bands are experimental results, in that they come from analyses by IceCube, while the blue one is theoretical and the brown one is a low-energy extrapolation.

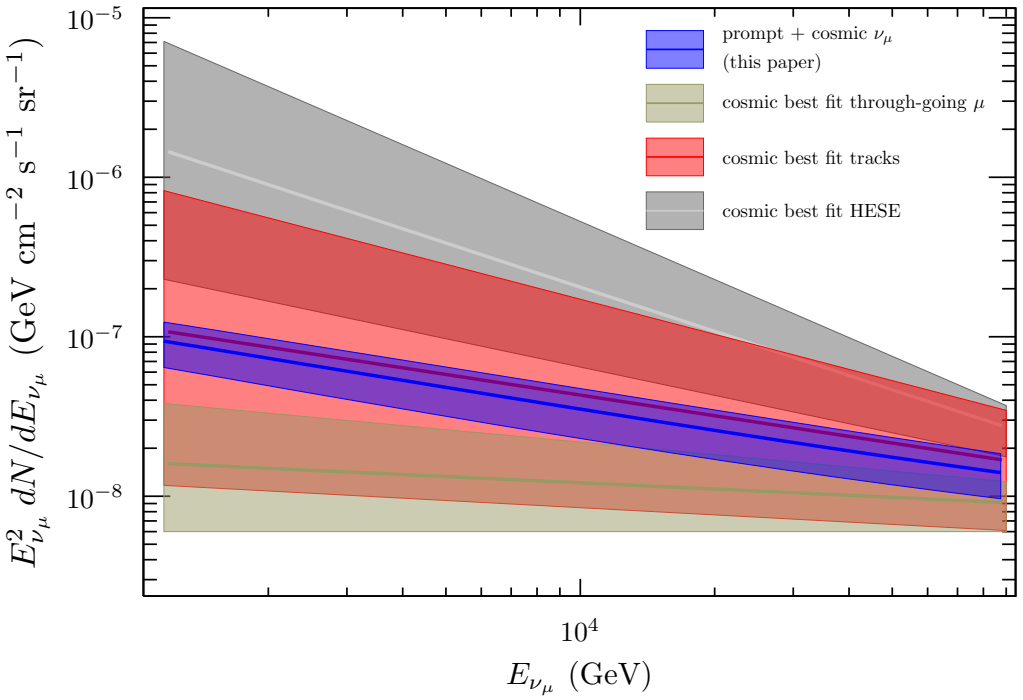

Figure 4.26: The sum of the prompt and cosmic components of the ν_μ spectrum as computed in this work (blue band) confronted to the astrophysical neutrino fluxes resulting from fitting the starting tracks sample [197] (red band), from the 6-year through-going muons analysis [172] (brown band), and from the 6-year HESE analysis [284] (grey band). The grey and red bands are experimental results, in that they come from analyses by IceCube, while the blue one is theoretical and the brown one is a low-energy extrapolation.

Summary and outlook

In this work we addressed a selection of the open problems in neutrino astrophysics. These open problems regard the fundamental properties of neutrinos, as well as their role as an astrophysical messenger, on which we focussed our efforts. However, we found it necessary, for a complete discussion on neutrinos, to review its description in the Standard Model of elementary particles, and the theory of neutrino mixing in vacuum and in dense media. We closed the introductory part with an overview of the commonly referred-to types of neutrinos: relic, solar, terrestrial, and cosmic. We will use this order in the following summary of our original work.

In the context of solar neutrinos, the main contribution of this thesis concerns the luminosity constraint, which is a strict relation between the solar luminosity in photons and in neutrinos. This constraint can be briefly expressed by saying that the power emitted in neutrinos is equal to the energy liberated in ^{4}He synthesis times the ^{4}He production rate. Such relation is based on the assumptions of energy conservation, of lepton number conservation, of stationarity of the Sun, and that ^{4}He is the only accumulating nuclear specie. Starting from the seminal work by Bahcall [101], we reformulated the derivation of said constraint in a simpler and clearer way. We then proceeded to generalise the luminosity constraint by relaxing the last two aforementioned assumptions; in fact, the Sun loses gravitational potential energy by expanding, and there are at least two more accumulating nuclear species, ^{3}He and ^{14}N. The contributions due to these phenomena to the luminosity constraint have been computed and assessed as sizable, because of the very high-precision measurement of the solar luminosity in

photons. We showed how this new, extended version of the luminosity constraint has the power to link with great accuracy *pp* and CNO neutrinos in a sufficiently model-independent way, also thanks to the precise observations of the current solar neutrino detectors. This is very powerful and interesting for:

- solar neutrino physics, as *pp* neutrinos are measured by Borexino with 10% uncertainty and there are only upper limits on the CNO flux
- solar physics, as the flux of CNO neutrinos is directly linked to the relative abundance of heavier-than-Helium elements (the so-called metallicity) in the Sun.

In the context of terrestrial neutrinos - in which we included accelerator, beam neutrinos, geoneutrinos, and atmospheric neutrinos - we focussed on certain open problems concerning atmospheric neutrinos. They are produced in the particle cascades which follow the collisions between cosmic rays (primaries) and the nuclei in the atmosphere. More precisely, atmospheric neutrinos are produced in the decay of secondary particles: pions and kaons produce the "conventional" component of atmospheric neutrinos, while heavier particles, like charmed mesons and baryons, decay into the "prompt" component, as their lifetime is very short (about 10^{-12} s). Both these components are predicted to keep memory of the spectral shape of the cosmic-ray energy spectrum; in particular, the conventional component follows an $E^{-3.7}$ distribution, while the prompt one is predicted to be distributed as $E^{-2.7}$ - no evidence for prompt neutrinos has been found yet. $E^{-2.7}$ is also the energy-dependence of the cosmic-ray energy spectrum before the knee, i.e. a transition region which is believed to correspond to the end of the light component (protons and Helium nuclei) of Galactic cosmic rays.

This feature in the cosmic ray spectrum is expected to be reflected also in the atmospheric neutrino spectrum; this observation is the foundation of the study published in [3]. In it, we tried to use the atmospheric neutrino data to discriminate between two incompatible values of the knee rigidity measured by ARGO-YBJ and KASCADE-Grande, respectively about 700 TV and 5 PV. To do so, we built a simple, power-law, model for the primary cosmic-ray spectrum which comprises only protons and Helium nuclei, and is fitted to the AMS-02 low-energy data; such spectrum is then modified by the presence of a knee feature, for which we considered two different functional forms. The final primary spectra

are obtained fitting the two high-energy datasets of ARGO-YBJ and KASCADE-Grande, so that the ensuing atmospheric neutrino fluxes could be numerically computed adopting various hadronic interaction models. We could then evaluate the theoretical uncertainties on the atmospheric neutrino fluxes, due to the fits to the data, to the chosen shape of the knee, and to the choice of hadronic interaction model. Unfortunately, the atmospheric neutrino data available at the energies of our interest (10 TeV - 1 PeV) have too large an uncertainty to discriminate the knee position; there is, however, a slight preference for the knee as measured by the KASCADE-Grande collaboration. With this work, we showed that it could be possible to use atmospheric neutrinos, if measured with much better precision, as a proxy for cosmic-ray measurements.

The results obtained on atmospheric neutrinos have been subsequently exploited to formulate suggestions for the detection of the prompt component in high-energy neutrino telescopes. In [4] we argued that the best chance for prompt neutrino detection is based on the study of inclined cascade-like events, rather than of the HESE and through-going muons dataset. In fact, neutrino-induced cascade events occur when all neutrino flavours interact via neutral current or electron and tau neutrinos interact via charged current; charged-current interactions of muon neutrinos produce muons, which have a very large mean free path along which they stochastically lose energy, thus generating tracks. Our results on the atmospheric neutrino components show that the spectrum of atmospheric muon neutrinos is dominated by the conventional component up to about 1 PeV, while for electron neutrinos conventional neutrinos dominate at most up to 50 TeV, and there are no conventional tau neutrinos. Using the IceCube effective areas for cascade-like events, given between 1 TeV and 10 PeV, we could compute the expected yearly rate of events due to conventional, prompt and astrophysical neutrinos, dividing by flavour and taking into account the presence of the atmospheric veto. The result is that the event rate due to prompt neutrinos above 1 TeV is smaller than 3% of that due to conventional neutrinos; however, conventional neutrinos are expected to be mainly distributed around the horizontal direction, and to vanish more quickly than prompt neutrinos for increasing energy. This means that, with the appropriate angular and energy cuts, it could be possible to extract the prompt component from the inclined cascades dataset.

An essential part of the previous work is the model of the astrophysical compo-

nent of the neutrino spectrum, which has been also the object of the other original papers I contributed to [1, 2]. This leads, in essence, to a power law distribution based on the *pp* assumption for astrophysical neutrino production. In particular, in [4] we combined the theoretical expectation by Loeb & Waxman of an $E^{-2.15}$ energy spectrum, connected to a starburst origin of the neutrinos, to the measurement resulting from the through-going muons analysis [172], so as to have a precise phenomenological muon neutrino flux. We then used the connection between gamma rays and neutrinos, which holds in the case of hadronic mechanism of neutrino production, to physically estimate the astrophysical fluxes of the other neutrino flavours. We could then compute the yearly rates of shower-like events, as mentioned above, as well as test whether the tension between the astrophysical neutrino fluxes resulting from the HESE [173] and through-going muons analyses could be somehow explained by a considerable atmospheric contribution to the HESE sample. This search was prompted also by a recent analysis of contained events [197], which resulted in a cosmic neutrino spectrum in between the fluxes from the HESE and through-going muons analyses. Upon visual comparison, see figure 4.25, it is apparent that the spectral tension may be due to the presence of prompt neutrinos. This conclusion seems somewhat weakened by the latest, preliminary results of the through-going muons and HESE analyses of [198, 190], which see a softening of the flux from the former and a hardening of the latter. Nonetheless, we argue that the best way to proceed in cosmic neutrino analyses would be:

- to be very careful when including $E \lesssim 100\,\mathrm{TeV}$ data, as the atmospheric component could produce an important number of events;
- to have a km^3-scale detector in the northern sky to have independent results and more statistics;
- to fit all datasets with a single theoretical framework, consisting in, say, the same, single-power-law, isotropic energy spectrum, and in the same model for the atmospheric component.

Further discussion on the open problem of the determination of the astrophysical neutrino spectrum can be found in [1], in which we showed that the results of the HESE and through-going muons analysis flux were incompatible with the assumptions of an unbroken power-law, cosmic neutrino spectrum (if

also isotropy is assumed), and with the available gamma-ray data. In fact, since the HESE and through-going muons analyses are relatively more sensitive to, respectively, the southern and the northern sky, assuming isotropy means that they should measure the same cosmic neutrino flux. However, if the through-going muons neutrino flux is prolonged down to few TeV, the two spectra are incompatible. Even if the HESE flux is prolonged down to lower energies, the connection between neutrinos and gamma rays, which are always expected whenever cosmic-rays are accelerated and produce neutrinos, would imply a gamma-ray flux which overshoots the limits by the experiments. This is a similar argument to the famous Waxman-Bahcall limit [178]. For these reasons, we considered a universal, two-component, cosmic neutrino spectrum which connects the low-energy part of the HESE flux to the high-energy part of the through-going muons flux. The flux of every flavour was computed using theoretical expectations and experimental constraints, and proved good compatibility with the IceCube measurements. We used this model to compute the number of events due to the Glashow resonance ($\overline{\nu}_e + e^- \to W^-$, $E_{\overline{\nu}_e} \approx 6.3\,\mathrm{PeV}$) for the pp and $p\gamma$ neutrino production mechanisms.

In [2] we focussed on the other flavour-specific, elusive kind of event, i.e. double cascades, the detection of which would be the definitive proof of the discovery of astrophysical neutrinos. The cascades are produced by tau neutrino charged current interactions (first cascade) and the subsequent hadronic decay of the tau lepton (second cascade). Due to the very short lifetime of tau leptons and the usual spacing of the optical modules, these events are visible in neutrino telescopes for energies of the tau lepton above few PeV - i.e. very rarely. In this paper we computed the yearly rate of double-cascade events in the current and next-generation neutrino telescopes, proposing analytical formulas, based on physical considerations, for the relevant effective areas. We concluded that paper claiming that IceCube was close to the detection of the first double cascade events: as a matter of fact, two such events are reported in the recent, preliminary work of [200]. On the one hand, this confirms the present theoretical framework on cosmic neutrinos; on the other hand, more statistics is needed to conclusively solve this problem. The possible consequences for the non-observation of double-cascade events have also been discussed: these are quite dramatic, consisting, alternatively, in the violation of standard three-flavour neutrino oscillations, in the disproof of the discovery of cosmic neutrinos, or in the existence of some

other new physics.

Naturally, there are other interesting problems in neutrino astrophysics, which include a more detailed study of Supernova explosions, a better characterisation of the atmospheric and cosmic neutrino fluxes, probing neutrino oscillations between 1 and 50 GeV (which is still a "dark" area) and finding cosmic neutrino sources. In the phenomenological spirit of this thesis, we underline that all these problems will most likely have an experimental solution:

- the current solar neutrino detectors will be able to precisely measure and characterise the neutrino flux resulting from the explosion of a Supernova - as soon as one such event occurs;
- PINGU and ORCA will be able to probe neutrino oscillations in the 1-50 GeV energy range;
- the study of ultra-high-energy neutrinos ($E_\nu \gg 1\,\mathrm{PeV}$) has already been started by Askaryan detectors, as well as Auger, and will be joined by POEMMA;
- the upgrade of IceCube to IceCube-gen2 and the finalisation of the KM3NeT construction will allow to better measure both the atmospheric and the cosmic neutrino flux, as well as collect enough statistics to unequivocally identify a source of neutrinos.

These prospects will take undoubtedly some years to few decades to become reality, nonetheless we believe it is still an exciting time for neutrino physics. As an example, the evidence for TXS 0506+056 as a cosmic-ray source finally earned neutrinos their place in multi-messenger astronomy. Also, if there is anything that neutrinos got us used to, it is surprises: it is then better to be open to the unexpected.

Bibliography

[1] Andrea Palladino, Carlo Mascaretti, and Francesco Vissani. "On the compatibility of the IceCube results with a universal neutrino spectrum". en. In: *The European Physical Journal C* 77.10 (Oct. 2017), p. 684. ISSN: 1434-6044, 1434-6052. DOI: 10.1140/epjc/s10052-017-5273-z. URL: https://epjc.epj.org/articles/epjc/abs/2017/10/10052_2017_Article_5273/10052_2017_Article_5273.html.

[2] Andrea Palladino, Carlo Mascaretti, and Francesco Vissani. "The importance of observing astrophysical tau neutrinos". In: *Journal of Cosmology and Astroparticle Physics* 2018.8 (Aug. 6, 2018), pp. 004–004. ISSN: 1475-7516. DOI: 10.1088/1475-7516/2018/08/004. arXiv: 1804.04965. URL: http://arxiv.org/abs/1804.04965.

[3] Carlo Mascaretti, Pasquale Blasi, and Carmelo Evoli. "Atmospheric neutrinos and the knee of the Cosmic Ray spectrum". In: *Astroparticle Physics* 114 (2019), pp. 22–29. ISSN: 09276505. DOI: 10.1016/j.astropartphys.2019.06.002. arXiv: 1906.05197. URL: http://arxiv.org/abs/1906.05197.

[4] Carlo Mascaretti and Francesco Vissani. "On the relevance of prompt neutrinos for the interpretation of the IceCube signals". In: *Journal of Cosmology and Astroparticle Physics* 2019.8 (Aug. 2019), pp. 004–004. ISSN: 1475-7516. DOI: 10.1088/1475-7516/2019/08/004. URL: https://doi.org/10.1088%5C%2F1475-7516%5C%2F2019%5C%2F08%5C%2F004.

[5] Abraham Loeb and Eli Waxman. "The Cumulative Bakground of High-Energy Neutrinos from Starburst Galaxies". In: *Journal of Cosmology and*

Astroparticle Physics 2006.5 (2006), pp. 003–003. ISSN: 1475-7516. DOI: 10.1088/1475-7516/2006/05/003. arXiv: astro-ph/0601695. URL: http://arxiv.org/abs/astro-ph/0601695.

[6] Carlo Giunti and Chung W. Kim. *Fundamentals of Neutrino Physics and Astrophysics*. Ed. by Oxford University Press. 2007.

[7] Laurie M. Brown. "The idea of the neutrino". In: *Physics Today* 31.9 (1978), p. 23. ISSN: 0031-9228. DOI: 10.1063/1.2995181.

[8] Enrico Fermi. "Tentativo di una teoria dell'emissione dei raggi beta". In: *La Ricerca Scientifica* 2.12 (1933). URL: https://www.phys.uniroma1.it/DipWeb/museo/collezione%20Fermi/documento1.htm.

[9] Edoardo Amaldi. "From the discovery of the neutron to the discovery of nuclear fission". In: *Physics Reports* 111.1 (Sept. 1, 1984), pp. 1–331. ISSN: 0370-1573. DOI: 10.1016/0370-1573(84)90214-X.

[10] C. L. Cowan et al. "Detection of the Free Neutrino: a Confirmation". In: *Science* 124.3212 (July 20, 1956), pp. 103–104. ISSN: 0036-8075, 1095-9203. DOI: 10.1126/science.124.3212.103. (Visited on 11/28/2019).

[11] Raymond Davis, Don S. Harmer, and Kenneth C. Hoffman. "Search for Neutrinos from the Sun". In: *Physical Review Letters* 20 (21 May 1968), pp. 1205–1209. DOI: 10.1103/PhysRevLett.20.1205.

[12] The SNO Collaboration. "Measurement of the Rate of $\nu_e + d \rightarrow p + p + e^-$ Interactions Produced by ^8B Solar Neutrinos at the Sudbury Neutrino Observatory". In: *Phys. Rev. Lett.* 87 (7 July 2001), p. 071301. DOI: 10.1103/PhysRevLett.87.071301.

[13] A. Bellerive et al. "The Sudbury Neutrino Observatory". In: *Nuclear Physics B* 908 (July 2016), pp. 30–51. DOI: 10.1016/j.nuclphysb.2016.04.035. arXiv: 1602.02469.

[14] Nakamura Mituhiro. "Result from DONUT - Direct observation of ν_τ interaction". In: *Nuclear Physics B - Proceedings Supplements* 77.1 (May 1, 1999), pp. 259–264. ISSN: 0920-5632. DOI: 10.1016/S0920-5632(99)00425-9.

[15] W. David Arnett et al. “Supernova 1987A”. In: *Annual Review of Astronomy and Astrophysics* 27.1 (Sept. 1, 1989), pp. 629–700. ISSN: 0066-4146. DOI: 10.1146/annurev.aa.27.090189.003213. URL: https://www.annualreviews.org/doi/10.1146/annurev.aa.27.090189.003213 (visited on 11/29/2019).

[16] A. Ianni et al. “Likelihood for supernova neutrino analyses”. In: *Physical Review D* 80.4 (Aug. 2009). ISSN: 1550-2368. DOI: 10.1103/physrevd.80.043007. URL: http://dx.doi.org/10.1103/PhysRevD.80.043007.

[17] IceCube Collaboration. “Evidence for High-Energy Extraterrestrial Neutrinos at the IceCube Detector”. In: *Science* 342.6161 (Nov. 22, 2013), pp. 1242856–1242856. ISSN: 0036-8075, 1095-9203. DOI: 10.1126/science.1242856. arXiv: 1311.5238. URL: http://arxiv.org/abs/1311.5238.

[18] The IceCube et al. “Multimessenger observations of a flaring blazar coincident with high-energy neutrino IceCube-170922A”. en. In: *Science* (July 2018). ISSN: 0036-8075, 1095-9203. DOI: 10.1126/science.aat1378. URL: http://science.sciencemag.org/content/early/2018/07/11/science.aat1378.

[19] M.E. Peskin and D.V. Schroeder. *An Introduction to Quantum Field Theory*. Avalon Publishing, 1995. ISBN: 978-0-201-50397-5.

[20] R. Ellis, W. Stirling, and B. Webber. *QCD and collider physics*. Vol. 8. Dec. 2003.

[21] Steven Weinberg. *The Quantum Theory of Fields*. Vol. 1 and 2. Cambridge University Press, 1995. DOI: 10.1017/CBO9781139644167.

[22] R. N. Mohapatra and P. B. Pal. “Massive neutrinos in physics and astrophysics”. In: *World Sci. Lect. Notes Phys.* 41 (1991), pp. 1–318.

[23] Guido Altarelli and Ferruccio Feruglio. “Neutrino masses and mixings: a theoretical perspective”. In: *Physics Reports* 320.1 (Oct. 1, 1999), pp. 295–318. ISSN: 0370-1573. DOI: 10.1016/S0370-1573(99)00067-8. URL: http://www.sciencedirect.com/science/article/pii/S0370157399000678.

[24] Ettore Majorana. “Teoria simmetrica dell’elettrone e del positrone”. In: *Il Nuovo Cimento* 14.4 (1937), p. 171. ISSN: 1827-6121. DOI: 10.1007/BF02961314. URL: https://doi.org/10.1007/BF02961314.

[25] S. M. Bilenky and B. Pontecorvo. "Lepton mixing and neutrino oscillations". In: *Physics Reports* 41.4 (May 1, 1978), pp. 225–261. ISSN: 0370-1573. DOI: 10.1016/0370-1573(78)90095-9. URL: http://www.sciencedirect.com/science/article/pii/0370157378900959.

[26] S. M. Bilenky and S. T. Petcov. "Massive neutrinos and neutrino oscillations". In: *Rev. Mod. Phys.* 59 (3 July 1987), pp. 671–754. DOI: 10.1103/RevModPhys.59.671. URL: https://link.aps.org/doi/10.1103/RevModPhys.59.671.

[27] Andrea Palladino and Francesco Vissani. "The natural parameterization of cosmic neutrino oscillations". In: *The European Physical Journal C* 75.9 (Sept. 1, 2015), p. 433. ISSN: 1434-6044, 1434-6052. DOI: 10.1140/epjc/s10052-015-3664-6.

[28] L. Wolfenstein. "Neutrino Oscillations in Matter". In: *Physics Review* D17 (1978), pp. 2369–2374. DOI: 10.1103/PhysRevD.17.2369.

[29] S. P. Mikheev and A. Yu Smirnov. "Resonant amplification of neutrino oscillations in matter and solar neutrino spectroscopy". In: *Nuovo Cimento* C9 (1986), pp. 17–26. DOI: 10.1007/BF02508049.

[30] Francesco Capozzi et al. "Global constraints on absolute neutrino masses and their ordering". In: *Physical Review D* 95.9 (May 30, 2017), p. 096014. DOI: 10.1103/PhysRevD.95.096014.

[31] A. D. Dolgov. "Neutrinos in cosmology". In: *Physics Reports* 370.4 (Nov. 2002), pp. 333–535. ISSN: 03701573. DOI: 10.1016/S0370-1573(02)00139-4. arXiv: hep-ph/0202122. URL: http://arxiv.org/abs/hep-ph/0202122.

[32] Brent Follin et al. "First Detection of the Acoustic Oscillation Phase Shift Expected from the Cosmic Neutrino Background". In: *Physical Review Letters* 115.9 (Aug. 26, 2015), p. 091301. DOI: 10.1103/PhysRevLett.115.091301. URL: https://link.aps.org/doi/10.1103/PhysRevLett.115.091301.

[33] S. E. Woosley and Thomas A. Weaver. "The physics of supernova explosions." In: *Annual Reviews of Astronomy and Astrophysics* 24 (Jan. 1986), pp. 205–253. DOI: 10.1146/annurev.aa.24.090186.001225.

[34] Scott M. Adams et al. “Observing the Next Galactic Supernova”. In: *The Astrophysical Journal* 778.2 (Nov. 2013), p. 164. ISSN: 1538-4357. DOI: 10.1088/0004-637x/778/2/164. URL: http://dx.doi.org/10.1088/0004-637X/778/2/164.

[35] K. Hirata et al. “Observation of a neutrino burst from the supernova SN1987A”. In: *Physical Review Letters* 58.14 (Apr. 6, 1987), pp. 1490–1493. DOI: 10.1103/PhysRevLett.58.1490. URL: https://link.aps.org/doi/10.1103/PhysRevLett.58.1490.

[36] R. M. Bionta et al. “Observation of a neutrino burst in coincidence with supernova 1987A in the Large Magellanic Cloud”. In: *Physical Review Letters* 58.14 (Apr. 6, 1987). DOI: 10.1103/PhysRevLett.58.1494. URL: https://link.aps.org/doi/10.1103/PhysRevLett.58.1494.

[37] E. N. Alekseev et al. “Detection of the Neutrino Signal From {SN1987A} in the {LMC} Using the Inr Baksan Underground Scintillation Telescope”. In: *Phys.Lett.* B205 (1988), pp. 209–214. DOI: 10.1016/0370-2693(88)91651-6.

[38] V. L. Dadykin et al. “Detection of a Rare Event on 23 February 1987 by the Neutrino Radiation Detector Under Mont Blanc”. In: *JETP Lett.* 45 (1987), pp. 593–595.

[39] A. De Rujula. “May a Supernova Bang Twice?” In: *Phys.Lett.* B193 (1987), pp. 514–524. DOI: 10.1016/0370-2693(87)91709-6.

[40] Thomas J. Loredo and Donald Q. Lamb. “Bayesian analysis of neutrinos observed from supernova SN 1987A”. In: *Physical Review D* 65.6 (Feb. 14, 2002), p. 063002. DOI: 10.1103/PhysRevD.65.063002. URL: https://link.aps.org/doi/10.1103/PhysRevD.65.063002.

[41] Andrea Gallo Rosso. “Analysis of supernova neutrino fluxes and neutron star properties”. PhD thesis. Gran Sasso Science Institute, Apr. 2019.

[42] David N. Schramm. “Neutrinos from Supernova SN 1987a”. In: *Comments Nucl. Part. Phys.* 17.5 (1987), pp. 239–278.

[43] Elena Amato and Pasquale Blasi. "Cosmic Ray Transport in the Galaxy: a Review". In: *Advances in Space Research* 62.10 (Nov. 2018), pp. 2731–2749. ISSN: 02731177. DOI: 10.1016/j.asr.2017.04.019. arXiv: 1704.05696. URL: http://arxiv.org/abs/1704.05696.

[44] Particle Data Group et al. "Review of Particle Physics". In: *Physical Review D* 98.3 (Aug. 17, 2018), p. 030001. DOI: 10.1103/PhysRevD.98.030001. URL: https://link.aps.org/doi/10.1103/PhysRevD.98.030001.

[45] T. K. Gaisser, R. Engel, and E. Resconi. *Cosmic Rays and Particle Physics*. Cambridge University Press, June 2016.

[46] P. Padovani et al. "Active Galactic Nuclei: what's in a name?" In: *The Astronomy and Astrophysics Review* 25.1 (Nov. 2017). ISSN: 0935-4956, 1432-0754. DOI: 10.1007/s00159-017-0102-9. arXiv: 1707.07134. URL: http://arxiv.org/abs/1707.07134.

[47] Walter Winter et al. "Multi-messenger interpretation of neutrinos from TXS 0506+056". In: *Proceedings of 36th International Cosmic Ray Conference — PoS(ICRC2019)*. 36th International Cosmic Ray Conference. Vol. 358. SISSA Medialab, Aug. 30, 2019, p. 1032. URL: https://pos.sissa.it/358/1032/ (visited on 12/15/2019).

[48] N. Agafonova et al. "Discovery of τ Neutrino Appearance in the CNGS Neutrino Beam with the OPERA Experiment". In: *Physical Review Letters* 115.12 (2015), p. 121802. DOI: 10.1103/PhysRevLett.115.121802. arXiv: 1507.01417 [hep-ex].

[49] Gernot Eder. "Terrestrial neutrinos". In: *Nuclear Physics* 78.3 (Apr. 1, 1966), pp. 657–662. ISSN: 0029-5582. DOI: 10.1016/0029-5582(66)90903-5. URL: http://www.sciencedirect.com/science/article/pii/0029558266909035.

[50] T. Araki et al. "Experimental investigation of geologically produced antineutrinos with KamLAND". In: *Nature* 436 (2005), pp. 499–503. DOI: 10.1038/nature03980.

[51] M. Agostini et al. *Comprehensive geoneutrino analysis with Borexino*. 2019. arXiv: 1909.02257 [hep-ex].

[52] Y. Fukuda et al. “Evidence for oscillation of atmospheric neutrinos”. In: *Phys. Rev. Lett.* 81 (1998), pp. 1562–1567. arXiv: hep-ex/9807003.

[53] Paschal Coyle. “KM3NeT-ORCA: Oscillation Research with Cosmics in the Abyss”. In: *Journal of Physics: Conference Series* 888 (Sept. 2017), p. 012024. ISSN: 1742-6596. DOI: 10.1088/1742-6596/888/1/012024. URL: http://dx.doi.org/10.1088/1742-6596/888/1/012024.

[54] H. A. Bethe. “Energy production in stars”. In: *Phys. Rev.* 55 (1939), pp. 434–456. DOI: 10.1103/PhysRev.55.434.

[55] William A. Fowler. “Experimental and theoretical nuclear astrophysics: the quest for the origin of the elements”. In: *Rev. Mod. Phys.* 56 (1984), pp. 149–179. DOI: 10.1103/RevModPhys.56.149.

[56] E. G. Adelberger et al. “Solar fusion cross sections. II. Theppchain and CNO cycles”. In: *Reviews of Modern Physics* 83.1 (Apr. 2011), pp. 195–245. ISSN: 1539-0756. DOI: 10.1103/revmodphys.83.195. URL: http://dx.doi.org/10.1103/RevModPhys.83.195.

[57] John N. Bahcall, M. H. Pinsonneault, and Sarbani Basu. “Solar Models: Current Epoch and Time Dependences, Neutrinos, and Helioseismological Properties”. In: *The Astrophysical Journal* 555.2 (July 2001), pp. 990–1012. ISSN: 1538-4357. DOI: 10.1086/321493. URL: http://dx.doi.org/10.1086/321493.

[58] J. N. Bahcall et al. “Solar neutrino flux”. In: *Astrophysical Journal* 137 (1963), pp. 344–346. DOI: 10.1086/147513.

[59] Núria Vinyoles et al. “A New Generation of Standard Solar Models”. In: *The Astrophysical Journal* 835.2 (Jan. 2017), p. 202. ISSN: 1538-4357. DOI: 10.3847/1538-4357/835/2/202. URL: http://dx.doi.org/10.3847/1538-4357/835/2/202.

[60] Andrea Gallo Rosso et al. “Introduction to neutrino astronomy”. In: *Eur. Phys. J. Plus* 133.7 (2018), p. 267. DOI: 10.1140/epjp/i2018-12143-6. arXiv: 1806.06339 [astro-ph.HE].

[61] D. Vescovi et al. “Effects of a revised7Be e^- capture rate on solar neutrino fluxes”. In: *Astronomy & Astrophysics* 623 (Mar. 2019), A126. ISSN: 1432-0746. DOI: 10.1051/0004-6361/201834993. URL: http://dx.doi.org/10.1051/0004-6361/201834993.

[62] E. E. Mamajek et al. “IAU 2015 Resolution B3 on Recommended Nominal Conversion Constants for Selected Solar and Planetary Properties”. In: *arXiv e-prints*, arXiv:1510.07674 (Oct. 2015), arXiv:1510.07674. arXiv: 1510.07674 [astro-ph.SR].

[63] N. Grevesse and A. J. Sauval. “Standard Solar Composition”. In: *Space Science Reviews* 85 (1998), pp. 161–174. DOI: 10.1023/A:1005161325181.

[64] Martin Asplund et al. “The Chemical Composition of the Sun”. In: *Annual Review of Astronomy and Astrophysics* 47.1 (2009), pp. 481–522. DOI: 10.1146/annurev.astro.46.060407.145222. eprint: https://doi.org/10.1146/annurev.astro.46.060407.145222. URL: https://doi.org/10.1146/annurev.astro.46.060407.145222.

[65] John N. Bahcall et al. “Helioseismological implications of recent solar abundance determinations”. In: *Astrophys. J.* 618 (2005), pp. 1049–1056. DOI: 10.1086/426070. arXiv: astro-ph/0407060 [astro-ph].

[66] Aldo M. Serenelli, W. C. Haxton, and Carlos Peña-Garay. “Solar models with accretion. I. Application to the solar abundance problem”. In: *The Astrophysical Journal* 743.1 (Nov. 2011), p. 24. ISSN: 1538-4357. DOI: 10.1088/0004-637x/743/1/24. URL: http://dx.doi.org/10.1088/0004-637X/743/1/24.

[67] B. T. Cleveland et al. “Measurement of the solar electron neutrino flux with the Homestake chlorine detector”. In: *Astrophys. J.* 496 (1998), pp. 505–526. DOI: 10.1086/305343.

[68] John N. Bahcall. “Solar models: An historical overview”. In: *Nuclear Physics B - Proceedings Supplements* 118 (Apr. 2003), pp. 77–86. ISSN: 0920-5632. DOI: 10.1016/s0920-5632(03)01306-9. URL: http://dx.doi.org/10.1016/S0920-5632(03)01306-9.

[69] M. Koshiba. “Observational neutrino astrophysics”. In: *Phys. Rept.* 220 (1992), pp. 229–381. DOI: 10.1016/0370-1573(92)90083-C.

[70] K. S. Hirata et al. “Real time, directional measurement of B-8 solar neutrinos in the Kamiokande-II detector”. In: *Phys. Rev.* D44 (1991). [Erratum: Phys. Rev.D45,2170(1992)], p. 2241. DOI: 10.1103/PhysRevD.44.2241, 10.1103/PhysRevD.45.2170.

[71] Y. Fukuda et al. “Solar neutrino data covering solar cycle 22”. In: *Phys. Rev. Lett.* 77 (1996), pp. 1683–1686. DOI: 10.1103/PhysRevLett.77.1683.

[72] Y. Fukuda et al. “The Super-Kamiokande detector”. In: *Nucl. Instrum. Meth.* A501 (2003), pp. 418–462. DOI: 10.1016/S0168-9002(03)00425-X.

[73] F. Kaether et al. “Reanalysis of the Gallex solar neutrino flux and source experiments”. In: *Physics Letters B* 685.1 (Feb. 2010), pp. 47–54. ISSN: 0370-2693. DOI: 10.1016/j.physletb.2010.01.030. URL: http://dx.doi.org/10.1016/j.physletb.2010.01.030.

[74] J. Hosaka et al. “Solar neutrino measurements in Super-Kamiokande-I”. In: *Physical Review D* 73.11 (June 2006). ISSN: 1550-2368. DOI: 10.1103/physrevd.73.112001. URL: http://dx.doi.org/10.1103/PhysRevD.73.112001.

[75] J. P. Cravens et al. “Solar neutrino measurements in Super-Kamiokande-II”. In: *Physical Review D* 78.3 (Aug. 2008). ISSN: 1550-2368. DOI: 10.1103/physrevd.78.032002. URL: http://dx.doi.org/10.1103/PhysRevD.78.032002.

[76] K. Abe et al. “Solar neutrino results in Super-Kamiokande-III”. In: *Physical Review D* 83.5 (Mar. 2011). ISSN: 1550-2368. DOI: 10.1103/physrevd.83.052010. URL: http://dx.doi.org/10.1103/PhysRevD.83.052010.

[77] Super-Kamiokande Collaboration. “Solar Neutrino Measurements in Super-Kamiokande-IV”. In: (2016). arXiv: 1606.07538 [hep-ex].

[78] J. N. Abdurashitov et al. “Measurement of the solar neutrino capture rate with gallium metal. III. Results for the 2002-2007 data-taking period”. In: *Physical Review C* 80.1 (July 2009). ISSN: 1089-490X. DOI: 10.1103/physrevc.80.015807. URL: http://dx.doi.org/10.1103/PhysRevC.80.015807.

[79] J Boger et al. "The Sudbury Neutrino Observatory". In: *Nuclear Instruments and Methods in Physics Research Section A: Accelerators, Spectrometers, Detectors and Associated Equipment* 449.1-2 (July 2000), pp. 172–207. ISSN: 0168-9002. DOI: 10.1016/s0168-9002(99)01469-2. URL: http://dx.doi.org/10.1016/S0168-9002(99)01469-2.

[80] H. H. Chen. "Direct Approach to Resolve the Solar Neutrino Problem". In: *Phys. Rev. Lett.* 55 (1985), pp. 1534–1536. DOI: 10.1103/PhysRevLett.55.1534.

[81] B. Aharmim et al. "Combined analysis of all three phases of solar neutrino data from the Sudbury Neutrino Observatory". In: *Physical Review C* 88.2 (Aug. 2013). ISSN: 1089-490X. DOI: 10.1103/physrevc.88.025501. URL: http://dx.doi.org/10.1103/PhysRevC.88.025501.

[82] Q. R. Ahmad et al. "Direct Evidence for Neutrino Flavor Transformation from Neutral-Current Interactions in the Sudbury Neutrino Observatory". In: *Physical Review Letters* 89.1 (June 2002). ISSN: 1079-7114. DOI: 10.1103/physrevlett.89.011301. URL: http://dx.doi.org/10.1103/PhysRevLett.89.011301.

[83] B. Aharmim et al. "Electron energy spectra, fluxes, and day-night asymmetries of8B solar neutrinos from measurements with NaCl dissolved in the heavy-water detector at the Sudbury Neutrino Observatory". In: *Physical Review C* 72.5 (Nov. 2005). ISSN: 1089-490X. DOI: 10.1103/physrevc.72.055502. URL: http://dx.doi.org/10.1103/PhysRevC.72.055502.

[84] M. Anderson et al. "Measurement of the ^{8}B solar neutrino flux in SNO+ with very low backgrounds". In: *Physical Review D* 99.1 (Jan. 2019). ISSN: 2470-0029. DOI: 10.1103/physrevd.99.012012. URL: http://dx.doi.org/10.1103/PhysRevD.99.012012.

[85] G. Alimonti et al. "The Borexino detector at the Laboratori Nazionali del Gran Sasso". In: *Nuclear Instruments and Methods in Physics Research Section A: Accelerators, Spectrometers, Detectors and Associated Equipment* 600.3 (Mar. 2009), pp. 568–593. ISSN: 0168-9002. DOI: 10.1016/j.nima.2008.11.076. URL: http://dx.doi.org/10.1016/j.nima.2008.11.076.

[86] C. Arpesella et al. “First real time detection of ^{7}Be solar neutrinos by Borexino”. In: *Physics Letters B* 658.4 (Jan. 2008), pp. 101–108. ISSN: 0370-2693. DOI: 10.1016/j.physletb.2007.09.054. URL: http://dx.doi.org/10.1016/j.physletb.2007.09.054.

[87] G. Bellini et al. “Precision Measurement of theBe7Solar Neutrino Interaction Rate in Borexino”. In: *Physical Review Letters* 107.14 (Sept. 2011). ISSN: 1079-7114. DOI: 10.1103/physrevlett.107.141302. URL: http://dx.doi.org/10.1103/PhysRevLett.107.141302.

[88] G. Bellini et al. “Absence of a day-night asymmetry in the 7Be solar neutrino rate in Borexino”. In: *Physics Letters B* 707.1 (Jan. 2012), pp. 22–26. ISSN: 0370-2693. DOI: 10.1016/j.physletb.2011.11.025. URL: http://dx.doi.org/10.1016/j.physletb.2011.11.025.

[89] M. Agostini et al. “Seasonal modulation of the 7 Be solar neutrino rate in Borexino”. In: *Astroparticle Physics* 92 (June 2017), pp. 21–29. ISSN: 0927-6505. DOI: 10.1016/j.astropartphys.2017.04.004. URL: http://dx.doi.org/10.1016/j.astropartphys.2017.04.004.

[90] G. Bellini et al. “Measurement of the solarB8neutrino rate with a liquid scintillator target and 3 MeV energy threshold in the Borexino detector”. In: *Physical Review D* 82.3 (Aug. 2010). ISSN: 1550-2368. DOI: 10.1103/physrevd.82.033006. URL: http://dx.doi.org/10.1103/PhysRevD.82.033006.

[91] G. Bellini et al. “Final results of Borexino Phase-I on low-energy solar neutrino spectroscopy”. In: *Physical Review D* 89.11 (June 2014). ISSN: 1550-2368. DOI: 10.1103/physrevd.89.112007. URL: http://dx.doi.org/10.1103/PhysRevD.89.112007.

[92] M. Agostini et al. “Simultaneous precision spectroscopy of pp, ^{7}Be, and pep solar neutrinos with Borexino Phase-II”. In: *Physical Review D* 100.8 (Oct. 2019). ISSN: 2470-0029. DOI: 10.1103/physrevd.100.082004. URL: http://dx.doi.org/10.1103/PhysRevD.100.082004.

[93] Ivan Esteban et al. “Updated fit to three neutrino mixing: exploring the accelerator-reactor complementarity”. In: *JHEP* 01 (2017), p. 087. DOI: 10.1007/JHEP01(2017)087. arXiv: 1611.01514 [hep-ph].

[94] The Borexino Collaboration et al. *Improved measurement of 8B solar neutrinos with 1.5 kt y of Borexino exposure*. 2017. arXiv: 1709.00756 [hep-ex].

[95] Fengpeng An et al. "Neutrino physics with JUNO". In: *Journal of Physics G: Nuclear and Particle Physics* 43.3 (Feb. 2016), p. 030401. ISSN: 1361-6471. DOI: 10.1088/0954-3899/43/3/030401. URL: http://dx.doi.org/10.1088/0954-3899/43/3/030401.

[96] Hyper-Kamiokande Proto-Collaboration. *Hyper-Kamiokande Design Report*. 2018. arXiv: 1805.04163 [physics.ins-det].

[97] The Borexino Collaboration. "'Neutrinos from the primary proton-proton fusion process in the Sun". In: *Nature* 512.7515 (2014), p. 383. DOI: 10.1038/nature13702.

[98] F. L. Villante et al. "A Step toward CNO solar neutrinos detection in liquid scintillators". In: *Physics Letters* B 701.336 (2011). DOI: 10.1016/j.physletb.2011.05.068. arXiv: 1104.1335 [hep-ph].

[99] Ranucci, G. on behalf of the Borexino Collaboration. "Report at the Gran Sasso Scientific Committee". In: 2019. URL: https://agenda.infn.it/event/20448/.

[100] M. Spiro and D. Vignaud. "Solar Model Independent Neutrino Oscillation Signals in the Forthcoming Solar Neutrino Experiments?" In: *Physics Letters* B 242.279 (1990). DOI: 10.1016/0370-2693(90)91471-M.

[101] John N. Bahcall. "The luminosity constraint on solar neutrino fluxes". In: *Physical Review C* 65.2, 025801 (Feb. 2002), p. 025801. DOI: 10.1103/PhysRevC.65.025801. arXiv: hep-ph/0108148 [hep-ph].

[102] Francesco Vissani. "Luminosity constraint and entangled solar neutrino signals". In: *Solar Neutrinos*. May 2019, pp. 121–141. DOI: 10.1142/9789811204296_0006.

[103] John N. Bahcall, M. H. Pinsonneault, and G. J. Wasserburg. "Solar models with helium and heavy-element diffusion". In: *Reviews of Modern Physics* 67.4 (Oct. 1995), pp. 781–808. DOI: 10.1103/RevModPhys.67.781. arXiv: hep-ph/9505425 [hep-ph].

[104] N. Grevesse and A. J. Sauval. "Standard Solar Composition". In: *Space Science Reviews* 85 (May 1998), pp. 161–174. DOI: 10.1023/A:1005161325181.

[105] H. Palme, K. Lodders, and A. Jones. "Solar System Abundances of the Elements". In: *Planets, Asteriods, Comets and The Solar System, Volume 2 of Treatise on Geochemistry (Second Edition)*. Vol. 2. Elsevier, 2014, pp. 15–36.

[106] L. Piersanti, O. Straniero, and S. Cristallo. "A method to derive the absolute composition of the Sun, the solar system, and the stars". In: *Astronomy and Astrophysics* 462.3 (Feb. 2007), pp. 1051–1062. DOI: 10.1051/0004-6361:20054505. arXiv: astro-ph/0611229 [astro-ph].

[107] J. Reiter, R. Bulirsch, and J. Pfleiderer. "A multiple shooting approach for the numerical treatment of stellar structure and evolution". In: *Astronomische Nachrichten* 315.3 (Apr. 1994), pp. 205–234. DOI: 10.1002/asna.2103150304.

[108] J. Reiter, L. Walsh, and A. Weiss. "Solar models: a comparative study of two stellar evolution codes". In: *Monthly Notices of the Royal Astronomical Society* 274.3 (June 1995), pp. 899–908. DOI: 10.1093/mnras/274.3.899.

[109] Anatoli Fedynitch et al. "A state-of-the-art calculation of atmospheric lepton fluxes". en. In: *Proceedings of 35th International Cosmic Ray Conference — PoS(ICRC2017)*. Vol. 301. SISSA Medialab, Aug. 2018, p. 1019. DOI: 10.22323/1.301.1019. URL: https://pos.sissa.it/301/1019/.

[110] Sally Robertson. "Measurement of the multi-TeV neutrino cross section with IceCube using Earth absorption". In: *36th International Cosmic Ray Conference (ICRC 2019) Madison, Wisconsin, USA, July 24-August 1, 2019*. 2019. arXiv: 1908.06123 [astro-ph.HE].

[111] Antonella Castellina and on behalf of the Pierre Auger Collaboration. "Highlights from the Pierre Auger Observatory". In: *Proceedings of 36th International Cosmic Ray Conference — PoS(ICRC2019)*. 36th International Cosmic Ray Conference. Vol. 358. SISSA Medialab, Oct. 25, 2019, p. 004. URL: https://pos.sissa.it/358/004/.

[112] G. T. Zatsepin and V. A. Kuz'min. "Upper Limit of the Spectrum of Cosmic Rays". In: *ZhETF Pisma Redaktsiiu* 4 (Aug. 1966), p. 114.

[113] V. S. Berezinsky and G. T. Zatsepin. "Cosmic rays at ultrahigh-energies (neutrino?)" In: *Phys. Lett.* 28B (1969), pp. 423–424. DOI: 10.1016/0370-2693(69)90341-4.

[114] K. S. Hirata et al. "Observation of a small atmospheric ν_μ/ν_e ratio in Kamiokande". In: *Phys. Lett.* B280 (1992), pp. 146–152.

[115] Y. Fukuda et al. "Atmospheric muon-neutrino / electron-neutrino ratio in the multiGeV energy range". In: *Phys. Lett.* B335 (1994), pp. 237–245.

[116] S. Hatakeyama et al. "Measurement of the flux and zenith angle distribution of upward through-going muons in Kamiokande II + III". In: *Phys. Rev. Lett.* 81 (1998), pp. 2016–2019. arXiv: hep-ex/9806038.

[117] R. Becker-Szendy et al. "A Search for muon-neutrino oscillations with the IMB detector". In: *Phys. Rev. Lett.* 69 (1992), pp. 1010–1013.

[118] Edward Kearns. "Experimental measurements of atmospheric neutrinos". In: *Nuclear Physics B - Proceedings Supplements* 70.1-3 (Jan. 1999), pp. 315–323. ISSN: 0920-5632. DOI: 10.1016/s0920-5632(98)00441-1. URL: http://dx.doi.org/10.1016/S0920-5632(98)00441-1.

[119] Yusuke Koshio and On behalf of the Super-Kamiokande Collaboration. "Solar and atmospheric neutrino oscillations in SuperKamiokande". In: *Proceedings of Neutrino Oscillation Workshop — PoS(NOW2016)*. Neutrino Oscillation Workshop. Vol. 283. SISSA Medialab, June 20, 2017, p. 001. DOI: 10.22323/1.283.0001. URL: https://pos.sissa.it/283/001/.

[120] Y. Ashie et al. "Evidence for an Oscillatory Signature in Atmospheric Neutrino Oscillations". In: *Physical Review Letters* 93.10 (Sept. 2004). ISSN: 1079-7114. DOI: 10.1103/physrevlett.93.101801. URL: http://dx.doi.org/10.1103/PhysRevLett.93.101801.

[121] M Ambrosio et al. "Atmospheric neutrino oscillations from upward through-going muon multiple scattering in MACRO". In: *Physics Letters B* 566.1-2 (July 2003), pp. 35–44. ISSN: 0370-2693. DOI: 10.1016/s0370-2693(03)00806-2. URL: http://dx.doi.org/10.1016/S0370-2693(03)00806-2.

[122] M. Ahlers and F. Halzen. "Opening a new window onto the universe with IceCube". In: *Progress in Particle and Nuclear Physics* 102 (Sept. 2018), pp. 73–88. DOI: 10.1016/j.ppnp.2018.05.001. arXiv: 1805.11112 [astro-ph.HE].

[123] Thomas Gaisser and Francis Halzen. "IceCube". In: *Annual Review of Nuclear and Particle Science* 64.1 (2014), pp. 101–123. DOI: 10.1146/annurev-nucl-102313-025321. URL: https://doi.org/10.1146/annurev-nucl-102313-025321.

[124] IceCube Collaboration. "IceTop: The surface component of IceCube". In: *Nuclear Instruments and Methods in Physics Research Section A: Accelerators, Spectrometers, Detectors and Associated Equipment* 700 (Feb. 2013), pp. 188–220. ISSN: 01689002. DOI: 10.1016/j.nima.2012.10.067. arXiv: 1207.6326. URL: http://arxiv.org/abs/1207.6326.

[125] Dennis Soldin and on behalf of the IceCube Collaboration. "Recent Results of Cosmic Ray Measurements from IceCube and IceTop". In: *Proceedings of 36th International Cosmic Ray Conference — PoS(ICRC2019)*. 36th International Cosmic Ray Conference. Vol. 358. SISSA Medialab, Aug. 30, 2019, p. 014. URL: https://pos.sissa.it/358/014/.

[126] The IceCube Collaboration. "Measurement of the Atmospheric ν_e Spectrum with IceCube". In: *Physical Review D* 91.12 (2015). ISSN: 1550-7998, 1550-2368. DOI: 10.1103/PhysRevD.91.122004. arXiv: 1504.03753. URL: http://arxiv.org/abs/1504.03753.

[127] The IceCube Collaboration. "Development of a General Analysis and Unfolding Scheme and its Application to Measure the Energy Spectrum of Atmospheric Neutrinos with IceCube". In: *The European Physical Journal C* 75.3 (2015). ISSN: 1434-6044, 1434-6052. DOI: 10.1140/epjc/s10052-015-3330-z. arXiv: 1409.4535.

[128] The IceCube Collaboration. "Measurement of the ν_μ energy spectrum with IceCube-79". In: *European Physical Journal C* 77, 692 (Oct. 2017), p. 692. DOI: 10.1140/epjc/s10052-017-5261-3. arXiv: 1705.07780 [astro-ph.HE].

[129] Mathis Börner. "Unfolding measurement of the Atmospheric Neutrino Spectrum using IceCube-79/86". In: *Proceedings of The 34th International Cosmic Ray Conference — PoS(ICRC2015)* 236 (2016), p. 1098. DOI: 10.22323/1.236.1098.

[130] Tobias Hoinka, Jan Soedingrekso, and Mathis Börner. "Model-independent Measurement of the Atmospheric Muon Neutrino Energy Spectrum up to 2.5 PeV". In: *HAWC Contributions to the 36th International Cosmic Ray Conference (ICRC2019)*. 2019. arXiv: 1909.05129 [astro-ph.HE].

[131] M. G. Aartsen et al. "Measurement of Atmospheric Neutrino Oscillations at 6-56 GeV with IceCube DeepCore". In: *Physical Review Letters* 120.7 (Feb. 2018). ISSN: 1079-7114. DOI: 10.1103/physrevlett.120.071801. URL: http://dx.doi.org/10.1103/PhysRevLett.120.071801.

[132] M. G. Aartsen et al. "Measurement of atmospheric tau neutrino appearance with IceCube DeepCore". In: *Physical Review D* 99.3 (Feb. 2019). ISSN: 2470-0029. DOI: 10.1103/physrevd.99.032007. URL: http://dx.doi.org/10.1103/PhysRevD.99.032007.

[133] Soebur Razzaque and Luis Salvador Miranda. "Revisiting constraints on sterile neutrino mixing parameters using IceCube atmospheric neutrino data". In: *Proceedings of 36th International Cosmic Ray Conference — PoS(ICRC2019)*. 36th International Cosmic Ray Conference. Vol. 358. SISSA Medialab, July 22, 2019, p. 987. URL: https://pos.sissa.it/358/987/.

[134] M. G. Aartsen et al. "Development of an analysis to probe the neutrino mass ordering with atmospheric neutrinos using three years of IceCube DeepCore data". In: *Eur. Phys. J.* C80.1 (2020), p. 9. DOI: 10.1140/epjc/s10052-019-7555-0.

[135] M G Aartsen et al. "PINGU: a vision for neutrino and particle physics at the South Pole". In: *Journal of Physics G: Nuclear and Particle Physics* 44.5 (Apr. 2017), p. 054006. ISSN: 1361-6471. DOI: 10.1088/1361-6471/44/5/054006. URL: http://dx.doi.org/10.1088/1361-6471/44/5/054006.

[136] M. Ageron et al. "ANTARES: The first undersea neutrino telescope". In: *Nuclear Instruments and Methods in Physics Research Section A: Accelerators, Spectrometers, Detectors and Associated Equipment* 656.1 (Nov. 2011), pp. 11–38. ISSN: 0168-9002. DOI: 10.1016/j.nima.2011.06.103. URL: http://dx.doi.org/10.1016/j.nima.2011.06.103.

[137] S Adriàn-Martìnez et al. "Letter of intent for KM3NeT 2.0". In: *Journal of Physics G: Nuclear and Particle Physics* 43.8 (June 2016), p. 084001. ISSN: 1361-6471. DOI: 10.1088/0954-3899/43/8/084001. URL: http://dx.doi.org/10.1088/0954-3899/43/8/084001.

[138] Jannik Hofestädt et al. "Atmospheric Neutrinos Detected with the First KM3NeT Detection Units of ARCA and ORCA". In: *Proceedings of 36th International Cosmic Ray Conference — PoS(ICRC2019)*. 36th International Cosmic Ray Conference. Vol. 358. SISSA Medialab, July 22, 2019, p. 910. URL: https://pos.sissa.it/358/910/.

[139] S. Adrián-Martínez et al. "Measurement of the atmospheric ν_μ energy spectrum from 100 GeV to 200 TeV with the ANTARES telescope". In: *The European Physical Journal C* 73.10 (Oct. 2013). ISSN: 1434-6052. DOI: 10.1140/epjc/s10052-013-2606-4. URL: http://dx.doi.org/10.1140/epjc/s10052-013-2606-4.

[140] ANTARES Collaboration. *Measuring the atmospheric neutrino oscillation parameters and constraining the 3+1 neutrino model with ten years of ANTARES data*. 2018. arXiv: 1812.08650 [hep-ex].

[141] T. Antoni, et al., and KASCADE Coll. "KASCADE measurements of energy spectra for elemental groups of cosmic rays: Results and open problems". In: *Astroparticle Physics* 24 (Sept. 2005), pp. 1–25. DOI: 10.1016/j.astropartphys.2005.04.001. eprint: astro-ph/0505413.

[142] B. Bartoli et al. "Energy spectrum of cosmic protons and helium nuclei by a hybrid measurement at 4300 m a.s.l." en. In: *Chinese Physics C* 38.4 (Apr. 2014), p. 045001. ISSN: 1674-1137. DOI: 10.1088/1674-1137/38/4/045001. URL: https://doi.org/10.1088%5C%2F1674-1137%5C%2F38%5C%2F4%5C%2F045001.

[143] G. Giacinti, M. Kachelrieß, and D. V. Semikoz. "Explaining the spectra of cosmic ray groups above the knee by escape from the Galaxy". In: *Physical Review D* 90.4, 041302 (Aug. 2014), p. 041302. DOI: 10.1103/PhysRevD.90.041302. arXiv: 1403.3380 [astro-ph.HE].

[144] P. Blasi. "The origin of galactic cosmic rays". In: *The Astronomy and Astrophysics Review* 21, 70 (Nov. 2013), p. 70. DOI: 10.1007/s00159-013-0070-7. arXiv: 1311.7346 [astro-ph.HE].

[145] M. Cardillo, E. Amato, and P. Blasi. "On the cosmic ray spectrum from type II supernovae expanding in their red giant presupernova wind". In: *Astroparticle Physics* 69 (Sept. 2015), pp. 1–10. DOI: 10.1016/j.astropartphys.2015.03.002. arXiv: 1503.03001 [astro-ph.HE].

[146] K. M. Schure and A. R. Bell. "From cosmic ray source to the Galactic pool". In: *Monthly Notices of the Royal Astronomical Society* 437 (Jan. 2014), pp. 2802–2805. DOI: 10.1093/mnras/stt2089. arXiv: 1310.7027 [astro-ph.HE].

[147] A. Fedynitch et al. "Calculation of conventional and prompt lepton fluxes at very high energy". In: *European Physical Journal Web of Conferences*. Vol. 99. European Physical Journal Web of Conferences. Aug. 2015, p. 08001. DOI: 10.1051/epjconf/20159908001. arXiv: 1503.00544 [hep-ph].

[148] J. M. Picone et al. "NRLMSISE-00 empirical model of the atmosphere: Statistical comparisons and scientific issues". In: *Journal of Geophysical Research (Space Physics)* 107, 1468 (Dec. 2002), p. 1468. DOI: 10.1029/2002JA009430.

[149] Felix Riehn et al. "The hadronic interaction model Sibyll 2.3c and Feynman scaling". en. In: *Proceedings of 35th International Cosmic Ray Conference — PoS(ICRC2017)* 301 (Aug. 2018), p. 301. DOI: 10.22323/1.301.0301. URL: https://pos.sissa.it/301/301/.

[150] The KASCADE-Grande Collaboration. "Ankle-like Feature in the Energy Spectrum of Light Elements of Cosmic Rays Observed with KASCADE-Grande". In: *Physical Review D* 87.8 (2013). ISSN: 1550-7998, 1550-2368. DOI: 10.1103/PhysRevD.87.081101. arXiv: 1304.7114.

[151] Di Sciascio on behalf of the ARGO-YBJ Collaboration. "ARGO-YBJ Highlights". In: *XI Multifrequency Behaviour of High Energy Cosmic Sources Workshop (MULTIF15)*. 2015, p. 50.

[152] Roberto Aloisio et al. "Selected Topics in Cosmic Ray Physics". In: *Multiple Messengers and Challenges in Astroparticle Physics*. Ed. by Roberto Aloisio, Eugenio Coccia, and Francesco Vissani. Cham: Springer International Publishing, 2018, pp. 1–95. ISBN: 978-3-319-65425-6. DOI: 10.1007/978-3-319-65425-6_1. arXiv: 1312.7459. URL: https://doi.org/10.1007/978-3-319-65425-6_1.

[153] O. Adriani et al. "PAMELA Measurements of Cosmic-Ray Proton and Helium Spectra". In: *Science* 332 (Apr. 2011), p. 69. DOI: 10.1126/science.1199172. arXiv: 1103.4055 [astro-ph.HE].

[154] The AMS-02 Collaboration. "Precision Measurement of the Proton Flux in Primary Cosmic Rays from Rigidity 1 GV to 1.8 TV with the Alpha Magnetic Spectrometer on the International Space Station". In: *Physical Review Letters* 114.17, 171103 (May 2015), p. 171103. DOI: 10.1103/PhysRevLett.114.171103.

[155] The AMS-02 Collaboration. "Precision Measurement of the Helium Flux in Primary Cosmic Rays of Rigidities 1.9 GV to 3 TV with the Alpha Magnetic Spectrometer on the International Space Station". In: *Physical Review Letters* 115.21, 211101 (Nov. 2015), p. 211101. DOI: 10.1103/PhysRevLett.115.211101.

[156] D. Maurin, F. Melot, and R. Taillet. "A database of charged cosmic rays". In: *The Astronomy and Astrophysics Review* 569, A32 (Sept. 2014), A32. DOI: 10.1051/0004-6361/201321344. arXiv: 1302.5525 [astro-ph.HE].

[157] P. Subedi et al. "Charged Particle Diffusion in Isotropic Random Magnetic Fields". In: *The Astrophysical Journal* 837, 140 (Mar. 2017), p. 140. DOI: 10.3847/1538-4357/aa603a. arXiv: 1612.09507 [physics.space-ph].

[158] Sven Schoo et al. "The energy spectrum of cosmic rays in the range from 10^{14} to 10^{18}eV". In: *PoS* ICRC2015 (2016), p. 263. DOI: 10.22323/1.236.0263.

[159] T. K. Gaisser, T. Stanev, and S. Tilav. "Cosmic ray energy spectrum from measurements of air showers". en. In: *Frontiers of Physics* 8.6 (Dec. 2013), pp. 748–758. ISSN: 2095-0470. DOI: 10.1007/s11467-013-0319-7. URL: https://doi.org/10.1007/s11467-013-0319-7.

[160] T. K. Gaisser. "Spectrum of cosmic-ray nucleons, kaon production, and the atmospheric muon charge ratio". In: *Astroparticle Physics* 35 (July 2012), pp. 801–806. DOI: 10.1016/j.astropartphys.2012.02.010. arXiv: 1111.6675 [astro-ph.HE].

[161] T. Pierog et al. "EPOS LHC: Test of collective hadronization with data measured at the CERN Large Hadron Collider". In: *Physical Review C* 92.3, 034906 (Sept. 2015), p. 034906. DOI: 10.1103/PhysRevC.92.034906.

[162] S. Ostapchenko. "Monte Carlo treatment of hadronic interactions in enhanced Pomeron scheme: QGSJET-II model". In: *Physical Review D* 83.1, 014018 (Jan. 2011), p. 014018. DOI: 10.1103/PhysRevD.83.014018. arXiv: 1010.1869 [hep-ph].

[163] A. Fedynitch and R. Engel. "Revision of the high energy hadronic interaction models PHOJET/DPMJET-III". In: *14th International Conference on Nuclear Reaction Mechanisms, Villa Monastero, Varenna*. 2015, p. 291.

[164] M. Thunman, G. Ingelman, and P. Gondolo. "Charm Production and High Energy Atmospheric Muon and Neutrino Fluxes". In: *Astroparticle Physics* 5.3 (1996), pp. 309–332. ISSN: 09276505. DOI: 10.1016/0927-6505(96)00033-3. arXiv: hep-ph/9505417. URL: http://arxiv.org/abs/hep-ph/9505417.

[165] Rikard Enberg, Mary Hall Reno, and Ina Sarcevic. "Prompt neutrino fluxes from atmospheric charm". In: *Physical Review D* 78.4 (2008). ISSN: 1550-7998, 1550-2368. DOI: 10.1103/PhysRevD.78.043005. arXiv: 0806.0418. URL: http://arxiv.org/abs/0806.0418.

[166] M. Honda et al. "Calculation of atmospheric neutrino flux using the interaction model calibrated with atmospheric muon data". In: *Physical Review D* 75.4 (2007). ISSN: 1550-7998, 1550-2368. DOI: 10.1103/PhysRevD.75.043006. arXiv: astro-ph/0611418. URL: http://arxiv.org/abs/astro-ph/0611418.

[167] Rhorry Gauld et al. "The prompt atmospheric neutrino flux in the light of LHCb". In: *Journal of High Energy Physics* 2016.2 (2016). ISSN: 1029-8479. DOI: 10.1007/JHEP02(2016)130. arXiv: 1511.06346. URL: http://arxiv.org/abs/1511.06346.

[168] M. Benzke et al. "Prompt neutrinos from atmospheric charm in the general-mass variable-flavor-number scheme". In: *Journal of High Energy Physics* 2017.12 (2017). ISSN: 1029-8479. DOI: 10.1007/JHEP12(2017)021. arXiv: 1705.10386.

[169] Atri Bhattacharya et al. "Prompt atmospheric neutrino fluxes: perturbative QCD models and nuclear effects". In: *Journal of High Energy Physics* 2016.11 (2016). ISSN: 1029-8479. DOI: 10.1007/JHEP11(2016)167. arXiv: 1607.00193. URL: http://arxiv.org/abs/1607.00193.

[170] A. M. Taylor, S. Gabici, and F. Aharonian. "Galactic halo origin of the neutrinos detected by IceCube". In: *Physical Review D* 89.10, 103003 (May 2014), p. 103003. DOI: 10.1103/PhysRevD.89.103003. arXiv: 1403.3206 [astro-ph.HE].

[171] P. Blasi and E. Amato. "Escape of cosmic rays from the Galaxy and effects on the circumgalactic medium". In: *arXiv e-prints* (Jan. 2019). arXiv: 1901.03609 [astro-ph.HE].

[172] M. G. Aartsen, et al., and Icecube Collaboration. "Observation and Characterization of a Cosmic Muon Neutrino Flux from the Northern Hemisphere Using Six Years of IceCube Data". In: *The Astrophysical Journal* 833, 3 (Dec. 2016), p. 3. DOI: 10.3847/0004-637X/833/1/3. arXiv: 1607.08006 [astro-ph.HE].

[173] Claudio Kopper and on behalf of the IceCube Collaboration. "Observation of Astrophysical Neutrinos in Six Years of IceCube Data". en. In: *Proceedings of 35th International Cosmic Ray Conference — PoS(ICRC2017)*. Vol. 301. SISSA Medialab, Aug. 2018, p. 981. DOI: 10.22323/1.301.0981. URL: https://pos.sissa.it/cgi-bin/reader/contribution.cgi?id=PoS(ICRC2017)981.

[174] The IceCube Collaboration. "Observation of High-Energy Astrophysical Neutrinos in Three Years of IceCube Data". In: *Physical Review Letters* 113.10 (Sept. 2, 2014). ISSN: 0031-9007, 1079-7114. DOI: 10.1103/PhysRevLett.113.101101. arXiv: 1405.5303. URL: http://arxiv.org/abs/1405.5303.

[175] Markus Ackermann et al. "Astrophysics Uniquely Enabled by Observations of High-Energy Cosmic Neutrinos". In: *Bull. Am. Astron. Soc.* 51 (2019), p. 185. arXiv: 1903.04334 [astro-ph.HE].

[176] F. L. Villante and F. Vissani. "How precisely can neutrino emission from supernova remnants be constrained by gamma ray observations?" In: *Physical Review D* 78.10 (Nov. 2008), p. 103007. DOI: 10.1103/PhysRevD.78.103007. URL: https://link.aps.org/doi/10.1103/PhysRevD.78.103007.

[177] Francesco Vissani. "Neutrinos from galactic sources of cosmic rays with known γ-ray spectra". In: *Astropart. Phys.* 26 (2006), pp. 310–313. DOI: 10.1016/j.astropartphys.2006.07.005. arXiv: astro-ph/0607249 [astro-ph].

[178] Eli Waxman and John Bahcall. "High energy neutrinos from astrophysical sources: An upper bound". In: *Physical Review D* 59 (Jan. 1, 1999), p. 023002. ISSN: 1550-7998. DOI: 10.1103/PhysRevD.59.023002. URL: http://adsabs.harvard.edu/abs/1999PhRvD..59b3002W.

[179] Kohta Murase, Dafne Guetta, and Markus Ahlers. "Hidden Cosmic-Ray Accelerators as an Origin of TeV-PeV Cosmic Neutrinos". In: *Phys. Rev. Lett.* 116.7 (2016), p. 071101. DOI: 10.1103/PhysRevLett.116.071101. arXiv: 1509.00805 [astro-ph.HE].

[180] Kohta Murase et al. "Testing the Dark Matter Scenario for PeV Neutrinos Observed in IceCube". In: *Phys. Rev. Lett.* 115.7 (2015), p. 071301. DOI: 10.1103/PhysRevLett.115.071301. arXiv: 1503.04663 [hep-ph].

[181] F. Halzen and E. Zas. "Neutrino fluxes from active galaxies: A Model independent estimate". In: *Astrophys. J.* 488 (1997), pp. 669–674. DOI: 10.1086/304741. arXiv: astro-ph/9702193 [astro-ph].

[182] Markus Ahlers and Lea Halser. "Neutrino fluence from gamma-ray bursts: off-axis view of structured jets". In: *Monthly Notices of the Royal Astronomical Society* 490.4 (Oct. 2019), pp. 4935–4943. ISSN: 1365-2966. DOI: 10.1093/mnras/stz2980. URL: http://dx.doi.org/10.1093/mnras/stz2980.

[183] Irene Tamborra, Shin'ichiro Ando, and Kohta Murase. "Star-forming galaxies as the origin of diffuse high-energy backgrounds: Gamma-ray and neutrino connections, and implications for starburst history". In: *JCAP* 1409 (2014), p. 043. DOI: 10.1088/1475-7516/2014/09/043. arXiv: 1404.1189 [astro-ph.HE].

[184] Enrico Peretti et al. "Cosmic ray transport and radiative processes in nuclei of starburst galaxies". In: *Monthly Notices of the Royal Astronomical Society* 487.1 (Apr. 2019), pp. 168–180. ISSN: 1365-2966. DOI: 10.1093/mnras/stz1161. URL: http://dx.doi.org/10.1093/mnras/stz1161.

[185] Enrico Peretti et al. *Contribution of starburst nuclei to the diffuse gamma-ray and neutrino flux*. 2019. arXiv: 1911.06163 [astro-ph.HE].

[186] Pasquale Blasi and Elena Amato. "Escape of Cosmic Rays from the Galaxy and Effects on the Circumgalactic Medium". In: *Physical Review Letters* 122.5 (Feb. 2019). ISSN: 1079-7114. DOI: 10.1103/physrevlett.122.051101. URL: http://dx.doi.org/10.1103/PhysRevLett.122.051101.

[187] K. Greisen. "Cosmic ray showers". In: *Ann. Rev. Nucl. Part. Sci.* 10 (1960), pp. 63–108. DOI: 10.1146/annurev.ns.10.120160.000431.

[188] M. A. Markov and I. M. Zheleznykh. "On high energy neutrino physics in cosmic rays". In: *Nucl. Phys.* 27 (1961), pp. 385–394. DOI: 10.1016/0029-5582(61)90331-5.

[189] Raj Gandhi et al. "Neutrino interactions at ultrahigh-energies". In: *Phys. Rev.* D58 (1998), p. 093009. DOI: 10.1103/PhysRevD.58.093009. arXiv: hep-ph/9807264 [hep-ph].

[190] Austin Schneider. "Characterization of the Astrophysical Diffuse Neutrino Flux with IceCube High-Energy Starting Events". In: *36th International Cosmic Ray Conference (ICRC 2019) Madison, Wisconsin, USA, July 24-August 1, 2019*. 2019. arXiv: 1907.11266 [astro-ph.HE].

[191] M. G. Aartsen et al. "Measurement of South Pole ice transparency with the IceCube LED calibration system". In: *Nucl. Instrum. Meth.* A711 (2013), pp. 73–89. DOI: 10.1016/j.nima.2013.01.054. arXiv: 1301.5361 [astro-ph.IM].

[192] M. G. Aartsen et al. "The IceCube Neutrino Observatory Part VI: Ice Properties, Reconstruction and Future Developments". In: *Proceedings, 33rd International Cosmic Ray Conference (ICRC2013): Rio de Janeiro, Brazil, July 2-9, 2013*. 2013. arXiv: 1309.7010 [astro-ph.HE].

[193] Dawn Williams. "Light propagation in the South Pole ice". In: *AIP Conf. Proc.* 1630.1 (2015), pp. 146–149. DOI: 10.1063/1.4902793.

[194] Christopher Weaver, Nancy Wandkowsky, and on behalf of the IceCube Collaboration. "All-flavor Multi-Channel Analysis of the Astrophysical Neutrino Spectrum with IceCube". In: *Proceedings of 35th International Cosmic Ray Conference — PoS(ICRC2017)*. 35th International Cosmic Ray Conference. Vol. 301. SISSA Medialab, Aug. 3, 2018, p. 976. DOI: 10.22323/1.301.0976. URL: https://pos.sissa.it/cgi-bin/reader/contribution.cgi?id=PoS(ICRC2017)976.

[195] Hans Martin Niederhausen, Yiqian Xu, and on behalf of the IceCube Collaboration. "High Energy Astrophysical Neutrino Flux Measurement Using Neutrino-induced Cascades Observed in 4 Years of IceCube Data". In: *Proceedings of 35th International Cosmic Ray Conference — PoS(ICRC2017)*. 35th International Cosmic Ray Conference. Vol. 301. SISSA Medialab, Aug. 3, 2018, p. 968. DOI: 10.22323/1.301.0968. URL: https://pos.sissa.it/cgi-bin/reader/contribution.cgi?id=PoS(ICRC2017)968.

[196] M. G. Aartsen et al. "Characteristics of the diffuse astrophysical electron and tau neutrino flux with six years of IceCube high energy cascade data". In: (2020). arXiv: 2001.09520 [astro-ph.HE].

[197] The IceCube Collaboration. "Measurements using the inelasticity distribution of multi-TeV neutrino interactions in IceCube". In: *Physical Review D* 99.3 (Feb. 2019). arXiv: 1808.07629, p. 032004. ISSN: 2470-0010, 2470-0029. DOI: 10.1103/PhysRevD.99.032004. URL: http://arxiv.org/abs/1808.07629.

[198] Jöran Stettner. "Measurement of the diffuse astrophysical muon-neutrino spectrum with ten years of IceCube data". In: *Proceedings of 36th International Cosmic Ray Conference — PoS(ICRC2019)*. 36th International Cosmic Ray Conference. Vol. 358. SISSA Medialab, July 22, 2019, p. 1017. URL: https://pos.sissa.it/358/1017/.

[199] M. G. Aartsen et al. "A combined maximum-likelihood analysis of the high-energy astrophysical neutrino flux measured with IceCube". In: *The Astrophysical Journal* 809.1 (Aug. 2015), p. 98. ISSN: 1538-4357. DOI: 10.1088/0004-637x/809/1/98. URL: http://dx.doi.org/10.1088/0004-637X/809/1/98.

[200] Juliana Stachurska. "First Double Cascade Tau Neutrino Candidates in IceCube and a New Measurement of the Flavor Composition". In: *Proceedings of 36th International Cosmic Ray Conference — PoS(ICRC2019)*. 36th International Cosmic Ray Conference. Vol. 358. SISSA Medialab, July 22, 2019, p. 1015. URL: https://pos.sissa.it/358/1015/.

[201] Dawn Williams and on behalf of the IceCube Collaboration. "Results from IceCube". In: *Proceedings of 36th International Cosmic Ray Conference — PoS(ICRC2019)*. 36th International Cosmic Ray Conference. Vol. 358. SISSA Medialab, July 22, 2019, p. 016. URL: https://pos.sissa.it/358/016.

[202] IceCube-Gen2 Collaboration. *IceCube-Gen2: A Vision for the Future of Neutrino Astronomy in Antarctica*. 2014. arXiv: 1412.5106 [astro-ph.HE].

[203] Giulia Illuminati. "ANTARES and IceCube combined search for neutrino point-like and extended sources in the Southern Sky". In: *Proceedings of 36th International Cosmic Ray Conference — PoS(ICRC2019)*. 36th International Cosmic Ray Conference. Vol. 358. SISSA Medialab, July 22, 2019, p. 919. URL: https://pos.sissa.it/cgi-bin/reader/contribution.cgi?id=PoS(ICRC2019)919.

[204] IceCube Collaboration. "Neutrino emission from the direction of the blazar TXS 0506+056 prior to the IceCube-170922A alert". In: *Science* (July 12, 2018), eaat2890. ISSN: 0036-8075, 1095-9203. DOI: 10.1126/science.aat2890. URL: http://science.sciencemag.org/content/early/2018/07/11/science.aat2890.

[205] Rosa Coniglione and on behalf of the KM3NeT {and} Antares collaborations. "Results from the Mediterranean neutrino detectors". In: *Proceedings of 36th International Cosmic Ray Conference — PoS(ICRC2019)*. 36th International Cosmic Ray Conference. Vol. 358. SISSA Medialab, Sept. 27, 2019, p. 006. URL: https://pos.sissa.it/358/006/.

[206] Luigi Antonio Fusco and Federico Versari. "Study of the high-energy neutrino diffuse flux with the ANTARES neutrino telescope". In: *Proceedings of 36th International Cosmic Ray Conference — PoS(ICRC2019)*. 36th International Cosmic Ray Conference. Vol. 358. SISSA Medialab, July 22, 2019, p. 891. URL: https://pos.sissa.it/358/891/.

[207] Julien Aublin. "ANTARES search for point sources of neutrinos with 11 yr of data: a likelihood stacking analysis". In: *Proceedings of 36th International Cosmic Ray Conference — PoS(ICRC2019)*. 36th International Cosmic Ray Conference. Vol. 358. SISSA Medialab, July 22, 2019, p. 840. URL: https://pos.sissa.it/358/840.

[208] Christian Glaser et al. *NuRadioMC: Simulating the radio emission of neutrinos from interaction to detector*. 2019. arXiv: 1906.01670 [astro-ph.IM].

[209] G. A. Askar'yan. "Excess negative charge of an electron-photon shower and its coherent radio emission". In: *Sov. Phys. JETP* 14.2 (1962). [Zh. Eksp. Teor. Fiz.41,616(1961)], pp. 441–443.

[210] Peter W. Gorham et al. "Radio-frequency measurements of coherent transition and Cherenkov radiation: Implications for high-energy neutrino detection". In: *Physical Review E* 62.6 (Dec. 2000), pp. 8590–8605. ISSN: 1095-3787. DOI: 10.1103/physreve.62.8590. URL: http://dx.doi.org/10.1103/PhysRevE.62.8590.

[211] S. Barwick et al. "South Polar in situ radio-frequency ice attenuation". In: *Journal of Glaciology* 51.173 (2005), pp. 231–238. DOI: 10.3189/172756505781829467.

[212] A. Anker et al. "Targeting ultra-high energy neutrinos with the ARIANNA experiment". In: *Advances in Space Research* 64.12 (Dec. 2019), pp. 2595–2609. ISSN: 02731177. DOI: 10.1016/j.asr.2019.06.016. arXiv: 1903.01609. URL: http://arxiv.org/abs/1903.01609.

[213] S. W. Barwick et al. “Design and Performance of the ARIANNA HRA-3 Neutrino Detector Systems”. In: *IEEE Transactions on Nuclear Science* 62.5 (Oct. 2015), pp. 2202–2215. ISSN: 1558-1578. DOI: 10.1109/TNS.2015.2468182.

[214] Christian Glaser. “Neutrino direction and energy resolution of Askaryan detectors”. In: *Proceedings of 36th International Cosmic Ray Conference — PoS(ICRC2019)*. 36th International Cosmic Ray Conference. Vol. 358. SISSA Medialab, Sept. 2, 2019, p. 899. URL: https://pos.sissa.it/358/899/.

[215] Christopher Persichilli. “Performance of the ARIANNA pilot array, and implications for the next generation of UHE neutrino detectors”. In: *Proceedings of 36th International Cosmic Ray Conference — PoS(ICRC2019)*. 36th International Cosmic Ray Conference. Vol. 358. SISSA Medialab, Sept. 2, 2019, p. 980. URL: https://pos.sissa.it/358/980/.

[216] ARA Collaboration. *Constraints on the Diffuse Flux of Ultra-High Energy Neutrinos from Four Years of Askaryan Radio Array Data in Two Stations*. 2019. arXiv: 1912.00987 [astro-ph.HE].

[217] P. W. Gorham et al. “Constraints on the ultra-high energy cosmic neutrino flux from the fourth flight of ANITA”. In: *Physical Review D* 99.12 (June 11, 2019), p. 122001. ISSN: 2470-0010, 2470-0029. DOI: 10.1103/PhysRevD.99.122001. arXiv: 1902.04005. URL: http://arxiv.org/abs/1902.04005 (visited on 02/04/2020).

[218] P. W. Gorham et al. “Observation of an Unusual Upward-going Cosmic-ray-like Event in the Third Flight of ANITA”. In: *Physical Review Letters* 121.16 (Oct. 18, 2018), p. 161102. ISSN: 0031-9007, 1079-7114. DOI: 10.1103/PhysRevLett.121.161102. arXiv: 1803.05088. URL: http://arxiv.org/abs/1803.05088.

[219] P. W. Gorham et al. “Characteristics of Four Upward-pointing Cosmic-ray-like Events Observed with ANITA”. In: *Phys. Rev. Lett.* 117.7 (2016), p. 071101. DOI: 10.1103/PhysRevLett.117.071101. arXiv: 1603.05218 [astro-ph.HE].

[220] F. Halzen and D. Saltzberg. "Tau-neutrino appearance with a 1000 megaparsec baseline". In: *Phys. Rev. Lett.* 81 (1998), pp. 4305–4308. DOI: 10.1103/PhysRevLett.81.4305. arXiv: hep-ph/9804354 [hep-ph].

[221] Alexander Aab et al. "The Pierre Auger Cosmic Ray Observatory". In: *Nucl. Instrum. Meth.* A798 (2015), pp. 172–213. DOI: 10.1016/j.nima.2015.06.058. arXiv: 1502.01323 [astro-ph.IM].

[222] A. Aab et al. "Probing the origin of ultra-high-energy cosmic rays with neutrinos in the EeV energy range using the Pierre Auger Observatory". In: *Journal of Cosmology and Astroparticle Physics* 2019.10 (Oct. 2019), pp. 022–022. ISSN: 1475-7516. DOI: 10.1088/1475-7516/2019/10/022. URL: http://dx.doi.org/10.1088/1475-7516/2019/10/022.

[223] John Krizmanic. "POEMMA: Probe Of Extreme Multi-Messenger Astrophysics". In: *EPJ Web Conf.* 210 (2019), p. 06008. DOI: 10.1051/epjconf/201921006008.

[224] Mary Hall Reno, John F. Krizmanic, and Tonia M. Venters. "Cosmic tau neutrino detection via Cherenkov signals from air showers from Earth-emerging taus". In: *Phys. Rev.* D100.6 (2019), p. 063010. DOI: 10.1103/PhysRevD.100.063010. arXiv: 1902.11287 [astro-ph.HE].

[225] Andrea Palladino and Francesco Vissani. "Can BL Lac emission explain the neutrinos above 0.2 PeV?" In: *Astronomy & Astrophysics* 604 (Aug. 2017), A18. ISSN: 0004-6361, 1432-0746. DOI: 10.1051/0004-6361/201730739. arXiv: 1702.08779. URL: http://arxiv.org/abs/1702.08779.

[226] Andrea Palladino and Francesco Vissani. "Extragalactic plus Galactic model for IceCube neutrino events". In: *The Astrophysical Journal* 826.2 (July 29, 2016), p. 185. ISSN: 1538-4357. DOI: 10.3847/0004-637X/826/2/185. arXiv: 1601.06678. URL: http://arxiv.org/abs/1601.06678.

[227] Atri Bhattacharya et al. "Perturbative charm production and the prompt atmospheric neutrino flux in light of RHIC and LHC". In: *Journal of High Energy Physics* 2015.6 (June 2015), p. 110. ISSN: 1029-8479. DOI: 10.1007/JHEP06(2015)110. arXiv: 1502.01076. URL: http://arxiv.org/abs/1502.01076.

[228] Andrea Palladino, Maurizio Spurio, and Francesco Vissani. "On the IceCube spectral anomaly". In: *Journal of Cosmology and Astroparticle Physics* 2016.12 (Dec. 2016). arXiv: 1610.07015, pp. 045–045. ISSN: 1475-7516. DOI: 10.1088/1475-7516/2016/12/045. URL: http://arxiv.org/abs/1610.07015.

[229] A. Neronov and D. V. Semikoz. "Evidence for the Galactic contribution to the IceCube astrophysical neutrino flux". In: *Astroparticle Physics* 75 (Feb. 2016). arXiv: 1509.03522, pp. 60–63. ISSN: 09276505. DOI: 10.1016/j.astropartphys.2015.11.002. URL: http://arxiv.org/abs/1509.03522.

[230] Peter B. Denton, Danny Marfatia, and Thomas J. Weiler. "The Galactic Contribution to IceCube's Astrophysical Neutrino Flux". In: *Journal of Cosmology and Astroparticle Physics* 2017.8 (Aug. 29, 2017), pp. 033–033. ISSN: 1475-7516. DOI: 10.1088/1475-7516/2017/08/033. arXiv: 1703.09721. URL: http://arxiv.org/abs/1703.09721.

[231] Sergio Palomares-Ruiz, Aaron C. Vincent, and Olga Mena. "Spectral analysis of the high-energy IceCube neutrinos". In: *Physical Review D* 91.10 (May 28, 2015), p. 103008. ISSN: 1550-7998, 1550-2368. DOI: 10.1103/PhysRevD.91.103008. arXiv: 1502.02649. URL: http://arxiv.org/abs/1502.02649.

[232] M. Chianese, G. Miele, and S. Morisi. "Dark Matter interpretation of low energy IceCube MESE excess". In: *Journal of Cosmology and Astroparticle Physics* 2017.1 (Jan. 3, 2017), pp. 007–007. ISSN: 1475-7516. DOI: 10.1088/1475-7516/2017/01/007. arXiv: 1610.04612. URL: http://arxiv.org/abs/1610.04612.

[233] Nagisa Hiroshima et al. "High-energy Neutrinos from Multi-body Decaying Dark Matter". In: *Physical Review D* 97.2 (Jan. 10, 2018), p. 023006. ISSN: 2470-0010, 2470-0029. DOI: 10.1103/PhysRevD.97.023006. arXiv: 1705.04419. URL: http://arxiv.org/abs/1705.04419.

[234] IceCube Collaboration. "Search for Astrophysical Tau Neutrinos in Three Years of IceCube Data". In: *Physical Review D* 93.2 (Jan. 12, 2016). ISSN: 2470-0010, 2470-0029. DOI: 10.1103/PhysRevD.93.022001. arXiv: 1509.06212. URL: http://arxiv.org/abs/1509.06212.

[235] Andrea Palladino et al. “Double pulses and cascades above 2 PeV in IceCube”. In: *The European Physical Journal C* 76.2 (Feb. 2016), p. 52. ISSN: 1434-6044, 1434-6052. DOI: 10.1140/epjc/s10052-016-3893-3. arXiv: 1510.05921. URL: http://arxiv.org/abs/1510.05921.

[236] Sheldon L. Glashow. “Resonant Scattering of Antineutrinos”. In: *Physical Review* 118 (Apr. 1, 1960), pp. 316–317. ISSN: 1536-6065. DOI: 10.1103/PhysRev.118.316. URL: http://adsabs.harvard.edu/abs/1960PhRv..118..316G.

[237] Zhi-zhong Xing and Shun Zhou. “The Glashow resonance as a discriminator of UHE cosmic neutrinos originating from p-gamma and p-p collisions”. In: *Physical Review D* 84.3 (Aug. 9, 2011), p. 033006. ISSN: 1550-7998, 1550-2368. DOI: 10.1103/PhysRevD.84.033006. arXiv: 1105.4114. URL: http://arxiv.org/abs/1105.4114.

[238] V. Barger et al. “Glashow resonance as a window into cosmic neutrino sources”. In: *Physical Review D* 90.12 (Dec. 12, 2014), p. 121301. ISSN: 1550-7998, 1550-2368. DOI: 10.1103/PhysRevD.90.121301. arXiv: 1407.3255. URL: http://arxiv.org/abs/1407.3255.

[239] Daniel Biehl et al. “Astrophysical Neutrino Production Diagnostics with the Glashow Resonance”. In: *Journal of Cosmology and Astroparticle Physics* 2017.1 (Jan. 16, 2017), pp. 033–033. ISSN: 1475-7516. DOI: 10.1088/1475-7516/2017/01/033. arXiv: 1611.07983. URL: http://arxiv.org/abs/1611.07983 (visited on 09/26/2019).

[240] Svenja Hümmer et al. “Simplified models for photohadronic interactions in cosmic accelerators”. In: *The Astrophysical Journal* 721.1 (Sept. 20, 2010), pp. 630–652. ISSN: 0004-637X, 1538-4357. DOI: 10.1088/0004-637X/721/1/630. arXiv: 1002.1310. URL: http://arxiv.org/abs/1002.1310.

[241] A. Palladino et al. “Which is the flavor of cosmic neutrinos seen by IceCube?” In: *Physical Review Letters* 114.17 (Apr. 28, 2015), p. 171101. ISSN: 0031-9007, 1079-7114. DOI: 10.1103/PhysRevLett.114.171101. arXiv: 1502.02923. URL: http://arxiv.org/abs/1502.02923.

[242] The Antares Collaboration. "New Constraints on all flavour Galactic diffuse neutrino emission with the ANTARES telescope". In: *Physical Review D* 96.6 (Sept. 11, 2017), p. 062001. ISSN: 2470-0010, 2470-0029. DOI: 10.1103/PhysRevD.96.062001. arXiv: 1705.00497. URL: http://arxiv.org/abs/1705.00497.

[243] The IceCube Collaboration. "Constraints on Galactic Neutrino Emission with Seven Years of IceCube Data". In: *The Astrophysical Journal* 849.1 (Oct. 31, 2017), p. 67. ISSN: 1538-4357. DOI: 10.3847/1538-4357/aa8dfb. arXiv: 1707.03416. URL: http://arxiv.org/abs/1707.03416.

[244] Peter Minkowski. "$\mu \to e\gamma$ at a rate of one out of 109 muon decays?" In: *Physics Letters B* 67.4 (Apr. 25, 1977), pp. 421–428. ISSN: 0370-2693. DOI: 10.1016/0370-2693(77)90435-X. URL: http://www.sciencedirect.com/science/article/pii/037026937790435X.

[245] Steven Weinberg. "Baryon- and Lepton-Nonconserving Processes". In: *Phys. Rev. Lett.* 43 (21 Nov. 1979), pp. 1566–1570. DOI: 10.1103/PhysRevLett.43.1566. URL: https://link.aps.org/doi/10.1103/PhysRevLett.43.1566.

[246] Robert E. Shrock. "Electromagnetic properties and decays of Dirac and Majorana neutrinos in a general class of gauge theories". In: *Nuclear Physics B* 206.3 (Oct. 18, 1982), pp. 359–379. ISSN: 0550-3213. DOI: 10.1016/0550-3213(82)90273-5. URL: http://www.sciencedirect.com/science/article/pii/0550321382902735.

[247] Marco Cirelli et al. "Probing oscillations into sterile neutrinos with cosmology, astrophysics and experiments". In: *Nuclear Physics B* 708.1 (Feb. 2005), pp. 215–267. ISSN: 05503213. DOI: 10.1016/j.nuclphysb.2004.11.056. arXiv: hep-ph/0403158. URL: http://arxiv.org/abs/hep-ph/0403158.

[248] Roberto Aloisio, Eugenio Coccia, and Francesco Vissani, eds. *Multiple Messengers and Challenges in Astroparticle Physics*. Springer International Publishing, 2018. ISBN: 978-3-319-65423-2. URL: https://www.springer.com/gp/book/9783319654232 (visited on 09/26/2019).

[249] Super-Kamiokande Collaboration. "Evidence for Oscillation of Atmospheric Neutrinos". In: *Physical Review Letters* 81.8 (Aug. 24, 1998), pp. 1562–1567. DOI: 10.1103/PhysRevLett.81.1562. URL: https://link.aps.org/doi/10.1103/PhysRevLett.81.1562 (visited on 09/26/2019).

[250] MACRO Collaboration. "Measurement of the atmospheric neutrino-induced upgoing muon flux using MACRO". In: *Physics Letters B* 434.3 (Aug. 27, 1998), pp. 451–457. ISSN: 0370-2693. DOI: 10.1016/S0370-2693(98)00885-5. URL: http://www.sciencedirect.com/science/article/pii/S0370269398008855.

[251] W. W. M. Allison et al. "The atmospheric neutrino flavor ratio from a 3.9 fiducial kiloton-year exposure of Soudan 2". In: *Physics Letters B* 449.1 (Mar. 4, 1999), pp. 137–144. ISSN: 0370-2693. DOI: 10.1016/S0370-2693(99)00056-8. URL: http://www.sciencedirect.com/science/article/pii/S0370269399000568.

[252] SNO Collaboration. "Direct Evidence for Neutrino Flavor Transformation from Neutral-Current Interactions in the Sudbury Neutrino Observatory". In: *Phys. Rev. Lett.* 89 (1 June 2002), p. 011301. DOI: 10.1103/PhysRevLett.89.011301. URL: https://link.aps.org/doi/10.1103/PhysRevLett.89.011301.

[253] KamLAND Collaboration. "First Results from KamLAND: Evidence for Reactor Antineutrino Disappearance". In: *Phys. Rev. Lett.* 90 (2 Jan. 2003), p. 021802. DOI: 10.1103/PhysRevLett.90.021802. URL: https://link.aps.org/doi/10.1103/PhysRevLett.90.021802.

[254] MINOS Collaboration. "Observation of Muon Neutrino Disappearance with the MINOS Detectors in the NuMI Neutrino Beam". In: *Phys. Rev. Lett.* 97 (19 Nov. 2006), p. 191801. DOI: 10.1103/PhysRevLett.97.191801. URL: https://link.aps.org/doi/10.1103/PhysRevLett.97.191801.

[255] T2K Collaboration. "Indication of Electron Neutrino Appearance from an Accelerator-Produced Off-Axis Muon Neutrino Beam". In: *Phys. Rev. Lett.* 107 (4 July 2011), p. 041801. DOI: 10.1103/PhysRevLett.107.041801. URL: https://link.aps.org/doi/10.1103/PhysRevLett.107.041801.

[256] F. P. An et al. “Observation of Electron-Antineutrino Disappearance at Daya Bay”. In: *Phys. Rev. Lett.* 108 (17 Apr. 2012), p. 171803. DOI: 10.1103/PhysRevLett.108.171803. URL: https://link.aps.org/doi/10.1103/PhysRevLett.108.171803.

[257] OPERA Collaboration. “Evidence for $\nu_\mu \to \nu_\tau$ appearance in the CNGS neutrino beam with the OPERA experiment”. In: *Phys. Rev. D* 89 (5 Mar. 2014), p. 051102. DOI: 10.1103/PhysRevD.89.051102. URL: https://link.aps.org/doi/10.1103/PhysRevD.89.051102.

[258] L. Wolfenstein. “Neutrino oscillations in matter”. In: *Phys. Rev. D* 17 (9 May 1978), pp. 2369–2374. DOI: 10.1103/PhysRevD.17.2369. URL: https://link.aps.org/doi/10.1103/PhysRevD.17.2369.

[259] John G. Learned and Sandip Pakvasa. “Detecting Nutau Oscillations as PeV Energies”. In: *Astroparticle Physics* 3.3 (May 1995), pp. 267–274. ISSN: 09276505. DOI: 10.1016/0927-6505(94)00043-3. arXiv: hep-ph/9405296. URL: http://arxiv.org/abs/hep-ph/9405296.

[260] V. S. Berezinsky and A. Z. Gazizov. “Cosmic neutrino and the possibility of Searching for W bosons with masses 30-100 GeV in underwater experiments”. In: *JETP Lett.* 25 (1977). Pisma Zh. Eksp. Teor. Fiz.25,276(1977), pp. 254–256.

[261] Soebur Razzaque and A. Yu. Smirnov. “Flavor conversion of cosmic neutrinos from hidden jets”. In: *Journal of High Energy Physics* 2010.3 (Mar. 2010). ISSN: 1029-8479. DOI: 10.1007/jhep03(2010)031. URL: http://dx.doi.org/10.1007/JHEP03(2010)031.

[262] M. Gasperini. “Testing the Principle of Equivalence with Oscillations”. In: *Phys. Rev.* D38 (1988), pp. 2635–2637. DOI: 10.1103/PhysRevD.38.2635.

[263] Floyd W. Stecker. “Testing Lorentz Symmetry using High Energy Astrophysics Observations”. In: *Symmetry* 9.201 (2017). arXiv: 1708.05672. URL: http://arxiv.org/abs/1708.05672 (visited on 09/26/2019).

[264] Veniamin Berezinsky, Mohan Narayan, and Francesco Vissani. “Mirror model for sterile neutrinos”. In: *Nuclear Physics B* 658.1-2 (May 2003), pp. 254–280. ISSN: 0550-3213. DOI: 10.1016/s0550-3213(03)00191-3. URL: http://dx.doi.org/10.1016/S0550-3213(03)00191-3.

[265] John F. Beacom et al. "Pseudo-Dirac Neutrinos: A Challenge for Neutrino Telescopes". In: *Physical Review Letters* 92.1 (Jan. 2004). ISSN: 1079-7114. DOI: 10.1103/physrevlett.92.011101. URL: http://dx.doi.org/10.1103/PhysRevLett.92.011101.

[266] Mauricio Bustamante, John F. Beacom, and Walter Winter. "Theoretically Palatable Flavor Combinations of Astrophysical Neutrinos". In: *Physical Review Letters* 115.16 (Oct. 2015). ISSN: 1079-7114. DOI: 10.1103/physrevlett.115.161302. URL: http://dx.doi.org/10.1103/PhysRevLett.115.161302.

[267] Rasmus W. Rasmussen et al. "Astrophysical neutrinos flavored with beyond the Standard Model physics". In: *Physical Review D* 96.8 (Oct. 2017). ISSN: 2470-0029. DOI: 10.1103/physrevd.96.083018. URL: http://dx.doi.org/10.1103/PhysRevD.96.083018.

[268] M. G. Aartsen et al. "Flavor Ratio of Astrophysical Neutrinos above 35 TeV in IceCube". In: *Physical Review Letters* 114.17 (Apr. 2015). ISSN: 1079-7114. DOI: 10.1103/physrevlett.114.171102. URL: http://dx.doi.org/10.1103/PhysRevLett.114.171102.

[269] M. G. Aartsen et al. "Evidence for Astrophysical Muon Neutrinos from the Northern Sky with IceCube". In: *Physical Review Letters* 115.8 (Aug. 2015). ISSN: 1079-7114. DOI: 10.1103/physrevlett.115.081102. URL: http://dx.doi.org/10.1103/PhysRevLett.115.081102.

[270] M. Tanabashi et al. "Review of Particle Physics". In: *Phys.Rev.* D98.3 (Aug. 17, 2018), p. 030001. DOI: 10.1103/PhysRevD.98.030001.

[271] Andrea Palladino and Walter Winter. "A multi-component model for observed astrophysical neutrinos". In: *Astronomy & Astrophysics* 615 (July 2018), A168. ISSN: 1432-0746. DOI: 10.1051/0004-6361/201832731. URL: http://dx.doi.org/10.1051/0004-6361/201832731.

[272] Marcel Usner and on behalf of the IceCube Collaboration. "Search for Astrophysical Tau Neutrinos in Six Years of High-Energy Starting Events in IceCube". In: *Proceedings of 35th International Cosmic Ray Conference — PoS(ICRC2017)*. 35th International Cosmic Ray Conference. Vol. 301. SISSA Medialab, Aug. 16, 2017, p. 974. URL: https://pos.sissa.it/

cgi-bin/reader/contribution.cgi?id=PoS(ICRC2017)974 (visited on 02/28/2018).

[273] D. Fargion. "Discovering Ultra–High-Energy Neutrinos through Horizontal and Upward τ Air Showers: Evidence in Terrestrial Gamma Flashes?" In: *The Astrophysical Journal* 570.2 (May 2002), pp. 909–925. ISSN: 1538-4357. DOI: 10.1086/339772. URL: http://dx.doi.org/10.1086/339772.

[274] D. Fargion et al. "Crown detectors arrays to observe horizontal and upward air-showers". In: *Advances in Space Research* 37.11 (Jan. 2006), pp. 2132–2138. ISSN: 0273-1177. DOI: 10.1016/j.asr.2006.03.037. URL: http://dx.doi.org/10.1016/j.asr.2006.03.037.

[275] Daniele Fargion and Pietro Oliva. *No Tau? No Astronomy!* 2017. arXiv: 1707.01982 [astro-ph.HE].

[276] Angela V. Olinto et al. "POEMMA: Probe Of Extreme Multi-Messenger Astrophysics". In: *Proceedings of 35th International Cosmic Ray Conference — PoS(ICRC2017)*. 35th International Cosmic Ray Conference. Vol. 301. SISSA Medialab, Aug. 3, 2018, p. 542. DOI: 10.22323/1.301.0542. URL: https://pos.sissa.it/301/542/ (visited on 09/26/2019).

[277] Yu Seon Jeong et al. "Tau energy loss and ultrahigh energy skimming tau neutrinos". In: *Physical Review D* 96.4 (Aug. 2017). ISSN: 2470-0029. DOI: 10.1103/physrevd.96.043003. URL: http://dx.doi.org/10.1103/PhysRevD.96.043003.

[278] Alexander Bulmahn and Mary Hall Reno. "Secondary atmospheric tau neutrino production". In: *Physical Review D* 82.5 (Sept. 2010). ISSN: 1550-2368. DOI: 10.1103/physrevd.82.057302. URL: http://dx.doi.org/10.1103/PhysRevD.82.057302.

[279] The IceCube Collaboration. "Observation of High-Energy Astrophysical Neutrinos in Three Years of IceCube Data". In: *Physical Review Letters* 113.10 (Sept. 2014). arXiv: 1405.5303. ISSN: 0031-9007, 1079-7114. DOI: 10.1103/PhysRevLett.113.101101. URL: http://arxiv.org/abs/1405.5303.

[280] The IceCube Collaboration. "The IceCube Neutrino Observatory - Contributions to ICRC 2017 Part II: Properties of the Atmospheric and Astrophysical Neutrino Flux". In: *arXiv:1710.01191 [astro-ph]* (2017). arXiv: 1710.01191. URL: http://arxiv.org/abs/1710.01191.

[281] Andrea Palladino et al. "IceCube Neutrinos from Hadronically Powered Gamma-Ray Galaxies". en. In: *arXiv* (Dec. 2018). URL: https://arxiv.org/abs/1812.04685.

[282] Carlos A. Argüelles et al. "Unified atmospheric neutrino passing fractions for large-scale neutrino telescopes". In: *Journal of Cosmology and Astroparticle Physics* 2018.07 (July 2018), pp. 047–047. ISSN: 1475-7516. DOI: 10.1088/1475-7516/2018/07/047. URL: http://dx.doi.org/10.1088/1475-7516/2018/07/047.

[283] Peter B. Denton and Irene Tamborra. "Invisible Neutrino Decay Resolves IceCube's Track and Cascade Tension". In: *Physical Review Letters* 121.12 (Sept. 2018). arXiv: 1805.05950, p. 121802. ISSN: 0031-9007, 1079-7114. DOI: 10.1103/PhysRevLett.121.121802. URL: http://arxiv.org/abs/1805.05950.

[284] Claudio Kopper and on behalf of the IceCube Collaboration. "Observation of Astrophysical Neutrinos in Six Years of IceCube Data". en. In: *Proceedings of 35th International Cosmic Ray Conference — PoS(ICRC2017)*. Vol. 301. SISSA Medialab, Aug. 2018, p. 981. DOI: 10.22323/1.301.0981. URL: https://pos.sissa.it/cgi-bin/reader/contribution.cgi?id=PoS(ICRC2017)981.

[285] Stefan Schönert et al. "Vetoing atmospheric neutrinos in a high energy neutrino telescope". en. In: *Physical Review D* (Dec. 2008). DOI: 10.1103/PhysRevD.79.043009. URL: https://arxiv.org/abs/0812.4308v1.

[286] M. Spurio. "Constraints to a Galactic Component of the Ice Cube cosmic neutrino flux from ANTARES". In: *Physical Review D* 90.10 (Nov. 2014). arXiv: 1409.4552, p. 103004. ISSN: 1550-7998, 1550-2368. DOI: 10.1103/PhysRevD.90.103004. URL: http://arxiv.org/abs/1409.4552.

[287] Sergey Troitsky. "Search for Galactic disk and halo components in the arrival directions of high-energy astrophysical neutrinos". In: *JETP Letters* 102.12 (Dec. 2015). arXiv: 1511.01708, pp. 785–788. ISSN: 0021-3640, 1090-6487. DOI: 10.1134/S0021364015240133. URL: http://arxiv.org/abs/1511.01708.

[288] Andrea Palladino and Francesco Vissani. "Extragalactic plus Galactic model for IceCube neutrino events". In: *The Astrophysical Journal* 826.2 (July 2016). arXiv: 1601.06678, p. 185. ISSN: 1538-4357. DOI: 10.3847/0004-637X/826/2/185. URL: http://arxiv.org/abs/1601.06678.

[289] G. Pagliaroli, C. Evoli, and F. L. Villante. "Expectations for high energy diffuse galactic neutrinos for different cosmic ray distributions". In: *Journal of Cosmology and Astroparticle Physics* 2016.11 (Nov. 2016). arXiv: 1606.04489, pp. 004–004. ISSN: 1475-7516. DOI: 10.1088/1475-7516/2016/11/004. URL: http://arxiv.org/abs/1606.04489.

[290] The IceCube and ANTARES Collaborations, D. Gaggero, and D. Grasso. "Joint constraints on Galactic diffuse neutrino emission from ANTARES and IceCube". In: *arXiv:1808.03531 [astro-ph]* (Aug. 2018). arXiv: 1808.03531. URL: http://arxiv.org/abs/1808.03531.

List of Figures

List of Tables